Enhancing Triple Phase Boundary Electrosynthesis

John Douglas Watkins

A thesis submitted for the degree of Doctor of Philosophy

University of Bath

Department of Chemistry

December 2011

Abstract

The first part of this thesis is concerned with the synthesis, characterisation and applications of surface functionalised carbon nanoparticles. Synthetic techniques are used to modify the existing surface architecture of carbon nanoparticles towards high surface area modified electrodes and pH sensing applications.

Electrochemical and synthetic techniques have been used to study triple phase boundaries and enhance their properties towards a bulk synthetic technique, in which an electrolyte phase and redox probe phase are held separate.

A salt matrix, ultrasound, high shear force and a carbon fibre membrane have all been used to form unique triple phase boundary environments in which electron and ion transfer processes can be studied and enhanced towards analytical and electrosynthetic applications.

A number of electro-reduction reactions have been shown to be feasible using the triple phase boundary methodology. Alkenes, aldehydes and imines have all been successfully electro-reduced, analysed and optimised to elucidate the synthetic triple phase boundary mechanism.

Acknowledgements

This thesis is dedicated to the memory of my mother Ellen Elizabeth Watkins, who instilled in me a passion for the sciences and mathematics throughout my childhood. She gave me the support to pursue a career in the subject she was never given the opportunity to study. Unfortunately, she was not able to see how much her support would affect my life.

I would like to thank my father Keith for his constant support throughout my childhood and adult life. He has always allowed me to make my own mistakes while always being there for guidance.

Also, I thank my supervisors Prof. Frank Marken and Dr. Steve Bull for their guidance throughout my undergraduate degree and postgraduate studies. They have made my experience in Bath a pleasure and given me a passion for research that will help me in my career far beyond my immediate future.

I have had the pleasure of supervising some excellent students during my studies that have helped me to achieve all that is presented in this thesis. These are; Ruth Lawrence, Sunyhik Ahn and Chris Hotchen.

I have also benefited from much collaboration both within the University of Bath and elsewhere, notably; Geoff Nelson (University of Oxford), Prof. John Foord (University of Oxford), Prof. Marcin Opallo (Warsaw), Katarzyna Szot (Warsaw), Dr. Jay Wadhawan (University of Hull), Fumihiro Amemiya (Tokyo Institute of Technology), Prof. Mahito Atobe (Tokyo Institute of Technology), Prof. Phil Page (University of East Anglia), everyone at the Bath Microscopy and Analysis Suite, Kate Lawrence (University of Bath), Dr. James Taylor (University of Bath), Charlie Cummings (University of Bath) and all past and present members of both the Bull and Marken labs. Namely: Andrew, Charlie, Richard, Jonny, Kate, Anne, Sara Dale and Fengjie for making the lab an enjoyable place to work.

Special thanks to Dr. Stuart MacDonald, currently employed at Shell, who has been something of a mentor to me during my time with the Marken lab. During my undergraduate degree, whilst he was working as a PhD student in the Marken lab, he inspired me to accept a PhD in electrosynthesis. Since graduating he has become a great friend and advisor, who is always willing to give me guidance despite the time restrictions of a high pressure job, for which I am very grateful. Also thanks to Liana Allen who has always challenged me to improve myself professionally and personally, without her I would not be the person I am today.

I have been very fortunate to be given the opportunity to travel to many conferences and other labs both in the UK and abroad. This has allowed me to meet new people and present my work to the wider scientific community. These have included Oxford, Hull, Liverpool, Warwick, Germany, Poland, Austria, Hawaii and San Francisco.

Finally I would like to thank the EPSRC for funding my PhD through the Doctoral Training Account.

Contents

1. Introduction

Contents

1.1 Introduction to Voltammetric Techniques

1.1.1 The Electrode Arrangement

Electrochemistry is concerned with the study of electron transfer between an electrode surface and molecules at the interface between two phases. By changing the potential the electron transfer can be carefully controlled and monitored, often yielding mechanistic, thermodynamic and kinetic data. Electrochemical investigations may be conducted using a variety of electrode configurations; (i) the two electrode arrangement commonly used for unreferenced electrolysis, by galvanostatic control, (ii) the four electrode arrangement commonly used for the polarisation of liquid | liquid interfaces in biphasic systems, and (iii) the three electrode setup which will henceforth be discussed as the core technique in this introduction. The three electrode arrangement is shown in Figure 1.1. The potential is controlled between the working and reference electrodes, with the counter electrode allowing the flow of current within the cell.

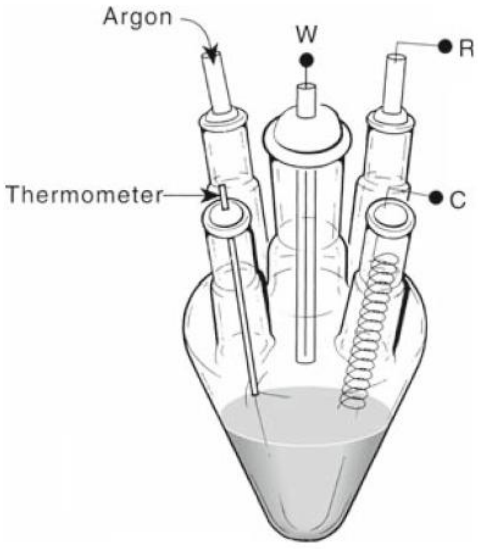

Figure 1.1 A three electrode cell setup showing W, working electrode C, counter electrode and R, reference electrode.

A commonly used reference electrode is the saturated KCl calomel reference electrode, which uses a $Hg^{I/0}$ redox couple Hg / Hg_2Cl_2 / KCl (saturated in water) in a fritted cell to maintain a constant and stable standard potential. The stability of the reference electrode is due to being very close to an ideal

non-polarisable interface as well as the concentration of KCl being assumed not to change during voltammetry due to its saturated nature. This electrode is designed to be largely unaffected by the electrolysis conditions and easier to work with than the standard hydrogen reference electrode which requires gaseous hydrogen.[1]

1.1.2 Measuring and Interpreting voltammograms

The electrochemical technique primarily used in this work is that of cyclic voltammetry. This is a powerful technique, which involves changing the potential applied to the cell in a linear fashion between a starting and ending potential (Figure 1.2). The gradient of the transition is the scan rate and can be adjusted to change the rate of electrochemical steps relative to chemical ones and can be used to elucidate the mechanism of the overall reaction.

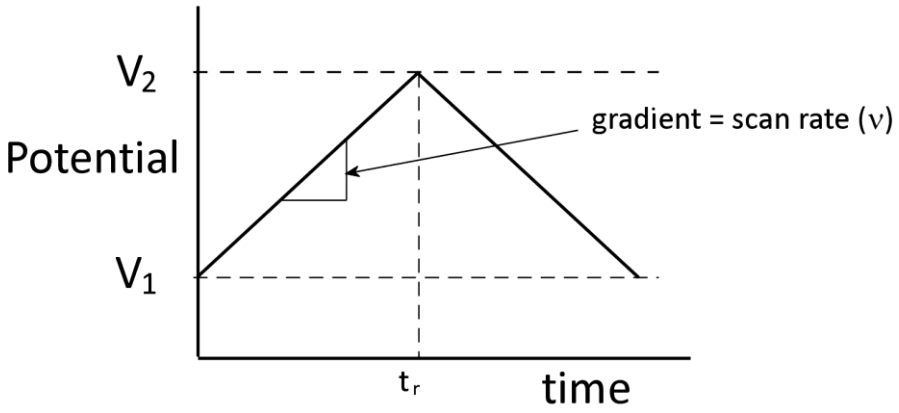

Figure 1.2 A graph showing the voltage *vs.* time wave applied during cyclic voltammetry with the scan rate being the gradient.

This change of potential is commonly plotted against the detected current to give a traditional voltammogram. The voltammogram signal can be split into two distinct components; (i) capacitive currents and (ii) faradaic currents. Capacitive currents are generally an unavoidable background which is inherent in all voltammetry due to the nature of the double layer existing at the electrode | solution interface. At this interface there is a potential gradient into the solution from the electrode and can act as a capacitor. Thus a charging current is visible on the voltammogram as illustrated in Figure 1.3.

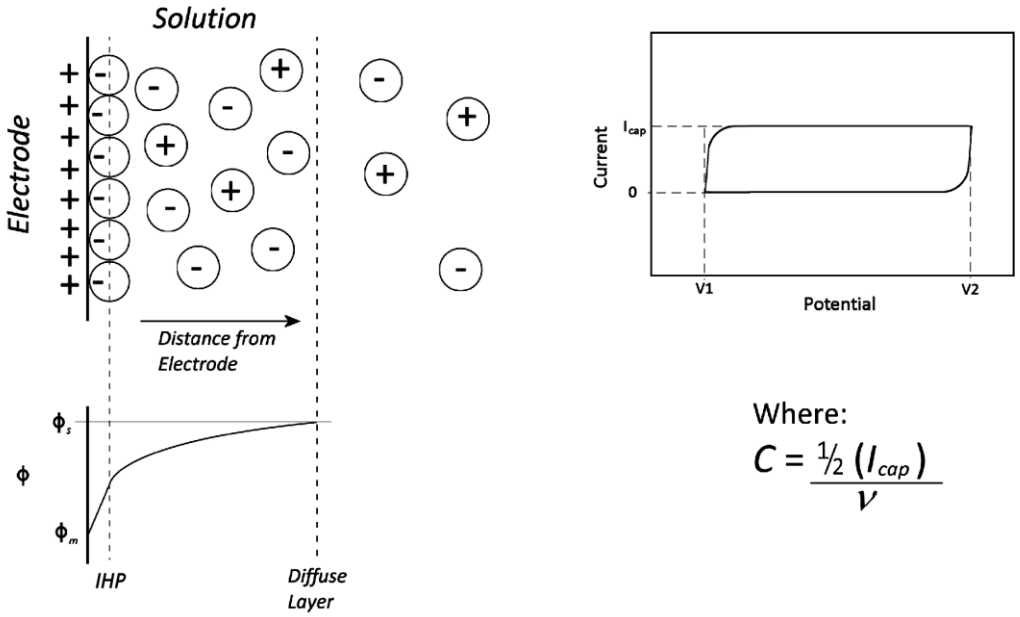

Figure 1.3 Diagrams showing the Stern model of the double layer at the electrode surface showing the change in potential from the electrode into the solution acting as a capacitor and the expected pure capacitance voltammogram. *C* is capacitance, I_{cap} is the current measured as shown *v* is the scan rate and IHP is the Inner Helmholtz Plane.

Faradaic currents are associated with the presence of a suitable redox probe around its reversible potential, suitable for redox reactions to occur, giving rise to a flow of current. In order for an electron transfer step to occur a redox active material must diffuse into the diffuse layer for electron tunnelling to be fast, since the probability of this process falls off exponentially with distance. The mechanism under static conditions proceeds in three steps; an associative step, which is mainly governed by the diffusion of A, an electron transfer step, which is controlled by the electron transfer kinetics of the surface and redox species and a dissociative step mainly governed by the diffusion of B, as shown in Figure 1.4. Voltammetry is used to measure the current arising from whichever of these steps is current limiting.

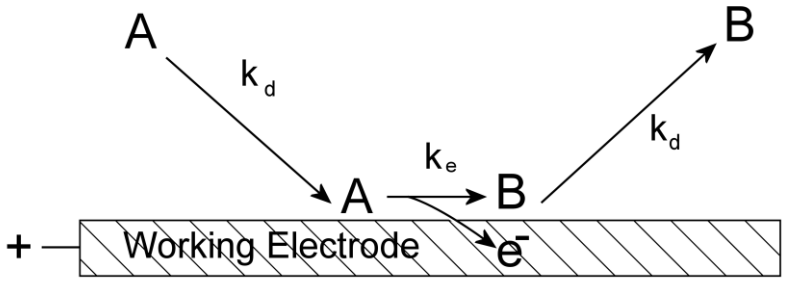

Figure 1.4 The mechanism for electron transfer at an electrode surface. Where A is the molecule to be reduced, B is the oxidised species k_e is a rate constant related to electron transfer and k_d is a rate constant related to the diffusion of A and B, assuming these have the same diffusion coefficient D.

For the fully reversible test system, shown in Equation 1, a cyclic voltammogram shown in Figure 1.5 may be expected. From this cyclic voltammogram it is possible to define a number of thermodynamic parameters, which are linked to the redox probe under interrogation and the reference electrode being used. The midpoint potential (E_{mid}) indicated in Figure 1.5 is defined as the potential halfway between oxidative and reductive peaks (Equation 2).

(1) $$R \rightleftarrows O + e^-$$

The formal potential may now be defined by Equation 3 in terms of E_{mid} (as obtained from the peak potentials in Figure 1.5) by taking into account the diffusion coefficients of both oxidised (D_{ox}) and reduced (D_{Red}) species.

(2) $$E_{mid} = \frac{E_{Red} + E_{Ox}}{2}$$

(3) $$E_{mid} = E^{\ominus\prime} + \frac{RT}{nF} \ln \frac{D_{ox}}{D_{Red}}$$

The thermodynamic region appearing before the peak is defined by the Nernst equation (Equations 4 and 5). The Nernst equation in Equation 4 is defined in terms of the standard potential ($E^{\ominus}$) and is thus dependent on the relative activities of O (a_O) and R (a_R). However, since these parameters are

seldom known it is more convenient to work in terms of concentrations and thus, the formal potential ($E^{\ominus'}$). The difference between the standard and formal potentials is subtle but important. The formal potential is the measured potential of a redox couple against the normal hydrogen electrode, incorporating activity coefficients and all background reagents in the measured medium. Thus $E^{\ominus}$ and $E^{\ominus'}$ are related by the relative reactivity coefficients (γ) [$E^{\ominus'} = E^{\ominus} + (RT/nF)\ln(\gamma_O/\gamma_R)$]. The consequence is that the medium can affect the formal potential, but it is assumed that the effect is negligible under standard conditions.

(4) $$E = E^{\ominus} + \frac{RT}{nF} \ln \frac{a_O}{a_R}$$

(5) $$E = E^{\ominus\prime} + \frac{RT}{nF} \ln \frac{[O]}{[R]}$$

Equations 4 and 5 show the Nernst equation in terms of chemical activities and concentrations. Here E is the equilibrium potential, $E^{\ominus}$ is the standard potential, $E^{\ominus'}$ is the formal potential, R is the gas constant, T is the absolute temperature, n is the number of transferring electrons, F is the faraday constant, a_O is the activity of O, a_R is the activity of R, [O] is the equilibrium concentration of oxidised species and [R] is the equilibrium concentration of the reduced species.

In the thermodynamic (Nernst) region the fully reversible system remains under sustained equilibrium and the applied potential causes a shift of this equilibrium. On an oxidative scan the equilibrium of oxidised and reduced species is gradually shifted in favour of the oxidised species by an increase in positive potential, consistent with the Nernst Equation (4/5), assuming a rapid equilibrium between reduced and oxidised species (Figure 1.5).

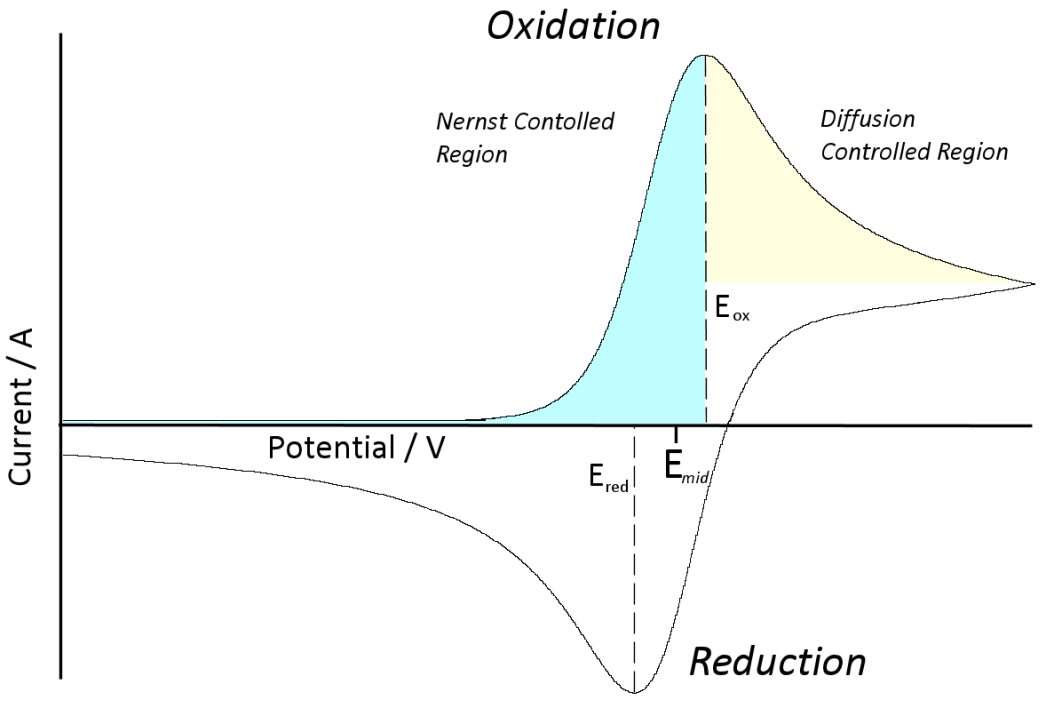

Figure 1.5 A cyclic voltammogram showing a reversible process with faradaic currents giving peaks. The midpoint potential, E_{mid}, is halfway between the two peak potentials E_{red} and E_{ox}. The Nernst controlled region is labelled in blue and the diffusion controlled region (governed by Fick's laws of diffusion) is labelled in yellow.

As redox active material is consumed at the electrode surface the concentration imbalance causes the diffusion of fresh material from the bulk as predicted by Fick's laws of diffusion. The distance over which the solution is affected by this diffusion is termed the diffusion layer thickness (δ) with a larger diffusion layer thickness leading to a shallower concentration gradient and a slower diffusion. As the redox process continues the diffusion layer grows and diffusion slows down. However, before the peak the current is subject only to the Nernst equation because despite the changing diffusion layer thickness plentiful redox material is present near to the electrode surface to satisfy the Nernst equation. Once the concentration of redox material at the electrode surface reaches zero this diffusion process becomes the limiting step of the reaction and the decaying current reflects the growing diffusion layer thickness and slowing diffusion. After the peak material must diffuse from the bulk before electrolysis is possible and so as the reaction continues and the diffusion layer thickness grows material must

diffuse from further and further away leading to a slowing of the diffusion speed and a decrease in the measured current (Figure 1.6A).

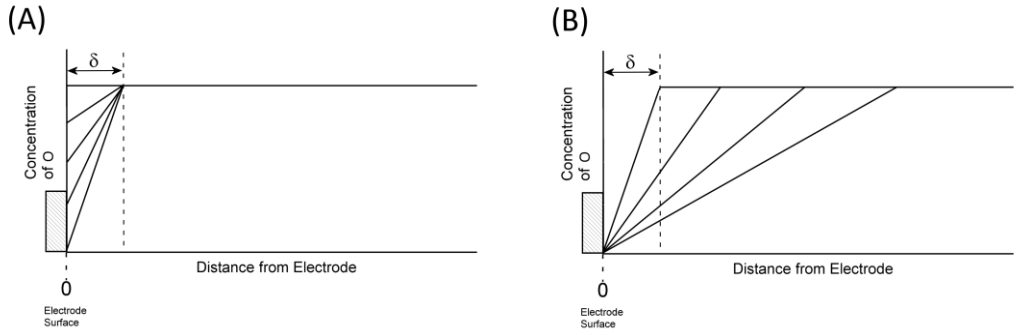

Figure 1.6 Concentration profiles of a redox active material showing the changes in concentration of O during a cyclic voltammogram **(A)** before the peak (Nernst control). The diffusion layer thickness is shown not to change over time in this case for ease (similar to a very fast scan rate) but actually will increase at all times when a concentration gradient is present. **(B)** After the peak (diffusion controlled by Fick's laws).

(6)

$$\frac{\partial[\mathrm{B}]}{\partial t} = D\,\frac{\partial^2[\mathrm{B}]}{\partial x^2}$$

Equation 6 shows Fick's second law, where [B] is the diffusing species with diffusion coefficient *D* which diffuses a distance *x* in a time *t*.

The idea of this thermodynamic overpotential can be thought of in terms of the Fermi level of the electrode, in comparison to the HOMO/LUMO of a redox active species. The Fermi level of the electrode can be modified by applying a potential such that if it is raised above the level of a redox species LUMO, then it is made thermodynamically favourable for electron transfer to occur from the electrode to the LUMO.

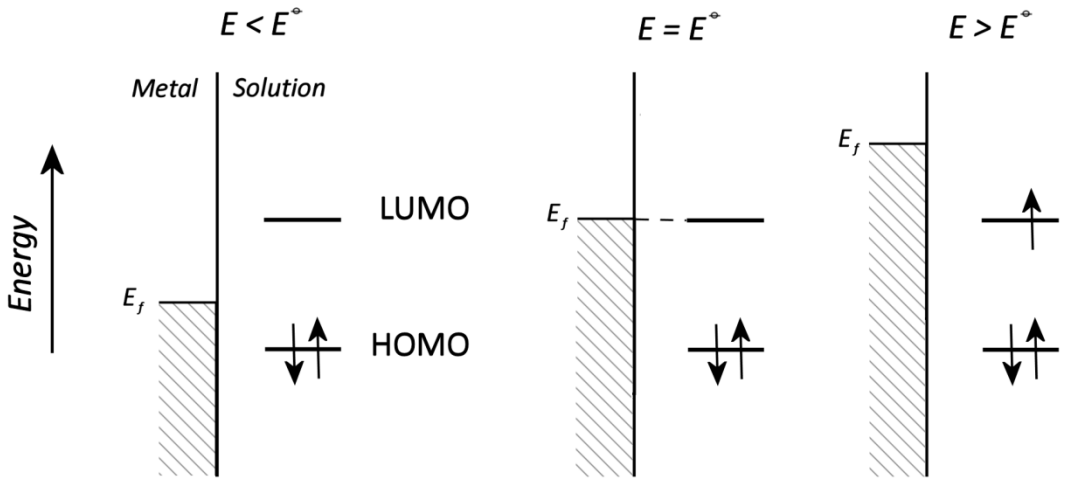

Figure 1.7 A Fermi level diagram showing that as the potential is changed the Fermi level of a metal can be changed such that electron transfer to LUMO (or from a HOMO) is promoted.

In this way it can be seen that at the standard potential the Fermi level and LUMO are of the same height and at strong overpotential the electron transfer process is strongly driven thermodynamically (Figure 1.7).

Most signals appear as a mixture of capacitive and Faradaic responses, with the capacitance being considered a background process and Faradaic current arises from the redox probe to be studied. Since the capacitance is dependant only on the electrode surface and the existence of conducting ions in solution, it is generally constant for a given electrode system and can easily be overcome by using a strong Faradaic signal from a suitably highly concentrated redox probe. Alternatively a Faradaic signal can be enhanced, compared to a capacitive background, by reducing the scan rate. Since, the capacitance is directly proportional to the scan rate but the Faradaic peak current is only proportional to the square root of the scan rate, (from the Randles-Sevcik, equation 7) the effect of lowering scan rate reduces the capacitance compared to the faradaic contribution and can lead to better peak resolution.

(7) $$I_p = 0.4463.nFAc.(nFvD/RT)^{1/2}$$

Equation 7 is the Randles-Sevcik equation where n, F, R, T and D have their previously stated definitions, I_p is the peak current, A is the electrode area, c is the bulk concentration and v is the scan rate, where all units are standard.

Microelectrodes may also be used for the resolution of low concentration redox probes as described in the next section. It is this faradaic signal which gives information about the redox probe. From the diffusion controlled region it is possible to extract the diffusion coefficient (D). The peak to peak separation also gives some important information. Assuming fast electron transfer, the peak separation is controlled only by the diffusion of species away from the surface of the electrode, after the redox step and before the back scan. Thus a perfect diffusion controlled process has a characteristic peak separation of *ca.* 57 mV for a one electron process at 25 ^{o}C, and can be reliably predicted using the equation $\Delta E = 2.218.RT/nF$. If the peaks are any closer than this, it is a sign that the species have some affinity for the surface in terms of electrostatic attraction or full surface immobilisation. If the species is in fact entirely attached to the surface then the peaks appear completely mirrored in a characteristic 'bell' shaped voltammogram, where the reversible potential appears at the same potential as the peak potential. In this case, there is no longer any diffusion controlled zone and the peak is a reflection of the surface coverage of redox material, where all surface attached species become completely converted.

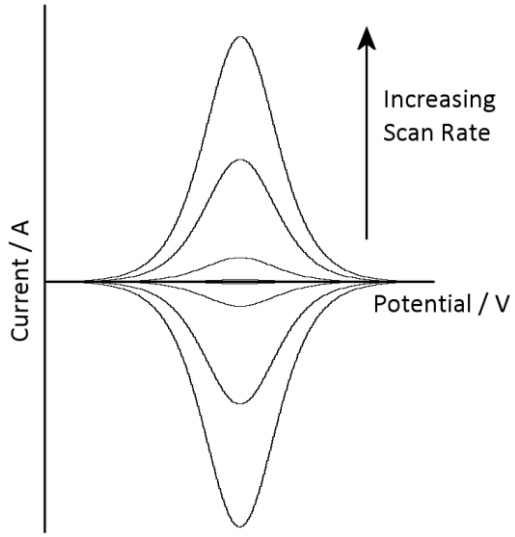

Figure 1.8 A voltammogram of a surface immobilised species showing a symmetrical 'bell' shaped curve with the oxidation and reduction peaks appearing directly on top of one another at the reversible potential.

If the peaks appear further apart and have a more drawn out shape, this usually indicates a slow electron transfer process and a so called 'quasi-reversible' voltammogram. A larger overpotential must then be applied before a response can be seen, due to a kinetic barrier to electron transfer. This discrepancy has been addressed by Marcus in several publications[2] as an extension of the classical Butler-Volmer model of kinetics,[1] in an attempt to explain the slow electron transfer characteristics of certain redox probes. It has been suggested in Marcus theory that since electron transfer is so rapid when compared to molecular motion, it must obey the Frank Condon principle. As such, the electron transfer can only happen once a reactant has rearranged sufficiently, to form a transition state which is more similar to the product. In this way the degree of rearrangement necessary is directly related to the activation energy of the electron transfer, and thus the electron transfer kinetics.

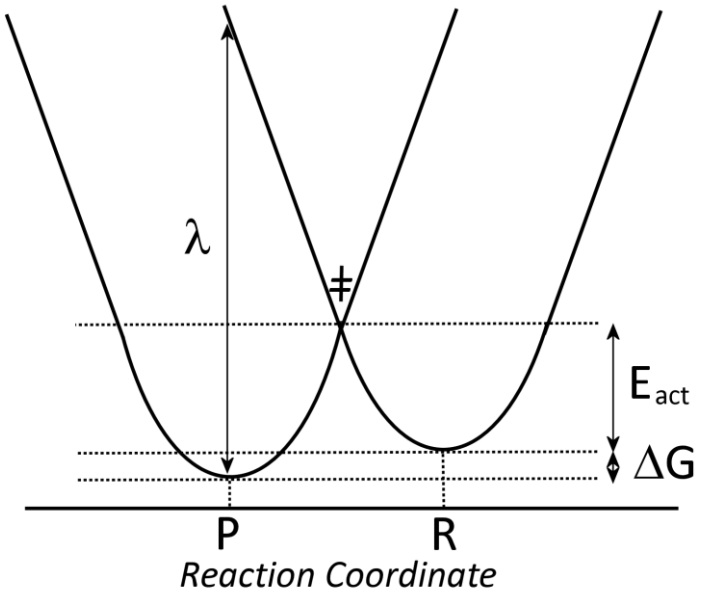

Figure 1.9 A diagram to illustrate Marcus Theory in which a spatial rearrangement of bonds is required to allow an electron transfer to occur. The quadratic rearrangement profiles of products and reactants cross to form a transition state where ΔG is the thermodynamic driving force, E_{act} is the activation energy and λ is the rearrangement energy.

From Figure 1.9, the activation barrier is clearly related to the crossing point of the rearrangement profiles. The activation barrier may be reduced in a number of ways as predicted by Marcus theory. The more similar the

reactants and products, the closer the quadratic curves are aligned on the reaction coordinate and the smaller the activation barrier. The thermodynamic driving force is also shown by the decrease in free energy for the transition, and it can be seen that increasing the vertical spacing of the curves, by creating a larger driving energy, will decrease the activation barrier. Both of these predictions of Marcus theory can be verified experimentally. The consequence for voltammetry is that a small rearrangement leads to a very fast electron transfer, whereas a large change in bond angle or length leads to slow electron transfer and quasi-reversible voltammetry. Examples are shown in Figure 1.10. In the first example, anthracene can be oxidised by one electron with almost no change to its structure and consequently has a very fast electron transfer rate constant. However the ferrous/ferric one electron oxidation involves a significant change in ligand to metal bond lengths to allow electron transfer, which is reflected by a high activation barrier and slow rate constant.

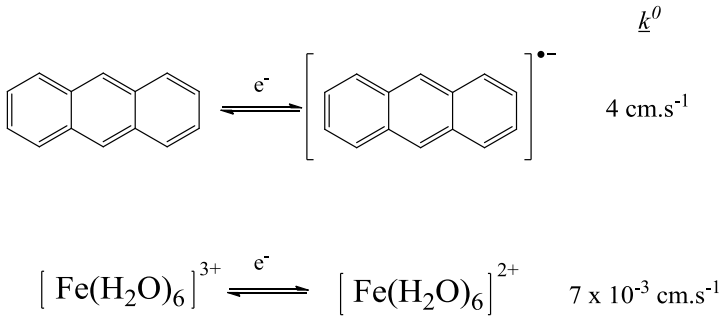

Figure 1.10 Anthracene an example of a fast electron transfer redox species and the ferrous/ferric redox couple an example of a slow electron transfer (adapted from Understanding Voltammetry 2nd ed, Compton, 2010).[3]

1.1.3 Mass Transport

So far the effects of diffusion have been discussed, but it is also known that migration (the movement of charged species with an electric field) and convection (the forced movement of species by agitation or thermal mixing) may affect the movement of redox species. It is for this reason that a large excess (*ca.* 100 fold) of conducting electrolyte is applied to all liquid phase voltammetric measurements. This excess of charged species act to screen the electronic field, and thus limit the effects involving migration of charged

redox species while remaining inert to electron transfer. Convection is harder to stop, but can be limited by using cryostatically controlled redox vessels to limit temperature gradients and by not agitating solutions during electrochemical interrogation.

If convection is studied with sufficient agitation, it is possible to speed up the transport of material to an electrode surface with a constant rate faster than diffusion would allow thus resulting in a voltammogram with no visible peak assuming a slow enough scan rate. Instead, a limiting current is seen, where current is directly related to the rate of mass transport. Once the redox active material at the surface is consumed then it is the mass transport rate which defines the current and, for a rotating disc arrangement, this effect can be predicted by the Levich Equation (Equation 8).

(8) $$I_L = 0.62nFA[B]_{bulk} D_B^{2/3} \nu^{-1/6} \omega^{1/2}$$

This is the Levich equation, where I_L is the limiting current A is the electrode area, D_B is the diffusion coefficient, v is the kinematic viscosity, n is the number of electrons transferred and ω is the rotation speed in rad.s^{-1}.

The Levich Equation for the rotating disc electrode in Equation 8, uses the rotation speed, ω, as a measure of mass transport. Other formulae can be used to predict the limiting currents for a simple flow channel electrode system, or a dual flow biphasic system.[4]

In general, the limiting current, $I_{L,}$ can be approximated for any mass transport limited system by the expression $I_L=nFDAc/\delta$. Where δ is the diffusion layer thickness, described previously in Figure 1.6, and is related to the rate of mass transport, k_{mt}, by the approximation $k_{mt}=D/\delta$. Where D is the appropriate diffusion coefficient.[1]

Microelectrodes can be considered a steady state system, despite there being no external mass transport. This is because the dimensions of a microelectrode are similar to the diffusion layer thickness, δ, and thus can no longer be approximated to have a planar diffusion field and must instead be approximated to a radial diffusion model. It is in this case that the mass flux is increased and thus so too is the current density. The signal shows a steady

state limiting current, which is often scan rate independent (Figure 1.11). These electrodes are commonly used for analytical applications.

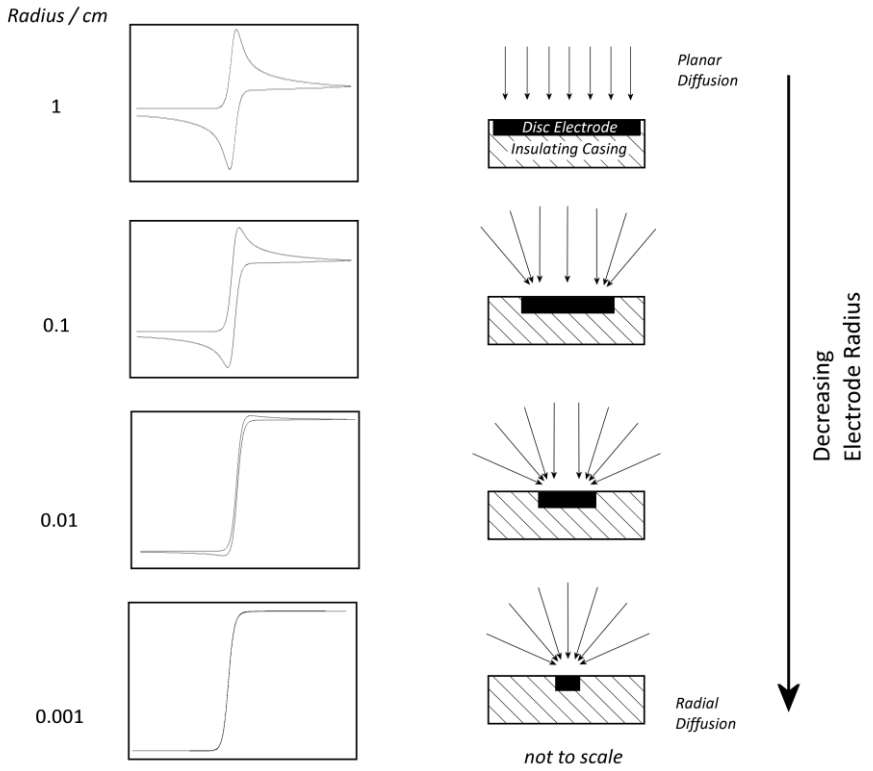

Figure 1.11 A series of diagrams showing simulated voltammograms at a scan rate of 1mVs^{-1} from Digisim for a changing disc electrode diameter where larger electrodes can be assumed to have purely planar diffusion but microelectrodes have purely radial diffusion. The schematic diagram shows the gradual change between these two extremes with anticipated voltammograms.

1.1.4 Electrochemical Reactions

As previously mentioned, cyclic voltammetry can yield a range of mechanistic details of a redox system, by analysing peak separation and shape. However, there are also a whole range of specific mechanisms that can be analysed by varying scan rates and observing the effect on relative peak sizes and positions. For example a voltammogram which appears quasi-reversible, where peak separation is much greater than 57 mV, can often be made reversible by decreasing the scan rate. The electron transfer kinetic and equilibration time for quasi-reversible voltammograms are only considered slow compared to the scan rate, and thus with a slower scan rate these parameters become relatively faster. Eventually, the electron transfer

stops being the rate limiting process at a given scan rate, and a reversible voltammogram is seen, which is again applicable to the Nernst equation. This change is characterised by the peaks shifting towards each other as the scan rate is decreased, until the separation becomes *ca.* 57 mV (Figure 1.12B). Note that scan rate also changes the peak heights so in order to effectively analyse the effect of scan rate on peak separation the peak charges must be normalised.

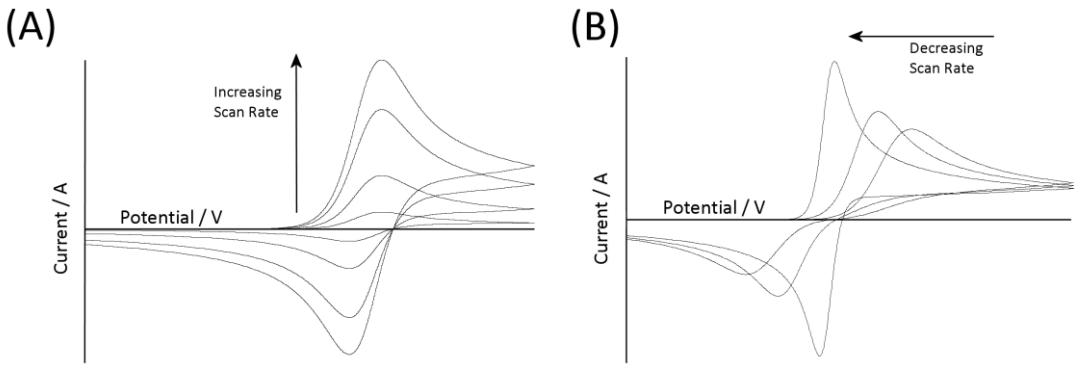

Figure 1.12 (A) Voltammograms showing the effect of increasing scan rate on the peak height, a reversible signal should show a square root relationship. **(B)** Voltammograms showing the effect of decreasing scan rate on the peak shift of a quasi-reversible signal, the peaks become reversible at slow enough scan rate by getting closer together as simulated by Digisim.

The peak size is also seen to change with scan rate. As the scan rate is increased, the peak height also increases with a square root relationship (Figure 1.12A) and this is another sign that the system is diffusion controlled. If the species appear surface attached, (as discussed previously) the peak height becomes directly proportional to the scan rate, and any case which lies between these two extremes shows some surface association is present.

The incorporation of chemical reactions can add another layer of complexity. The simplest is the EC mechanism, (Figure 1.13) where an electrochemical step is followed by a chemical one, which leads to an irreversible voltammogram where the reverse peak appears smaller or nonexistent. If the electrochemical step is sufficiently reversible then in the chemically irreversible case the forward scan would be expected to shift to lower potentials, a phenomenon not shown in Figure 1.13 for simplicity. The electrochemically generated material can undergo a reaction and be

consumed chemically before the back scan can occur. The rate of the chemical step is fixed, but the rate of the electrochemical step can be changed with scan rate. Thus, a faster scan rate (or slow reaction k_r) leads to the re-emergence of the peak, since the chemical step can be outrun by the reverse electrochemical step by scanning faster and not giving the chemical reaction enough time to occur.

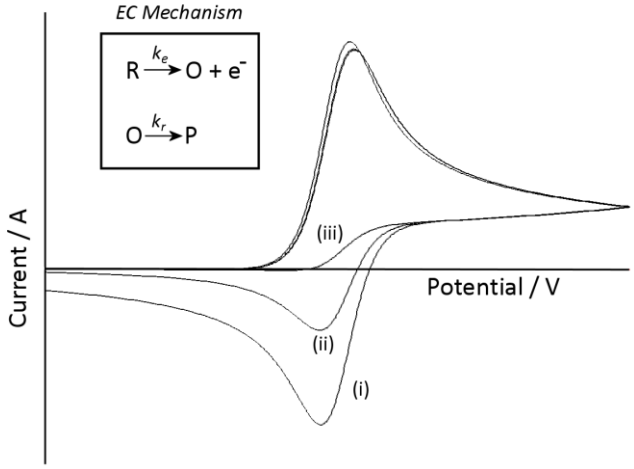

Figure 1.13 Voltammograms showing the effect of k_r on mechanism in an EC mechanism, if k_r is slow compared to the electron transfer back reaction (i) the signal appears reversible but if k_r is fast compared to the electron transfer back reaction (iii) then the reverse peak disappears.

Another mechanism is the ECE mechanism (Figure 1.14), very similar to the EC mechanism, except that the chemically generated product is electrochemically active and thus a second signal is seen. The first being irreversible and the second being reversible or quasi reversible, if the reaction constant, k_r, is fast enough to compete with the reverse electron transfer in process (A). If this is the case then a second reversible signal is seen (B). If k_r is not sufficiently fast, then a simple reversible process (A) is seen with no (B) visible, since product X is not significantly produced.

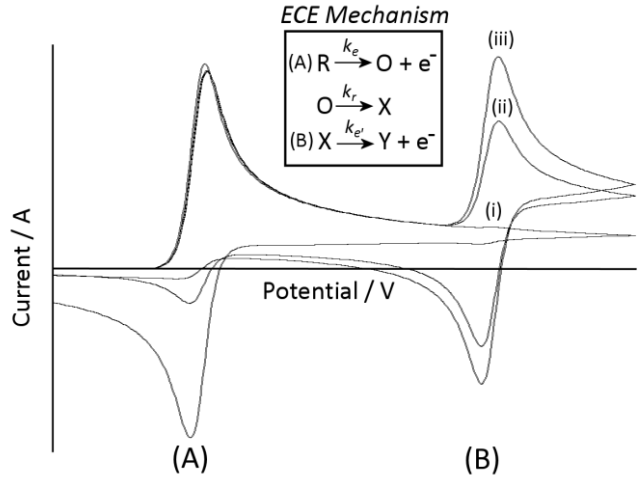

Figure 1.14 Voltammograms showing the effect of scan rate on the ECE mechanism, at fast k_r (iii) the back peak of the first redox couple is not seen and a signal for the second redox reaction is larger. At slower k_r (i) the back peak is much larger and the second redox peak disappears.

The last example is that of a catalytic reaction. The EC' mechanism (Figure 1.15) involves a chemical reaction, which regenerates the initial electrochemically active species. Therefore, if the reaction k_r is sufficiently fast, the peak current increases due to a catalytic step regenerating the redox active material which can be oxidised again. Due to this redox probe recycling effect, the EC' mechanism is characterised by the emergence of a limiting current (iii) at sufficiently slow scan rates.

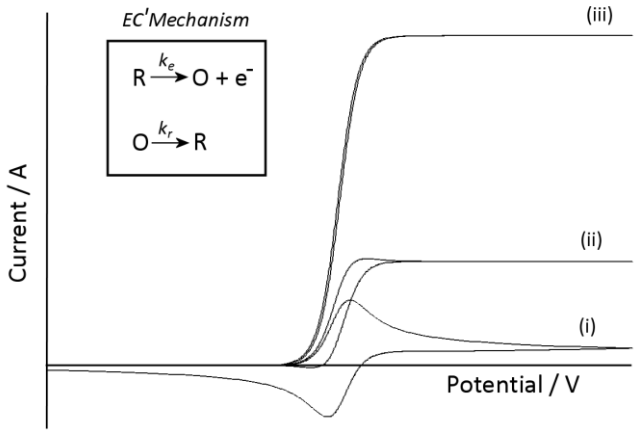

Figure 1.15 Voltammograms showing the EC' mechanism in which the forward peak is greatly enhanced by an increased k_r (iii) and the back peak disappears since the chemical step becomes faster relative to the reverse peak.

1.2 Triple Phase Boundary Electrochemistry

1.2.1 Introduction to the Triple Phase Boundary

Interfacial chemistry is an integral part of electrochemistry, even in common 'single phase' electrochemistry the interface of the working electrode surface and the liquid is under interrogation, by the double layer effect first proposed by Helmholtz (1853).

Of particular interest are the interfaces between immiscible liquids and the mobilisation of ions between the liquid phases, to mimic those processes already prevalent in nature. Previously ion transfer across a liquid | liquid boundary was conducted using a 'four electrode' system, (Figure 1.16A) where each liquid phase contained electrolyte and had a separate reference electrode to effectively polarise the interface leading to ion transport across the phases.[5] Alternatively, thin films (Figure 1.16B) have been used where the organic film thickness was very small, but coated the entire electrode surface. This allowed three electrode controlled ion transfer when coupled with a redox probe in the organic phase, although electrolyte must be present in both phases in large excess. The thin film system was originally developed by Shi and Anson[6] who found that by using a graphite electrode coated in a thin nitrobenzene film, containing various redox probes, voltammetry could be performed at the liquid | liquid interface with a three electrode system. This study used redox reactions in one or both phases to measure the rates of electron and ion transfer at the organic | aqueous boundary. The thin film system has been further studied by Quentel *et al.* who analysed the kinetics and thermodynamics of ion and electron transfer at the thin film modified electrode using decamethylferrocene or lutetium bis(tetra-*tert*-butylphthalocyaninato) redox probes in nitrobenzene,[7] *n*-octanol,[8] 2-nitrophenyloctyl ether[9] and compared the results with mathematical models.[10] This study was extended by using square wave voltammetry and impedance spectroscopy.[11]

The liquid | liquid | solid triple phase boundary is formed at the contact line where aqueous, organic and solid (electrode) phases meet and allow

electron transfer processes to occur. For this technique it is only necessary for one liquid phase to contain electrolyte (Figure 1.16C).

The advantages of a triple phase boundary method are not only that three electrodes are required and the volume of organic solvents is comparatively small, but also that the current response is not limited by the electrode size and electrolyte is not required in the organic phase. This means that under the correct conditions the triple phase boundary may be approximated to a molecular width band electrode or microband electrode for greater analytical precision.[12]

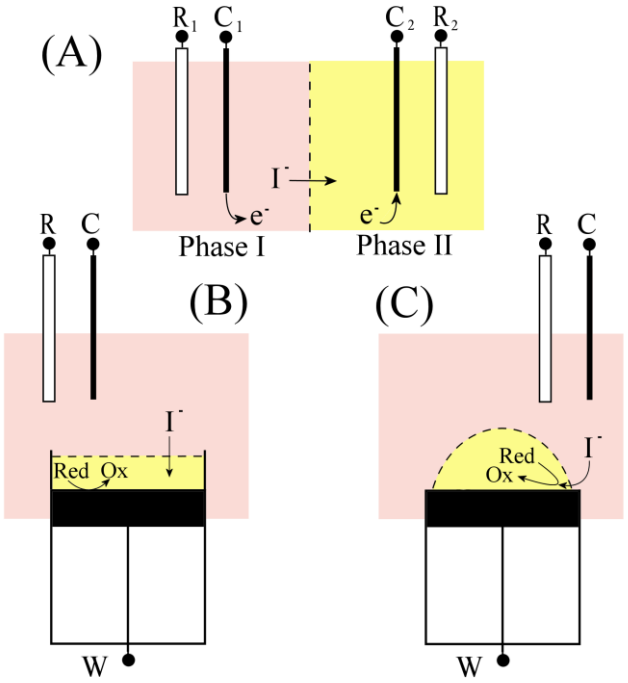

Figure 1.16 Schematics of three ion transfer systems with two immiscible liquids **(A)** A four electrode system polarising the interface of two supported liquids stimulating ion migration **(B)** A thin film system with two supported liquids using a redox probe to stimulate ion migration **(C)** A triple phase boundary with unsupported yellow phase and redox probe *vide infra.*

The concept of a triple phase boundary was first investigated by Marken *et al.* in 1997.[13] It was shown that an array of water immiscible micro-droplets of N,N,N',N'-tetrahexylphenylene diamine (THPD) could be dispersed onto a basal plane pyrolytic graphite (BPPG) electrode from a solution of acetonitrile. When the modified electrode was immersed in an aqueous solution containing electrolyte, a redox process could be seen to occur at the

boundary of the three phases (aqueous | THPD | BPPG surface). Thus, even without electrolyte present in the THPD (oil) phase, the voltammetry of THPD was studied. Marken suggested that the mechanism involved the creation of a new phase adjacent to the oil (Figure 1.17A) and this was supported by visual microscopy of the highly coloured product, showing a ring of oil beads around the original oil droplets.

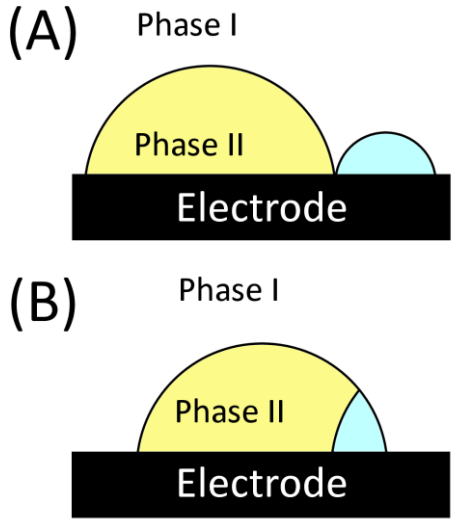

Figure 1.17 (A) without carrier phase a separate phase formed outside of the redox droplet (Marken). **(B)** with carrier solvent the new redox material is incorporated into the same droplet (Scholz).

Later this investigation was extended to include systems where almost any redox probe could be incorporated into water immiscible oil and deposited as a triple phase interface redox system, by Scholz *et al.*[14] The mechanism differed slightly from that used by Marken *et al.*[13] and can be seen in Figure 1.17B. This shows that in a system with no electrolyte in the organic phase the reaction can only proceed at the triple phase interface, where all the phases meet. This is because the simultaneous oxidation of *n*-butylferrocene (*n*-BuFc), shown in Equation 1, was accompanied by the transfer of an electrolyte anion (ClO_4^-) from the aqueous phase into the organic phase (Figure 1.18). The driving force of this migration was that the oxidation of the *n*-BuFc generated a positive charge at the interface of the liquids, which must be balanced. This meant that a negative charge must be brought into the organic phase or a positive charge must leave it.

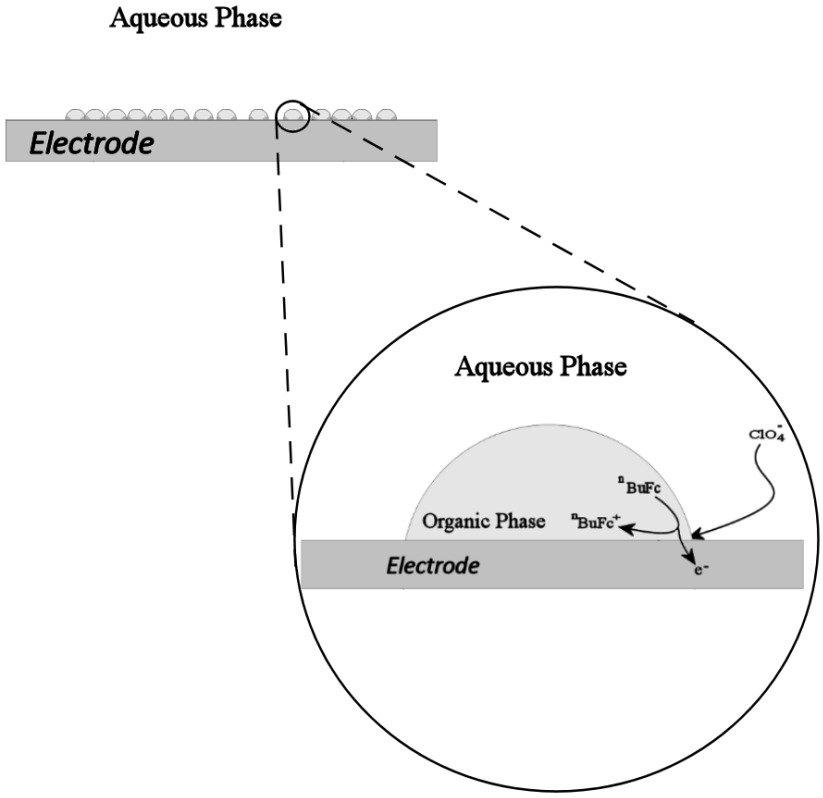

Figure 1.18 A diagrammatic representation of the triple phase boundary showing the proposed mechanism of the oxidation of *n*-butylferrocene with a perchlorate insertion as a test system. The micro droplet array is pictured first with a zoomed in image of just one micro droplet.

(1)

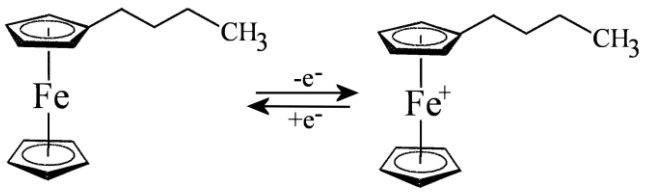

1.2.2 Triple Phase Boundary Mechanism: Thermodynamics

Since the redox reaction stimulates the ion transfer step, it might be sensible to assume a two step process in which an electron transfer step is followed by an ion transfer step. However, it has been found experimentally that for scan rates less than 40 Vs^{-1}, the process appeared concerted over the experimental timescale.[15] This mechanism is however only active when an ionic insertion mechanism is considered. In the case that the organic phase

is also electrolyte supported, an expulsion mechanism of a supporting ion is also possible and in this case the whole electrode contact area (electrode | organic interface) is redox active giving rise to much higher currents but is not a true triple phase boundary reaction.

This ion transfer is not necessarily a by-product of a redox process and can undergo a reaction within the droplet after transfer. It is theoretically appropriate to assume that this triple phase boundary is in fact a molecular width line boundary. However, the real boundary is better represented as a mixed phase of organic and aqueous phases with a real size dependant on the partitioning of the two phases together. To some degree, even immiscible liquids are found to mix at their boundary and this is what gives the triple phase boundary real dimension. The liquid | liquid interface has been extensively investigated in simulations by Benjamin.[16] It may be estimated from average density calculations that the organic | water boundary has a mixed phase of *ca.* 10 Å at the interface. Furthermore, Benjamin has predicted the existence of interlocking 'fingers' of one solvent penetrating into the opposing solvent appearing periodically at the microscopic level.

Water immiscible oils that are used to dissolve the redox probe and set up the triple phase boundary, can also be altered with further additives to facilitate the transfer of certain ions. It was found by Katif *et al.*[17] that adding boronic acids to the oil phase, facilitated the transfer of sugar based ions that can bind to the boronic acid. It was also found by Quentel *et al.*[18] that cholesterol modified thin film interfaces could selectively allow anion transfer, while the competing cation transfer was retarded.

There is much evidence supporting the anion insertion mechanism outlined in Figure 1.18 using both oils and ionic liquids.[19] The first finding was that the identity and pH of the supporting electrolyte anion was very important in the process, and as such, a shift in the reversible potential was seen depending on this parameter. Further studies have been conducted using single oil droplets on electrodes in an attempt to understand diffusion conditions within the droplet, with and without electrolyte in the oil phase.

The relationship between the reversible ion transfer potential and Gibbs' energy of ion transfer showed that, it was the hydrophobicity of the anions that affected the ion transfer mechanism.[14] It was found that hydrophobic ions such as hexafluorophosphate (PF_6^-) were easier to transfer to the oil phase, shown by their less positive transfer potential. However halides and other more hydrophilic ions have more of a tendency to remain in the water phase and require a much higher driving potential to move.[14]

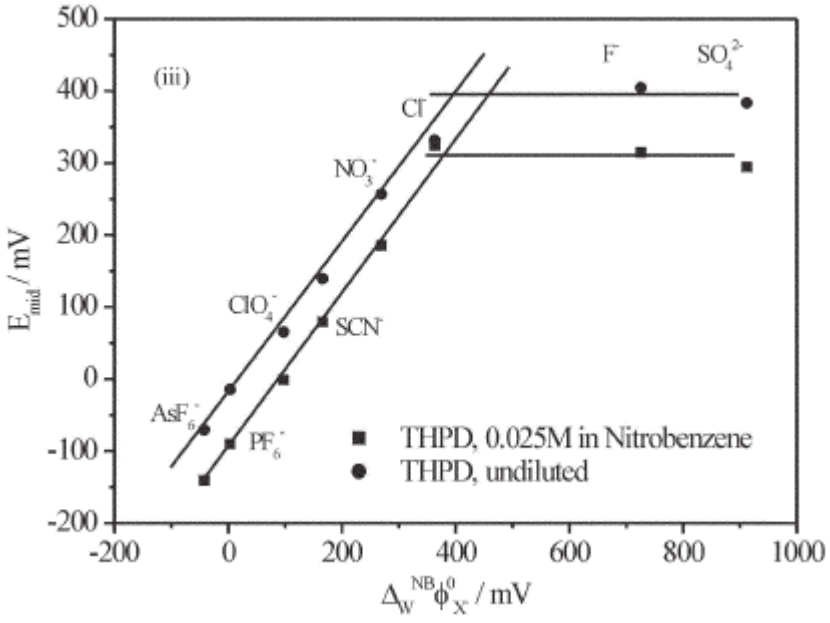

Figure 1.19 A plot of the reversible redox potential for *para-N,N,N',N'*-tetrahexylphenylenediamine (THPD) against the standard Gibbs' energy of ion transfer for each given anion from water into nitrobenzene[19a].

The data in Figure 1.19 above, shows that there is a linear relationship between the standard Gibbs' energy of ion transfer and the potential seen for the *para-N,N,N',N'*-tetrahexylphenylenediamine (THPD) redox couple. In this case, the standard Gibbs' energy of transfer was being taken as a measure of hydrophobicity and thus, it was deduced that a linear relationship between the hydrophobicity and the ion transfer exists.[19a] This relationship, however, leveled off for ions with a much higher Gibbs' energy of transfer, since the transfer was now too energetically unfavourable. In order to balance the charge due to the THPD oxidation, the $THPD^+$ was forced to leave the oil phase because this was energetically preferable, compared to the entry of more hydrophilic ions. Of course, this mechanistic change meant that the

reversible redox potential was now unaffected by the anion since it was no longer involved in the mechanism and the graph levelled off to reflect this.[19a] Successive scans for the hydrophilic ion case showed a reduction in concentration of THPD.

This effect can be altered by using different redox probes. Lutetium bisphthalocyanines allowed the transfer of much more hydrophilic anions, as the cation formed in this case was highly hydrophobic, disfavouring its transfer into water.[20] Similar results show, that decamethylferrocene had a lower plateau point within a nitrobenzene oil droplet on a basal plane pyrolytic graphite working electrode. This was because the ferrocenium ion was more hydrophilic than $THPD^+$ and was able to transfer more easily into an aqueous phase.[21] Finally, the effect of the electrode material could be significant, and studies have been conducted on boron doped diamond,[22] graphite[23] and glassy carbon,[12] with successful electron transfer at the triple phase boundary.

An important aspect of triple phase boundary reactions, is the method by which the reaction proceeds over time. This area has been extensively investigated by Donten *et al.* using platinum probe microelectrodes,[24] pierced droplet experiments[25] and deposition methods.[26] Some key findings will be discussed within this review.

In the data shown in Figure 1.20, ferrocenium ions (Fc^+) were generated at the triple phase boundary using a glassy carbon working electrode, onto which the droplets of nitrobenzene were deposited. A platinum microelectrode was used to detect the presence of Fc^+ at various positions, pictured in Figure 1.20, by applying a constant reduction potential. It was found that at position 2, at the top of the droplet, almost no Fc^+ was detected, even after a long time period. In contrast at position 3, it was found that Fc^+ is almost immediately detected, and at position 1 there was a slight delay before detection. This further supports that ferrocene was oxidised at the triple phase boundary, position 3, where detection was instantaneous. The reaction propagated into the droplet and was detected with a delay at all other positions.

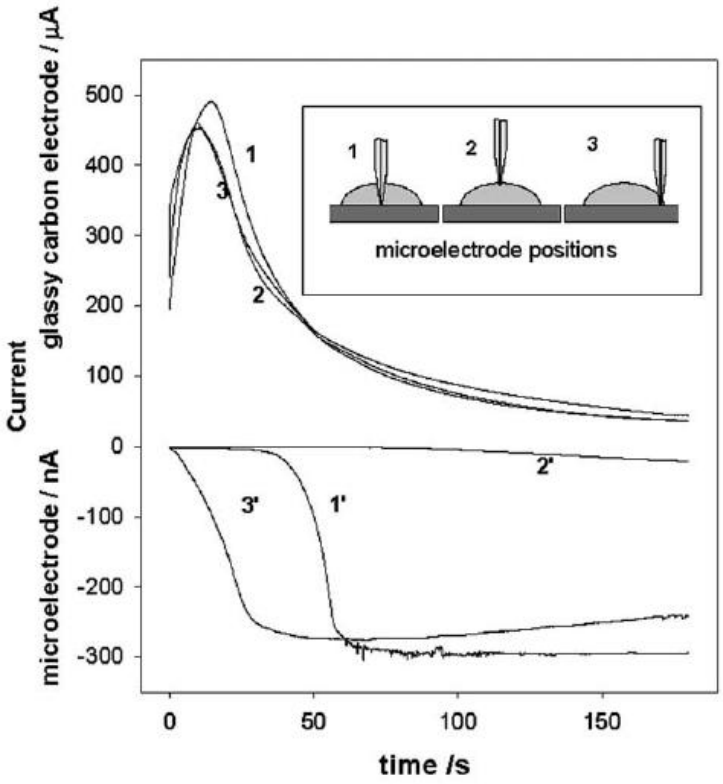

Figure 1.20 Results using a ferrocene oxidation to generate ferrocenium ions at the triple phase boundary with a platinum microelectrode detector system at various points in the droplet to monitor the reaction.[23]

Recent work into the mechanism of triple phase boundary chemistry, has focused on the propagation of the reaction into the organic phase, and how the triple phase boundary changed over time. Even though at the start of any reaction there was no electrolyte within the organic phase, assuming insignificant partitioning of electrolytes prior to electrolysis. It must be considered that, as the reaction proceeds, the creation of cationic products and accompanying inclusion of anions, must lead to an increase in the conductivity of the organic phase.

Furthermore, it was suggested by Tasakorn *et al.*[27] that a true triple phase boundary reaction is thus very unlikely, since the reaction area was changed drastically with the extra conductivity afforded by the entering ions. As such, the only true triple phase boundary reaction is one where ions instead are ejected from the oil phase to balance the generated charge. In this case, it truly was only at the triple phase boundary that this reaction could occur, as no extra conductivity is created. Although true, this statement does not take

into account the use of an organic redox probe, where the movement of protons are now used to balance any generated charge. In this case no extra conductivity can be afforded, as the protons moving into an oil droplet during a reductive electrolysis, may become involved in a chemical step and thus are no longer just a by-product of an electrochemical step.

The ion transfer and propagation mechanisms were investigated by Bak *et al.*[28] using a micro wire electrode system. Bak used two immiscible liquids in a container separated with the denser towards the bottom. By placing a wire into the container that broke the plain of the liquids, a triple phase 'ring' boundary was formed, the size of which was varied by the diameter of the wire used (Figure 1.21A). As well as giving further credence to ion transfer chemistry occurring at the triple phase boundary, this work has also explored the temperature dependence of the ion transfer.[29] By using a reaction that yielded an insoluble and highly coloured polymer, visualisation of the triple phase mechanism was achieved.[26] A time dependent study was undertaken using visual means, to see where triple phase reactions occurred and how the boundary migrated over time.

Further insight into the propagation mechanism in the triple phase boundary reaction by Donten and Bak *et al.*[25] was carried out using a 'hanging droplet' (Figure 1.21B). In this experiment an organic droplet was formed in an aqueous bulk phase, and then pierced by a platinum micro-wire electrode. The system was analysed by different puncturing depths, and also by completely skewering the droplet to form two triple phase boundaries. By looking at the time dependent current change of a redox process, the diffusion layer propagation into the droplet was analysed, since a current drop was observed when the diffusion layers from opposite ends of the droplet merged.[25] Using two wires separated by a given distance piercing the droplet adjacent to each other, the perpendicular diffusion zone was also be estimated.[25]

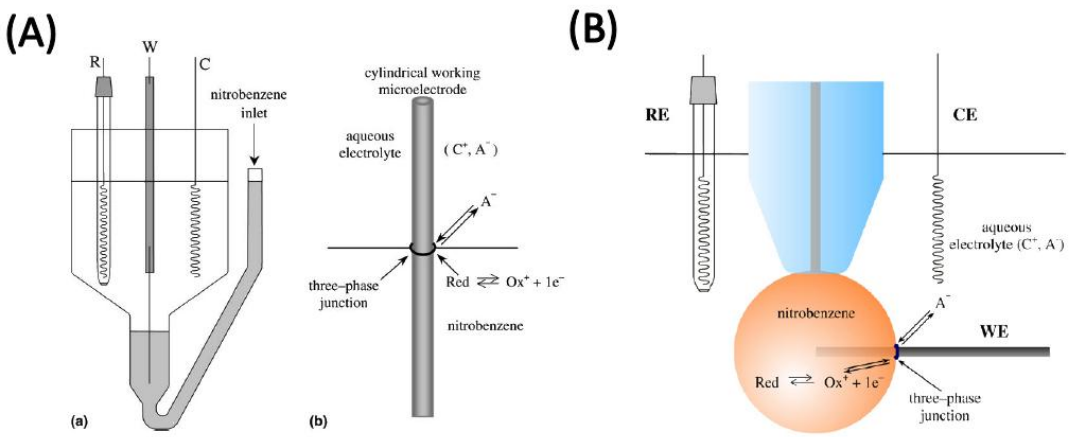

Figure 1.21 A diagrammatic summary of work carried out by Donten and Bak et al. **(A)** shows the 'ring boundary' model with two liquid phases in a container.[24,28b] **(B)** This shows the hanging droplet model with working electrode piercing the droplet to form the triple phase boundary.[25]

It was possible to analyse the triple phase boundary mechanism using other techniques, both visual and electrochemical. Shul *et al.*[30] have used a scanning electrochemical microscopy (SECM) method, with a decamethylferrocene (DMFc) oxidation at a 2-nitrophenyloctyl ether (NPOE) water interface, in the presence of a hydrophilic ion such as chloride. It was found that this system favoured the ejection of $DMFc^+$ ions into the aqueous phase, as detected by the SECM tip. However, in the presence of a more hydrophobic ion such as perchlorate, much less $DMFc^+$ ejection was observed. This finding again supported the conclusion that perchlorate, is instead moved into the organic phase to balance the charge of the newly formed cation. Takakorn *et al.*[27] arrived at the same conclusion by using the analysis of a single droplet and suggested the presence of a pure aqueous redox process for removed $DMFc^+$, as well as the triple phase redox process.

Spectroscopic measurements *in situ* have been attempted for triple phase boundary processes. In the original publication by Marken *et al.*[13] *in situ* ESR spectroscopy, showed the reversible creation and destruction of a radical species within a micro-droplet array, during electrolysis.

In a later publication by Komorsky-Lovric *et al.*[15] visible light spectrometry on a transparent ITO electrode was used to detect the presence of $DMFc^+$ at

several positions, within and outside of a nitrobenzene droplet in aqueous solution. This confirmed that with hydrophobic aqueous anions $DMFc^+$ ions were detected within the droplet, first near to the triple phase boundary and later in the centre of the droplet. For these hydrophobic ions, there was no detection of $DMFc^+$ outside of the droplet and the reaction progression was seen, to migrate into the droplet from the triple phase boundary. With hydrophilic aqueous anions, it was confirmed that $DMFc^+$ was instead ejected from the nitrobenzene phase and was detected in the aqueous phase.[15]

1.2.3 Triple Phase Mechanism: Kinetics

The kinetics of the electron transfer processes have been studied[3b] and lead to the conclusion that in a standard two phase (electrode | solution) system, the electron transfer is highly dependent on the rearrangement parameters of the redox active species itself, as well as the solvation energy, as predicted by Marcus theory.[2,31] In a triple phase system the electron transfer undergoes similar conditions, however, an ion must now also transfer in a concerted fashion to avoid a charge imbalance.

It was shown by Quentel *et al.*[8] that in a thin film system it was the ion transfer itself which is rate limiting, and thus the most important kinetic parameter. This investigation was achieved in a water | *n*-octanol thin film system with an electronically supported organic phase, but is a similar enough case to be extrapolated to explain some features of triple phase boundary processes in microdroplets.[7b] A similar study has yielded similar results for a water | nitrobenzene interface.[7c,10]

For boron doped diamond electrodes slow heterogeneous electron transfer kinetics are often observed due to variations in doping levels between diamond crystals. In a triple phase system a comparison of THPD and tetramethylphenylenediamine (TMPD) microdroplets in a heterogeneous aqueous phase showed, that THPD gave much faster electron transfer at the triple phase boundary than TMPD at the aqueous | electrode interface.[21]

1.2.4 Different Types of Triple Phase Boundaries

Triple phase boundaries can exist in a range of environments, with a varied combination of different phases forming the boundary. For example, the saturated KCl calomel electrode, used extensively as an electrochemical reference electrode, itself possesses a triple phase boundary of Hg (l) | $HgCl_2$ (s)| sat. KCl (aq). It is only at the point where each of these phases meet that electron transfer is possible and this gives the inherent stability of the electrode.[3b]

The use of microdroplets as systems for triple phase boundary analysis has already been discussed as single droplets[26] and droplet arrays.[13] The arrays discussed up until now have been random in nature, both from a position and size perspective. Highly structured arrays have also been developed in an attempt to study the surface effects of electron transfer at the liquid | liquid phase boundary[32] or to demonstrate diffusion properties by perturbing the deposition of copper metal onto gold electrodes.[33]

Permeable membrane electrodes are also being created for applications in sensing, based on the triple phase boundary protocol. Shul *et al.* report a procedure for the creation of a silica based matrix doped with graphite nanoparticles[34] or carbon nanofibres[35] towards ion sensing applications. These electrodes utilised an implanted redox probe, which was suitably lipophyllic to remain immobilised in the organic phase, favouring instead, the movement of ions from aqueous phases for detection. The large electrode volume acted as a reservoir for redox mediated organic phase, giving similar triple phase boundary effects as microdroplets, but with a greatly increased organic phase volume, to ensure incomplete electrolysis. The degree of oxidised ferrocene leaving the organic phase in favour of anion insertion, was estimated using scanning electrochemical microscopy (SECM).[30]

A limitation of the triple phase boundary methodology is, that the process, in general, can only occur where all three phases are in contact. In a hemispherical droplet, this line boundary accounts for only a very tiny fraction of the contact area with the. The current achieved is proportional to the triple phase line boundary length, as well as the diffusion of redox mediator to the

boundary from within the organic phase. The rate of electron transfer is not usually limited by the anion diffusion from the aqueous phase, since the anion concentration is kept sufficiently high to be in large abundance close the triple phase boundary interface. Of course if the path of diffusion of anions is perturbed, for example in a restricted environment, then it can be supposed that this assumption may not be true.

The triple phase boundary process can be greatly enhanced in one of two ways: i) The triple phase boundary interface length is increased, or ii) A mass transport effect is utilised to move redox active material to the triple phase boundary interface faster *vide infra*.

The former seems to have an obvious solution, smaller droplets inherently have a larger triple phase boundary interface compared to their volume and thus, should give better signal resolution. However the lower limit of droplet size, when distributed on an electrode surface, is governed by surface tension and viscosity parameters. These micro-droplets, although useful for sensing applications, are not so useful for electrosynthetic processes.

This problem has been approached by Marken *et al.*[36] using a carbon nanoparticle stabilised interface. The carbon nanoparticles were found to naturally stabilise a liquid | liquid phase boundary. By an electron hopping mechanism, the triple phase boundary was effectively extended around the liquid | liquid interface by the inherent conductivity of the carbon nanoparticles. This electron hopping permitted the use of triple phase boundaries at the carbon nanoparticle | organic | aqueous boundary interface. A second publication explored the use of a boron doped diamond pore array as a support for small volumes of organic liquids.[37] This system utilised the extra stability of the pores as a solid support for microdroplets, as well as incorporating carbon nanofibres into the organic solution to enhance the electrochemical signal in detecting antioxidants.

A more recent study has seen a similar methodology applied to the use of room temperature ionic liquids (RTILs) mixed with graphite nanoparticles.[38] In this case the RTIL acted as both the immiscible carrier phase, as well as providing inherent electrical conductivity within the modified electrode. This

inherent conductivity extended the triple phase area into the RTIL phase making the redox process more efficient and increasing the observed signal.

The triple phase boundary system is not just limited to organic droplets on modified electrodes in an aqueous medium. A 'reverse' triple phase system has also been published by Davies *et al.*[39] in which water droplets contained a redox active species and were immobilised on a graphite electrode in an electrolyte supported 1,2-dichloroethane (DCE) phase. This has lead to further evidence of the triple phase mechanism by using time resolved copper deposition to monitor the reaction progression. The same mechanism as has been reported previously, for immobilised organic droplets, was seen.

Many redox probes have been utilised to study the triple phase mechanism, each with different properties and advantages. Quentel *et al.*[7a,20] often utilise the lutetium *bis*(tetra-*tert*-butylphthalocyaninato) redox probe. The advantage of this is that the Lu^{2+} undergoes a facile one electron oxidation or one electron reduction (Scheme 2). Thus, both oxidation and reduction reactions can easily be studied for triple phase boundary processes. Lu^{n+} ions are also very hydrophobic, meaning it is highly unfavourable for the redox cation to be expelled into the aqueous phase, thus simplifying the mechanism.

(2) $\underset{\text{Lu(I)}}{Lu[(^tBu)_4Pc]_2^-} \overset{-0.08V}{\rightleftharpoons} \underset{\text{Lu(II)}}{\mathbf{Lu[(^tBu)_4Pc]_2}} \overset{+0.3V}{\rightleftharpoons} \underset{\text{Lu(III)}}{Lu[(^tBu)_4Pc]_2^+}$

Another redox triple phase boundary redox reaction used by Adamiak *et al.*[40] was the six consecutive reversible reductions of C^{60}. The advantage of this system was not only the stability gained by the redox probe in the organic phase, but also the ability to study multiple triple phase reductions consecutively.

1.2.5 Dynamic Triple Phase Boundaries

The triple phase boundary reaction is often limited by the diffusion of active species to the triple phase boundary interface. This diffusion is often slow in relation to standard hemispherical or thin film diffusion. Due to the restrictive nature of the contact angle of organic droplets to the electrode surface, the

pathway to the interface is often perturbed. A mass transport system can be used to overcome this problem, by replenishing redox material at the triple phase boundary faster than a diffusion limited system would allow. This assumes however, that the reaction being studied is based on an ionic insertion mechanism and that the aqueous ion species is in large excess compared to the redox probe.

Several methods have been studied in an attempt to enhance the mass transport to the triple phase boundary interface. MacDonald *et al.* have used the lamellar flow of two immiscible liquids (Figure 1.22) as a dynamic triple phase boundary interface at a gold,[4] glassy carbon,[41] and platinum[42] electrode. The mechanism was the same as for a static micro-droplet system, with a redox probe (*n*-BuFc) being oxidised in the organic phase, leading to the insertion of an anion (ClO_4^-) from the aqueous phase to balance the charge (Figure 1.18).

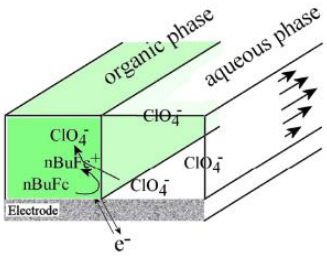

Figure 1.22 A schematic cross section through a lamellar two phase flow cell showing an *n*-BuFc oxidation anion insertion reaction at the triple phase boundary.[43]

A dynamic triple phase boundary could also be found in an emulsion phase, where not only are the droplets being used small enough, so as to have a large triple phase boundary contact zone, but also the turbulent effect of the emulsion stirring, can also cause localised mixing within the droplets themselves. In general, high powered ultrasound can be used to emulsify an organic phase in water. This approach has been utilised in triple phase boundary processes to enhance electrochemical signals for analytical[44] and electrosynthetic[45] purposes. Further illumination of the effects of ultrasound in voltammetry and emulsification can be found later in Chapter 5.

1.2.6 Applications of Triple Phase Boundaries

For analytical applications, the triple phase boundary interface is an ideal system. It utilises a pseudo micro-band electrode array, as well as an unsupported carrier phase. This leads to the remarkable ability of the triple phase boundary, to allow the detection of analytes in extremely non-polar solvents, such as hexane. This could allow the facile detection of a range of trace molecules in traditionally inaccessible media such as crude oil, even potentially leading to the online monitoring of potentially harmful additives.

It has already been discussed, that the triple phase boundary length is critical in the detection of low concentrations of analytes. This can be achieved by using microdroplet arrays and nanoparticle additives, an example was shown by Zhang *et al.*[37] It was the analyte in the organic phase that was being detected as a redox active species, usually shown as a voltammetric response related to the concentration of the analyte. However, the mechanism of the triple phase boundary reaction also allows the use a known redox system to stimulate ions to migrate across the phase boundary, to be detected. This movement can be monitored by analysing the shift in reversible redox signal, of course assuming that the migration energy of the redox probe itself is too large to allow it to transfer phases, in preference to the ion to be detected.

It is this unique ionic migration mechanism that has initially been investigated by Marken *et al.*[13] as a system for ion detection. This study used simple transfer anions (ClO_4^-, PF_6^-, NO_3^- and SCN^-) with a *N*,*N*,*N*',*N*'-Tetrahexyl-phenylenediamine (THPD) redox probe to show the change in midpoint potentials with ion identity,[46] as well as the shift with pH.[47] This very simple initial concept has lead to the detection of much more exotic ions, using more robust electrochemical redox probes. This work has even extended as far as the detection of chiral ions, as demonstrated first by Scholz *et al.* in 2002.[48] This work used a thermodynamic rationale to observe a slight shift in optical isomer transfer, from an achiral solvent into a chiral oil containing the decamethylferrocene redox probe. The oil used was either (D) or (L)–menthol[48b] or (D) or (L)–2-octanol,[48a] with the transfer of either (D) or (L)–tryptophan or (D) or (L)-phenylalanine being studied. Since the solvation

energy change from phase to phase is a large contributing factor to the thermodynamic transfer energy, it was reasonable to assume that the energy of solvation for chiral molecules would be different when in the presence of a chiral oil. This was indeed observed with the (D)–tryptophan transfer into (D)–menthol being favoured over (L)–tryptophan transfer. This energy difference, as previously explained, was shown by a shift in the oxidation of the decamethylferrocene, with a greater driving force being needed to induce the transfer of a mismatched chirality and thus a shift to more positive potentials.

In 2009 Mirčeski *et al.*[49] proposed a kinetic method for the triple phase boundary detection of chiral ions, using a similar electrochemical system to that described by Scholz.[48] Square wave voltammetry was applied and since the system was rate limited by ion transfer a quasi reversible response was given. By varying the frequency of the square wave a quasi reversible maximum, which is directly related to the kinetics of the reaction, could be calculated and from this a kinetic difference in the transfer of D and L ions into a given chirally pure solvent. The chirally paired ions (D_{ion} to $D_{solvent}$ or L_{ion} to $L_{solvent}$) were thermodynamically lower in energy as shown previously, which lead, to the fact that it is also a less 'driven' process and occurred kinetically slower.

Further applications in analytical chemistry of the triple phase boundary system have used a 'generator-collector' system.[50] This type of experiment used two working electrodes separated by a nano-gap (Figure 1.23). The primary working electrode (the 'generator') performed a standard cyclic voltammetry experiment, while the secondary working electrode (the 'collector') provided a constant potential which would oxidise or reduce the generated ions of the primary working electrode as appropriate. As such, the secondary electrode acted as a detector for generated ions at the generator. Provided it is only separated by a nano-gap, this response was independent of the scan rate of the generator and was seen as a steady state signal only controlled by the diffusion of the ion across the gap.

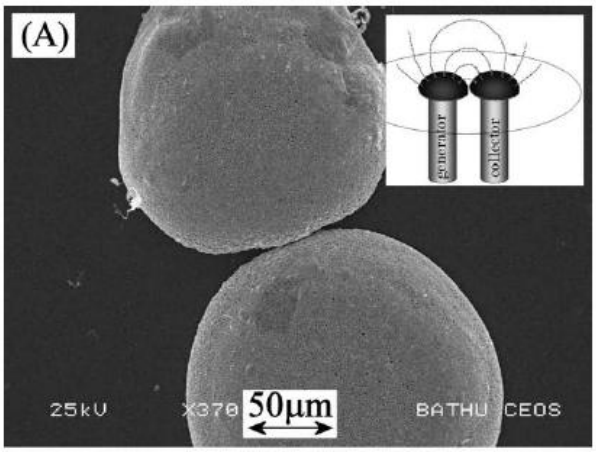

Figure 1.23 An SEM image of the gold micro-junction electrode used by French et al.[50a]

This kind of experiment has been used very effectively to assess low concentrations of redox active materials, by using the collector's steady state response. The sensitivity permitted detections in the nanomolar range, with the sensitivity being limited by the gap size.

This methodology has been successfully applied to triple phase boundary chemistry[51] by placing an oil droplet in the gap, as shown in Figure 1.24. The generator electrode acted to oxidise a Co^{2+} couple causing the incorporation of a transfer anion from the aqueous phase, as seen in other triple phase systems. This anion then diffused across the gap between generator and collector within the oil, where it was ejected in the opposite redox reaction, the reduction of Co^{3+}. The collector signal is a scan rate independent steady state response, which modelled the anion transfer process and was used to elucidate the mechanism of ion diffusion in the organic oil. Vagin, Vuorema *et al.*[52] have also found, that by using band electrodes with a larger electrode face area between generator and collector, signal responses were further improved.

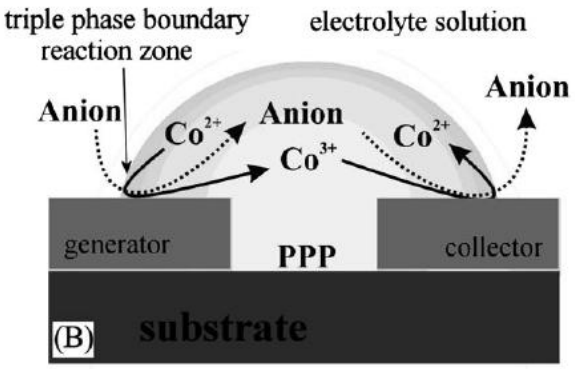

Figure 1.24 A schematic diagram of a generator-collector system at a micro-gap electrode by Vuorema *et al.*[52a]

As a method for synthetic electrochemistry, triple phase electrochemistry is potentially ideal. The benefits of this system, over conventional electrosynthesis, would allow small volumes of organic solvents to be used in a much 'greener' approach than single phase reactions. Only the aqueous phase must contain electrolyte and is held separate from the organic phase which has a two fold benefit: (i) Separation of the reaction material from the far more concentrated salt is easy. (ii) The aqueous phase may be reused since the salt concentration is only slightly depleted by the triple phase boundary reaction and contains no organic materials.

Triple phase boundary processes have already been used in the synthesis of many materials. Bak *et al.* [26] have shown that a polymer can be synthesised at the triple phase boundary interface as a marker for the triple phase reaction zone. Niedziolka *et al.*[53] have further shown that the triple phase boundary interface can also be effectively utilised to synthesise sol-gel materials.

In this thesis triple phase boundary processes of electrodes are studied in particular for the case of electrosynthetic applications. New types of electrodes are introduced to improve efficiency and explore a wider range of potential applications.

In order to provide an overview of the recent developments in electrosynthesis the next section provides an introduction to the key aspects of electrosynthesis.

1.3 Electrosynthetic Reactions

1.3.1 Introduction to Electrosynthesis

Traditional electrosynthesis in stationary reactor systems already offers a clean and experimentally easy method of synthesis, often excluding the need for strong acids and bases.[54] Also, otherwise unstable intermediates,[55] for efficient reaction, can be generated *in situ*. Electrosynthesis exerts a high level of control over traditional syntheses. By using an applied voltage as a driving force for a thermodynamic reaction, a reaction rate can be increased or even stopped completely by removing the potential bias all together. Another significant advantage of electrosynthesis is that the use of electrons as a reagent provided by solid electrodes, means that the synthesis is atom efficient and highly controlled. There are also examples of modified electrodes giving examples of heterogeneous catalysis, a most controversial topic in organic synthesis.[56] By using a selective membrane at the electrode surface, reaction routes can be controlled by permitting only certain redox processes. Alternatively, using catalytic nanoparticles, reaction rates can be improved.[57] Chiral control can also be applied by using a chiral surface,[58] attached chiral catalyst,[59] or chiral electrolyte[60] and this chirality has been used to influence enantiomeric product distribution. Further control has been shown by using an individually addressable microelectrode array with surface attached organic redox probes and has allowed large libraries of compounds to be generated simultaneously.[61]

Of course there are also disadvantages to the electrosynthetic approach. A high electrolyte concentration is required to ensure charge contact between the electrodes. This electrolyte salt must then be separated from the reaction mixture to allow products to be isolated, adding an extra separation step which is often not facile. A limitation of the electrosynthetic approach is that for effective electrosynthesis polar solvents are preferred to aid in dissolution of charge carriers. Therefore water, with its high dielectric constant (80.100,[62]) is an ideal solvent for electrolysis, but many organic functional groups are either not stable or not soluble in water. so a compromise must be reached. Either a solvent mixture must be prepared, or more commonly

acetonitrile is used due to its relatively high dielectric constant (36.64,[62]) but with the advantage over water that organics are much more soluble in it.

1.3.2 Paired Processes

The first challenge with all electrosynthesis is that electrochemical reactions must occur in pairs for electro-neutrality, *i.e.* one species is oxidised as another is reduced. Often only one of these processes is focused on with the other being unimportant, but chosen specifically not to interfere with the desired products. This is achieved by using a divided cell with a fritted counter electrode, allowing electrical contact but not the movement of material between chambers.[63] In 'paired' reactions the difference is that both half reactions contribute to the overall reaction and thus less waste is generated. Much of the early work on paired syntheses was accomplished and summarised in the 1980s by Baizer *et al.*[64] These reactions require a delicate balance of reaction materials and diffusion of intermediates, it is for example important that a generated intermediate does not simply diffuse to the opposing electrode and become deactivated before it can react.

More recently paired electrosynthesis have been extensively reviewed by Paddon *et al.*[65] showing that there are 3 key types of paired process. The easiest example of a paired synthesis is that of a 'parallel' reaction, which involves two unreactive materials separately converted into two different products, this is electrochemically uncomplicated but requires separation. A 'divergent' synthesis is also electrochemically uncomplicated, where one reactant is simultaneously reduced and oxidized into two different products, but must again be separated. A third example is that of 'convergent' synthesis a useful but rare transformation, where oxidation and reduction both yield the same product. This method is highly atom efficient, reduces waste and negates the need for separation techniques. One such example is shown in Figure 1.25, where both the cathodic and anodic processes yield the same glyoxalic acid product.[66]

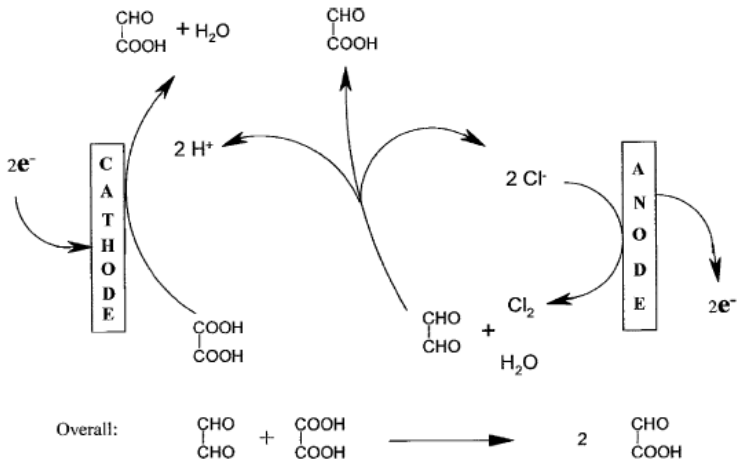

Figure 1.25 An example of a convergent electrosynthesis of glyoxalic acid by Jalbout *et al.*[66]

In most cases, electrosynthesis follows very simple acid / base type reaction steps, where the acid or base is first electrochemically generated (Figure 1.26). This occurs either directly, by one of the reagents, or indirectly using a carrier species to add or remove protons accordingly. There are three different potential pathways for these reactions; direct electrolysis where the reaction takes place at an electrode, indirect electrolysis where a reagent is generated electrochemically before reaction,[67] and mediated electrolysis[68] where an electron transfer reagent is used. The key intermediates in all electrosynthetic reactions are radicals. The radicals created are often affiliated with anions or cations and are highly unstable, which can result in them reacting indiscriminately with other radicals or reactive species almost immediately. As a consequence, they are never produced in significant concentrations and often lead to a mixture of products from multiple reaction pathways. It is the challenge of electrochemistry to control these radicals and there are a range of methods for doing so.

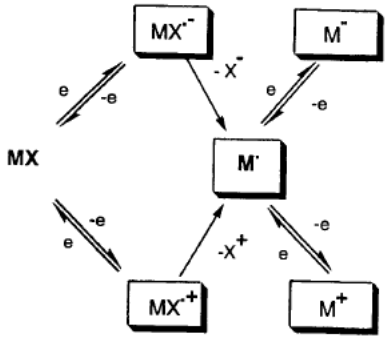

Figure 1.26 Pathways of electrochemistry[55]

In many simple cases where there is only one redox centre this problem is not significant, with only one significant reaction pathway leading to one product, but in more complex molecules where multiple redox centres may be present a different strategy is required.

1.3.3 Electrolyte Free Electrosynthesis

Another challenge facing electrosynthesis is that the incorporation of electrolytes means an extra separation step is necessary after the synthetic step. To this end the method of biphasic electrolysis is discussed, but another area of great interest with a view to synthesis is an approach without the need for intentionally added electrolyte at all. This would require very small inter-electrode separation, where the electrochemically generated materials act as their own electrolyte. This negates the need to add electrolyte and from an economy point of view makes the synthesis far more cost effective for both logistics and materials cost.

Horcajada *et al.*[69] have described an electrolyte free electrolysis process using a flow system though porous electrodes and separated only by a very thin membrane. The charge was carried by charged materials involved in the synthesis. This has yielded a simple methoxylation process in a flow cell without intentionally added electrolyte (Figure 1.27).

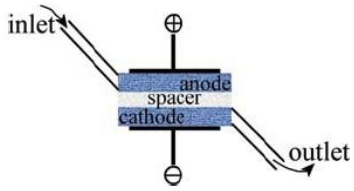

Figure 1.27. A schematic diagram of Yoshida's electrochemical flow cell.[69]

The flow cell design is simple, with the inter-electrode separation being determined by the spacer and easily varied by changing the spacer width. In this case, the generation of protons reduced the resistance in the inter-electrode gap acting as a generated electrolyte, the dimethoxylated product was formed in about 70% yield.

Many microreactor flow cell examples have been reported by He *et al.*[70] using the principle of no intentionally added electrolyte. These have been

used in the cathodic dimerisation of 4-nitrobenzylbromide[70a] and the coupling reaction of benzyl bromides with acetic anhydrides[70d] or activated olefins.[70b,70c] In this micro-gap flow cell electrodes are parallel to the channel and facing each other. Typically the gap is 10 μm up to 500 μm and is comparable to the electrode diffusion layer thickness, meaning no electrolyte should be required as ionic species formed *in situ* are capable of sustaining charge transport.

1.3.4 Electroauxiliaries

One such method that has been used extensively is the incorporation of electroauxiliaries. Electroauxiliaries are functional groups which promote an electron transfer, making transformations occur at lower potentials, in a more selective and predictable manner.[71] A good example of such an electroauxiliary is in the oxidation of ethers and amines where α-silyl groups cause the oxidation to appear at a less positive potential.[72] The silyl group has the effect of raising the HOMO of the molecule (Figure 1.28), thus making the loss of an electron by oxidation easier, and thus selectively cleaving the Si-C to form the cation. This idea of silane based group has been extended to their use as nucleophiles in the form of allylsilane, in which the allyl fragment was used to capture radical intermediates and form C-C bonds.

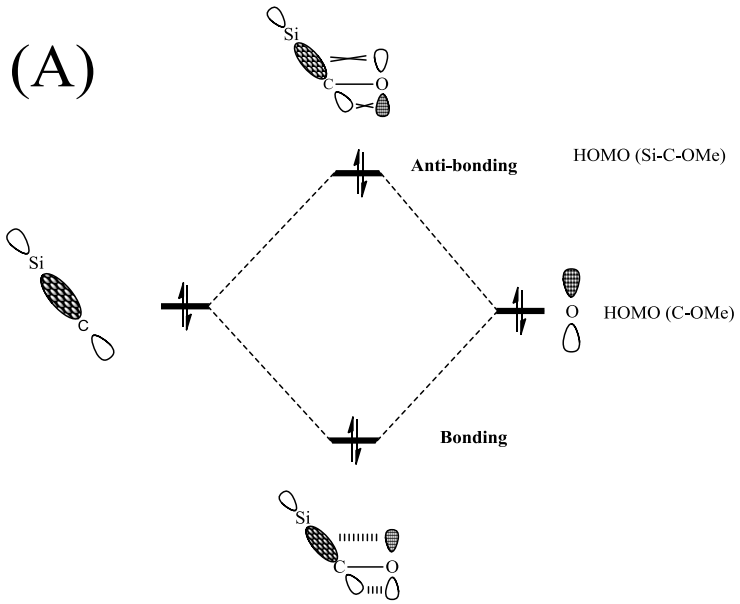

(B)

	E / V
MeO, C_7H_{15}	>2.50
$SiMe_3$, MeO, C_7H_{15}	1.72

Figure 1.28 (A) A molecular orbital diagram to describe the HOMO raising effect of $SiMe_3$ groups. **(B)** An example by Yoshida *et al.* of this effect in lowering the oxidation potential of ethers.

1.3.5 Mediators

It is often an obstacle in direct electrosynthesis that since all the reactive intermediates are directly produced at the electrode surface, polymerization reactions can cause non conducting films to build on the electrode surface and block further reaction. One way to overcome this problem is to use indirect synthesis where much lower potentials are required to generate reagents electrochemically. A further variation of this is to use a mediator, which undergoes facile electron transfer at the electrode surface before diffusing into the bulk, whereby it is able to transfer electrons to reagents for bulk reaction. A review of such mediators is extensively shown by Ogibin *et al.*[73] An interesting and highly relevant example of a mediated process is the Sharpless asymmetric dihydroxylation[74] of an alkene. This reaction used an Os^{VI} | Os^{VIII} coupling and ferricyanide as a mediator system. The ferricyanide

acts as a mediator maintaining the concentrations of Os^{VIII} indirectly, as shown below in Figure 1.29.

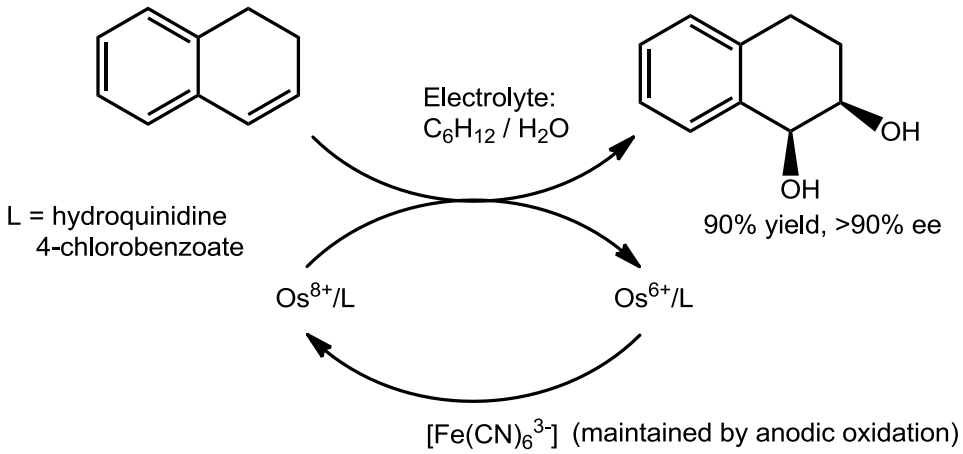

Figure 1.29 An example of a Sharpless asymmetric dihydroxylation of an alkene with Osmium ions used as a mediator (Adapted from Utley 1997).[55]

This reaction was also a two phase reaction with a cyclohexane | water interface making it highly suitable for biphasic flow. The Os^{VIII} reacted with the alkene in the organic phase and was regenerated by the ferrocyanide at the interface. This is an excellent example of a biphasic phase transfer mechanism and is one example of a reaction where products are kept separate from redox materials making separation easier.

1.3.6 Biphasic Reactions

Biphasic media offer a further useful dimension for electrosynthesis. This concept has already been mentioned briefly using a high power ultrasonic emulsion[45,75] and in a mediated biphasic process.[76] Biphasic systems are of particular importance in electrosynthetic approaches since many drawbacks of electrosynthesis can be, at least in part, solved.

It has been stated previously that water is an ideal electrosynthetic solvent due to its high dielectric constant (80.10,[62]) with the only drawback being its incompatibility with many organic functional groups. Biphasic systems allow the conductivity of a fully supported electrolytic phase to be utilised along side a fully solubilised organic phase, containing the redox material of interest.

Asami *et al.*[77] utilised an ultrasonic biphasic system where electrolysed material in an electrolytic phase (containing electrolyte), partitioned into an unsupported organic phase containing a capture reagent. the electrolytic phase used was an ionic liquid, 1-ethyl-3-methylimidazolium tetrafluoroborate, and contained a redox probe which upon being oxidised partitioned into the organic phase containing a nucleophile. The product remained in the organic phase and thus acted as a self extraction proceedure. Nucleophilic species, such as allyltrimethylsilane, tend to be easily oxidised due to their electron-poor nature. To prevent this the organic phase contained no supporting electrolyte and oxidation of material dissolved in it was greatly inhibited, thus the competing oxidation of the nucleophile and product was avoided.

Similarly, nucleophilic redox processes can be avoided by using the 'cation pool' method pioneered by Yoshida *et al.*[78] This method uses high concentrations of cations that are created in solution before adding a nucleophile to react with the cations. This avoids the problem of competing oxidation of nucleophiles, which are often easily oxidised.

1.3.7 Example I : The Kolbe Reaction

A most important class of reactions is that of the carbon-carbon bond formation in which carbon radicals are paired to form a new bond. This is most easily achieved by forming a symmetrical molecule from two of the same carbon radical as shown in Figure 1.30.

The most highly studied carbon-carbon bond formation in electrosynthesis is that of the Kolbe electrolysis, as shown in Figure 1.27. Originally proposed by Hermann Kolbe in 1849, the basic reaction involves the oxidation of a carboxylic acid followed by the thermodynamically driven loss of carbon dioxide. The resulting radical could then be shown to form a range of products that can be divided into two classes: the 'one electron' products and the 'two electron' products. The 'one electron' products are formed by the initial one electron oxidation followed by a subsequent radical reaction. The 'two electron' products are often referred to as Hofer-Moest products and are formed by a second electron oxidation to the cation.[79] A detailed mechanism

shows that the 'one electron' products are dimers, alkanes and alkenes, whereas the 'two electron' products are alkenes, alcohols and esters.[80]

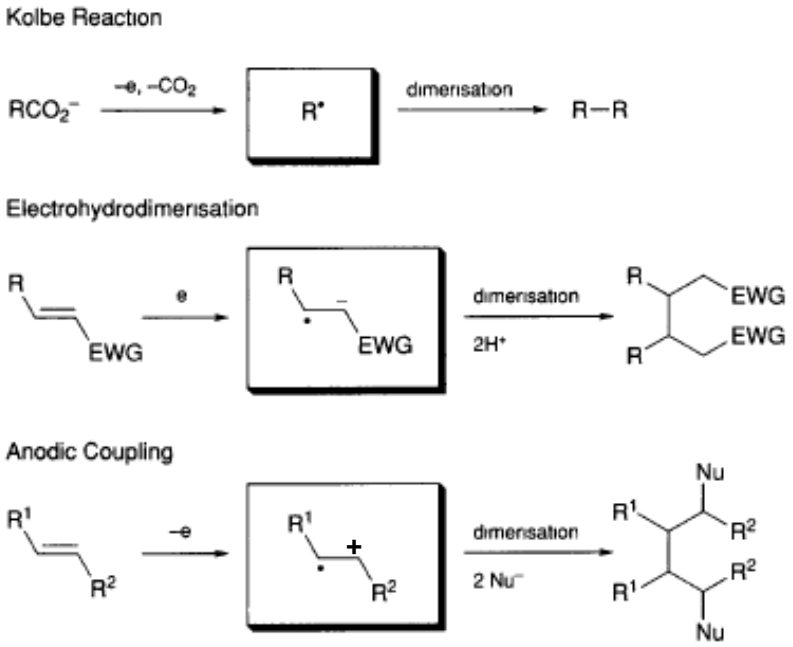

Figure 1.30 Examples of theoretical electrochemical carbon-carbon bond forming reactions.[55]

What makes the Kolbe electrolysis so powerful is that the products and reaction mechanism are very easily tuned by changing the electrolysis conditions. The product distributions tend to favour radical dimerisation over disproportionation, a trend not observed in homogeneous electrochemistry. It is found in general that platinum electrodes, solvents such as methanol and electron poor carboxylic acids tend to yield the carbon radical and thus the single electron products.[79] Conversely, the carbonium ion is favoured by carbon electrodes and electron rich carboxylic acids, thus yielding primarily the Hofer-Moest products.[79] Another interesting feature of the Kolbe electrolysis is that water oxidation is effectively eliminated with surface reaction of the carboxylic acid blocking this process.[81] This allows a large overpotential to be used to drive the process without concern about solvent processes lowering current efficiency. Overall the scope of the Kolbe electrolysis is huge, with more recent developments in cross coupling of carboxylic acids becoming feasible.[79,64b] Radical capture reagents such as alkenes can also be used to intercept intermediates and form new

products,[82] which has lead to an oxidative cyclisation mechanism for carboxylic acids.[83]

A biphasic sonoemulsion process has also been used to control product distribution. Wadhawan *et al.*[84] have shown that under sonoemulsion conditions the dimer is favoured even at carbon based electrodes, which would usually be expected to yield two electron products. This discrepancy was attributed to a trapping mechanism in which radicals are sequestered within the mobile non-conducting oil phase after a single electron transfer, and are unable to be further oxidised. The major products are thus the dimer, from the elimination of two molecules of carbon dioxide and the ester, from the elimination of one molecule of carbon dioxide.

1.3.8 Example II Pharmaceutical Electrosynthesis

Practically, the use of electrosynthesis is on the rise in the fields of pharmaceutical synthesis and industrial production. An interesting example of such an electrosynthesis is that of a β-lactam synthesis by Feroci *et al.*[85] in which an N – C4 bond[85a] and later the C3 – C4 bond[85b] are formed electrochemically. β-lactams are particularly interesting because of their widespread incorporation into many antibiotics, and with bacterial strains becoming ever more resistant it is crucial that antibiotic discovery keeps ahead of the curve. Electrosynthesis is fast and clean allowing easy β-lactam synthesis for new antibiotic development.

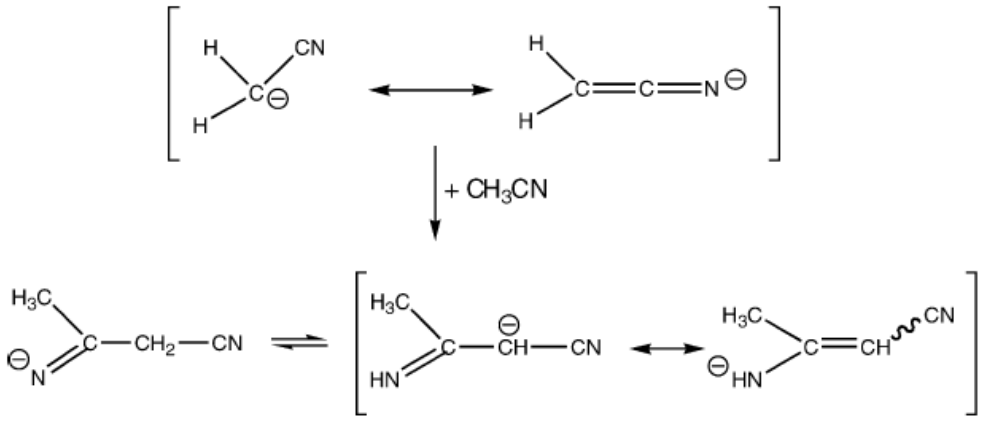

Figure 1.31 Formation of basic MeCN ion as a precursor for β-lactam synthesis[85b]

It was found that the use of the acetonitrile (solvent) and supporting electrolyte under galvanostatic conditions yielded an electro-generated base, most notably the MeCN- TEAP system (Figure 1.31). This figure shows how the MeCN anion was made and acted as a base. The electro-generated base was used to deprotonate the amine giving a nitrogen anion. This anion was used as a precursor to cyclisation by intramolecular nucleophilic substitution of the bromine (Figure 1.32). It must be noted, that the formation of product 3 is the result of a deprotonation at the C3 position, consistent with enolate formation, which can result in a displacement of the bromine as the conjugated α, β unsaturated amide is instead formed. This reduction of the bromoamide was avoided by electro-generation of the base before the bromoamide was added.

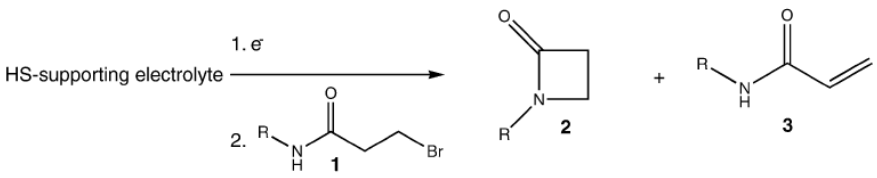

HS (solvent)	Supporting electrolyte
MeCN	$Et_4N^+ClO_4^-$ (TEAP)
EtCN	$Me_4N^+ClO_4^-$ (TMAP)
$MeNO_2$	$Et_4N^+Cl^-$ (TEACl)
DMSO	$Bu_4N^+Cl^-$ (TBACl)
DMF	$Et_4N^+F_6P^-$ (TEAFP)
	$Bu_4N^+F_6P^-$ (TBAFP)

1, 2, 3	R
a	Ph-CH_2-
b	Ph-
c	*c*-C_5H_9-
d	*p*-CH_3-Ph-
e	*o*-CH_3-Ph-
f	*p*-CH_3O-Ph-
g	*p*-Cl-Ph-
h	*p*-Br-Ph-
i	*p*-NO_2-Ph-

Figure 1.32. Reaction scheme for the formation of β-lactam electrochemically[85b]

The effect of the R group identity has been investigated and it was found that R groups changing the acidity of the N-H proton affect the relative yields of the two products, where electron withdrawing substituents favour the formation of the β-lactam ring. The effects of the solvent, electrolyte and charge applied before reaction were also analysed.

1.3.9 Example III : Electrosynthesis in Industry

From an environmental point of view electrosynthesis also has a great advantage over traditional synthetic approaches. A large problem with current syntheses is the significant amount of solvent waste discarded. Now there is a green directive in place to either reduce solvent wastes in volume or to replace more harmful solvents with lesser ones. As discussed previously microfluidics by definition fits these criteria, since they use micro channels with very little solvent for synthesis.

Another benefit of electrochemistry to the environment is that using electrochemistry often negates the need to use harmful bases and acids, as they can easily be generated *in situ* from probases and proacids. Thus these potentially harmful materials are never in a sufficiently high concentration as to be dangerous. This also means that operators need not be exposed to potentially harmful conditions. An example is chlorine gas activation to form reactive intermediates. Chlorine is a toxic gas both to humans and the environment and also gives a HCl by-product, a strong and harmful acid. In electrosynthesis weaker activating groups can be used such as methanol,[86] which is less harmful and easier to transport, store and use efficiently and safely.

Industry is starting to embrace the idea of electrosynthetic processes. From an industrial point of view these syntheses are generally far less hazardous than their purely organic counterparts and lend themselves to sustainability. Although this parameter relies on new renewable energy sources being adopted. Since it is also the use of electrons as a reagent, the logistics of reagent transportation are lowered as less need for heating due to the nature of highly reactive intermediates being produced.

Currently the most widely used organic electrosynthetic process adopted by industry is the production of adiponitrile ($CNCH_2CH_2CH_2CH_2CN$) by cathodic hydrodimerisation of acrylonitrile (Figure 1.33) in the Monsanto Process.[65,87] The production scale is *ca.* 340,000 tonnes.yr^{-1}, and is based on a principle founded in the 1960s. The modern production version uses cadmium cathodes and steel anodes, in an acetonitrile | aqueous emulsion with a

bisquaternary salt electrolyte. The aqueous phase is continually treated to prevent electrode coating and corrosion. The industrial significance of adiponitrile is as a precursor in the production of Nylon-6,6 and thus a key to manufacturing this highly abundant synthetic fibre as cheaply and efficiently as possible.

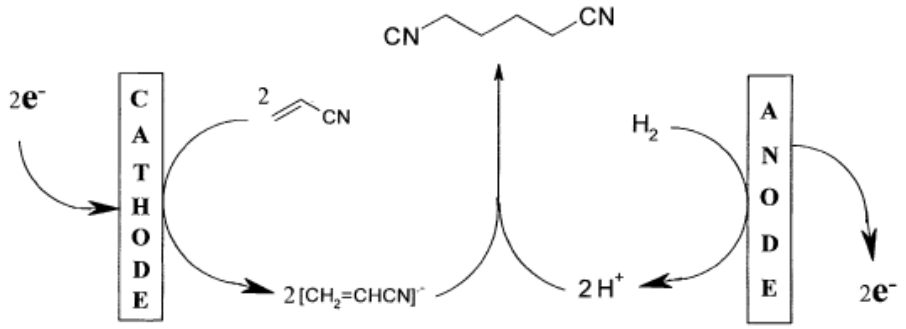

Figure 1.33 The Monsanto Process (Paddon, *Journal of Applied Electrochemistry*, 2006)[65]

Interestingly, the adiponitrile process is fraught with the same challenges that have been described previously. The potential of acrylonitrile reduction is so low as to rival hydrogen evolution from water, but it is by using cadmium electrodes and a quaternary ammonium salt electrolyte that the hydrogen evolution is almost completely eliminated. The quaternary ammonium salt simply excludes water and protons from the electrode surface favouring the reduction of acrylonitrile, which can reach current efficiencies of 95%.

With the constant competition of standard chemical process, the next generation of commercially viable processes must show ever increasing efficiency and ease of use. It is to this end that paired synthesis is receiving much attention on the industrial scale, such as that shown in Figure 1.34. These processes are, as previously described, highly efficient in terms of current and atom efficiency, assuming that both cathodic and anodic products are of some commercial use and the starting materials are sufficiently inexpensive.

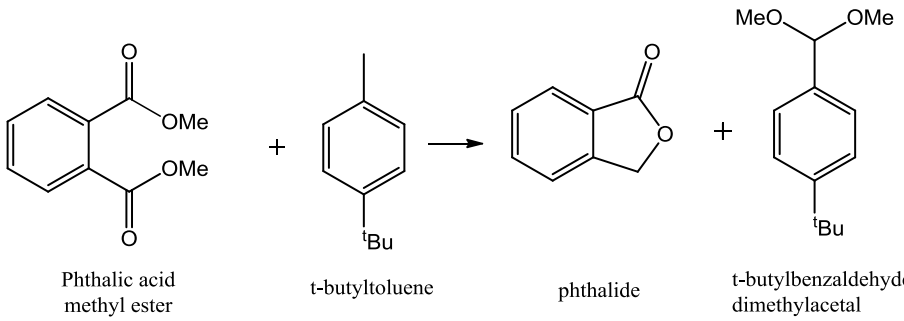

Figure 1.34. A paired electrochemical process (adapted from Sequeira, *Journal of the Brazilian Chemical Society*, 2009)[87]

Why then is it that more electrosynthetic processes are not becoming industrially adopted despite the high yields, high efficiencies and lack of dangerous materials? An interesting review of this topic by Sequeira *et al.*[87] seeks to provide an explanation for this disinterest. It is suggested that current electrosynthesis is being too heavily targeted at the high volume low added value market, where it would be better suited to the lower volume high added value market usually seen in the pharmaceuticals industry. Scale up is not required on as grand a scale, which is often a problem in electrochemistry. This may more correctly be attributed to a disconnect between pharmaceutical research development scientists, who seldom turn to an electrochemical synthetic route as a synthetic solution, and synthetic electrochemists who become too focused on commercially unviable syntheses.

A second point made by the author is the lack of relevant skills of researchers in all required areas; electrochemistry, organic synthesis, electrochemical engineering and chemical economics. This list is however a difficult set of stipulations even in standard syntheses so the reason for the lack of electrochemical development must stem from the trepidation that any non-electrochemists have for the subject. To compound the problem, electrochemistry is mainly an academically driven subject and suffering more than most areas from the huge void often seen between academia and industry.

In general, it is the research arm of the pharmaceuticals industry driving the commercialisation of synthetic processes and finding new routes *via* literature, rather than academics pushing their techniques to be synthetically

viable. As postulated by Sequeira, companies are often not willing to venture into electrochemistry when standard syntheses are available, so it is the job of purpose built companies to make this leap.

Finally, it is suggested that the overall cost of scale up and running an electrochemical plant is putting off industrial growth. This could be further elaborated to the extent that using huge amounts of electricity for synthetic gain is frowned upon as a general practice, due to the fossil fuel conscious state of the current world. Electrochemistry suffers from having a very obvious demand for electricity in the form of electrons, but many other synthetic processes use electricity as well in the form of heating and stirring. With current efficiencies as high as 95% for the adiponitrile process, this accounts for far less waste of power than heating. Overall, electrochemistry would become a far more attractive prospect on the grand scale if coupled with a renewable energy source such as photovoltaic cells. Unfortunately, thus far the renewable energy industry has not become widespread enough to sustain a large development on industrial scale electrosynthetic processes.

This thesis aims to combine the liquid | liquid | solid triple phase boundary mechanism with an electrosynthetic reaction, to create a novel electrosynthetic protocol capable of synthesising products in a rapid and clean reaction, without the need for a separation step to remove electrolytes post-reaction.

In doing so, new triple phase boundary procedures have been analysed and optimised to scale up the existing microdroplet experiments. The aim is to increase current densities and product turnover to the point where it is experimentally easy, fast and applicable to multiple functional groups by potentiostatic electrolysis.

1.4 References

(1) Bard, A. J.; Faulkner, L. R. *Electrochemical Methods, 2nd Ed.*; 2nd ed.; Wiley, 2001.

(2) Marcus, R. A. *Journal of Chemical Physics* **1956**, *24*, 966.

(3) Compton, R. G.; Banks, C. E. *Understanding Voltammetry, 2nd Ed*; 2nd ed.; Imperial College Press, 2010.

(4) MacDonald, S. M.; Watkins, J. D.; Gu, Y.; Yunus, K.; Fisher, A. C.; Shul, G.; Opallo, M.; Marken, F. *Electrochemistry Communications* **2007**, *9*, 2105.

(5) Marken, F. *Philosophical Transactions of the Royal Society of London Series A-Mathematical Physical and Engineering Sciences* **2004**, *362*, 2611.

(6) (a) Shi, C. N.; Anson, F. C. *Journal of Physical Chemistry B* **1999**, *103*, 6283. (b) Shi, C. N.; Anson, F. C. *Analytical Chemistry* **1998**, *70*, 3114; (c) Shi, C. N.; Anson, F. C. *Journal of Physical Chemistry B* **1998**, *102*, 9850;

(7) (a) Njanja, E.; Nassi, A.; Ngameni, E.; Elleouet, C.; Quentel, F.; L'Her, M. *Electrochemistry Communications* **2007**, *9*, 1695; (b) Quentel, F.; Mirceski, V.; L'Her, M.; Mladenov, M.; Scholz, F.; Elleouet, C. *Journal of Physical Chemistry B* **2005**, *109*, 13228; (c) Quentel, F.; Mirceski, V.; L'Her, M. *Analytical Chemistry* **2005**, *77*, 1940; (d) Charreteur, K.; Quentel, F.; Elleouet, C.; L'Her, M. *Analytical Chemistry* **2008**, *80*, 5065.

(8) Quentel, F.; Mirceski, V.; L'Her, M. *Journal of Solid State Electrochemistry* **2008**, *12*, 31.

(9) Quentel, F.; Mirceski, V.; Elleouet, C.; L'Her, M. *Journal of Physical Chemistry C* **2008**, *112*, 15553.

(10) Mirceski, V.; Quentel, F.; L'Her, M.; Pondaven, A. *Electrochemistry Communications* **2005**, *7*, 1122.

(11) Gulaboski, R.; Mirceski, V.; Pereira, C. M.; Cordeiro, M.; Silva, A. F.; Quentel, F.; L'Her, M.; Lovric, M. *Langmuir* **2006**, *22*, 3404.

(12) Aoki, K.; Tasakorn, P.; Chen, J. Y. *Journal of Electroanalytical Chemistry* **2003**, *542*, 51.

(13) Marken, F.; Webster, R. D.; Bull, S. D.; Davies, S. G. *Journal of Electroanalytical Chemistry* **1997**, *437*, 209.

(14) Scholz, F.; Komorsky-Lovric, S.; Lovric, M. *Electrochemistry Communications* **2000**, *2*, 112.

(15) Komorsky-Lovric, E.; Mirceski, V.; Kabbe, C.; Scholz, F. *Journal of Electroanalytical Chemistry* **2004**, *566*, 371.

(16) (a) Benjamin, I. *Science* **1993**, *261*, 1558; (b) Benjamin, I. *Chemical Reviews* **1996**, *96*, 1449.

(17) Katif, N.; Harries, R. A.; Kelly, A. M.; Fossey, J. S.; James, T. D.; Marken, F. *Journal of Solid State Electrochemistry* **2009**, *13*, 1475.

(18) Quentel, F.; Mirceski, V.; L'Her, M.; Spasovski, F.; Gacina, M. *Electrochemistry Communications* **2007**, *9*, 2489.

(19) (a) Schroder, U.; Wadhawan, J.; Evans, R. G.; Compton, R. G.; Wood, B.; Walton, D. J.; France, R. R.; Marken, F.; Page, P. C. B.; Hayman, C. M. *Journal of Physical Chemistry B* **2002**, *106*, 8697; (b) Schroder, U.; Compton, R. G.; Marken, F.; Bull, S. D.; Davies, S. G.; Gilmour, S. *Journal of Physical Chemistry B* **2001**, *105*, 1344.

(20) Quentel, F.; Mirceski, V.; L'Her, M. *Journal of Physical Chemistry B* **2005**, *109*, 1262.

(21) Komorsky-Lovric, S.; Lovric, M.; Scholz, F. *Journal of Electroanalytical Chemistry* **2001**, *508*, 129.

(22) Marken, F.; Compton, R. G.; Goeting, C. H.; Foord, J. S.; Bull, S. D.; Davies, S. G. *Journal of Solid State Electrochemistry* **2001**, *5*, 88.

(23) Scholz, F. *Annu. Rep. Prog. Chem., Sect. C* **2006**, *102*, 28.

(24) Donten, M.; Stojek, Z.; Scholz, F. *Electrochemistry Communications* **2002**, *4*, 324.

(25) (a) Donten, M.; Bak, E.; Gniadek, M.; Stojek, Z.; Scholz, F. *Electrochimica Acta* **2008**, *53*, 5608; (b) Bak, E.; Donten, M.; Stojek, Z.; Scholz, F. *Electrochemistry Communications* **2007**, *9*, 386.

(26) (a) Bak, E.; Donten, M.; Skompska, M.; Stojek, Z. *Journal of Physical Chemistry B* **2006**, *110*, 24635; (b) Bak, E.; Donten, M. L.; Donten, M.; Stojek, Z. *Electrochemistry Communications* **2005**, *7*, 1098.

(27) Tasakorn, P.; Chen, J. Y.; Aoki, K. *Journal of Electroanalytical Chemistry* **2002**, *533*, 119.

(28) (a) Bak, E.; Donten, M.; Stojek, Z. *Journal of Electroanalytical Chemistry* **2007**, *600*, 45; (b) Bak, E.; Donten, M.; Stojek, Z. *Electrochemistry Communications* **2005**, *7*, 483.

(29) Bak, E.; Donten, M.; Stojek, Z. *Electrochemistry Communications* **2008**, *10*, 1074.

(30) Shul, G.; Nogala, W.; Zakorchemna, I.; Niedziolka, J.; Opallo, M. *Journal of Solid State Electrochemistry* **2008**, *12*, 1285.

(31) Marcus, R. A. *Discussions of the Faraday Society* **1960**, 21.

(32) Rayner, D.; Fietkau, N.; Streeter, I.; Marken, F.; Buckley, B. R.; Page, P. C. B.; del Campo, J.; Mas, R.; Munoz, F. X.; Compton, R. G. *Journal of Physical Chemistry C* **2007**, *111*, 9992.

(33) Simm, A. O.; Chevallier, F. G.; Ordeig, O.; del Campo, F. J.; Munoz, F. X.; Compton, R. G. *Chem. Phys. Chem.* **2006**, *7*, 2585.

(34) Shul, G.; Opallo, M. *Electrochemistry Communications* **2005**, *7*, 194.

(35) Shul, G.; Murphy, M. A.; Wilcox, G. D.; Marken, F.; Opallo, M. *Journal of Solid State Electrochemistry* **2005**, *9*, 874.

(36) MacDonald, S. M.; Fletcher, P. D. I.; Cui, Z. G.; Opallo, M. C.; Chen, J. Y.; Marken, F. *Electrochimica Acta* **2007**, *53*, 1175.

(37) Zhang, X. H.; Paddon, C. A.; Chan, Y. H.; Bulman-Page, P. C.; Fordred, P. S.; Bull, S. D.; Chang, H. C.; Rizvi, N.; Marken, F. *Electroanalysis* **2009**, *21*, 1341.

(38) Shul, G.; Sirieix-Plenet, J.; Gaillon, L.; Opallo, M. *Electrochemistry Communications* **2006**, *8*, 1111.

(39) Davies, T. J.; Wilkins, S. J.; Compton, R. G. *Journal of Electroanalytical Chemistry* **2006**, *586*, 260.

(40) (a) Adamiak, W.; Opallo, M. *Journal of Electroanalytical Chemistry* **2010**, *643*, 82; (b) Adamiak, W.; Shul, G.; Opallo, M. *Electrochemistry Communications* **2009**, *11*, 149.

(41) MacDonald, S. M.; Opallo, M.; Klamt, A.; Eckert, F.; Marken, F. *Physical Chemistry Chemical Physics* **2008**, *10*, 3925.

(42) Watkins, J. D.; MacDonald, S. M.; Fordred, P. S.; Bull, S. D.; Gu, Y. F.; Yunus, K.; Fisher, A. C.; Bulman-Page, P. C.; Marken, F. *Electrochimica Acta* **2009**, *54*, 6908.

(43) MacDonald, S. M.; Watkins, J. D.; Bull, S. D.; Davies, I. R.; Gu, Y.; Yunus, K.; Fisher, A. C.; Page, P. C. B.; Chan, Y.; Elliott, C.; Marken, F. *Journal of Physical Organic Chemistry* **2009**, *22*, 52.

(44) Marken, F.; Goldfarb, D. L.; Compton, R. G. *Electroanalysis* **1998**, *10*, 562.

(45) (a) Marken, F.; Compton, R. G.; Bull, S. D.; Davies, S. C. *Chemical Communications* **1997**, 995; (b) Marken, F.; Compton, R. G.; Davies, S. G.; Bull, S. D.; Thiemann, T.; Melo, M.; Neves, A. C.; Castillo, J.; Jung, C. G.; Fontana, A. *Journal of the Chemical Society-Perkin Transactions 2* **1997**, 2055.

(46) Banks, C. E.; Davies, T. J.; Evans, R. G.; Hignett, G.; Wain, A. J.; Lawrence, N. S.; Wadhawan, J. D.; Marken, F.; Compton, R. G. *Physical Chemistry Chemical Physics* **2003**, *5*, 4053.

(47) Marken, F.; Compton, R. G.; Goeting, C. H.; Foord, J. S.; Bull, S. D.; Davies, S. G. *Electroanalysis* **1998**, *10*, 821.

(48) (a) Scholz, F.; Gulaboski, R.; Mirceski, V.; Langer, P. *Electrochemistry Communications* **2002**, *4*, 659; (b) Scholz, F.; Gulaboski, R. *Faraday Discussions* **2005**, *129*, 169.

(49) Mirceski, V.; Quentel, F.; L'Her, M. *Electrochemistry Communications* **2009**, *11*, 1262.

(50) (a) French, R. W.; Gordeev, S. N.; Raithby, P. R.; Marken, F. *Journal of Electroanalytical Chemistry* **2009**, *632*, 206; (b) French, R. W.; Marken, F. *Journal of Solid State Electrochemistry* **2009**, *13*, 609; (c) French, R. W.; Collins, A. M.; Marken, F. *Electroanalysis* **2008**, *20*, 2403.

(51) French, R. W.; Chan, Y. H.; Bulman-Page, P. C.; Marken, F. *Electrophoresis* **2009**, *30*, 3361.

(52) (a) Vuorema, A.; Meadows, H.; Bin Ibrahim, N.; Del Campo, J.; Cortina-Puig, M.; Vagin, M. Y.; Karyakin, A. A.; Sillanpaa, M.; Marken, F. *Electroanalysis* **2010**, *22*, 2889; (b) Vagin, M. Y.; Karyakin, A. A.; Vuorema, A.; Sillanpaa, M.; Meadows, H.; Del Campo, F. J.; Cortina-Puig, M.; Page, P. C. B.; Chan, Y. H.; Marken, F. *Electrochemistry Communications* **2010**, *12*, 455.

(53) Niedziolka, J.; Opallo, M. *Electrochemistry Communications* **2008**, *10*, 1445.

(54) Moeller, K. D. *Tetrahedron* **2000**, *56*, 9527.

(55) Utley, J. *Chemical Society Reviews* **1997**, *26*, 157.

(56) Kyriakou, G.; Beaumont, S. K.; Humphrey, S. M.; Antonetti, C.; Lambert, R. M. *Chem. Cat. Chem.* **2010**, *2*, 1444.

(57) (a) Yin, Z.; Zheng, H.; Ma, D.; Bao, X. *Journal of Physical Chemistry C* **2009**, *113*, 1001; (b) Pan, W.; Zhang, X.; Ma, H.; Zhang, J. *Journal of Physical Chemistry C* **2008**, *112*, 2456.

(58) (a) Attard, G. *Journal of Physical Chemistry B* **2001**, *105*, 3158; (b) Ahmadi, A.; Attard, G.; Feliu, J.; Rodes, A. *Langmuir* **1999**, *15*, 2420.

(59) Watkins, B. F.; Behling, J. R.; Kariv, E.; Miller, L. L. *Journal of the American Chemical Society* **1975**, *97*, 3549.

(60) Maekawa, H.; Itoh, K.; Goda, S.; Nishiguchi, I. *Chirality* **2003**, *15*, 95

(61) (a) Tesfu, E.; Maurer, K.; Ragsdale, S. R.; Moeller, K. D. *Journal of the American Chemical Society* **2004**, *126*, 6212; (b) Bi, B.; Maurer, K.; Moeller, K. D. *Journal of the American Chemical Society* **2010**, *132*, 17405; (c) Hu, L.; Stuart, M.; Tian, J.; Maurer, K.; Moeller, K. D. *Journal of the American Chemical Society* **2010**, *132*, 16610

(62) Lide, D. R. *CRC Handbook of Chemistry and Physics, 89th Ed.*; CRC Press, **2008**.

(63) (a) Lingane, J. J.; Swain, C. G.; Fields, M. *Journal of the American Chemical Society* **1943**, *65*, 1348; (b) Zhang, L.; Zha, Z. G.; Wang, Z. Y.; Fu, S. Q. *Tetrahedron Letters* **2010**, *51*, 1426.

(64) (a) Baizer, M. M.; Hallcher, R. C. *Journal of the Electrochemical Society* **1976**, *123*, 809; (b) Lund, H.; Baizer, M. M.; Marcel Dekker: New York, **1991**.

(65) Paddon, C. A.; Atobe, M.; Fuchigami, T.; He, P.; Watts, P.; Haswell, S. J.; Pritchard, G. J.; Bull, S. D.; Marken, F. *Journal of Applied Electrochemistry* **2006**, *36*, 617.

(66) Jalbout, A. F.; Zhang, S. H. *Acta Chim. Slov.* **2002**, *49*, 917.

(67) (a) Utley, J. H. P.; Oguntoye, E.; Smith, C. Z.; Wyatt, P. B. *Tetrahedron Letters* **2000**, *41*, 7249; (b) Utley, J. H. P.; Ramesh, S.; Salvatella, X.; Szunerits, S.; Motevalli, M.; Nielsen, M. F. *Journal of the Chemical Society-Perkin Transactions 2* **2001**, 153.

(68) Coleman, J. P.; Hallcher, R. C.; McMackins, D. E.; Rogers, T. E.; Wagenknecht, J. H. *Tetrahedron* **1991**, *47*, 809.

(69) Horcajada, R.; Okajima, M.; Suga, S.; Yoshida, J. *Chemical Communications* **2005**, 1303.

(70) (a) He, P.; Watts, P.; Marken, F.; Haswell, S. J. *Electrochemistry Communications* **2005**, *7*, 918; (b) He, P.; Watts, P.; Marken, F.; Haswell, S. J. *Angewandte Chemie-International Edition* **2006**, *45*, 4146; (c) He, P.; Watts, P.; Marken, F.; Haswell, S. J. *Lab on a Chip* **2007**, *7*, 141; (d) He, P.; Watts, P.; Marken, F.; Haswell, S. J. *Green Chemistry* **2007**, *9*, 20.

(71) Yoshida, J.; Kataoka, K.; Horcajada, R.; Nagaki, A. *Chemical Reviews* **2008**, *108*, 2265.

(72) Yoshida, J.; Maekawa, T.; Murata, T.; Matsunaga, S. I.; Isoe, S. *Journal of the American Chemical Society* **1990**, *112*, 1962.

(73) Ogibin, Y. N.; Elinson, M. N.; Nikishin, G. I. *Russ. Chem. Rev.* **2009**, *78*, 89.

(74) Amunsden, A. R.; Balko, E. N. *Journal of Applied Electrochemistry* **1992**, *22*, 810

(75) Wadhawan, J. D.; Del Campo, F. J.; Compton, R. G.; Foord, J. S.; Marken, F.; Bull, S. D.; Davies, S. G.; Walton, D. J.; Ryley, S. *Journal of Electroanalytical Chemistry* **2001**, *507*, 135.

(76) (a) Khan, F. N.; Jayakumar, R.; Pillai, C. N. *Journal of Molecular Catalysis a-Chemical* **2003**, *195*, 139(b) Davies, T. J.; Garner, A. C.; Davies, S. G.; Compton, R. G. *Chemphyschem* **2005**, *6*, 2633.

(77) (a) Asami, R.; Fuchigami, T.; Atobe, M. *Organic & Biomolecular Chemistry* **2008**, *6*, 1938; (b) Asami, R.; Fuchigami, T.; Atobe, M. *Chemical Communications* **2008**, 244.

(78) Yoshida, J.; Suga, S. *Chemistry-A European Journal* **2002**, *8*, 2651.

(79) Fry, A. J.; 2 ed.; Wiley-Interscience, 1989.

(80) Rand, L.; Mohar, A. F. *Journal of Organic Chemistry* **1965**, *30*, 3885.

(81) Vijh, A. K.; Conway, B. E. *Chemical Reviews* **1967**, *67*, 623.

(82) Chkir, M.; Lelandai.D *Journal of the Chemical Society D-Chemical Communications* **1971**, 1369.

(83) Lebreux, F.; Buzzo, F.; Marko, I. E. *Synlett* **2008**, 2815.

(84) Wadhawan, J. D.; Marken, F.; Compton, R. G. Workshop on Electchemistry and Interfacial Chemistry in Environmental Clean-Up and Green Chemical Processes, Coimbra, Portugal, **2001**; p 1947.

(85) (a) Feroci, M.; Orsini, M.; Palombi, L.; Rossi, L.; Inesi, A. *Electrochimica Acta* **2005**, *50*, 2029; (b) Feroci, A.; Orsini, M.; Rossi, L.; Sotgiu, G.; Inesi, A. *Electrochimica Acta* **2006**, *51*, 5540.

(86) Tajima, T.; Fuchigami, T. *Chemistry-A European Journal* **2005**, *11*, 6192.

(87) Sequeira, C. A. C.; Santos, D. M. F. *Journal of the Brazilian Chemical Society* **2009**, *20*, 387.

2. Synthesis, Characterisation and Applications of Cationic Carbon Nanoparticles

Contents

Aims

- To synthesise cationically charged carbon nanoparticles as a complimentary conductive binder for layer by layer electrode modification.
- To characterise the novel cationic carbon nanoparticles by X-ray photoelectron spectroscopy, atomic force microscopy, raman spectroscopy and cyclic voltammetry.
- To assess the number of cationic binding sites per nanoparticle by complementary binding of the redox active material indigo carmine.

Publication

Watkins JD, Lawrence R, Taylor JE, Bull SD, Nelson GW, Foord JS, Wolverson D, Rassaei L, Evans NDM, Gascon SA and Marken F, *Physical Chemistry Chemical Physics*, **2010**, 12, 737 – 739.

CHAPTER 2: Synthesis, Characterisation and Applications of Cationic Carbon Nanoparticles

2.1 Introduction

2.1.1 Introduction to Traditional Carbon Electrode Materials

Carbon is highly useful as an electrode material due to its high conductivity and large electrochemical window. It is also non-hazardous and easy to modify for selectivity. Carbon electrodes can be divided into a few categories by structure; i) glassy carbon, ii) boron doped diamond and iii) graphite based.

Glassy carbon is a ceramic form of carbon which has a high stability to chemicals, high temperature resistance and is impermeable to gases and liquids. It has been suggested by Harris *et al.*[1] that the structure of glassy carbon is of a random collection of fullerene based shapes. The high electrochemical window of glassy carbon makes it ideal for voltammetry, and combined with its hardness it is also easy to clean the surface by mechanical polishing. For glassy carbon electrodes the pre-treatment method has been shown to be important for the heterogeneous electron transfer rate especially for surface sensitive 'inner sphere' redox processes.[2]

Boron doped diamond is a more ordered form of carbon based on the diamond structure. In its natural form diamond is not conducting enough for voltammetry but when doped with an acceptor impurity such as boron this can be resolved, as summarised by Pleskov.[3] With moderate doping a p-type semiconductor is created but more commonly a larger amount of dopant is used to create a metal-like electrode. It is at these semi-metal electrodes that many unique effects of boron doped diamond are observed. Adsorption based electron transfers (such as O_2 or H_2 evolution) are mostly eliminated, as these are 'inner sphere' processes and involve a substantial chemical change as well as an electronic change. Meanwhile, 'outer sphere' electron transfers such as standard aqueous redox couples appear kinetically slower than on glassy carbon.[4] In a review by McCreery[5] a summary of the

electrochemical properties of boron doped diamond is presented, showing evidence that local dopant levels and grain boundaries are highly important in the electrochemistry seen at this material. Thus it must be appreciated that much of the voltammetry presented is a result of the average electrochemical behaviour and often boron doped diamond must be appreciated to have poor electron transfer homogeneity. Boron doped diamond can be easily fabricated by chemical vapour deposition from volatile carbon species such as methane, trimethylboron and hydrogen.[6] Boron doped diamond possesses remarkable chemical and electrochemical stability on repeated cycling, even in harsh acidic media[7] and is often robust enough to allow stable voltammetry without pre-treatment. As an electrode material boron doped diamond shows an incredible potential window of over 3 V, with considerably lower capacitive current than glassy carbon.[6] Boron doped diamond, however, shows poor catalytic activity compared to metal electrodes but has many applications in analysis as a microelectrode array, reviewed by Lawrence *et al.*[8] and in conjunction with ultrasound, reviewed by Compton *et al.*[9] Other uses of boron doped diamond are summarised by Panizza and Cerisola[10] and include waste water treatment and electrosynthetic processes where its high resistance to fouling make it an ideal material.

A common carbon material used for electrodes is graphite, a highly ordered carbon with a distinctive planar structure. It is this structure that gives rise to two distinctive electrochemical sites, the edge plane and the basal plane. Both of which have different electrochemical properties, as controlled by their different electron transfer capabilities.

In general, a graphite electrode contains both edge and basal plane sites and appears as a series of interlocking plates of basal plane electrode with steps between plates containing edge plane sites as reviewed by Banks *et al.*[11] It is suggested that these edge plane sites give faster electron transfer kinetics than the basal plane sites. Thus is may be beneficial for highly ordered graphite to be roughened in order to introduce edge plane sites for useful electrochemistry. McCreery and co-workers have published many studies aimed at a robust comparison of electron transfer rates at pristine graphite

surfaces and glassy carbon electrodes.[5,12] By using highly ordered pyrolytic graphite (HOPG) surfaces created with almost no defect edge plane sites it was further found that glassy carbon regularly exhibits electron transfer speeds 1-5 orders of magnitude faster than HOPG. The actual results were often subject to the redox probe in question with surface structure and impurities being important for some cases. $Ru(NH_3)_6^{2+/3+}$ is often considered close to an ideal 'outer sphere' electron transfer case and is thus not affected by surface impurities and treatments and was found to vary by roughly a factor of 1000.[5] As with the boron doped diamond case however it is important to take into account that the use of cyclic voltammetry at macro-electrodes as a measure of electron kinetics gives an average of the surface and not the true site comparison. More recently a study by Unwin, Macpherson *et al.*[13] have shown a new method utilising a scanning micropipette contact method to analyse the local electron transfer characteristics of electrode surfaces. This has shown that the basal plane graphite is considerably more active than traditionally thought. The electrochemical window of edge plane pyrolytic graphite electrodes (EPPG) is also such that it is a suitable material for electro-analytical methodologies as summarised by Banks and Compton.[14]

2.1.2 Introduction to Nanoscale Carbon Electrode Materials

Nanoscale carbon materials are now of significant interest in electrochemistry, especially in the field of electrode modification. An important group of carbon nanostructured materials are carbon nanotubes. first reported by Iijima[15] in 1991. Carbon nanotubes are characterised as a rolled graphene sheet with a diameter in the nanoscale. These can be single walled or, if more than one sheet is sequentially rolled, multiwalled nanotubes. Originally carbon nanotubes were grown by an arc discharge technique,[15] common in the production of C_{60} species. Now it is more common to use a plasma assisted CVD method for more precise control of size and length. Nanotubes are also naturally occurring in all forms of combustion soot much like fullerenes but require separation which can generally be achieved by centrifugation.

Carbon nanotube structures are inherently linked to graphite due to their layered nature and as such possess the same basal plane and edge plane type sites. The edge planes occur at the tube ends or at defects in the tube walls and are active sites of fast electron transfer kinetics. Since the walls are analogous to basal planes of graphitic carbon they are often assumed to suffer from slow electron transfer kinetics. However, as with BPPG carbon nanotubes walls are being shown to be more electrochemically active than first thought at areas other than defects.[16] It is these findings which have lead to aligned carbon nanotube 'forests' being grown or immobilised on electrode surfaces. These aligned nanotubes posses superior electron transfer kinetics over random arrays of nanotubes due to the higher density of edge sites available per electrode area.[17] The use of carbon nanotubes in sensor applications has been reviewed by Ahammad *et al.*[18] who demonstrate their particular importance in biosensing applications due to biocompatibility and ease of functionalisation. One specific example showed that sub-attomolar detection of DNA strands was possible at an aligned low density nanotube electrode.[19]

Carbon nanoparticles, in comparison to carbon nanotubes, are more randomly distributed both in terms of size and activity. Conversely, nanoparticles are far cheaper and easier to manufacture. These nanoparticles generally consist of a carbon black sphere with inherent surface functionality, usually influenced by the manufacture process and can be either hydrophobic or hydrophilic. These modified carbon nanoparticles are often commercially available for use in modifying electrodes and provide a useful platform for surface modification. On a commercial scale nanoparticles can be made by an oil furnace process from the incomplete combustion of aromatic hydrocarbons. Separation and filtration of the resulting soot (Cabot Corporation *ca.* 1995) is achieved by acid treatment. The carbon nanoparticles are often substituted by oxygen groups and these can be used to create a range of carbon surface functionalisation.[20] For electroanalysis, carbon nanoparticles can be easily affixed to traditional carbon electrodes by evaporation from water[21] to form an inexpensive sensor with a large surface area. This large surface area can be used to adsorb analytes from solution to have a concentrating effect at the surface allowing

facile low concentration detection.[22] Alternatively, carbon nanoparticles can be used in conjunction with insulating polymer matrices, which can easily be functionalised and coated onto an electrode surface but do not usually allow conductivity within the film. In this case the nanoparticles act as a conductive bridge creating many active sites within the polymer and a large surface area electrode.[23]

It has been shown previously by Rassaei *et al.*[23b] that a positively charged carbon nanoparticle electrode film can be made using commercially available carbon nanoparticles combined with chitosan polymer. The resulting film contained terminating amine groups that could become positively charged under certain conditions (Figure 2.1). In this example, the carbon nanoparticles provided a conducting support matrix for the insulating chitosan film which can bind negatively charged ions.

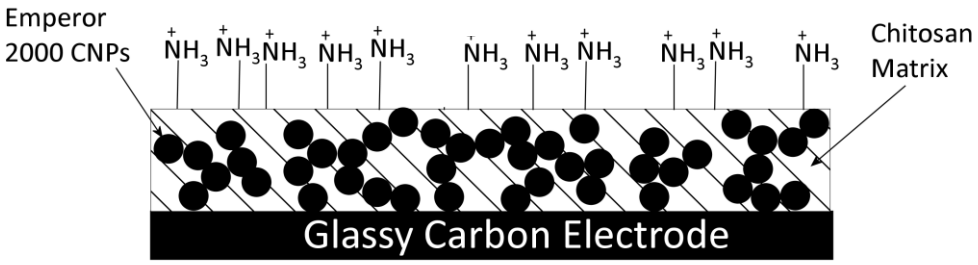

Figure 2.1 This schematic representation shows the previously reported positively charged carbon nanoparticle / chitosan matrix.[23b]

Carbon nanostructures are utilised in a range of applications. As sensor materials they benefit from a high conductivity and large surface area as well as good selectivity once modified, as described in Section 2.1.3. Often these carbon materials are combined with metal nanoparticles using the carbon nanostructure as a scaffold of high surface area so as to enhance electrochemical signals. For example a biosensor for oxalate has been recently reported by Pundir *et al.*[24] which showed that gold nanoparticles adsorbed onto multiwalled carbon nanotubes act as an electrocatalytic support for the oxalate oxidase enzyme. The most commonly used group of carbon nanomaterials for sensor applications are carbon nanotubes, which provide a robust self supporting matrix for electrochemical detection[25] and biological electroanalysis.[26]

2.1.3 Surface Modification of Carbon Electrode Materials

As mentioned previously, one of the major advantages of carbon electrodes are that they are highly resistant to chemical degradation during electrolysis. Carbon materials are also highly functionalisable by a few key reactions which can give synthetic handles for further modification even including biological markers. The many methods for functionalisation are summarised in a review by Downard[20] and shown in Figure 2.2.

The key methods for functionalisation utilise radical generating reactions to couple directly with carbon surfaces. Most well studied is the use of diazonium as a coupling reagent[27] (Figure 2.2A) which can be easily bound to carbon surfaces without pre-existing architecture. If the aryl diazonium salt is first isolated, a single electron reduction or non-electrochemical binding can be achieved.[28] Alternatively the ion can be electro-generated *in situ* from the oxidation of the corresponding aryl amine with almost the same results.[29] A second option for the direct functionalisation of carbon surfaces is the use of silane linking groups (Figure 2.2C). For this process a silane group is non-electrochemically attached to a carbon surface *via* the pendant alcohol functional groups on the surface.[30] It has even been shown by Andrieux *et al.*[31] that the Kolbe reaction can be used to modify surfaces by binding the electro-generated radicals of an electro-decarboxylation reaction to the surface.

Once a suitable synthetic handle is in place 'click' chemistry has been used highly successfully for the further rapid modification of surfaces by a multitude of useful functionalisation as reviewed by Mahouche-Chergui *et al.*[27] 'Click' chemistry uses the easy coupling of small molecules for the rapid and efficient synthesis of useful functional groups. A common example for surface modification is the reaction between alkynes and azides forming triazoles in high yield.[32]

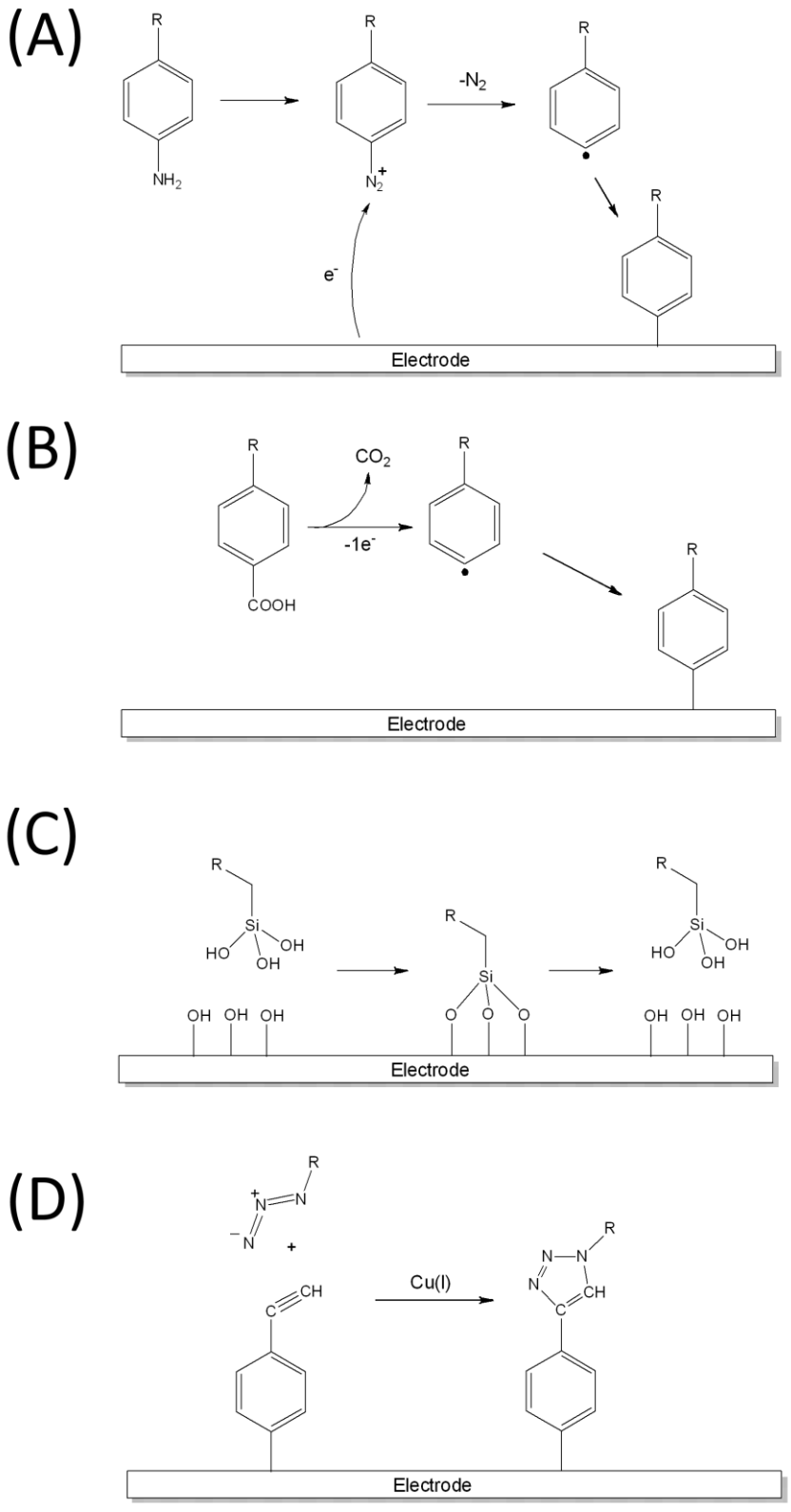

Figure 2.2 A summary of commonly used surface functionalisation reactions; **(A)** Diazonium reduction, **(B)** Kolbe reaction, **(C)** Silane attachment, **(D)** 'Click' reaction.

The results presented in this chapter seek to simplify the approach used by Rassaei, by combining the conductivity of the carbon nanoparticle matrix with

the cationic sites provided by the chitosan into a single species (Figure 2.3). This was achieved by modifying the surface of commercially available anionic carbon nanoparticles to incorporate a terminal amine, which was easily protonated to create cationic behaviour. This type of carbon nanoparticle was then of use in a layer by layer technique as a conducting cationic complementary layer, capable of binding with anionic polymers. This approach was used to create completely novel carbon electrode materials, by layer by layer deposition of anionic and cationic carbon nanoparticles to create inexpensive, thin and porous carbon nanoparticle films without the limitations of insulating polymeric binders.

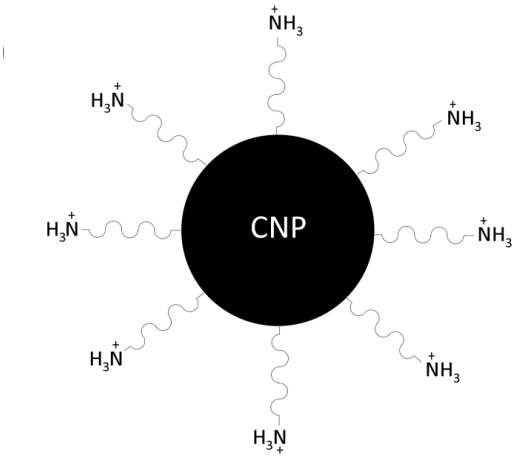

Figure 2.3 This shows a schematic diagram of the proposed cationic carbon nanoparticles with tethered protonated terminal amines creating a positive surface charge.

2.2 Experimental

2.2.1 Reagents

Emperor 2000™ carbon nanoparticles used as the starting material were obtained from Cabot Corporation. Other reagents were used without further purification: sodium nitrate (Sigma Aldrich, 99.0%), indigo carmine, certified (Aldrich), acetic acid (Aldrich, 99.7+%), *ortho*-phosphoric acid (Fisher Scientific), boric acid (Aldrich, 99.5%). Britton–Robinson buffer was prepared from 0.04 M of each of boric acid, phosphoric acid, and acetic acid and adjusting with sodium hydroxide to the desired pH. Demineralised and filtered

water was taken from a Thermo Scientific water purification system (Barnstead Nanopure) with not less than 18.2 MΩ cm resistivity. Experiments were conducted at 20 - 21^{o}C.

2.2.2 Instrumentation

For voltammetric studies a microAutolab III potentiostat system (EcoChemie, Netherlands) was employed with a Pt wire counter electrode, a saturated calomel (SCE) reference electrode (Radiometer, Copenhagen) and a surface modified (as shown in 2.2.3) 3mm glassy carbon disc working electrode. Atomic force microscopy (AFM) was conducted in tapping mode under ambient conditions using a Nanoscope IIIA (V6.14) and a Nanosensors NCH-16 tip. Raman spectroscopy studies were carried out with a Renishaw Raman microscope system with a resolution of about 2 cm^{-1} and using an excitation energy of 5.08 eV (244 nm) provided by a frequency-doubled continuous wave argon ion laser (reference diamond = 1332 cm^{-1}). X-ray photoelectron spectroscopy (XPS) was conducted using a VSW hemispherical analyser, excited using a monochromatic Al Ka X-ray source at 1486.6 eV. Spectra were background corrected using a Shirley background scan and peak fitting was conducted using the XPSPEAK (ver. 4.1) software package. A Malvern Zetamaster S (Malvern Instruments) was used for zeta potential measurements. Each sample was measured 10 times, and each of these measurements took *ca.* 30 s.

2.2.3 Procedure I: surface modification of carbon nanoparticles

For step (A) (Scheme 2.1) typically 1 g of carbon nanoparticles (Emperor 2000™) were sonicated in dry dichloromethane in a round bottom flask for 30 minutes. The flask was degassed with nitrogen gas at 0 ^{o}C and 10 cm^3 of thionyl chloride was added dropwise under continuous stirring. The flask was then allowed to warm to room temperature whilst stirring for 2–3 hours. Excess thionyl chloride and solvent were removed by rotary evaporation to yield sulphonyl chloride modified nanoparticles. For Step (B) (Scheme 2.1) 10 cm^3 of ethylene diamine was added into a 250 cm^3 round bottom flask with 30 cm^3 of dry dichloromethane and the temperature cooled to 0 ^{o}C. The sulphonylchloride functionalised carbon nanoparticles were added in small

portions, and then the reaction was allowed to warm to room temperature whilst stirring for 2 h. Excess amine and dichloromethane were removed by rotary evaporation. The resulting black tar was washed under Büchner filtration with aliquots of dichloromethane and 1 M aqueous HCl and allowed to dry to form a sulphonamide modified nano-particular powder (*ca.* 1 g).

2.2.4 Procedure II: deposition of carbon nanoparticle films onto glassy carbon electrodes

For deposition 3.5 mg of the sulphonamide-functionalised nanoparticles were added into 1.5 cm^3 distilled water. The resulting solution/suspension was initially sonicated for 1 hour (in a low power ultrasound bath, Fisher FB11012) and then shaken vigorously prior to each use. Aliquots of this solution/ suspension were pipetted directly onto a polished 3 mm diameter glassy carbon electrode and allowed to evaporate at 80 ^oC in an oven. The resulting film exhibited good adhesion to glassy carbon and was used directly in further experiments.

2.2.5 Procedure III: Indigo carmine adsorption into carbon nanoparticle films

For modification by indigo carmine the carbon nanoparticle films on glassy carbon electrodes (see above) were dipped into aqueous solutions of indigo carmine of varying concentration and left to equilibrate for 5 min. The electrodes were then rinsed with distilled water and placed into aqueous 1 M sodium nitrate for electrochemical experiments.

2.3 Results and Discussion

2.3.1 Synthesis of Ethylene diamine modified nanoparticles

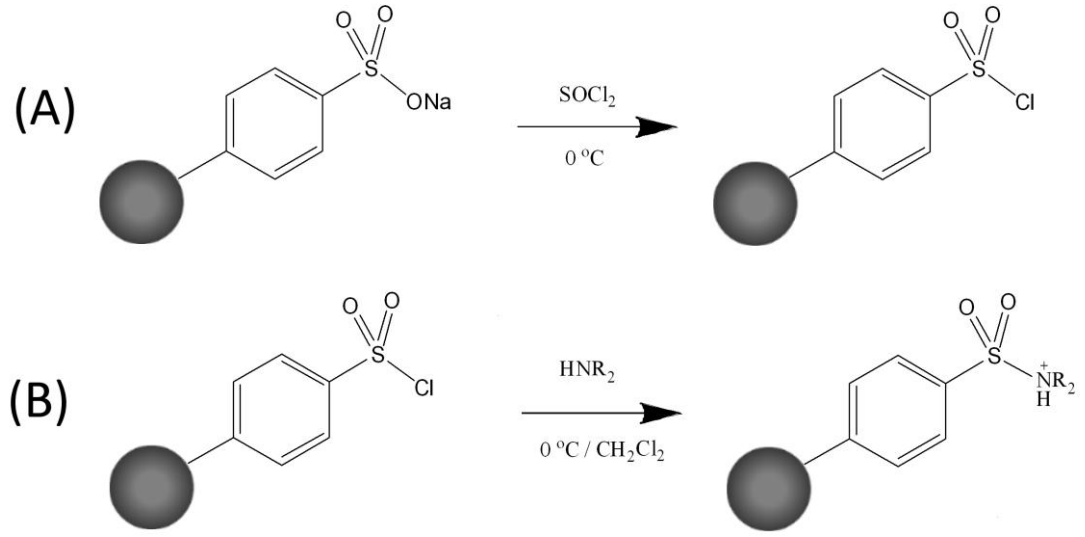

Scheme 2.1 The general two step synthesis of positively charged carbon nanoparticles

The precursor material chosen was a commercially available pre-functionalised carbon black dye, Emperor 2000™, from the Cabot Corporation. The Emperor 2000™ nanoparticles have a sulphonate based surface functionality giving rise to the inherent negative charge. This starting material was first treated with thionyl chloride to create a reactive intermediate of sulphonyl chloride which upon treatment with a range of amine reagents formed various sulphonyl amines (Scheme 2.1). Two amines were initially investigated (Figure 2.4); i) ethylene diamine, a straight chain diamine, with the potential for one protonation site and ii) *tris*-(2-aminoethyl) amine, a branched amine, which would hopefully yield 2 or 3 protonation sites and thus a higher charge. The ethylene diamine terminated carbon nanoparticles were water soluble and were easily dispersed in pure water by low power ultrasound, with suspensions being stable for several months. The *tris*-(2-aminoethyl) amine modified carbon nanoparticles were entirely insoluble in water, possibly due to a high degree of cross-linking between nanoparticles during synthesis and therefore a lower degree of protonation.

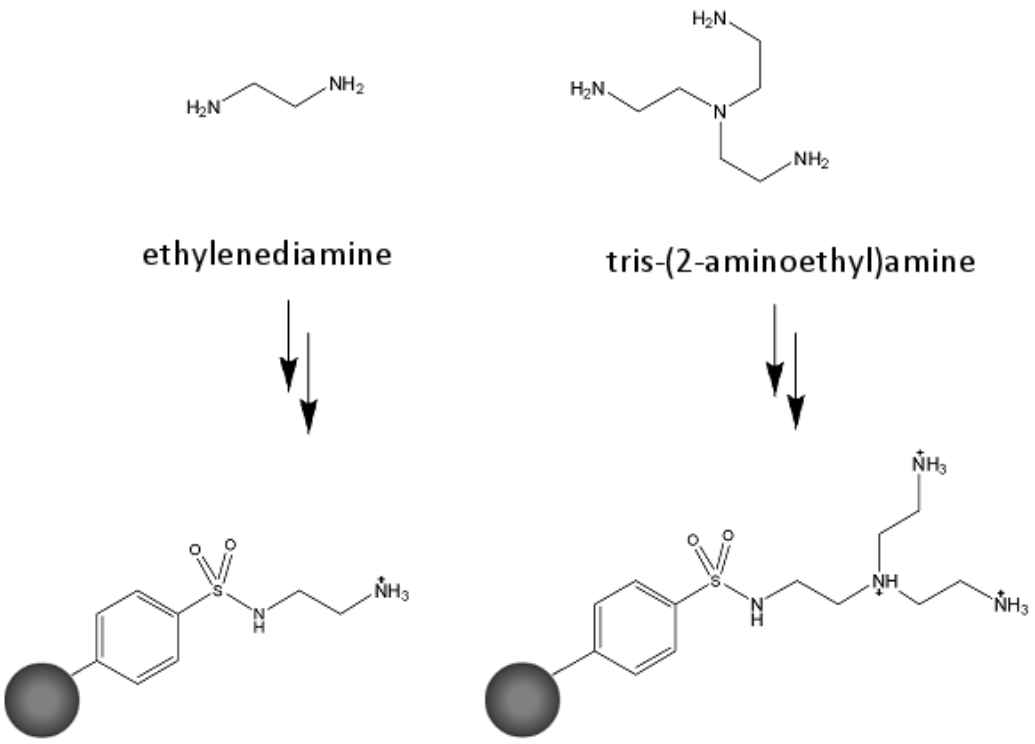

Figure 2.4 The two amines used to modify carbon nanoparticles.

2.3.2 Characterisation of ethylene diamine modified carbon nanoparticles.

2.3.2.1 Atomic force microscopy

A layer by layer approach was used to modify negatively charged glass slides with carbon nanoparticles by using concurrent layers of positively charged nanoparticles (post synthesis) and commercially available negative carbon nanoparticles (Emperor 2000™, Cabot Corporation). The glass was first cleaned with washes of acetone, ethanol and distilled water under sonication conditions. This built a porous carbon film on the glass slides without the need for polymeric binders. The carbon film was visible as a darkening of the affected area after the application of approximately 20 layers of carbon.

Atomic force microscopy (AFM) was used to visualise a single layer of positively charged carbon nanoparticles on the surface of a glass slide (Figure 2.5A). Carbon aggregate microstructures were visible by AFM on the glass surface, showing that the carbon nanoparticles were positively charged as they electrostatically affix to the negative glass. When compared with negatively charged Emperor 2000™ nanoparticles no adhesion to glass was

seen. AFM images were also taken for a 20 layer 100% carbon film (10 layers of positively and 10 layers of negatively charged carbon) terminating in negatively charged Emperor 2000™ (Figure 2.5C). The images show clustered carbon aggregates on the glass surface with height variations of 40 – 50 nm, showing that the carbon coating is very rough.

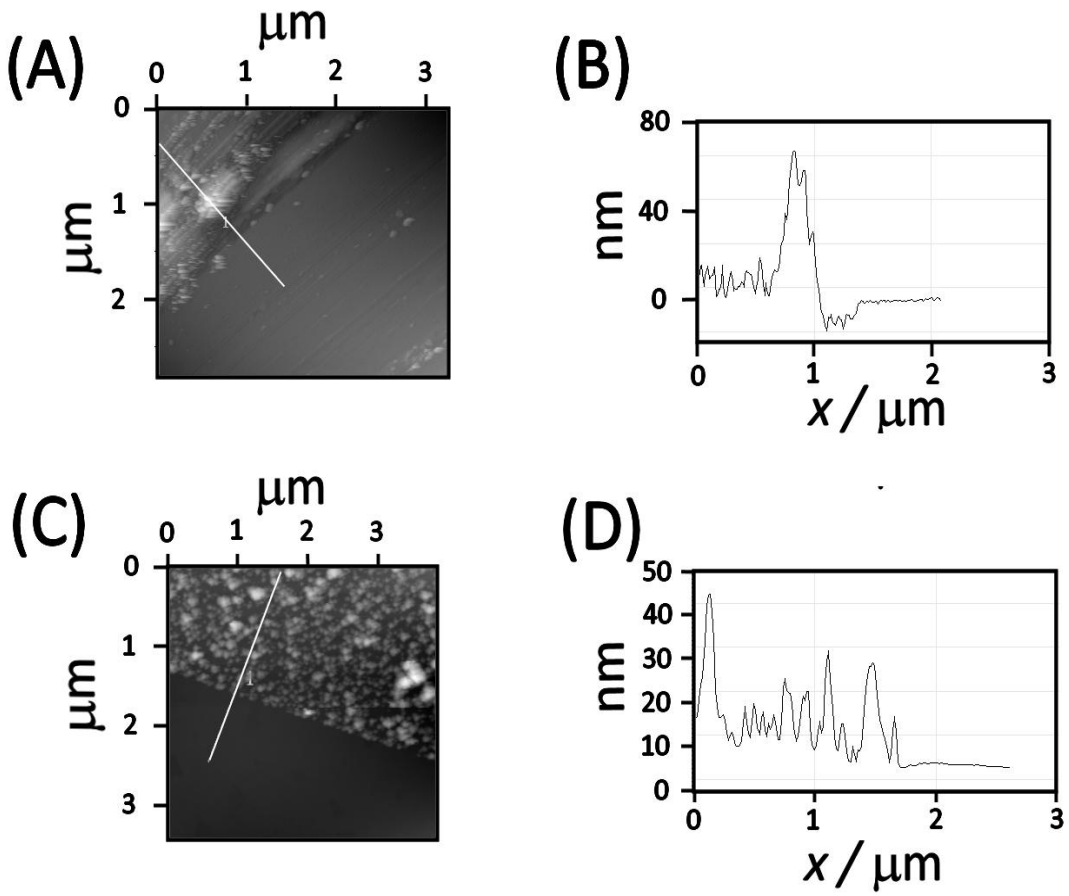

Figure 2.5 (**A)** AFM image of 1 layer of cationic carbon nanoparticles. **(B)** Height variation along the path shown in A. **(C)** AFM image of a 20 layer 100% carbon film. **(D)** Height variation along the path shown in C.

2.3.2.2 Zeta potential

The zeta potential is described as the potential difference between a layer of bound solvent to a surface and a point beyond the double layer in solution and is measured in mV. This technique is most useful when applied to various samples as a measure of relative charge. The zeta potential not only determined the relative surface charge of nanoparticles in solution but also gave an idea of their colloidal stability. A colloidal solution is stable if the particles are sufficiently small, with a sufficiently large surface charge to

cause enough repulsion to overcome flocculation forces. Attractive Van der Waals forces can act over only a very small distance so particles must come into close proximity in order to interact attractively. With highly charged surfaces, the electronic double layer has a much larger range and will cause repulsion of similarly charged molecules, not allowing surfaces close enough for attractive forces to act.

The zeta potential of the negatively charged Emperor 2000™ nanoparticles was measured to be -44.5 mV and is thus proven to be negatively charged. With an average particle diameter of *ca.* 10nm a colloid of good stability was formed. The ethylene diamine functionalised positive nanoparticles were measured to have a zeta potential of +29.8 mV proving that these nanoparticles were positively charged and form a moderately stable colloid. For comparison the zeta potential of SiO_2 nanoparticles has been found to be *ca.* -35 mV (at pH 7).[33] The discrepancy maybe attributed to less than 100% conversion of either or both steps of the synthesis, less than 100% protonation or of aggregates of several nanoparticles in solution masking some of the positive charges. These shortcomings were deemed to be insignificant for further experimentation given the substantial conversion to a highly charged nanoparticle of good colloidal stability.

2.3.2.3 Raman spectroscopy

Raman spectroscopy measurements were also undertaken to get an idea of the nature of the composition of the nanoparticles and it was shown that a well defined G mode peak appeared at *ca.*1576 cm^{-1} suggesting an ordered graphitic structure with a low number of defects. This technique is not however surface sensitive and gave information only about the bulk carbon.

2.3.2.4 X-ray photoelectron spectroscopy (XPS)

The most useful method for determining the surface composition of the newly synthesised carbon nanoparticles was the use of XPS. Unlike many other spectroscopic techniques, XPS showed very clear peaks consistent with the presence of atoms in certain structural circumstances giving a fingerprint of atomic composition. This meant that the high level of carbon intrinsic in any technique is contained to a secluded part of the spectrum, without

overshadowing the far less abundant surface attached atoms. XPS is concerned with the binding energy of core shell electrons, which are far less easily influenced by environment and thus give rise to single diagnostic peaks for atomic identity.

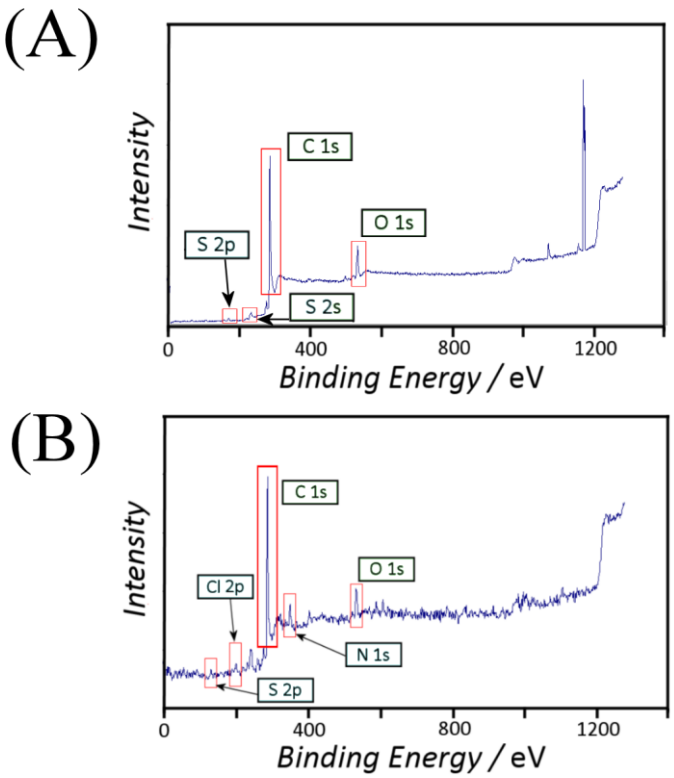

Figure 2.6 XPS spectra of **(A)** Emperor 2000 negatively charged nanoparticles and **(B)** ethylene diamine substituted positively charged carbon nanoparticles.

The XPS spectra shown in Figure 2.6 represent the survey scans for both the Emperor 2000™ starting material (A) and the ethylene diamine modified positive product (B). The survey scans are fast scans over a wide binding energy range and are useful for identifying the presence or absence of key elements. From the spectra shown in Figure 2.6 it was clear that the positively charged product material contained nitrogen atoms, not found in the starting material, at *ca.* 400 eV representing the 1s core shell electrons. With a more detailed survey of this region it was seen that the nitrogen 1s peaks were split into two peaks, at 394.7 eV and 400.8 eV, with a separation which suggested a protonated and unprotonated amine (Figure 2.7C), as was expected in the dry form of the nanoparticles. Interestingly, the product nanoparticles also showed a slight chlorine 2p peak, suggesting the

presence of chloride counter ions associated with the protonated amine sites. It was unlikely that this peak reflected unreacted sulphonyl chloride since this functionality would be highly unstable and liable to hydrolysis.

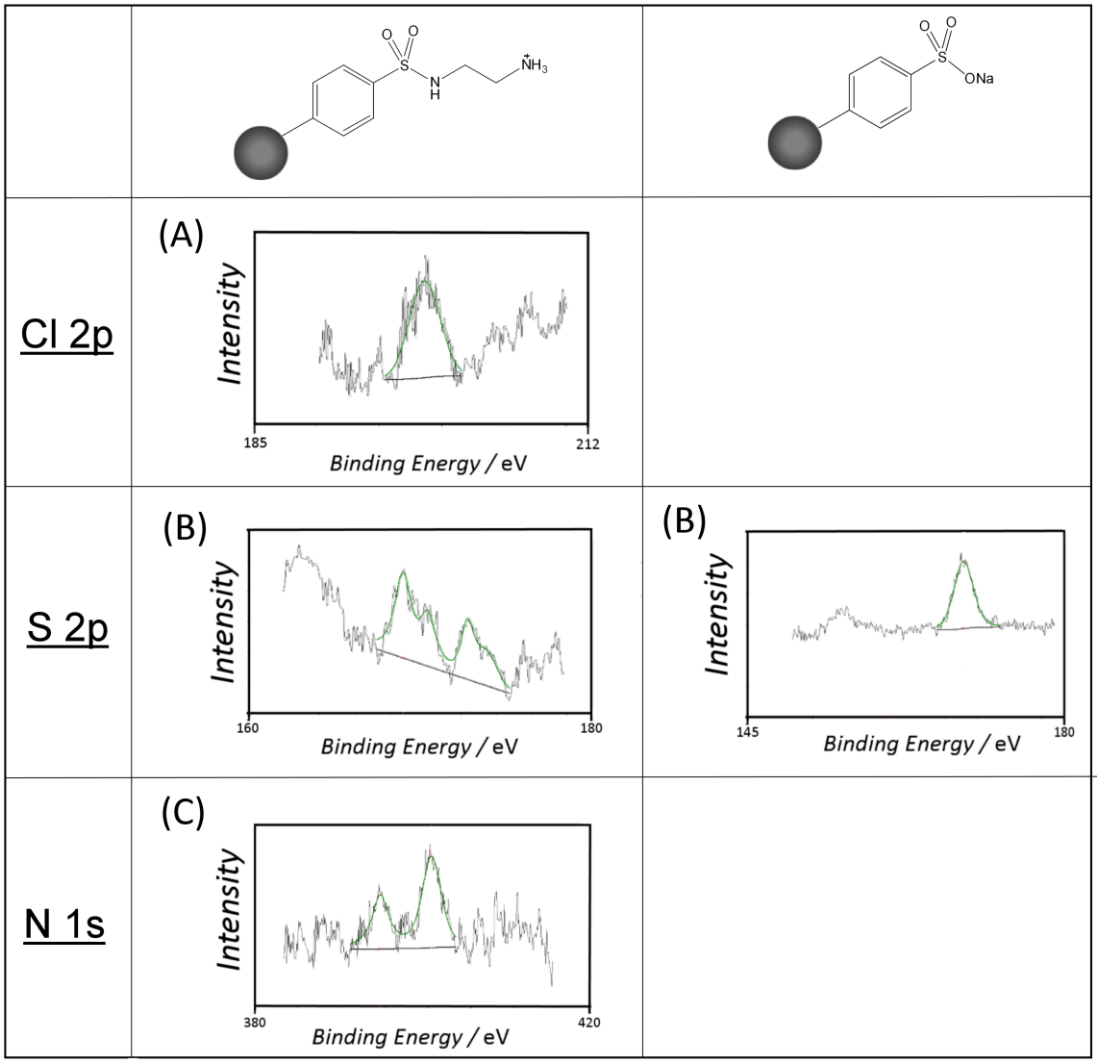

Figure 2.7 XPS data for Emperor 2000 and ethylene diamine modified carbon nanoparticles with slow scans for the regions associated with **(A)** Cl 2p **(B)** S 2p and **(C)** N 1s. Spectra are fitted by prediction software to elucidate different atomic environments.

When analysing the sulphur 2p peaks there was a key difference between the Emperor 2000™ nanoparticles and the ethylene diamine modified alternative. The Emperor 2000™ nanoparticles showed only a single S 2p peak, whereas the ethylene diamine modified nanoparticles showed a number of adjacent peaks. This result was possibly due to some protonation of the sulphonamide or, more likely due to some Emperor 2000™ starting material still being present. The key result from this technique was that a ratio

of 2 : 1 of nitrogen to sulphur was found which is further strong evidence that the surface modified product was indeed correct.

2.3.3 Capacitance Analysis of Cationic Carbon Nanoparticles

The capacitance is defined as the ability of a material to store charge and is an important parameter to characterise new electrode modifying materials. Since capacitive currents appear in voltammetric techniques as a background current it is often detrimental to electroanalytical techniques, masking very low faradaic responses of analytes in low concentration.

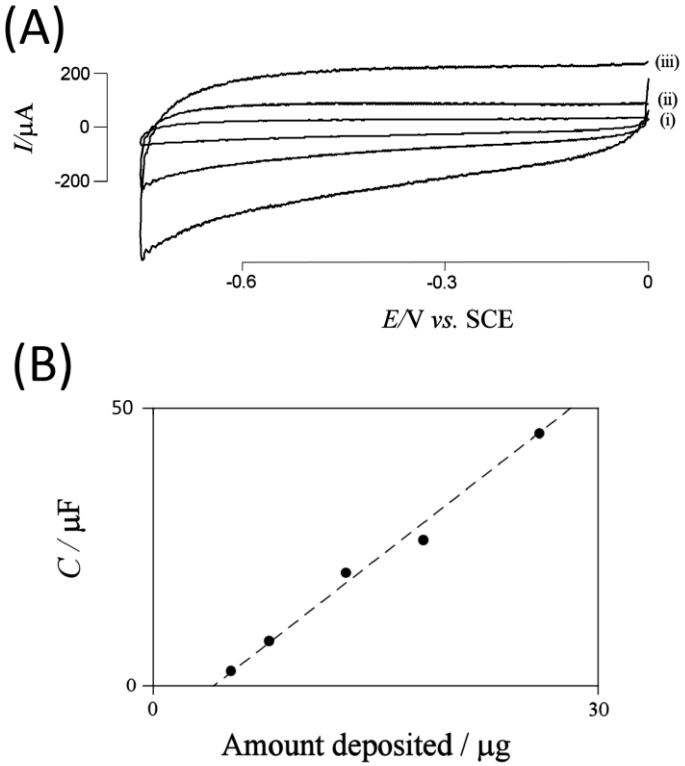

Figure 2.8 (A) Cyclic voltammograms showing the capacitive response of cationic carbon nanoparticles at a scan rate of 10 mVs^{-1} with a modified 3mm diameter glassy carbon electrode for i)4.6 μg ii) 7.0 μg and iii) 11.7 μg. **(B)** A plot of the capacitance against the mass of carbon nanoparticles used.

The capacitance is measured as the current difference between oxidation and reduction waves divided by the scan rate. For the ethylene diamine modified nanoparticles the capacitive responses were well defined and a plot of capacitance against the mass of carbon nanoparticles in the film was plotted, in Figure 2.8B, showing a linear relationship. The intercept of the plot would suggest an impossible negative value for unmodified glassy carbon so

it may be assumed that at small depositions losses of material are possible with further additions yielding better adhesion. The carbon nanoparticles were attached as a film onto glassy carbon electrodes, as described in Section 2.4. with the volume of the water solution determining the mass of nanoparticles attached. From this linear relationship a specific capacitance can be found of 3.3 Fg^{-1}, which was moderate compared to more structured carbon nanomaterials but consistent with their magnitudes.[34]

2.3.4 Cyclic voltammetry of adsorbed indigo carmine on cationic carbon nanoparticles: surface coverage

The amine terminated nanoparticle surface was believed to be protonated over a wide pH range in aqueous solution and thus becoming cationic. Indigo carmine was employed as an anionic binding ion, a two electron reversible redox probe and a pH sensitive surface modifier. Indigo carmine is dianionic and undergoes a reversible two electron / two proton redox process (Scheme 2.2) and by the procedure described in Section 2.5 the cationic carbon nanoparticles surface was modified with indigo carmine redox probes.

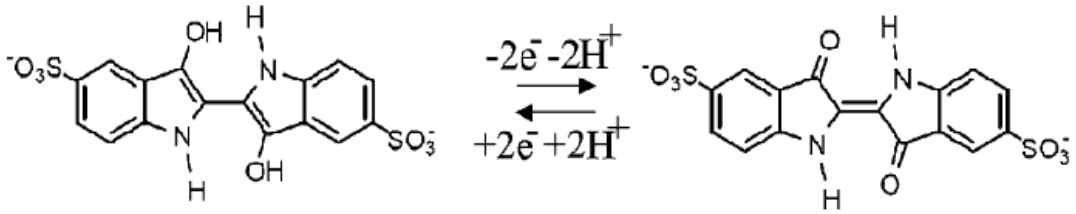

Scheme 2.2. The reduction of indigo carmine by a $2e^-/2H^+$ process pH < 7.7.

Voltammetry was conducted with a three electrode configuration in an aqueous 1 M $NaNO_3$ solution, after being degassed with inert argon for several minutes. The voltammetry shown in Figure 2.9A was typical of a surface attached redox species, with no diffusion controlled region being visible and no peak to peak separation. The redox signal also appeared quite stable, with very little drop in Faradaic charge over 20 scans (not shown), suggesting that almost no material was lost into the aqueous solution by leaching. A surface attached signal was further confirmed by Figure 2.9B which showed a linear agreement of peak current with scan rate. A reversible

diffusion controlled process would instead show a linear relationship of peak current with the square root of scan rate.

The charge associated with the redox process was defined by the area under the Faradaic portion of the voltammogram and should be the same for both oxidative and reductive peaks, assuming a completely reversible process. In this work the oxidative charge was concentrated on to eliminate possible error associated with the reduction of trace amounts of oxygen, which may cause unwanted background currents. This charge was directly related to the number of indigo carmine groups present, since the process involved two electrons. With the charge on an electron being known, the number of indigo carmine molecules attached to the surface was calculated with this corresponding to half the number of positive sites, due to the indigo carmine being a dianion. Initially, a saturating concentration of indigo carmine was applied to the surface by using a 1 mM dipping solution. This ensured that 100% of the positive sites available were able to be detected. Figure 2.9C shows a plot of the mass of carbon nanoparticles immobilised on the surface against the charge showing, as expected, a linear relationship. However, with a very large amount of nanoparticles present the charge appeared less than predicted, which was rationalised by the permeability of the film by indigo carmine becoming more difficult, with some deeper positively charged sites not able to associate with indigo carmine.

For further investigation, the concentration of the indigo carmine dipping solution was changed with a constant amount of carbon nanoparticles. By monitoring the change in charge for each concentration a Langmuir plot was realised as a first approximation of the binding. By fitting a Langmuir graph to this plot a rough binding constant for the indigo carmine nanoparticles interaction was calculated and the total number of binding sites found. This procedure was followed for two different masses of carbon nanoparticles, as shown in Figure 2.9D/E, and has lead to a binding constant of *ca.* 4000 $mol^{-1}dm^3$. This value was comparable with a similar study by Rassaei mentioned previously.[23b]

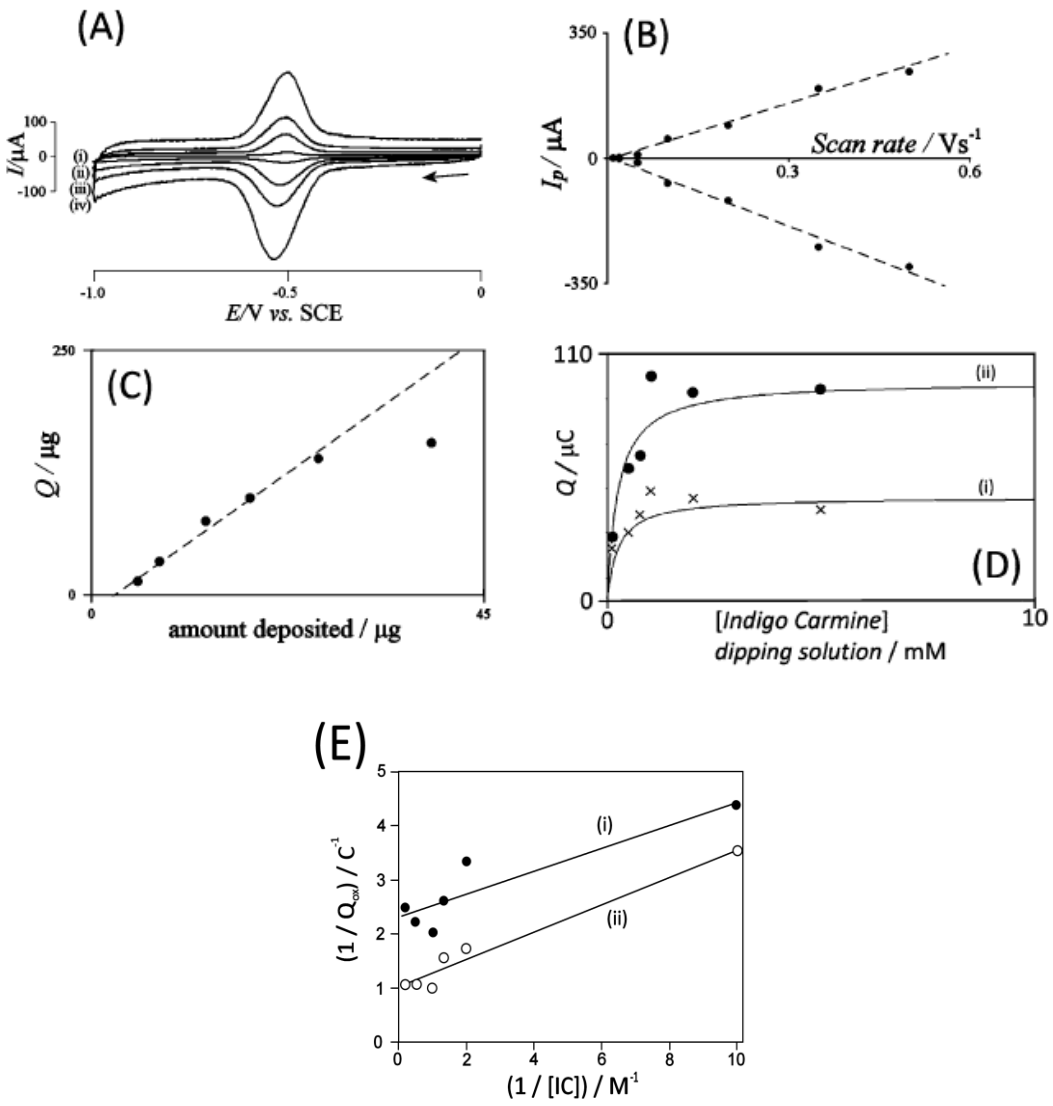

Figure 2.9 **(A)** Cyclic voltammograms of surface attached indigo carmine (1mM dipping solution for 5mins) at scan rates (i) 50 mVs^{-1}, (ii) 100 mVs^{-1}, (iii) 200 mVs^{-1}, and (iv) 500 mVs^{-1} obtained with a deposit of 7 mg of ethylene diamine functionalised carbon nanoparticles at a 3 mm diameter glassy carbon electrode in 1 M $NaNO_3$. **(B)** Plot of anodic peak current for indigo carmine reduction versus scan rate. **(C)** Plot of the anodic peak charge for indigo carmine reduction versus amount of carbon nanoparticles deposited. **(D)** Plots of the anodic peak charge for indigo carmine reduction versus the concentration in the indigo carmine dipping solution for (i) 7 mg and (ii) 16 mg carbon nanoparticle deposit. **(E)** Linear plot of Langmuir isotherm for (i) 7 mg and (ii) 16 mg.

From the Langmuir plot (Figure 2.9D), it was also possible to confirm a saturating concentration of indigo carmine and thus a number of positive binding sites as described previously. Assuming a density of carbon

nanoparticles was 2.2 gcm^{-3}, with an average diameter of 12 nm, it was possible to calculate the number of carbon nanoparticles in a film of a given mass and thus the number of cationic sites per carbon nanoparticle. Given these assumptions it was calculated that there were 600 – 700 cationic sites per carbon nanoparticle, giving a reasonable 'molecular footprint' of 75 $Å^2$ for the sulphonamide functionality.

2.3.5 Cyclic voltammetry of adsorbed indigo carmine on cationic carbon nanoparticles: pH effects

The final effect investigated with the indigo carmine attached carbon nanoparticles was the effect of pH. Since the indigo carmine couple involved the transfer of two protons as well as two electrons, at pH 7, it was anticipated that a significant effect of pH would be seen.

The effect of pH on the midpoint potential of the surface immobilised redox couple of indigo carmine is summarised in Figure 2.10A. It was seen that with increasing pH, less proton availability meant that the redox process became more difficult and a higher overpotential was required for reduction, as shown by a more negative reduction process occurring. The shift of a proton dependent signal with pH is termed the Nernstian shift. If no protons are involved in the redox process then no such shift occurs and the redox couple is pH independent. For a two electron/ two proton process, such as that shown for indigo carmine, the midpoint potential (defined as halfway between the oxidative and reductive peak potentials) is expected to shift by 57 mV per pH unit at room temperature.

In Figure 2.10B this trend was seen at acidic pHs between pH 1 and pH 7 by reduction Scheme 2.2. However at more alkaline pH a shift of about half that number was seen, which now corresponded to a two electron/ one proton reduction process (Scheme 2.3). The implication of this change in gradient was that in the *leuco*-indigo carmine, one of the protonation sites now remained unprotonated and thus the pKa value of this site was estimated to be about 7.7, which compared favourably to a literature value found of 8.[35] By extrapolation of the literature it would be expected that a second change in gradient should occur around pH 11, representing the second *leuco*-indigo

protonation site becoming deprotonated at a pKa of *ca.* 11. The mechanism for this range is depicted in Scheme 2.4 and since it would now be a two electron/ zero proton process a pH independent signal would be anticipated.

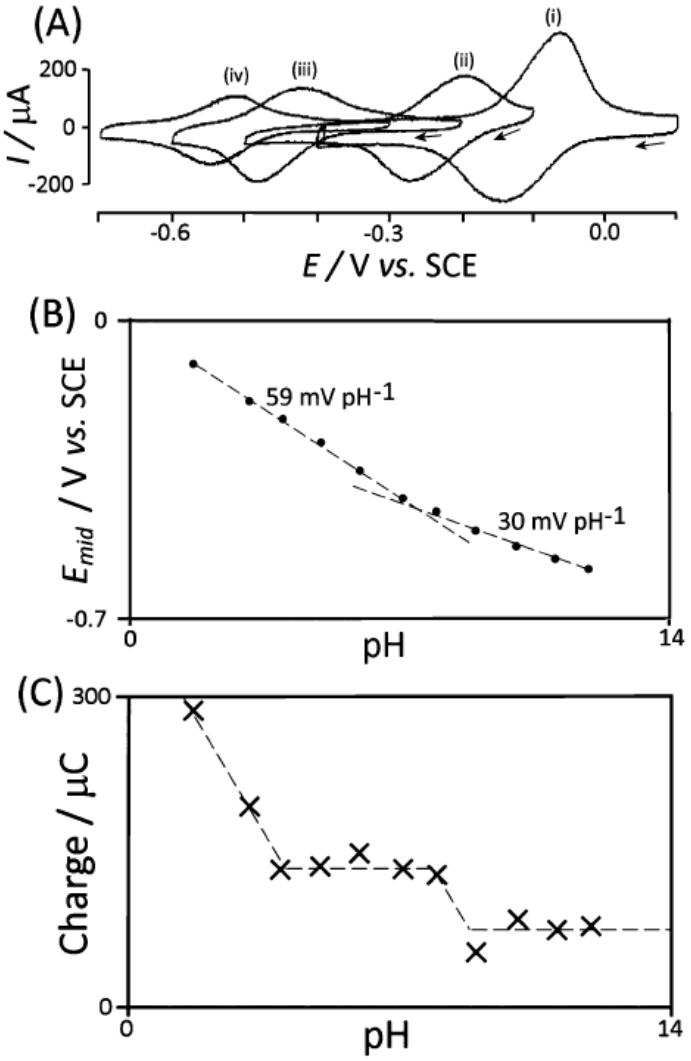

Figure 2.10 (**A)** Cyclic voltammograms for the reduction of indigo carmine (adsorbed from a 1 mM dipping solution of indigo carmine in Britton–Robinson buffer onto 16 µg carbon nanoparticles at a 3 mm diameter glassy carbon electrode and a scan rate of 100 mVs^{-1}) immersed in 0.12 M Britton–Robinson at pH (i) 2, (ii) 4, (iii) 8, and (iv) 10. **(B)** Plot of the midpoint potential ($E_{mid}=1/2E_p^{ox}+1/2E_p^{red}$) against pH. **(C)** Plot of the anodic charge for the indigo carmine reduction against pH.

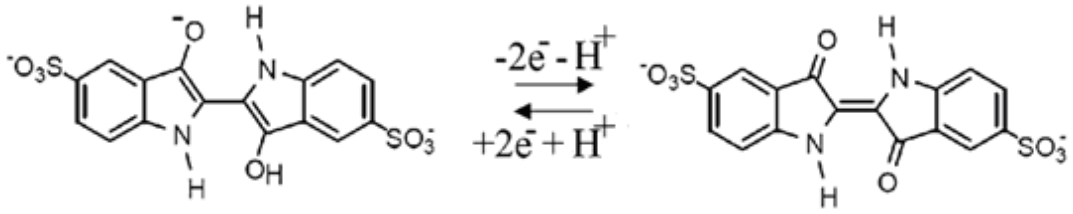

Scheme 2.3 Reduction of indigo carmine by a $2e^-/1H^+$ process (pH > 7.7).

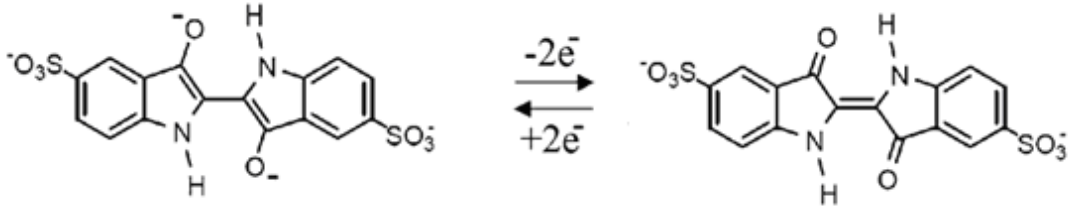

Scheme 2.4 Reduction of indigo carmine by a $2e^-$ process with no proton transfer (not seen at any pH during this study).

By considering Figure 2.10C, it is seen that the anodic charge also changes as a function of the pH, thus showing that the number of positive binding sites is also a function of pH. This trend was not unexpected, since it was the protonation of the amine functionality that afforded the positive surface charge. Thus, the degree of protonation depended on the pH and dictated the number of positive binding sites. In the pH range between 4 and 8 a steady anodic charge was seen, which suggested no change in the number of binding sites with the terminal amine remaining protonated in this pH range. At lower pH (below pH 4) a linear increase in the anodic charge was found suggesting that more cationic sites were emerging at lower pH. This result was explained by the protonation of the amide functionality, as well as the terminal amine. This protonation required a much lower pH to occur but this possibility has been suggested previously by the XPS measurements presented earlier (Section 2.3.2.4). Conversely at pH higher than 8 it was found that the charge, and thus number of cationic sites, decreased. This result was explained by the deprotonation of the terminal amine at these pH values and in this case the pKa of the terminal amine was estimated to be roughly 9.

2.4 Conclusions

In conclusion, positively charged nanoparticles were synthesised in a facile and reliable two step process *via* a sulphonyl chloride intermediate. This intermediate was shown to be substituted by simple amine groups and could lead to alternative modifications in the future. The positive carbon nanoparticles were analysed by zeta potential comparison, atomic force microscopy, Raman spectroscopy and X-ray photoelectron spectroscopy. The voltammetry of ionically attached indigo carmine on the cationic carbon nanoparticles lead to an estimate of the number positive binding sites being *ca.* 400 per nanoparticle. For further applications the nanoparticles were shown to be useful in layer by layer techniques for the catalytic reduction of oxygen by enzymes, in collaboration with the Institute of Physical Chemistry at the Polish Academy of Sciences.[36]

2.5 References

(1) Harris, P. J. F. *Philosophical Magazine* **2004**, *84*, 3159

(2) (a) Chen, P. H.; Fryling, M. A.; McCreery, R. L. *Analytical Chemistry* **1995**, *67*, 3115; (b) Chen, P. H.; McCreery, R. L. *Analytical Chemistry* **1996**, *68*, 3958.

(3) Pleskov, Y. V. *Russ. J. Electrochem.* **2002**, *38*, 1275.

(4) Alehashem, S.; Chambers, F.; Strojek, J. W.; Swain, G. M.; Ramesham, R. *Analytical Chemistry* **1995**, *67*, 2812.

(5) McCreery, R. L. *Chemical Reviews* **2008**, *108*, 2646.

(6) Swain, G. M.; Ramesham, R. *Analytical Chemistry* **1993**, *65*, 345.

(7) Swain, G. M. *Journal of the Electrochemical Society* **1994**, *141*, 3382.

(8) Lawrence, N. S.; Pagels, M.; Meredith, A.; Jones, T. G. J.; Hall, C. E.; Pickles, C. S. J.; Godfried, H. P.; Banks, C. E.; Compton, R. G.; Jiang, L. *Talanta* **2006**, *69*, 829.

(9) Compton, R. G.; Foord, J. S.; Marken, F. *Electroanalysis* **2003**, *15*, 1349.

(10) Panizza, M.; Cerisola, G. *Electrochimica Acta* **2005**, *51*, 191.

(11) Banks, C. E.; Compton, R. G. *Analyst* **2006**, *131*, 15.

(12) Kneten, K. R.; McCreery, R. L. *Analytical Chemistry* **1992**, *64*, 2518.

(13) Williams, C. G.; Edwards, M. A.; Colley, A. L.; Macpherson, J. V.; Unwin, P. R. *Analytical Chemistry* **2009**, *81*, 2486.

(14) Banks, C. E.; Compton, R. G. *Anal. Sci.* **2005**, *21*, 1263.

(15) Iijima, S. *Nature* **1991**, *354*, 56.

(16) Day, T. M.; Unwin, P. R.; Wilson, N. R.; Macpherson, J. V. *Journal of the American Chemical Society* **2005**, *127*, 10639.

(17) Pumera, M. *Chemistry-A European Journal* **2009**, *15*, 4970.

(18) Ahammad, A. J. S.; Lee, J. J.; Rahman, M. A. *Sensors* **2009**, *9*, 2289.

(19) Li, J.; Ng, H. T.; Cassell, A.; Fan, W.; Chen, H.; Ye, Q.; Koehne, J.; Han, J.; Meyyappan, M. *Nano Letters* **2003**, *3*, 597.

(20) Downard, A. J. *Electroanalysis* **2000**, *12*, 1085.

(21) Amiri, M.; Shahrokhian, S.; Marken, F. *Electroanalysis* **2007**, *19*, 1032.

(22) Amiri, M.; Shahrokhian, S.; Psillakis, E.; Marken, F. *Analytica Chimica Acta* **2007**, *593*, 117.

(23) (a) Rassaei, L.; Bonne, M. J.; Sillanpaa, M.; Marken, F. *New Journal of Chemistry* **2008**, *32*, 1253; (b) Rassaei, L.; Sillanpaa, M.; Marken, F. *Electrochimica Acta* **2008**, *53*, 5732.

(24) Pundir, C. S.; Chauhan, N.; Rajneesh; Verma, M.; Ravi *Sens. Actuator B-Chem.* **2011**, *155*, 796.

(25) Pan, W.; Zhang, X.; Ma, H.; Zhang, J. *Journal of Physical Chemistry C* **2008**, *112*, 2456

(26) Yang, M. Q.; He, J. H.; Hu, X. C.; Yan, C. X.; Cheng, Z. X.; Zhao, Y. Q.; Zuo, G. M. *Sens. Actuator B-Chem.* **2011**, *155*, 692.

(27) Mahouche-Chergui, S.; Gam-Derouich, S.; Mangeney, C.; Chehimi, M. M. *Chemical Society Reviews* **2011**, *40*, 4143.

(28) Barriere, F.; Downard, A. J. *Journal of Solid State Electrochemistry* **2008**, *12*, 1231.

(29) (a) Liu, G. Z.; Chockalingham, M.; Khor, S. M.; Gui, A. L.; Gooding, J. J. *Electroanalysis* **2010**, *22*, 918; (b) Breton, T.; Belanger, D. *Langmuir* **2008**, *24*, 8711.

(30) Pust, S. E.; Szunerits, S.; Boukherroub, R.; Wittstock, G. *Nanotechnology* **2009**, *20*.

(31) Andrieux, C. P.; Gonzalez, F.; Saveant, J. M. *Journal of the American Chemical Society* **1997**, *119*, 4292.

(32) (a) Evrard, D.; Lambert, F.; Policar, C.; Balland, V.; Limoges, B. *Chemistry-a European Journal* **2008**, *14*, 9286; (b) Rana, S.; Yoo, H. J.; Cho, J. W.; Chun, B. C.; Park, J. S. *Journal of Applied Polymer Science* **2011**, *119*, 31.

(33) Hees, J.; Kriele, A.; Williams, O. A. *Chemical Physics Letters* **2011**, *509*, 12.

(34) Simon, P.; Gogotsi, Y. *Nature Materials* **2008**, *7*, 845.

(35) Etters, J. N. *Journal of the Society of Dyers and Colourists* **1993**, *109*, 251.

(36) Szot, K.; Watkins, J. D.; Bull, S. D.; Marken, F.; Opallo, M. *Electrochemistry Communications* **2010**, *12*, 737.

3. Covalent Modification of Carbon Nanoparticles and Pore Reactivity of 9,10-Anthraquinone

Contents

Aims

- To use the terminal amine of the deprotonated cationic carbon nanoparticles as a synthetic handle for further modification by covalent substitution reactions.
- To characterise the covalently bound redox probe anthraquinone by cyclic voltammetry and analyse changes in behaviour with pH and scan rate.
- To assess the number of covalent binding sites per nanoparticle by analysis of anthraquinone voltammetry.

Publication

Watkins JD, Lawrence K, Taylor JE, James TD, Bull SD and Marken F, *Electroanalysis*, **2011**, 23, 1320 – 1324.

CHAPTER 3: Covalent Modification of Carbon Nanoparticles and Pore Reactivity of 9,10-Anthraquinone

3.1 Introduction

In Chapter 2 traditional and nanoscale carbon materials in electrochemistry were introduced and discussed with their relative benefits and limitations. It was shown that carbon nanoparticles represent an excellent balance of functionality and cost compared to carbon nanotubes and graphene. Some surface modifications of carbon nanoparticles were detailed in Section 2.1.3 when starting from an unfunctionalised surface. For ease however, a pre-functionalised nanoparticle was used as a synthetic starting point, which by functional group interconversion lead to a facile surface modification.

In this chapter a further surface modification by the anthraquinone redox probe is presented. Anthraquinone is a useful functional group for redox processes and is readily incorporated onto surfaces. The common uses of anthraquinone based redox probes are pH detection,[1] the catalytic reduction of oxygen[2] and electrochemical mediation.[3]

One of the most common electrochemical sensors is for the detection of pH, which can be measured accurately and simply even in harsh conditions. For this type of sensor a redox probe which also undergoes a proton transfer over a wide pH range as part of a fully reversible electrochemical signal is required. Since the redox process involves a known transfer of protons as well as electrons, a shift in the reversible potential will occur with pH. More acidic conditions will cause a shift towards positive potential. A commonly used probe is anthraquinone (AQ) which undergoes a reversible two electron, two proton process, as shown in Scheme 3.1. In conjunction with a non pH active redox probe, such as ferrocene, a sensitive reference electrode free pH sensor can be made as an immobilised film,[1a] attached to a carbon nanomaterial[1b] or grafted onto electrode surfaces as shown previously.[4]

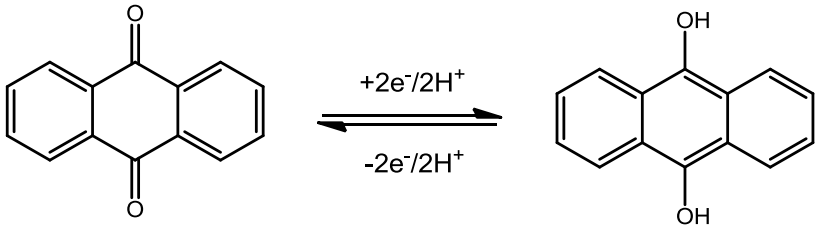

Scheme 3.1 The two electron / two proton reversible redox process for anthraquinone

It is also well known that AQ can act as an effective mediator for catalytic oxygen reduction and so an electrode modified with AQ can also be used in this application.[4] The catalytic reduction of oxygen is a widely studied electrochemical system for applications in fuel cell research and peroxide production. Schiffrin and co workers present several studies[2b,c] performed on a rotating ring disc electrode for electrochemically grafted anthraquinone by the diazonium method. In this case, where the rotating disc acts as the generator and the electrode ring as a peroxide sensor, it was shown that this procedure yielded quantitative amounts of peroxide. From kinetics, it was also shown that two adjacent anthraquinone groups were required for the catalytic reduction of one oxygen molecule. The mechanism of such catalytic reductions is *via* the electro-generated semi-quinone which can bind molecular oxygen before being further reduced, as investigated by Maia *et al.* [2a]

The use of anthraquinone as a redox mediator has been studied in solution and as an immobilised system for catalytic reduction processes. One such example, by Vuorema *et al.*[3] showed that the incorporation of anthraquinone into an indigo dye allowed the catalytic reduction of indigo by glucose under sonotrode conditions.

Anthraquinone has been used, with further functionalisation, as a redox tag for electrochemical detections. For example Kowalczyk *et al.*[5] have found that by functionalising with known intercalating groups the AQ couple can be used as a DNA hybridisation sensor.

This chapter seeks to incorporate the useful redox probe anthraquinone onto a conducting carbon nanoparticle. This new nanoparticle was useful for the construction of highly porous three dimensional carbon rich films for sensing

and mediator applications. The methodology presented represents a new surface modification technique for carbon nanoparticles, by using a highly efficient and simple modification of the existing cationic carbon nanoparticles introduced in Chapter 2.

3.2 Experimental

For details of reagents and equipment used please refer to Section 2.2 in the previous nanoparticles section. The procedures for the synthesis of amine functionalised nanoparticles have been previously discussed in Section 2.2.3. The amine functionalised nanoparticles were used as the initial step in the anthraquinone functionalisation summarised in Scheme 3.2A below.

3.2.1 Procedure I: further modification of carbon nanoparticles by anthraquinone

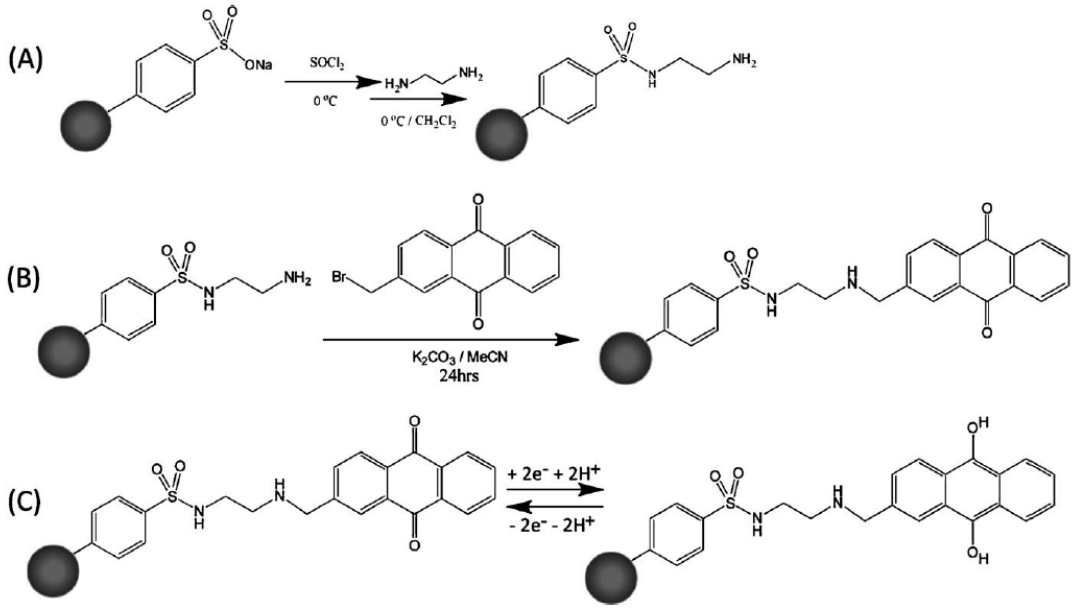

Scheme 3.2 (A) Modification of Emperor 2000 nanoparticles with ethylene diamine. **(B)** Further modification of ethylene diamine nanoparticles with anthraquinone. **(C)** The reversible $2e^-/2H^+$ redox process of surface attached anthraquinone.

For step B (see Scheme 3.2) 0.5 g of ethylene diamine surface-modified carbon nanoparticles were sonicated for 30 minutes in 10 cm^3 acetonitrile before 0.5 g of potassium carbonate was added. This suspension was stirred for 10 minutes at room temperature to deprotonate the nanoparticles, and then 0.5 g 2-bromomethyl-anthraquinone was added and the mixture left to

stir for 24 hours. The resulting nanoparticle suspension was dried under reduced pressure, and the residue washed with distilled water. The resulting nanoparticles were then washed carefully with dichloromethane to remove unreacted material and the remaining black solid was dried at 60 ^{o}C in air. A black hydrophobic powder (*ca.* 0.1 g) is obtained which is readily dispersed in organic solvents such as ethanol but highly insoluble in aqueous media.

3.2.2 Procedure II: deposition of anthraquinone modified carbon onto glassy carbon electrodes

A dispersion of nanoparticles (2 mg.cm^{-3}) was made by sonication for 30 minutes in ethanol. The resulting suspension was stable for up to one hour and used to deposit 10 μL aliquots of solution onto polished 3 mm diameter glassy carbon electrodes. After evaporation of ethanol in air, non-uniform aggregates were visible on the electrode surface to increase the surface coverage. The resulting modified electrode was treated with multiple coatings of 10 μL nanoparticle solution. The resulting films were stable during measurements in aqueous solution.

3.3 Results and Discussion

3.3.1 Synthesis of covalently modified carbon nanoparticles with anthraquinone

The terminal amine group of the ethylene diamine functionalised carbon nanoparticles can be effectively utilised as a synthetic handle for further covalent modification. This modification was attempted *in situ* using a dipping solution containing a bromomethyl substituted anthraquinone, to be substituted by the amine. This procedure showed very little functionalisation and was more likely to yield functionalisation by intermolecular attraction of the hydrophobic anthraquinone than by covalent modification, so a synthetic approach was instead utilised.

The procedure outlined in Section 3.2.1 was used to couple anthraquinone to the terminal amine by a simple S_N2 substitution reaction. This yielded a new carbon nanoparticle which appeared waxy and was insoluble in water. A

suspension was achieved by sonication in ethanol but the colloid was unstable and required re-sonication before all applications to ensure homogeneity. Furthermore, deposition *via* ethanol yielded less uniform films than the deposition of hydrophilic nanoparticles from water, leading to non uniform coverage of a 3 mm diameter glassy carbon electrode. The resultant film had the appearance of carbon aggregates on the surface and some carbon became immobilised on the inert Teflon© surrounding the active carbon electrode.

3.3.2 Characterisation of anthraquinone modified carbon nanoparticles

3.3.2.1 Cyclic voltammetry of covalently attached anthraquinone on carbon nanoparticles: Surface coverage

Cyclic voltammetry was applied for the surface immobilised anthraquinone particles in order to characterise the surface coverage and reversibility of the redox probe. Anthraquinone undergoes a two electron / two proton reversible redox process in solution and, as shown in Figure 3.1A, appears reversible as a surface attached species.

The voltammetry seen in Figure 3.1A for anthraquinone appeared quite resistive, with a peak to peak separation higher than expected for a surface immobilised redox probe. The reason for this is likely to be a pH gradient within the carbon nanoparticle aggregates. The charge (Faradaic area under the peak) was related to the number of anthraquinone groups attached to the carbon nanoparticle deposit. Figure 3.1B shows the linear relationship between anodic charge and the volume of carbon nanoparticle solution deposited onto the glassy carbon surface. These results suggested a complete reduction of anthraquinone. The gradient of this plot gave a charge of 75 μC per μL of deposition solution and was used to estimate 250 anthraquinone groups per carbon nanoparticle (assuming an average carbon nanoparticle diameter of 12 nm and a density of 2.2 gcm^{-3}). This corresponded to a 'molecular footprint' of 180 $Å^2$ per anthraquinone molecule.

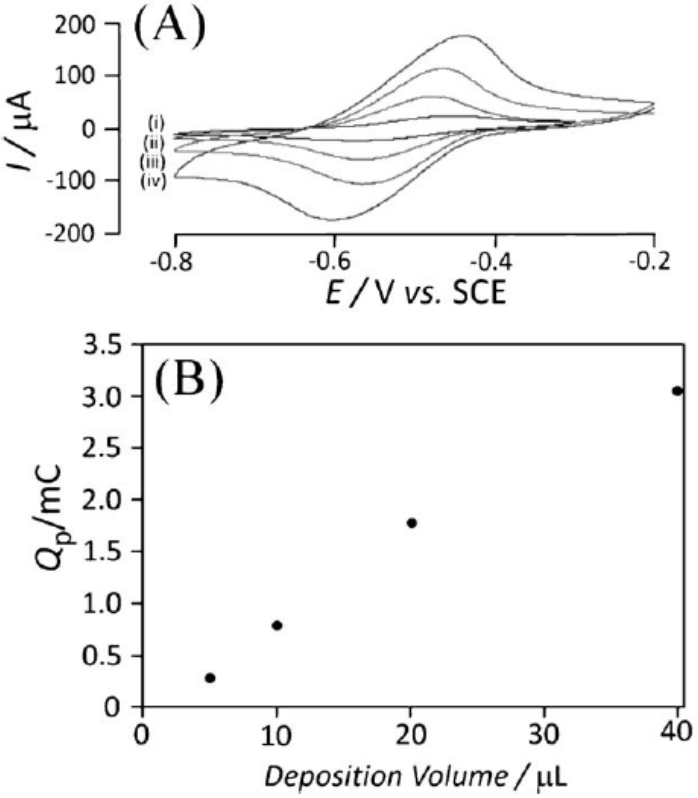

Figure 3.1 (A) Cyclic voltammograms for the reduction of CNP-anthraquinone at 10 mVs^{-1} and various volumes of deposit (i) 5, (ii) 10, (iii) 20, and (iv) 40 µL dispersion of 2 mg cm^{-3} on 3 mm diameter glassy carbon immersed in 0.5 M phosphate buffer pH 7. **(B)** Plot of the anodic peak charge against deposition volume.

Figure 3.2A shows the effect of scan rate on the surface attached anthraquinone redox probe and a plot of the scan rate against the anodic peak current is shown in Figure 3.2B. The relationship of scan rate against anodic peak current was shown to be linear at low scan rates with a negative deviation at much higher scan rates. This suggested that at the low scan rates used to analyse the surface coverage, the conversion of anthraquinone to its reduced form was complete.

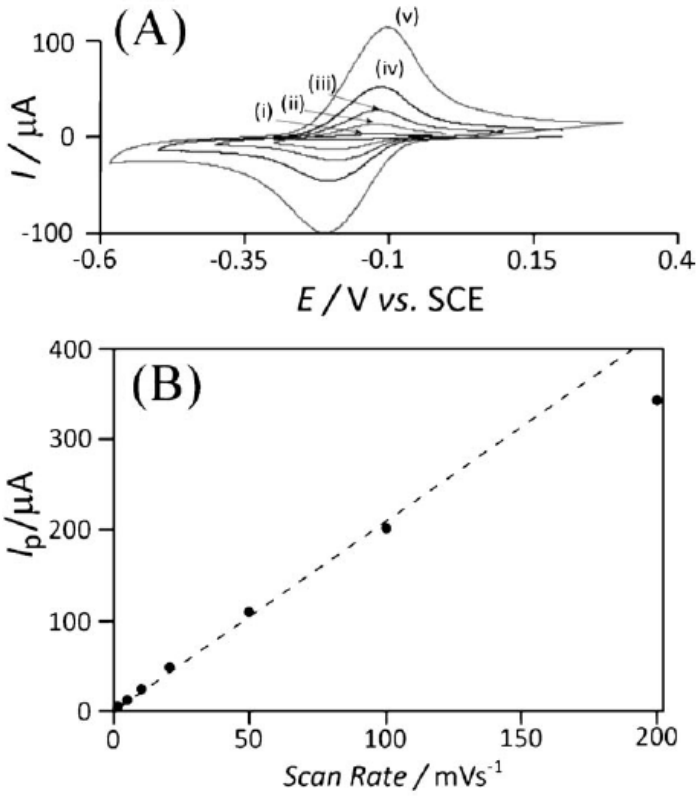

Figure 3.2 (A) Cyclic voltammograms (scan rate (i) 1, (ii) 5, (iii) 10, (iv) 20, and (v) 50 mVs^{-1}) for the reduction of CNP-anthraquinone (deposit of 10 mL dispersion of 2 mg cm^{-3} on 3 mm diameter glassy carbon) immersed in 0.5 M phosphate buffer pH 2. **(B)** Plot of the anodic peak current versus scan rate.

3.3.2.2 Cyclic voltammetry of covalently attached anthraquinone on carbon nanoparticles: pH effects

Much like the ionically bound indigo carmine probe seen at the cationically modified carbon nanoparticles surface (Section 2.3.4), immobilised anthraquinone undergoes a two electron / two proton process and thus displayed a pH dependant redox couple.

Figure 3.3A again shows the anticipated negative shift at higher pH associated with a reversible two electron / two proton process. By plotting the midpoint potential against the pH the anticipated Nernstian shift of 57mV per pH unit was found (Figure 3.3B). Furthermore, Figure 3.3B also shows both the anodic and cathodic peak potential as plotted against the pH, highlighting an interesting trend in the peak shape and peak to peak separation. This trend may also be visualised in Figure 3.3A where the peaks become smaller and broader at certain discrete pH values, with a large peak to peak

separation associated with the poor buffer capacity of phosphate buffers (pH 4.7 and 8.5). Conversely, in high buffer capacity regions (pH2, 7, 12) sharper peaks with a smaller peak to peak separation were seen.

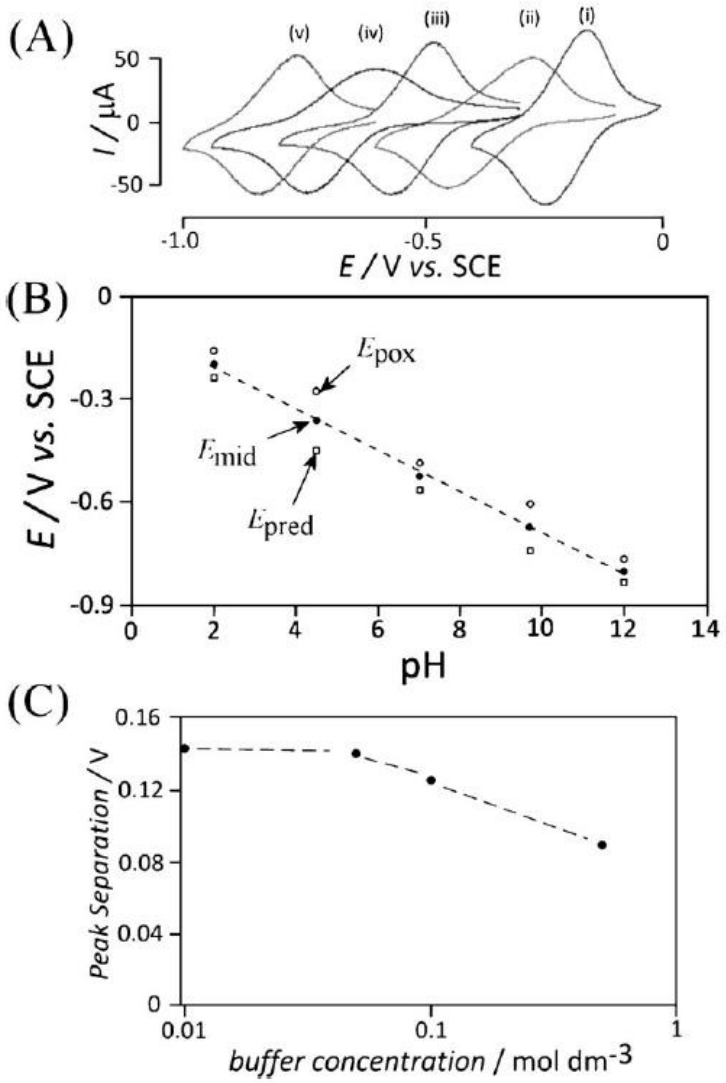

Figure 3.3 (A) Cyclic voltammograms for the reduction of CNP-anthraquinone with deposits of 10 µL dispersion of 2 µgcm^{-3} on 3 mm diameter glassy carbon immersed in 0.5 M phosphate buffer i) pH 2.0, ii) pH 4.5, iii) pH 7.0, iv) pH 9.7, and v) pH 12.0. at a scan rate of 10mVs^{-1} **(B)** Plot of the reduction and oxidation peak potentials and the midpoint potential versus pH. **(C)** Plot of the peak separation between cathodic and anodic peak versus logarithm of phosphate buffer concentration at pH 7.

It was observed that the anthraquinone modified carbon nanoparticles readily formed aggregates with a likely pore size of 2 – 6 nm resulting in an estimated 50% volume of buffer solution within the aggregate. If, as previously calculated, there were 250 anthraquinone groups per carbon nanoparticle then an effective anthraquinone concentration of 0.46 M could

be estimated within the pores. When compared to an effective buffer concentration of 0.92 M, it was envisaged that a pH drift was relatively likely within the pores and was amplified in low buffer capacity conditions. The effect of the buffer concentration is seen in Figure 3.3C, at low buffer concentrations a high peak to peak separation was observed but even at relatively strong buffer conditions an appreciable peak to peak separation was found. The sometimes poor stability of these signals with pH limit the effectiveness of this surface immobilised system in pH sensing applications.

Since the anthraquinone modified nanoparticles still contained secondary amine functionality, it was still possible that they will become positively charged, generating a net positively charge carbon nanoparticle. This meant that large anions may bind to the surface, as seen with indigo carmine, and may also affect the voltammetry shape within the pores.

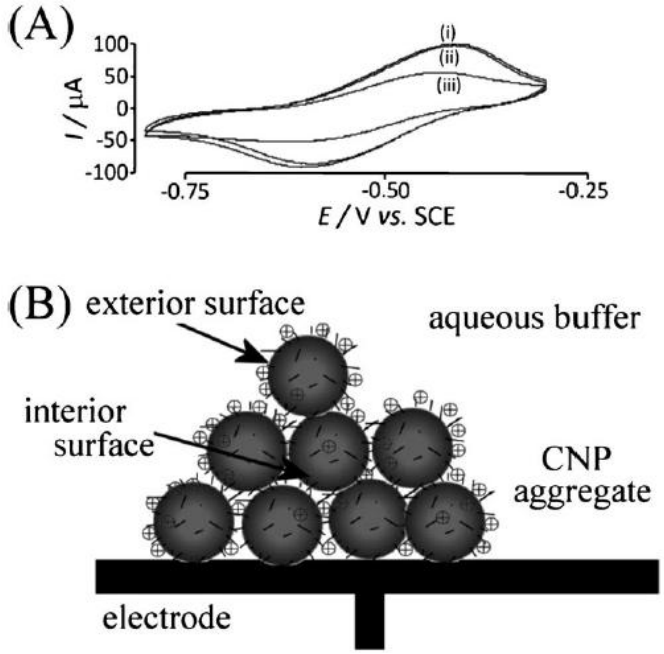

Figure 3.4 (A) Cyclic voltammograms for the reduction of CNP-anthraquinone deposits of 10 µL dispersion of 2 $mg.cm^{-3}$ on 3 mm diameter glassy carbon electrode at 10 mVs^{-1} immersed in 0.1 M phosphate buffer pH 7 (i) without pretreatment, (ii) immersed into aqueous 1 mM NBu_4Cl, rinsed, and dried, and (iii) immersed into aqueous 1 mM $KBPh_4$, rinsed and dried. **(B)** Schematic drawing of the CNP-anthraquinone aggregate on the electrode surface with interior and exterior surfaces showing different reactivity.

Figure 3.4A shows the effects of binding ions on the pore reactivity of the surface immobilised anthraquinone. When the nanoparticle modified electrode was first pre-treated by immersion in a solution of tetrabutylammonium chloride, no effect was seen on the voltammetry, when compared with a non-pre-treated electrode. In this case the large positive ions were unable to bind to the cationic nanoparticles and do not obscure the pore based reaction. However, when pre-treated with potassium tetraphenylborate, the peak size is roughly halved. This can be attributed to the tetraphenylborate anions ability to bind to the cationic surface and obstruct the electrochemical pore reaction, whilst leaving the exterior surface reaction essentially uninterrupted.

3.4 Conclusion

The cationic amine functionalised carbon nanoparticles were functionalised by deprotonation of the amine group for use as a synthetic modification site. Anthraquinone was attached to the surface and dispersed on a glassy carbon electrode, whereby the voltammetry was analysed to show an average 250 covalent sites per carbon nanoparticle. This number is of a similar magnitude to the value of cationic sites estimated in Chapter 2 but is less due to the steric hindrance of some sites for complete modification by anthraquinone. The effect of pH shift was shown for the surface immobilised anthraquinone, with the anticipated 57 mV/pH, Nernstian shift expected for a one proton per electron redox process. However, the peak to peak separation showed that the redox process was highly sensitive to the buffer capacity with a small separation shown for the phosphate buffer regions at pH 2, 7 and 12. This suggested that the surface chemistry was highly sensitive to ionic strength effects within the carbon nanoparticle film with pore reactivity shown to be high. Therefore, this was a suitable system for sensitive pH sensing.

3.5 References

(1) (a) Lafitte, V. G. H.; Wang, W. X.; Yashina, A. S.; Lawrence, N. S. *Electrochemistry Communications* **2008**, *10*, 1831; (b) Wildgoose, G. G.; Pandurangappa, M.; Lawrence, N. S.; Jiang, L.; Jones, T. G. J.; Compton, R. G. *Talanta* **2003**, *60*, 887.

(2) (a) Maia, G.; Maschion, F. C.; Tanimoto, S. T.; Vaik, K.; Maeorg, U.; Tammeveski, K. *Journal of Solid State Electrochemistry* **2007**, *11*, 1411; (b) Sarapuu, A.; Vaik, K.; Schiffrin, D. J.; Tammeveski, K. *Journal of Electroanalytical Chemistry* **2003**, *541*, 23; (c) Tammeveski, K.; Kontturi, K.; Nichols, R. J.; Potter, R. J.; Schiffrin, D. J. *Journal of Electroanalytical Chemistry* **2001**, *515*, 101.

(3) Vuorema, A.; John, P.; Keskitalo, M.; Mahon, M. F.; Kulandainathan, M. A.; Marken, F. *Physical Chemistry Chemical Physics* **2009**, *11*, 1816.

(4) Seinberg, J. M.; Kullapere, M.; Maeorg, U.; Maschion, F. C.; Maia, G.; Schiffrin, D. J.; Tammeveski, K. *Journal of Electroanalytical Chemistry* **2008**, *624*, 151.

(5) Kowalczyk, A.; Nowicka, A. M.; Jurczakowski, R.; Niedzialkowski, P.; Ossowski, T.; Stojek, Z. *Electroanalysis* **2010**, *22*, 49.

4. Salt Cell Voltammetry: Triple Phase Boundary Redox Processes in Highly Non-Polar Solvents

Contents

Aims

- To use a hydrated solid salt matrix as a medium to support redox processes at the solid | salt | organic solvent triple phase boundary.
- To use the salt cell technique as a mechanism for detections of redox probes in highly non-polar solvents hexane and toluene and comparison with polar 1,2-dichloroethane.
- To grow gold nanowires by electrodeposition at the triple phase boundary.

Publication

Watkins JD, Hotchen CE, Mitchels JM and Marken F, *Organometallics*, **2011**, Submitted.

CHAPTER 4: Salt Cell Voltammetry: Triple Phase Boundary Redox Processes in Highly Non-Polar Solvents

4.1 Introduction

Highly non-polar solvents such as hexane and toluene are notoriously challenging for electrochemistry due to their poor conductivity and incompatibility with standard electrolytes. One attempt to view voltammetry in toluene by Bond *et al.*[1] has used an ionic liquid dissolved in the toluene as an effective charge carrier.

An alternative, the triple phase boundary methodology, has been extensively discussed in Chapter 1.2 and gives a unique platform on which to perform analytical measurements in non-polar media. The nature of keeping analyte and electrolyte separate allows the problems of low solubility and low conductivity to be circumvented.[2] Another advantage of the triple phase boundary is that it can be considered a non-destructive analysis method, since sample preparation can be almost entirely eliminated with feasible scope for online detection.

Triple phase boundary electrochemistry allowed the use of undiluted oils in an organic phase to be kept separated from a clean electrolyte containing aqueous phase. In a study by Zhang *et al.*[3] the utility of a triple phase boundary in this manor was demonstrated, by the detection of antioxidant molecules in mineral oil at a pore array electrode.

In general, electroanalysis has moved towards smaller and smaller electrode sizes to enhance sensitivity and reduce capacitance background signals. Nano-electrodes and nano-electrode arrays,[4] often fabricated from carbon nanotubes,[5] can now be reliably created and used for analytical purposes. This effect can be roughly mimicked by triple phase boundary electrochemistry since the boundary can be thought of as a microband electrode, especially when an expulsion mechanism is utilised.[6] Further

enhancement is also often found with dynamic electrode setups *via* sonotrodes[7] or flowing micro channels.[8]

The oil industry is a good example of a situation where rapid and cost effective trace analysis of crude oil samples for antioxidant materials and trace heavy metal complexes is essential. Traditionally, this analysis is conducted in an off-site laboratory and requires intensive sample treatment in the form of dilution and cleaning. From an electrochemical standpoint, crude oil is also a highly unsuitable medium due to its very low polarity and insufficient solubility towards ionic charge carriers, as well as having a high content of potential fouling agents. For these reasons, samples are commonly diluted in methanol or other solvents with electrolytes being added before analysis.[9]

The concept of a solid salt matrix voltammetric analysis was originally investigated by Dale *et al.*[10] This work used analytes ground into the salt which could be detected in a two electrode system, with humidified air being used instead of carrier solvent. It was found that by using humidified air the hydrated layer can be maintained on a hydrophilic salt matrix, creating a charge carrying pathway between electrodes *via* interconnected salt crystals. Further publications using this salt cell matrix for electroanalytical applications at the gas | aqueous | electrode phases have also been investigated.[11]

Here, water saturated organic solvent was inserted into the salt matrix (Figure 4.1). At each point where a salt crystal was in contact simultaneously with the electrode surface and the organic solvent, a triple phase boundary was formed. In this case, the aqueous phase was the salt saturated hydrated layer encapsulating the salt crystals, the organic phase carries the redox probe, as previously shown, and the electrode surface at which nano-contact points of salt exist created the solid phase.

The concept of a solid electrolyte is not novel and has been investigated by Tajima *et al.* who have used solid supported bases to generate *in situ* electrolytes from methanol[12] and acetic acid.[13] In these cases, the solid

supported base is able to deprotonate the solvent leaving a charge pair that can act as electrolyte.

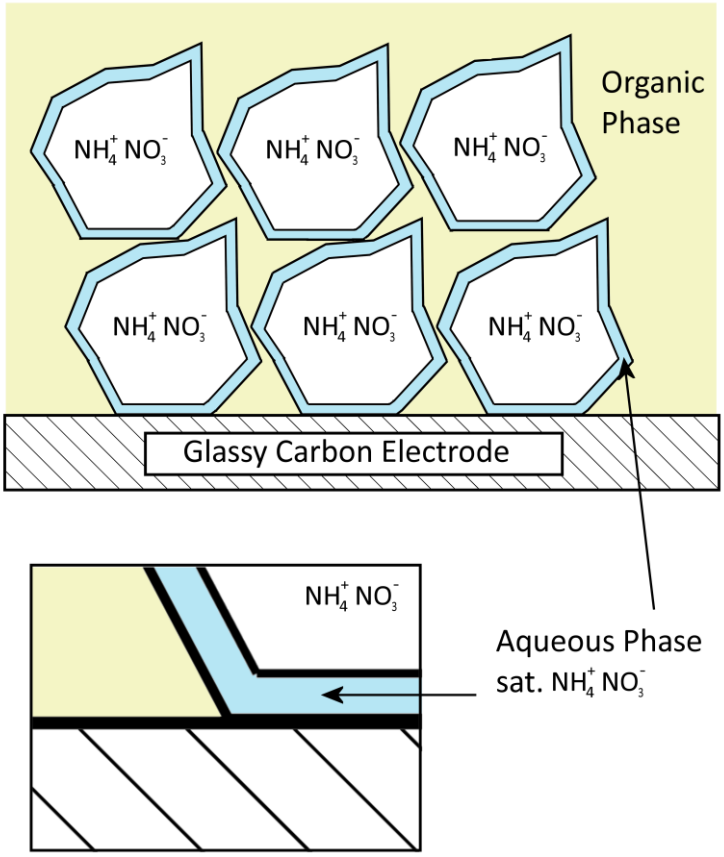

Figure 4.1 A schematic diagram of the triple phase boundary between an oil phase, glassy carbon electrode surface and the aqueous layer of a solid electrolyte.

Here, a new concept for an electroanalytical triple phase boundary technique is presented based on the salt matrix electrochemical cell shown by Dale *et al.* allowing electrochemical detection in highly non-polar media. This cell incorporated a high contact area triple phase boundary array. A solid 'aqueous phase' was created by the thin water layer around the hydrated crystals in contact with the electrode surface as shown in Figure 4.1. The analyte oil solution filled all the space not occupied by the densely packed salt crystals and formed a triple phase boundary at the boundary between the glassy carbon electrode, organic phase and the aqueous layer on the salt crystal. A key part of this cell was that the thin liquid layer of water remained intact to ensure conductivity. This meant that any solvent applied to the cell must be saturated with water to allow the water layer to remain in place, otherwise insufficient ionic contact between the electrodes would occur. Post-

analysis, the analyte solution could then be recovered by filtration from the solid electrolyte.

4.2 Experimental

4.2.1 Procedure: Salt matrix voltammetry cell design

The salt matrix cell was made of solvent resistant PTFE with four holes cut into a 70 mm x 30 mm x 50 mm block. The large top and bottom holes allowed the insertion of a working and counter / reference electrode creating a small cavity which was filled with *ca.* 1 g compacted solid electrolyte. The electrolytes used were ammonium chloride and ammonium sulphate due to their high hydration ability. The counter / reference electrode used was a saturated calomel electrode (SCE) and was screwed into the base of the cell. Next, the cavity was loaded with electrolyte and the glassy carbon working electrode was screwed into the top of the cell to compact the salt and create conductivity between itself and the counter / reference *via* the thin water layer surrounding the salt crystals. The two small side holes acted as an inlet and outlet for analyte solutions as shown in Figure 4.2.

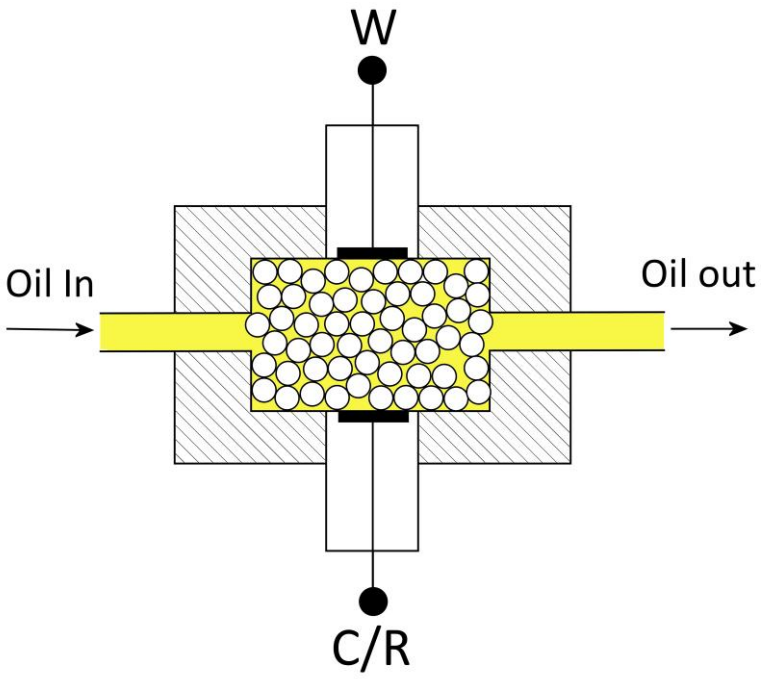

Figure 4.2 A schematic diagram of the salt matrix cell.

4.2.2 Procedure: Salt cell voltammetry in non-polar media

For measurements in unsupported non-polar solvents the dry salt matrix cell, described in Section 4.2.1, was created. The non-polar solvent containing the redox probe to be studied was first saturated with water by creating an immiscible mixture of the solvent with water and vigorously shaking. This was repeated several times and the mixture left to equilibrate for several minutes. The solvent layer was extracted by syringe and passed through the salt matrix cell by syringe pump through one of the side holes. Gentle pressure was applied to the syringe pump until liquid was seen to flow out through the opposite hole. Care was taken that salt was not washed out of the cell and leaking around either electrode was not seen. The water saturated analyte solution was prepared similarly and flowed in through the same side hole. Roughly 5 cm^3 of analyte solution was flowed through the cell to ensure homogeneity prior to electrochemical experimentation. After each electrochemical scan fresh analyte solution was allowed to flow through the salt matrix and between different concentrations of analyte fresh solvent solution was used to wash the salt matrix. A fresh aliquot of salt was used for each different solvent and consistency was ensured by repeating measurements in many clean salt matrix conditions.

4.2.3 Procedure: Salt cell electro-deposition of Au

Gold deposition experiments were carried out using a 1 mM solution of tetrachloroaurate / 5 mM tetraoctylammonium bromide in toluene under static conditions. The solution was prepared following a literature preparation by Brust *et al.*[14] A volume of 3 mL of a solution of 30 mM of hydrogen chloride and 30 mM gold (III) trichloride was added to 8 mL of a solution of 50 mM tetraoctylammonium bromide toluene. The mixture was shaken and left to equilibrate for several minutes until the aqueous layer (bottom) became decolourised and the toluene layer (upper) became bright red in colour. The toluene layer was recovered by syringe and diluted with a further 80 mL of clean toluene to give a solution with *ca.* 1 mM Au(III) and *ca.* 5 mM tetraoctylammonium bromide. The deposition potential in the salt cell was chosen to provide roughly 10 µA of current (*ca.* -3V vs. SCE). The electro-deposition of gold was carried out for 30 minutes after which the electrode

was removed, thoroughly rinsed with acetone and distilled water, and dried. Gold deposits were seen by optical microscopy and further confirmed by energy dispersive X-ray spectroscopy (EDS) and scanning electron microscopy (SEM) methods.

4.3 Results and Discussion

4.3.1 Salt Matrix Voltammetry: Redox processes of decamethylferrocene in non-polar solvents

Decamethylferrocene was used as a highly stable test system to show how triple phase boundary chemistry in the salt matrix cell was possible. The voltammetry of decamethylferrocene is well understood to be a one electron highly reversible redox probe (Scheme 4.1) and no significant partitioning into the water phase was expected. Figure 4.4A shows the voltammetry of decamethylferrocene (2 mM) in three different solvents of varying polarity. The polarity of a solvent can be related to its relative dielectric constant (relative to the permittivity of free space) where polar molecules have a high dielectric constant and non-polar molecules have a dielectric constant close to zero.

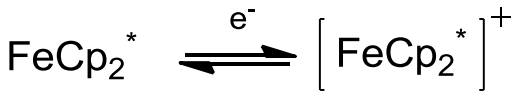

Scheme 4.1 The one electron reversible oxidation of decamethylferrocene in aqueous conditions.

Solvent	Dielectric Constant (relative to ε_0 at 15 - 30 °C)[15]	Water Content / mM
Water	80.100	-
Acetonitrile	36.64	-
Ethanol	25.3	-
1,2-Dichloroethane	10.42	130 [16]
Toluene	2.379	28 [17]
Hexane	1.8865	4.6 [18]

Figure 4.3 A table showing the dielectric constants of some common electrochemical solvents compared to non-polar solvents.[15]

As shown in the table (Figure 4.3), hexane has a very low dielectric constant due to its lack of electronegative sites. Conversely water has a high dielectric constant due to the high polarity afforded by the electronegativity difference between oxygen and hydrogen, as well as its orientation being that based on a tetrahedral structure. The table in Figure 4.3 shows that acetonitrile is an ideal choice for most organically based electrochemical processes. This is due to its ability to dissolve organic molecules as well as its high relative polarity compared to other organic solvents.

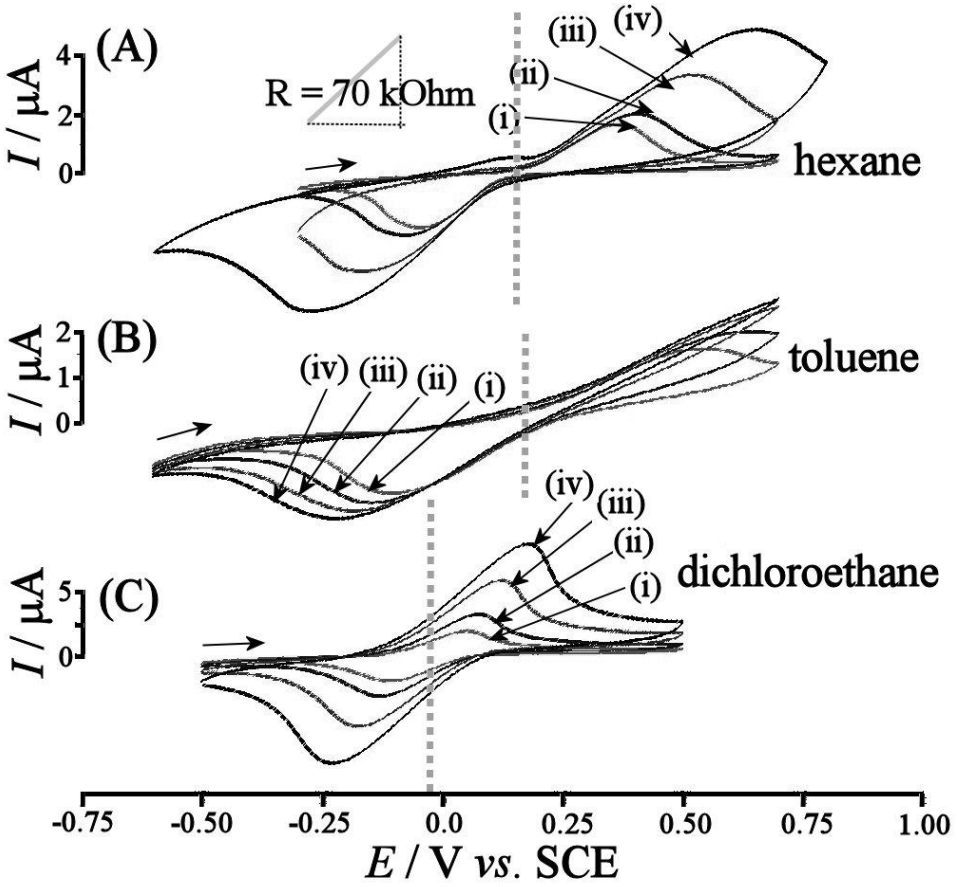

Figure 4.4 (A) Cyclic voltammograms for the oxidation and reduction of 2 mM decamethylferrocene in humidified hexane in contact to NH_4NO_3 | glassy carbon at scan rates (i) 10, (ii) 20, (iii) 50, and (iv) 100 mVs^{-1}. **(B)** As above but in toluene. **(C)** As above but in 1,2-dichloroethane.

$$FeCp_2^*(Hexane) + NO_3^-(Salt) \rightleftharpoons \left[FeCp_2^*\right]^+ NO_3^-(Solid) + e^-(Electrode)$$

Scheme 4.2. The one electron oxidation of decamethylferrocene in the salt cell with a highly polar solvent such as Hexane or Toluene to yield an insoluble product salt.

The voltammetry of decamethylferrocene (Figure 4.4A) showed an unusual shape absent of the commonly seen diffusional profile. Instead a symmetrical shape was shown at low scan rate (≤10 mVs^{-1}) suggesting an electrode blocking mechanism was operating. This result could be explained by the insolubility of the product decamethylferrocenium salt which deposited at the triple phase boundary and caused a blocking effect of the triple phase boundary mechanism. On the reverse scan the solid deposit was redissolved. This deposition mechanism (Scheme 4.2) also explained the high peak to peak separation of oxidative and reductive processes. At higher scan rates an increase in peak height was achieved, as well as a decrease in the charge, suggesting that there is not sufficient time for the deposition to occur to the extent of blocking the electrode. Furthermore, there appeared to be a large iR-drop, estimated to be 70 kOhms, associated with the voltammetry in the salt matrix cell, probably due to the resistivity between the working and counter-reference electrodes through the salt matrix. Similar resistivity effects have been seen in previous liquid-liquid triple phase boundary systems. It is also worth noting, that in a dry hexane system, without using a pre-saturation with water step, no electrochemical signal was seen for decamethylferrocene (not shown). A water saturated solution of hexane is known to contain 4.6 mM of water[18] and is sufficient to uphold the water layer model required for ionic conductivity between electrodes.

At slow scan rates similar behaviour was shown by the triple phase boundary voltammetry of decamethylferrocene in toluene (Figure 4.4B) to that seen in hexane and a similar deposition model was applied. This model explained the lack of oxidative peak at high scan rate, where deposition did not have time to occur, but where a symmetrical peak was seen at lower scan rates, akin to that shown for hexane. The slight discrepancy at fast scan rate however showed that the deposition from toluene occurred slower than that from hexane, consistent with the change in polarity of the solvent. At all scan rates tested blocking was found from hexane at all scan rates. The less efficient deposition from toluene lead to smaller peak heights an the lack of complete blocking at fast scan rates, shown by the lack of oxidative peak.

Scheme 4.3. The one electron oxidation of decamethylferrocene in the salt cell with a DCE solvent to yield a soluble product salt.

1,2-Dichloroethane (DCE) however, showed a markedly different voltammetric response for the decamethylferrocene redox couple from the two less polar solvents (Figure 4.4C). The most obvious difference initially was the midpoint potential which appeared negatively shifted (*ca.* -0.02 V) compared to the values shown for hexane (*ca.* +0.16 V) and toluene (*ca.* +0.17 V). This change could be explained, at least in part, by the increased solubility of the decamethylferrocenium product in DCE and the switch to a different mechanism where no deposition occured and the redox reaction remained confined to the organic phase (Scheme 4.3). Additional effects from membrane potentials at the reference electrode were however also possible. The voltammetric response now showed a shape consistent with a diffusion based process, with charge analysis of the area under the peaks suggesting a planar diffusion of material away from the electrode which may be analysed by the Randle-Sevcik expression (Equation 1). This expression relates the peak height and the scan rate given a known electron transfer mechanism and can be used to calculate the diffusion coefficient, assuming a uniformly accessible planar electrode.

(1)
$$I_p = 0.446nFAc\sqrt{\frac{nF\nu D}{RT}}$$

Here: I_p is the peak current, n is the number of electrons transferred, F is the Faraday constant (96485 $Cmol^{-1}$), A is the active electrode area, c is the bulk concentration of the diffusing molecule, v is the scan rate, R is the gas constant (8.314 $Jmol^{-1}K^{-1}$), T is the absolute temperature and D is the diffusion coefficient.

The Wilke-Chang expression[19] was used to estimate diffusion coefficients for comparison. This expression is most effective for estimated diffusion coefficients of organic species in organic solvents taking into account intermolecular interactions. When this expression was used to estimate the

expected diffusion coefficient of decamethylferrocene in DCE for this reaction, a discrepancy was found. The value was estimated to be 0.7 ± 0.1 x 10^{-9} m^2s^{-1} which would suggest a peak current of about 10 μA at a scan rate of 10 mVs^{-1}. Experimentally a peak current of *ca* 2 μA is seen, which is 20% of that expected for a full 3 mm diameter glassy carbon electrode and thus, it was estimated that only 20% of the electrode area is active in this reaction assuming that the point contacts did not have overlapping diffusion fields. This small active area was indicative of the triple phase boundary reaction since only the point contacts where the electrode was in contact with a salt crystal and organic phase simultaneously can the reaction occur. At the electrode-organic and electrode-salt interfaces no reaction was possible. It was reasonable to infer from the results that a more finely ground solid electrolyte would lead to smaller crystals, more triple phase contact points and a higher active electrode area. Furthermore, the random distribution of salt crystals on the electrode surface lead to less than perfect reproducibility. In order to overcome this, salt samples were washed with the relevant solvent between samples and the same salt matrix used for multiple experiments to ensure reproducibility.

As a direct comparison between the three solvent systems, Figure 4.5A shows scans for equal scan rates for hexane, toluene and DCE. The shift in midpoint potential has been explained previously but the DCE signal also showed much less iR-drop in comparison to the less polar solvents. This was a result of far less resistivity in the organic phase between the working and counter, reference electrodes due to the much higher conductivity of DCE. The peak shape was also much different for the DCE case where sharper peaks were seen, including the expected ‘diffusional tail’, for a reversible redox process. This reversibility was also reflected by the greatly reduced peak to peak separation also suggesting that the deposition mechanism proposed for non-polar solvents was no longer in effect and the ionic product decamethylferrocenium remained soluble in the organic phase. When the effect of the decamethylferrocene concentration was analysed in hexane (Figure 4.5B), it was seen that the peak shape changed dramatically as peaks became sharper with a smaller peak to peak separation at higher concentrations. At these large concentrations however, the area under the

peak was not seen to change which further supported the deposition theory, with larger concentrations giving rise to a faster deposition at the salt | organic | electrode interface but not increasing the total amount of deposition occurring.

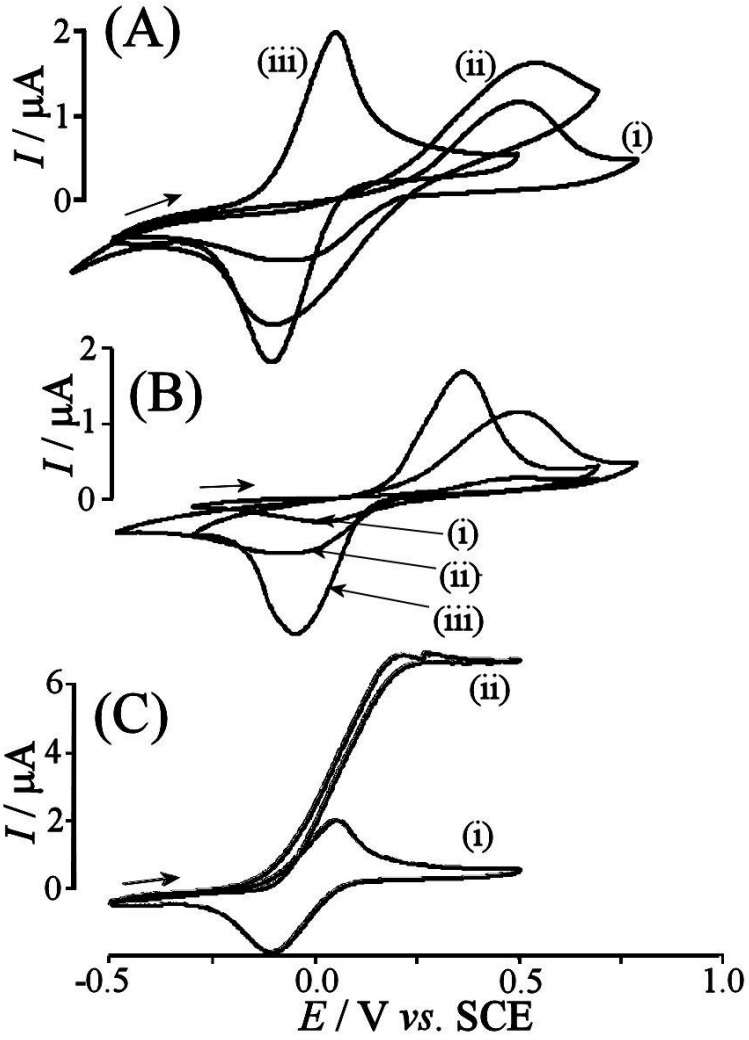

Figure 4.5 (A) Cyclic voltammograms for the oxidation of 2 mM decamethylferrocene in humidified (i) hexane, (ii) toluene, and (iii) dichloroethane obtained at a NH_4NO_3 salt | glassy carbon electrode contact at a scan rate of 10 mVs^{-1} **(B)** Cyclic voltammograms for the oxidation of (i) 1 mM, (ii) 2 mM, and (iii) 5 mM decamethylferrocene in hexane conditions as above **(C)** Cyclic voltammograms for the oxidation of 2 mM decamethylferrocene in dichloroethane in (i) static and (ii) flowing solution at 400 $\mu Lmin^{-1}$ conditions as previous.

The effect of flow on triple phase boundary voltammetry was then investigated. In the cases of hexane and toluene no effect of flow was seen on the voltammetry with a peak still visible (not shown) due to the blocking

effect of deposition discussed previously. In the case of DCE an increase in current was seen for a flow rate of 400 $\mu Lmin^{-1}$ giving the expected limiting current (Figure 4.5C) and showing that no deposition process acts in this case. The effluent stream also appeared as a green colour indicative of the ferrocenium ion, showing substantial conversion of the redox probe.

4.3.2 Salt matrix voltammetry: Electro-deposition of Au as nanowires at the salt | electrode | toluene interface.

To visualise the reaction zone available at the triple phase boundary between the non-polar solvent, salt and electrode phases a gold (III) solution of $Au(III)Cl_4^-$ was used. The gold salt was prepared in toluene using a literature method,[14] as given in Section 4.2.3, and passed through the salt cell. This transfer was achieved using a phase transfer reagent tetraoctylammonium bromide (5 mM) with a dilution step used prior to electrolysis to make a gold (III) concentration of *ca.* 1 mM. The voltammetry reflected a high level of resistance (not shown) in the organic phase, possibly due to the sequestered nature of the gold salt. For this reason a large deposition current of *ca.* 10 µA was used by applying a potential of 3 V (*vs.* SCE) for 30 minutes.

After deposition, the electrode was rinsed thoroughly with acetone followed by distilled water to ensure only deposited gold was visualised. The deposited gold was first analysed by optical microscopy showing macrostructures of gold in ring like shapes.

Further visualisation by scanning electron microscopy (SEM) (Figure 4.6) showed significant coverage of the glassy carbon electrode with macrostructured rings of gold. This was confirmed by energy-dispersive X-ray spectroscopy (EDS) (not shown). The ring shaped deposit was attributed to the outline of the salt crystals against the electrode surface and thus the triple phase boundary reaction zone. Previous estimates of electrode activity being *ca.* 20% are justified by this coverage of gold, showing only the edges of surface adjacent crystals to be active at the triple phase boundary. Upon closer inspection the rings also exhibited a fine structure in the form of gold nanorods (Figure 4.6C/D). This ordered shape could be explained by the existence of a liquid crystal phase domain favouring the growth of gold in a

single dimension due to the micellular properties of the tetraoctylammonium bromide transfer agent. The nanowires appeared grouped into clusters with individual filament diameters of less than 10 nm. The nanowire structured deposition could be explained by the formation of a lyotropic liquid crystal phase at the triple phase boundary, as shown in Figure 4.7.

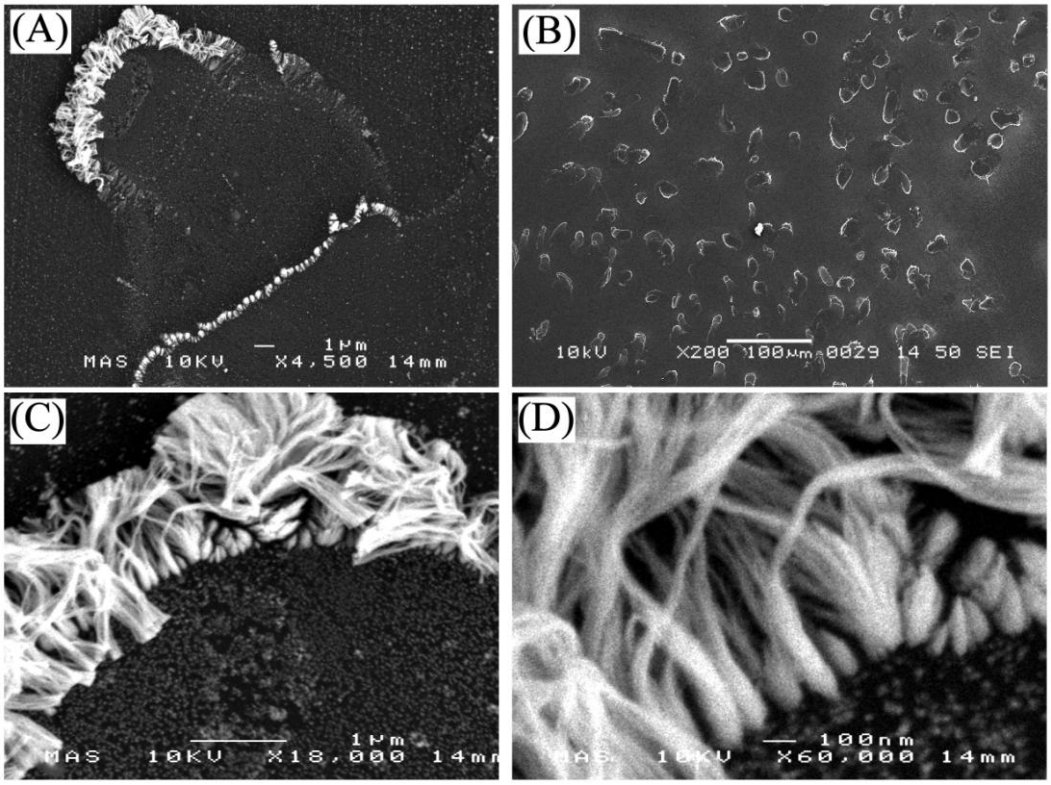

Figure 4.6 SEM images for gold deposits formed at -3 V (*vs.* SCE) at NH_4NO_3 | electrode contact points with *ca.* 10 µA deposition current and 30 minutes deposition time in 1 mM $AuCl_4^-$ and 5 mM tetraoctylammonium bromide in toluene (see experimental).

In a highly non-polar solvent such as toluene the aqueous soluble gold ions were stabilised by the transfer agent, which also acted as a surfactant. A micelle was formed where surfactant tetraoctylammonium bromide (TOABr) encapsulated the ions making them soluble in toluene. As shown in Figure 4.7Bii the initial deposition occurred as nano structures. Further deposition occurred in a stepwise manner on the existing nanostructures forming evenly spaced nano-wires stabilised by surfactant. When the surface was rinsed with organic materials and water, the toluene and surfactant were removed leaving the templated gold nano-wires.

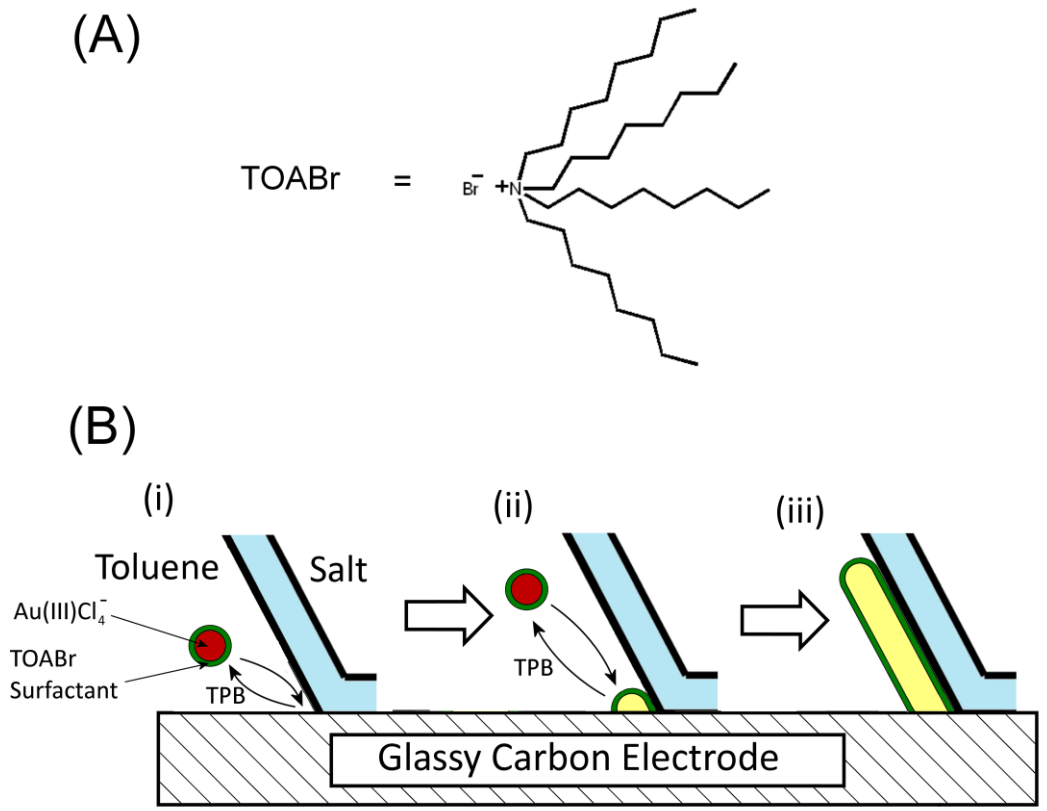

Figure 4.7 A schematic diagram of the liquid crystal phase leading to nanowire deposition. The structure of TOABr is shown in **(A)** and stabilises the aqueous $Au(III)Cl_4^-$ toluene. **(B)** Growth of a single gold nanowire at the triple phase boundary of the salt crystal | toluene and the electrode surface, where TPB represents the triple phase boundary reaction of a three electron reduction and the concerted transfer of ions to balance the charge.

4.4 Conclusions

In conclusion a new type of triple phase boundary process was presented with possible analytical applications in the detection of molecules in highly non-polar solvents. The triple phase boundary used was the boundary formed between the solid glassy carbon electrode, water saturated organic solvent phase and a water saturated crystal surface aqueous phase. The salt crystals created nanoscale points of contact with the electrode surface and it was only at these points that the triple phase reaction could occur, thus acting as a nanoelectrode array. This mechanism allowed the analysis of redox materials in highly non-polar and electrically non-conducting organic phases.

The differences in mechanism for the non-polar solvent (toluene and hexane) phases and the more polar 1,2-dichloroethane were shown. For the less polar solvents a deposition mechanism was seen at the triple phase boundary whereas a more traditional liquid contained mechanism was seen for the more polar DCE.

Finally, gold deposition from the organic phase was demonstrated resulting in the growth of nanowires likely due to a suspected liquid crystal mechanism caused by the surfactant used to solubilise the gold salt in toluene. The resulting nanowires were imaged by SEM (Figure 4.6) showing the deposition pattern around the perimeter of the salt crystals.

4.5 References

(1) Duffy, N. W.; Bond, A. M. *Electrochemistry Communications* **2006**, *8*, 892.

(2) Marken, F.; Watkins, J. D.; Collins, A. M. *Physical Chemistry Chemical Physics* **2011**, *13*, 10036.

(3) Zhang, X. H.; Paddon, C. A.; Chan, Y. H.; Bulman-Page, P. C.; Fordred, P. S.; Bull, S. D.; Chang, H. C.; Rizvi, N.; Marken, F. *Electroanalysis* **2009**, *21*, 1341.

(4) Li, J.; Ng, H. T.; Cassell, A.; Fan, W.; Chen, H.; Ye, Q.; Koehne, J.; Han, J.; Meyyappan, M. *Nano Letters* **2003**, *3*, 597.

(5) Tu, Y.; Lin, Y. H.; Yantasee, W.; Ren, Z. F. *Electroanalysis* **2005**, *17*, 79.

(6) (a) Chen, J. Y.; Sato, M. *Journal of Electroanalytical Chemistry* **2004**, *572*, 153; (b) Aoki, K.; Tasakorn, P.; Chen, J. Y. *Journal of Electroanalytical Chemistry* **2003**, *542*, 51.

(7) Floate, S.; Hardcastle, J. L.; Cordemans, E.; Compton, R. G. *Analyst* **2002**, *127*, 1094.

(8) Grieshaber, D.; MacKenzie, R.; Voros, J.; Reimhult, E. *Sensors* **2008**, *8*, 1400.

(9) Welter, K.; Salazar, E.; Balladores, Y.; Márquez, O. P.; Márquez, J.; Martínez, Y. *Fuel Processing Technology* **2009**, *90*, 212.

(10) Dale, S. E. C.; Cummings, C. Y.; Marken, F. *Electrochemistry Communications* **2011**, *13*, 154.

(11) (a) Shariki, S.; Dale, S. E. C.; Marken, F. *Electroanalysis* **2011**, *23*, 2149; (b) Ibrahim, N. B.; Lawrence, K.; James, T. D.; Xia, F.; Pan, M.; Mu, S.; Mitchels, J. M.; Marken, F. *Sensors and Actuators B: Chemical* **2011;** (c) Xia, F.; Dale, S. E. C.; Webster, R. A.; Pan, M.; Mu, S.; Tsang, S. C.; Mitchels, J. M.; Marken, F. *New Journal of Chemistry* **2011**, *35*, 1855.

(12) Tajima, T.; Fuchigami, T. *Journal of the American Chemical Society* **2005**, *127*, 2848.

(13) Tajima, T.; Fuchigami, T. *Angewandte Chemie-International Edition* **2005**, *44*, 4760.

(14) Brust, M.; Walker, M.; Bethell, D.; Schiffrin, D. J.; Whyman, R. *Journal of the Chemical Society-Chemical Communications* **1994**, 801.

(15) Lide, D. R. *CRC Handbook of Chemistry and Physics, 89th Ed.*; CRC Press, **2008**.

(16) Horvath, A. L.; Getzen, F. W.; Maczynska, Z. *Journal of Physical and Chemical Reference Data* **1999**, *28*, 395.

(17) Neely, B. J.; Wagner, J.; Robinson, R. L.; Gasem, K. A. M. *Journal of Chemical and Engineering Data* **2008**, *53*, 165.

(18) Maczynski, A.; Shaw, D. G.; Goral, M.; Wisniewska-Goclowska, B.; Skrzecz, A.; Owczarek, I.; Blazej, K.; Haulait-Pirson, M. C.; Hefter, G. T.; Kapuku, F.; Maczynska, Z.; Young, C. L. *Journal of Physical and Chemical Reference Data* **2005**, *34*, 709.

(19) Wilke, C. R.; Chang, P. *Aiche Journal* **1955**, *1*, 264.

5. Ultrasound Mobilization of Liquid | Liquid | Solid Triple Phase Boundary Redox Systems

Contents

Aims

- To use low power ultrasound to mobilise macrodroplets on electrode surfaces in order to enhance triple phase boundary processes.
- To optimise the enhanced triple phase boundary for droplet volume, ultrasound power and transfer ion identity.
- To use the enhanced triple phase boundary for synthetic reactions in organic droplets by proton transfer.

Publication

- Watkins JD, Bull SD and Marken F, *Journal of Physical Chemistry C*, **2009**, 113, 15629 – 15633.

CHAPTER 5: Ultrasound Mobilization of Liquid | Liquid | Solid Triple Phase Boundary Redox Systems

5.1 Introduction to Ultrasound

5.1.1 Ultrasound in Electrochemistry and Synthesis

Ultrasound is defined as a cyclic sound wave with a frequency above the range of human hearing, about 20 kHz.[1] The frequency and power used often play a key role in the application of ultrasound. Generally a distinction can be made between two frequency bands of ultrasound.[2] High frequencies, above 1 MHz are termed 'diagnostic ultrasound', result in negligible cavitation effects and are used for imaging. Frequencies between 20 and 100 kHz are termed 'power ultrasound' and often cause cavitation. This leads to its use in cleaning and chemical reaction manipulation.

Ultrasonic devices are widely used in both household and business. In the home, ultrasonic baths are used to clean metallic objects such as jewellery and also in toothbrushes to dislodge materials from between the teeth. In medical applications it can be used for breaking up gallstones, treating tumours and sterilising medical equipment.[2] One of the advantages of ultrasound over other agitation methods is that it can be accurately targeted onto a mass or surface. Other less destructive applications use much higher frequencies to avoid cavitation effects (attributed to the destructive nature of ultrasound) and include ultrasonic imaging which can give images of foetuses in the womb, analyse microscopic flaws in materials or give images of solid objects in otherwise opaque materials.[1,2]

Ultrasound is already used successfully in many fields of chemistry such as photochemistry,[3] synthetic chemistry,[4] phase transfer catalysis[5] and single phase electrochemistry both for electrosynthetic[6] and electro-analytical[7] applications. The use of ultrasound for triple phase boundary electro-organic reactions has been studied previously by Atobe *et al.*[8]

Ultrasound gives a few key benefits in electrochemistry, the first of which is the very high degree of mass transport, especially for traditionally 'slow diffusers,[9] and is gained through two key mechanisms. (i) 'Acoustic streaming', where a directed turbulent flow of bulk material is in effect causing fast material transport to the electrode surface and a heating effect of the bulk solution. (ii) Cavitation (Figure 5.1), where the effect of the ultrasonic wave causes a compression and rarefaction cycle in the bulk liquid leading to voids being created at the electrode surface. Upon collapse these voids lead to a roughening of the electrode surface and mass transport being increased. This effect leads to localised temperatures and pressures of around 5000 K and 1700 bar and can create radicals in solution which react rapidly.[10]

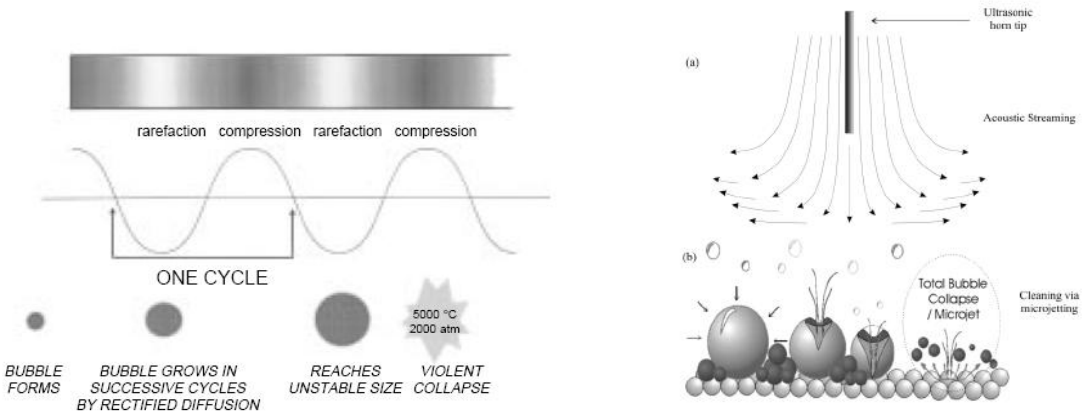

Figure 5.1 (left) Shows the compression rarefaction cycle in ultrasound that leads to cavitation[10] and (right) it's effect on a surface.[11]

In the case of the ultrasonic horn being positioned perpendicular to the electrode surface ('face on', Figure 5.2), it is likely that 'acoustic streaming' is the dominant method of mass transport in this system. The effects of sonic power on various electrode to sonic horn configurations and separations has been thoroughly investigated by Marken *et al.*[12] showing evidence that in a 'face-on' configuration the diffusion layer thickness is related to the limiting current. In addition to this it is also the case that a lower limit of the diffusion layer thickness is imposed by the solvent.

The mass transport effect has been extensively investigated for a number of years, not just from a power and frequency perspective, but also as a geometry effect between the sonic horn and the electrode surface. The three most common geometries are demonstrated in Figure 5.2 from a review by Compton *et al*. The 'side on[13] and 'sonotrode[14] configurations will not be discussed in this report since it is exclusively the 'face on' method that has been used.

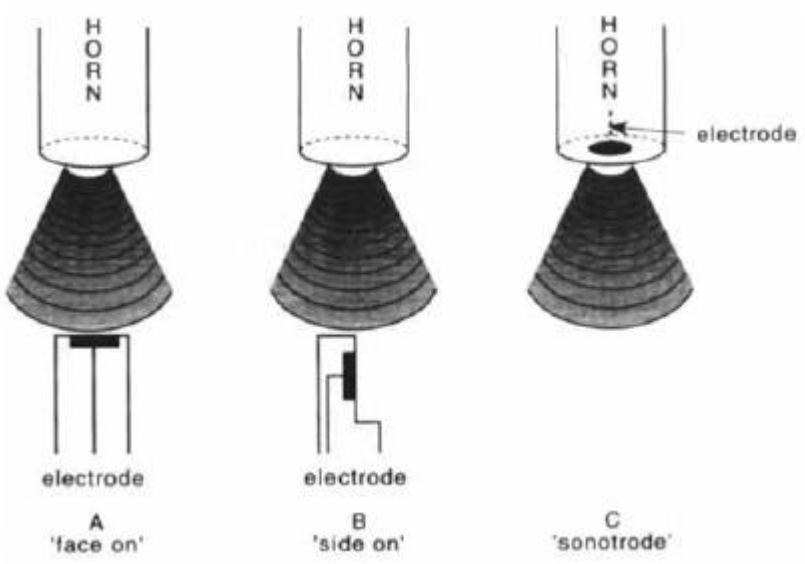

Figure 5.2 The three common geometries of electrodes with ultrasonic horns.[7c]

Each of the geometries possesses its own benefits and drawbacks. The most common geometry is that of the 'face on' configuration where the sonic horn is held a set distance from the electrode surface. The action of mass transport, in this case, has the effect of decreasing the diffusion layer thickness.[7c] The relationship of limiting current I_{lim} to diffusion layer δ is given by Equation 1. This is in contrast to the 'side on' configuration which can be modelled by a flow over a surface given by the Nernst diffusion layer equation.

(1)
$$i_{lim} = \frac{nFADc_{bulk}}{\delta}$$

Here n is the number of electrons transferred per molecule diffusing to the surface, F is the faraday constant, D is the diffusion coefficient of the redox

active material in the medium, A is the electrode area and c_{bulk} is the concentration of the redox active material.

This equation assumes that the concentration gradient is linear across a thin layer next to the electrode surface. Compton *et al.*[15] have exploited this ability to control the diffusion layer thickness by changing the power of ultrasound in order to investigate the fast electron transfer properties of an ECE mechanism. It is usual in these cases to use a microelectrode with a very small diffusion layer, since macroelectrodes mask fast electron transfer processes with a diffusion effect. Compton found however, that by using power ultrasound the small diffusion layer created on a standard 3 mm diameter glassy carbon electrode was sufficient to measure fast electron transfer kinetics.

It should be noted that investigations of the effect of direct high power ultrasound on electron transfer kinetics show that this parameter remains unaffected for the heterogeneous system and it is only the mass transport which leads to the dramatically increased currents seen in the presence of ultrasound.[16]

Compton *et al.*[17] have also investigated the relationship of power and limiting current which shows a relationship given by Equation 2.

(2)
$$I_{Lim} = C(h,\upsilon) D^{2/3} A C_{Bulk} P_W^{1/2}$$

Here P_w is the sonication power, A is the electrode area, C_{bulk} is the concentration of the redox active species, D is the diffusion coefficient, and C is a function of ν (scan rate) and of the electrode-to-horn separation, h which falls off strongly as h increases.

Mass transport effects are not the only benefit from ultrasound in electrochemical applications. Ultrasound can also change electrochemical processes[18] especially in the field of electrosynthesis. In electrosynthesis ultrasound is useful not only for increasing reaction rates but also for stopping electrode surfaces from being fouled by polymers and other solid materials in a depassivation effect.[19] This is especially useful for performing

analytical electrochemistry in non-ideal environments such as blood,[11,20] a notoriously difficult medium to address directly. Depassivation is also beneficial when a redox reaction generates blocking materials, either intentionally or as a by-product, since it means that the electrode surface is always replenished and reactions may be driven to completion. The depassivation is mainly achieved through the cavitation mechanism and depending on the conditions of frequency, sonication power, electrode area and solvent this surface cleaning can also lead to the electrode surface becoming rough and damaged.[21]

Ultrasonic chemistry has also been successfully applied to organic synthetic chemistry, even in the field of natural product synthesis.[22] In this case, the ultrasound possesses many potentially beneficial effects useful for synthetic chemistry; (i) A high agitation effect, especially useful for heterogeneous reactions, (ii) a high localised heating effect, similar to directed microwave heating although not as precise, and (iii) a cleaning effect to prevent a solid catalyst surface becoming fouled. Ultrasound can often provide unique conditions in organic reaction, which can facilitate unusual reactivity, greater yields or faster reactions.[10] This effect can be attributed to a combination of mechanical and chemical activation parameters. For example, metal components of a reaction can become surface activated by ultrasound *via* cavitation. This is a so called physical process and often leads to a reaction becoming faster. In general, physical effects of ultrasound can be matched by very rapid stirring and are thus not true sonochemical effects.

It was found by Ando *et al.*[23] that radical reactions were promoted by ultrasound which can lead to different major products. This process is called ‘sonochemical switching’ (Figure 5.3.), but ionic based reactions remain unaffected chemically. This was attributed to the localised heating effect of cavitation of, up to 1000s of degrees hotter than the bulk, and increased pressure leading to radical generation, which was a chemical effect. Under these extreme conditions the generation of methyl radicals from the ligands followed by a radical attack of the alkene bond is favoured.

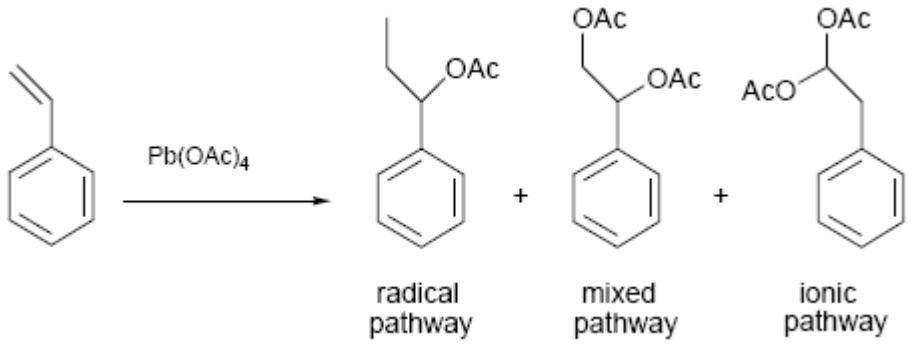

Figure 5.3. This reaction shows the different products of the decomposition of lead tetraacetate in acetic acid with styrene. Under ultrasound the favoured product is the 1-phenylpropyl acetate.[23]

Finally, the use of ultrasound as a technique can be considered relatively 'green', especially in the use in biphasic systems. In these cases the volume of potentially hazardous solvents is limited. Higher yields and faster reactions also lead to less waste as summarised in a review by Cintas *et al.*[24]

In this chapter a low powered ultrasound system was used in a 'face on' mode with an electrode surface. An unsupported organic phase, of *ca.* 1 ml, containing redox probe was placed onto the electrode. To this ultrasound power was applied so as to agitate the droplet and create a localised emulsion in contact with the electrode without bulk emulsion formation. This highly mobile microdroplet emulsion was then used as a hydrodynamic triple phase boundary benefitting from an increase in triple phase boundary contact area and agitation of both aqueous and organic phases. After the experiment was complete, removal of the ultrasonic horn resulted in the reformation of the bulk organic phase.

5.2 Experimental

5.2.1 Chemical Reagents

Sodium perchlorate (99%, Aldrich), hexaammineruthenium (III) chloride (analytical reagent grade, Alfa Aesar), 1,2-dichloroethane (Fluka, HPLC grade ≥99.8%), n-butylferrocene (98%, Alfa Aesar), Potassium hexafluorophosphate (Sigma Aldrich, 99.9+%), tetrabutylammonium hexafluorophosphate (Fluka analytical reagent, ≥99.0%), potassium

tetraphenylborate (Sigma Aldrich, ≥99.5%), phosphoric acid (Sigma Aldrich ACS reagent, 85 wt%), Benzil (98%, Aldrich), 1,2,3,4-tetrahydro-1-naphthol (Aldrich), benzyl alcohol (99+%, Aldrich), and filtered demineralised water was taken from a Millipore water purification system with not less than 18 MOhm cm resistivity.

5.2.2 Instrumentation

Voltammetric measurements were conducted with a μ-Autolab III potentiostat system (Eco Chemie, Netherlands) in staircase voltammetry mode with a 2.83 cm^2 geometric area glassy carbon working electrode (glassy carbon from Alfa Aesar, type I). In some other experiments two types of graphite electrodes were used (basal plane pyrocarbon and graphite 2120PT both from Le Carbone Ltd.) for comparison, of 2.83 cm^3 geometric area. A platinum counter electrode and a saturated calomel reference electrode (SCE, REF401, Radiometer) were placed in the 32 ml of aqueous phase. All experiments were conducted at 22 +/- 2 ^oC with sonication time and intensity chosen to minimise ultrasonic heating during the experiment. An ultrasound processor (Hielscher UP 200G, 24 kHz, 200 W, maximum ultrasound intensity 30 Wcm^{-2}, calibrated based on the thermal effect of ultrasound absorption in aqueous media[25]) was fitted with a 13 mm diameter glass horn and used for only short periods of time to prevent a sizable temperature rise of the solution above room temperature.

5.2.3 Procedure

In this chapter, a new methodology for the creation of a dynamic triple phase boundary based on a low power ultrasound system is outlined. This is used to break down and agitate a single macro-droplet of the scale 100 μL up to 2 ml into surface localised micro-droplets without significant loss of organic phase as emulsion into the aqueous phase. This effect was two fold (i) The macro-droplet upon being broken down acted as a localised emulsion of micro-droplets which greatly increased the active triple phase boundary contact zone, and (ii) a mass transport effect of the ultrasound was in effect agitating the micro-droplets on the surface and leading to increased triple phase boundary activity. This methodology was especially synthetically

useful for electrolyte separation. When the ultrasound was stopped, the droplet quickly reformed into its original size from which a syringe can draw a sample for characterisation, without the need to separate electrolyte. This effect is shown schematically in Figure 5.4.

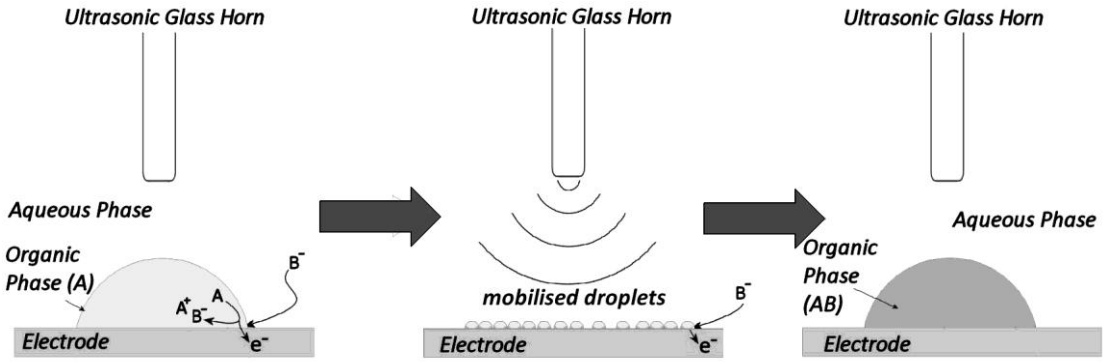

Figure 5.4 This shows a schematic drawing of the mobilisation effect of low power ultrasound on a surface droplet of DCE on a glassy carbon surface. The anodic triple phase boundary process causes extraction of B^- from the aqueous phase into the organic phase. Upon mobilisation of the organic phase an extended and dynamic triple phase boundary enhances the anodic process.

To achieve this process a relatively low power of 24 kHz ultrasound was used provided from the modest distance of 15 mm perpendicular to the electrode surface being a 2.83 cm^2 glassy carbon working electrode in 32 cm^3 of aqueous solution.

This investigation was carried out using the electrode setup shown in Figure 5.5, with the saturated calomel reference and a platinum wire counter electrode in the positions indicated. The glassy carbon working electrode formed the bottom of the electrochemical cell, with the cell being sealed to it by a rubber ring. Droplets of between 50 and 5000 µL were deposited into the middle of the working electrode by a syringe after the cell was already filled 32 cm^3 with aqueous electrolyte solution. The glass ultrasonic horn was inserted for direct sonication of the droplet perpendicular to the working electrode.

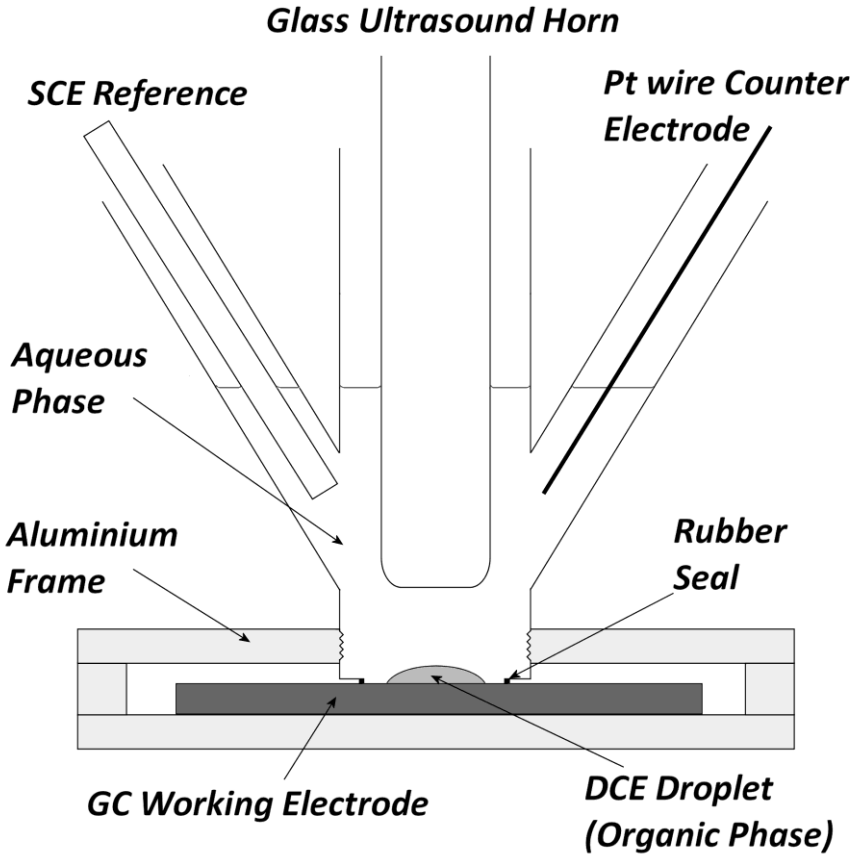

Figure. 5.5 A schematic diagram showing the electrode setup used and the position of the ultrasonic horn perpendicular to the electrode surface on which the droplet exists.

5.3 Results and Discussion

5.3.1 The Effect of Ultrasound Power on Mass Transport in the Aqueous Phase Containing the $Ru(NH_3)_6^{3+}$ Redox Probe

The first step was to calibrate the power ultrasound system with a simple single aqueous phase test system of 2 mM $Ru(NH_3)_6^{3+}$. The one electron redox couple for this transformation is given below in Scheme 5.1.

The shape of the voltammograms were characterised by a reduction of $Ru(NH_3)_6^{3+}$, at about -0.1 V *vs.* SCE, with a steady state shape. The limiting current reflected the ultrasonic mass transport of the redox active material to the surface and explained why at higher powers of ultrasound this limiting current became higher, as shown in Figure 5.6B. When using a 'face on' ultrasound system there was a large amount of noise present, especially in the mass transport limiting part of the voltammograms, due to the turbulent nature of the ultrasound and interfacial cavitation effects. The signals appeared very drawn out due to the size of the electrode causing ohmic drop and a high resistance (*ca.* 100 Ω) effect. The results are summarised in Figure 5.6A and 5.6B and as expected show a roughly linear relationship between the limiting current and the ultrasonic power. It was found that under these conditions the diffusion layer thickness ranged from *ca.* 30 – 120 μm.

$$Ru(NH_3)_6^{3+}{}_{(aq)} + e^- \rightleftharpoons Ru(NH_3)_6^{2+}{}_{(aq)}$$

Scheme 5.1 The reversible one electron redox couple $Ru(NH_3)_6^{3+}$.

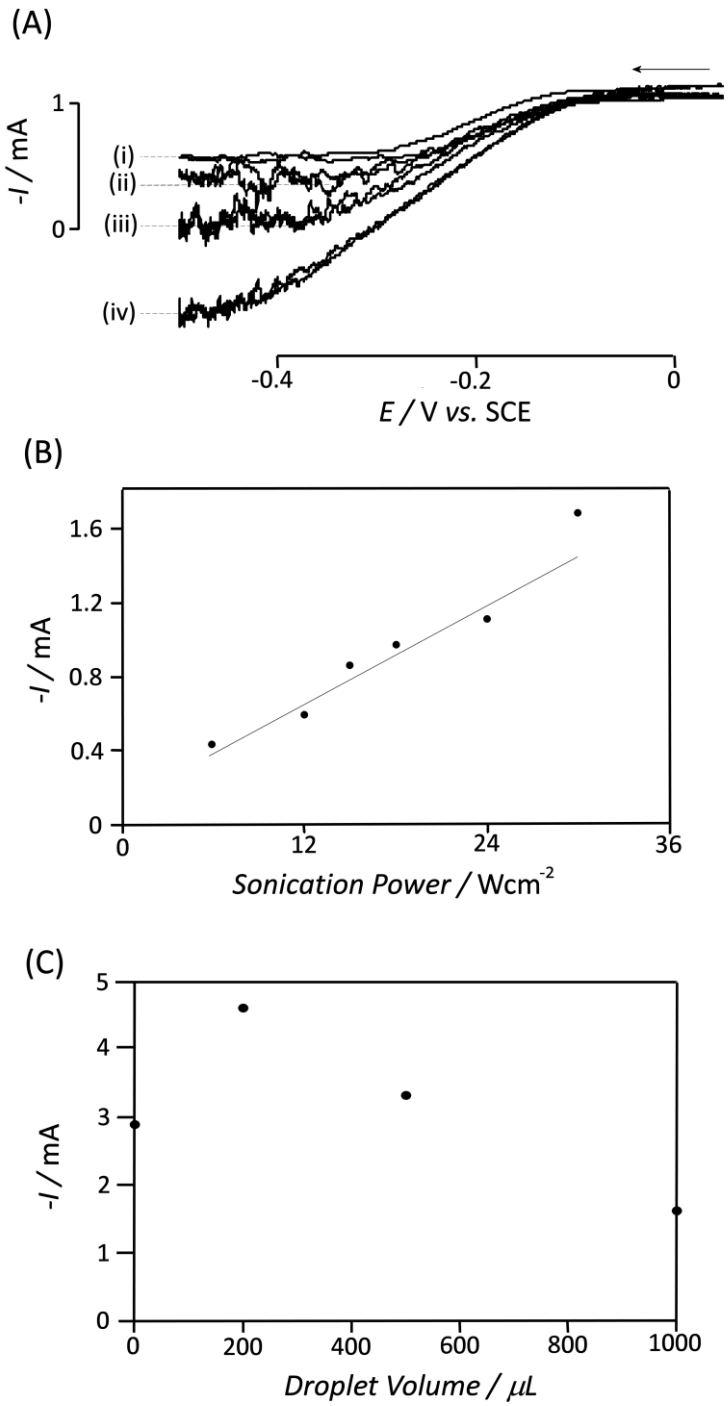

Figure. 5.6 (**A)** Voltammograms (scan rate 5 mVs^{-1}) for a single homogeneous aqueous phase of 2 mM $Ru(NH_3)_6^{3+}$ and 0.1 M KCl on a glassy carbon working electrode, with sonication at 15 mm from the electrode surface. (i) 6 Wcm^{-2} (ii) 12 Wcm^{-2} (iii) 18 Wcm^{-2} (iv) 30 Wcm^{-2}. **(B)** A plot of limiting current vs. sonication power for single phase calibration showing a linear agreement. **(C)** A plot of limiting current vs. droplet size calibration for a single electrochemically active aqueous phase of 10 mM $Ru(NH_3)_6^{3+}$ and 0.1 M KCl at a power of 15 Wcm^{-2} at a distance of 15 mm from the electrode surface with varying organic droplet size of DCE.

The same methodology was then applied for the same aqueous phase system (10 mM $Ru(NH_3)_6^{3+}$) with an electrochemically inactive droplet of 1,2-dichloroethane (DCE) placed on the surface. This experiment gave an idea of the effect that the organic phase had on the single phase mass transport. The results showed similar limiting currents to those seen with no DCE present (Figure 5.6C). However, in the presence of small droplets (200 µL) the limiting currents increased. This effect was possibly due to an increased streaming effect brought about by the presence of a surface immobilized droplet. It was anticipated that the major effect would be a blocking of the electrode surface by the droplet and hence a decrease in limiting current. After the initial increase in limiting current with a 200 µL DCE droplet being present this expected trend was indeed observed as a roughly linear decrease in limiting current. This was due to the contact area of the aqueous phase and electrode surface becoming reduced by the presence of a masking DCE phase.

5.3.2 The Effect of Ultrasound Power on Mass Transport in the Organic Phase Containing the *n*-Butylferrocene Redox Probe

The next stage of experiment was concerned with the dynamic triple phase boundary formed between the surface immobilized droplet, the solid electrode surface and the bulk aqueous phase containing electrolyte. In this case, the sonication effect was two fold. (i) The large DCE macro-droplet applied to the surface was broken up into smaller droplets to increase the triple phase contact area and (ii) agitation effects of both phases due to acoustic streaming from the sonicator. The system used was a 10 mM *n*-butylferrocene redox probe in the DCE organic phase with 0.1 M $NaClO_4$ in the aqueous phase, acting as a transfer reagent to balance the positive charge associated with ferrocenium formation. It is worth noting that no intentionally added electrolyte was present in the organic phase initially but that the oxidation stimulated the transport of anions from the aqueous phase into the organic phase as part of the triple phase boundary mechanism.

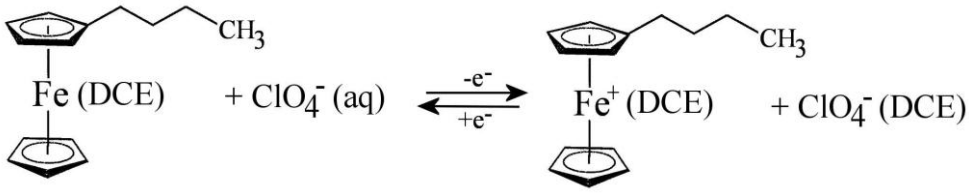

Scheme 5.2 The reversible one electron redox process of *n*-butylferrocene at a triple phase boundary.

An example of the limiting current scan obtained for a triple phase system is shown in Figure 5.7A for the case using 15 Wcm^{-2} sonication power. The onset of oxidation appeared at *ca.* 0.2 V *vs.* SCE and the response appeared drawn out due to a high resistance (*ca.* 1000 Ω), from the low conductivity within the droplet without any electrolyte. There was also evidence of a cathodic process occurring, showing that some bulk electrolysis was in effect over the time scale of the cyclic voltammetry, further supporting the hypothesis that the macro-droplets were broken up effectively into micro-droplets. Scans (ii)-(iv) in Figure 5.7A show the effect of the surface identity on the triple phase boundary signals.

For basal plane pyrolytic graphite (BPPG) electrode there was a slight increase over glassy carbon in the limiting current. However, for another type of commercially available graphite tested, 2120PT, a large increase in the limiting current was seen. This was possibly due to a roughening of the electrode surface changing the surface energy and interaction with droplets of different sizes and thus an increased triple phase zone.

As shown in Figure 5.7B, greater sonication power created more droplet agitation and a larger triple phase contact zone, which in turn lead to an increased limiting current. There was however a point around 15 Wcm^{-2} where the droplet became dispersed and organic material was lost from the surface, as shown by a decrease in the observed limiting current. This electrochemical trend was supported by a coinciding visual trend in which a bulk emulsion started to form in the aqueous phase. This was in contrast to the '2-dimensional' emulsion, closely associated with the electrode surface, seen at lower ultrasonic power. The optimal power for potential bulk electrolysis was found to be 15 Wcm^{-2} for this electrode and solvent system.

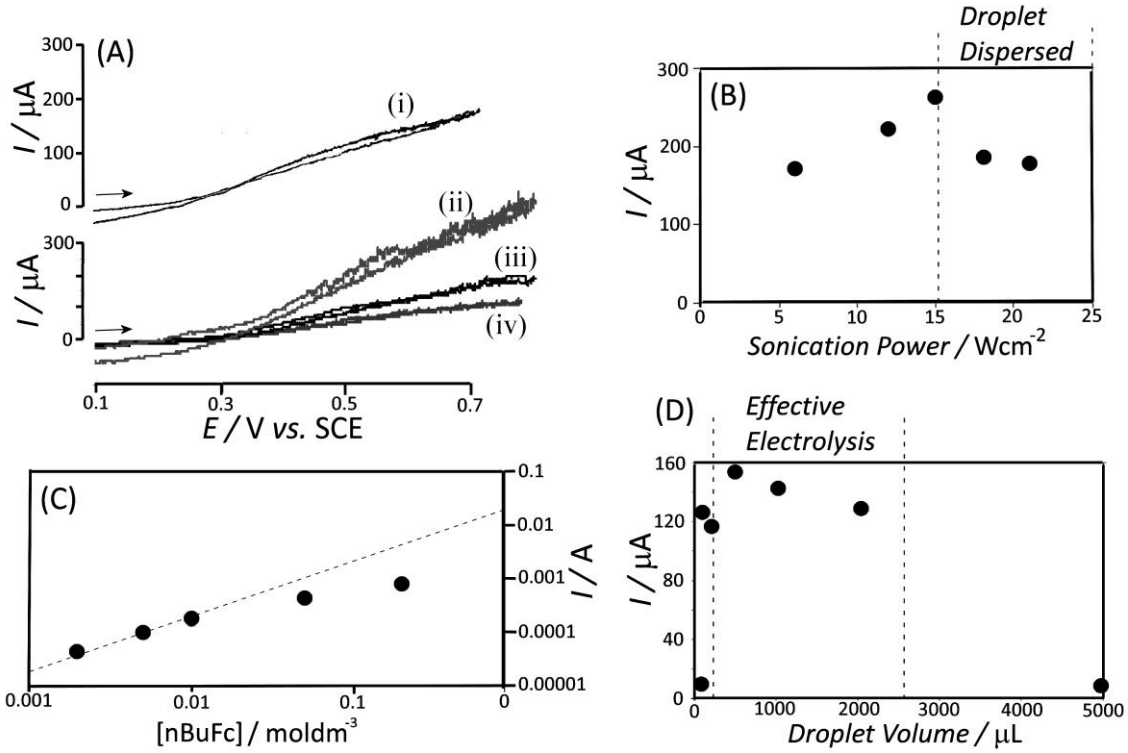

Figure 5.7 (A) Cyclic voltammograms (scan rate 5 mVs^{-1}) for the oxidation of 10 mM nBuFc in (i) 500 µL and (ii-iv) 200 µL 1,2-dichloroethane | aqueous 0.1 M $NaClO_4$ with sonication (15 Wcm^{-2} power, distance 15 mm). The electrode materials are (i) glassy carbon, (ii) graphite 2120PT, (iii) basal plane pyrolytic graphite, and (iv) glassy carbon. **(B)** Plot of the mass transport controlled limiting currents versus the sonication power (at a threshold of ca. 15 Wcm^{-2} the droplets become emulsified and disperse). **(C)** Logarithmic plot of the mass transport controlled limiting currents (recorded at a scan rate of 5 mVs^{-1} in the presence of aqueous 0.1 M KPF_6, sonication power 15 Wcm^{-2}, 15 mm distance) versus *n*-BuFc concentration in a 500 µL 1,2-dichloroethane droplet. **(D)** Plot of the mass transport controlled limiting currents (scan rate 5 mVs^{-1}, 5 mM *n*-BuFc, aqueous 0.1 M $NaClO_4$, sonication power 15 Wcm^{-2}, 15 mm distance) versus the droplet volume.

The effect of *n*-butylferrocene concentration was much as expected with an increase in *n*-butylferrocene concentration accompanying a linear increase in limiting current, shown in Figure 5.7C.

It was also of interest to explore the effect of the size of the droplet on the triple phase boundary process. A constant sonication power of 15 Wcm^{-2} at a distance of 15 mm perpendicular to the glassy carbon electrode surface (the optimum value found in Figure 5.7B) was used. This time the size of the DCE droplet was changed cumulatively with limiting currents reported at each

volume. The results in Figure 5.7D show there was a lower threshold at about 100 µL, above which effective electrolysis could be achieved using this methodology. Below this threshold it was found that droplets were too easily dispersed even at the low power conditions and redox material was lost to the bulk aqueous phase causing low limiting currents.

There was also an upper limit of about 2 mL, where the onset of electrode blocking occurs. The organic phase was now too large and entirely coated the electrode surface affording no triple phase boundary on which to perform oxidation. This observation suggested that the mechanism proposed previously was correct, with both phases needing simultaneous contact with the electrode surface. It is worth noting that this upper limit was far greater under the conditions of ultrasound than in a silent mode, in a silent mode the surface was obscured at about 500 µL.

The agitation of the low power ultrasound allowed a triple phase boundary to form by forcing aqueous phase to the electrode and breaking up the organic phase so it did not form a single continuous film on the electrode. In between these two limits existed a synthetically useful area where the limiting currents appeared to be comparable with each other and only a small dependence on the droplet volume was observed. The small volume dependence in this area however suggested that 500 µL was the optimal volume, but that any volume in this range had potential for effective electrosynthesis. It is important to note that this value was only applicable to this particular electrode, surface area and cell geometry used. A larger electrode could yield very different results and potentially allow a greater sonication power to be applied without the droplet becoming completely dispersed into the bulk.

5.3.3 The Effect of electrolyte ion identity on the Triple Phase Boundary n-Butylferrocene Oxidation Process

The identity of the transferring anion was of critical importance to the mechanism of the triple phase boundary process and the reversible potential of the processes. Hydrophobic ions transferred more readily, since they had greater affinity with the organic DCE phase and thus a lower energy of transfer. The electrolyte anions tested were perchlorate (ClO_4^-),

hexafluorophosphate (PF_6^-), tetraphenylborate (Ph_4B^-) and phosphate ions in a pH 1 buffer solution.

The mechanism for the hydrophobic ions (ClO_4^-, PF_6^- and Ph_4B^-) was proven to be the transfer of anions into the DCE phase as the *n*-BuFc was oxidised to ferrocenium, shown previously in Figure 5.4. The shift in the half wave potential is clearly shown in Figure 5.8A, with hydrophobic ions being transferred more easily and thus at lower potential, with a constant limiting current. Figure 8B shows a summary of the E_{mid} values plotted against the standard potential of ion transfer[26] where E_{mid} is defined as the potential at which half the limiting current has been reached. This plot shows that for the most hydrophobic ions (ClO_4^-, PF_6^- and Ph_4B^-) there was good correlation with an ideal unity gradient line. This suggested a directly proportional relationship between the standard transfer energy of the ion and the potential recorded for its transfer, as driven by the ferrocene oxidation at the triple phase boundary. This proved that the triple phase boundary mechanism was correct and the electrolyte ion identity was critical.

In the case of phosphate pH 1, it was found that a different mechanism dominated. The phosphate was too hydrophilic and instead of diffusing into the DCE to balance the positive charge of the ferrocenium, it was the ferrocenium ion which diffused into the bulk aqueous phase. The aqueous unstable ferrocenium ion was decomposed into iron (III) phosphate crystals on the electrode surface.[28] This effect is shown in Figure 5.8B by the negative deviation from the straight line relationship given by more hydrophobic ions. This showed that the E_{mid} value became independent of the electrolyte ions and reached a hydrophobicity point, after which it was more energetically favourable for the ferrocenium ion to transfer instead.

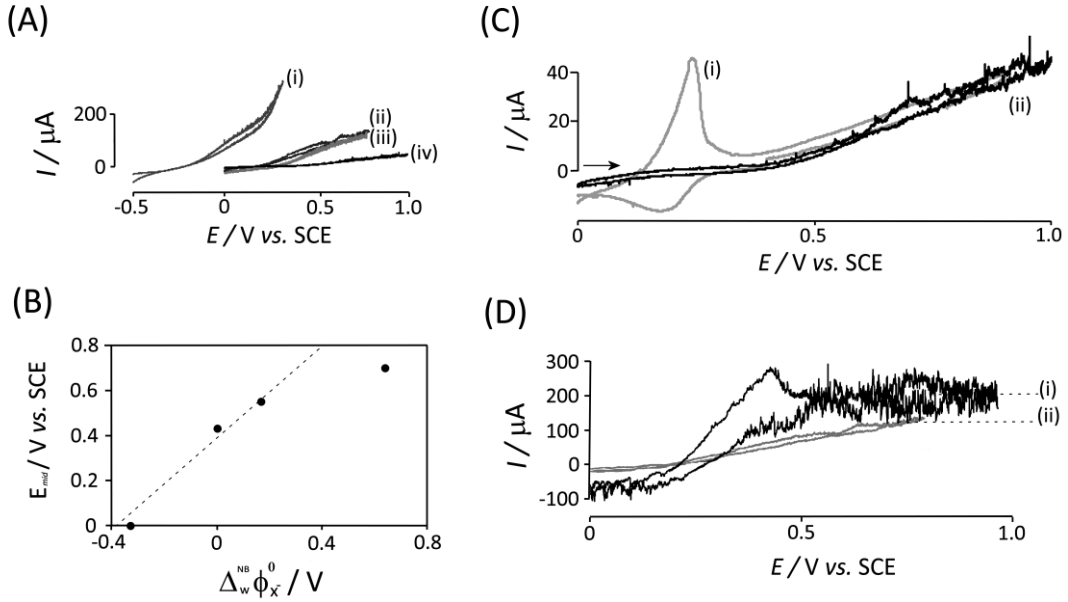

Figure 5.8 **(A)** Cyclic voltammograms recorded at 5 mVs^{-1} showing the effects of changing the transferring anion identity in the aqueous phase, whilst keeping the organic phase unchanged with 5 mM *n*-BuFc in a 200 µL DCE droplet, at a sonication power of 15 Wcm^{-2} and the sonic horn held 15 mm away from the glassy carbon working electrode (i) Ph_4B^- (ii) PF_6^- (iii) ClO_4^- (iv) Phosphate (ph 1). **(B)** A plot of the Gibbs energy of transfer for each transferring ion[27] against the potential at half the limiting current (E_{mid}). **(C)** This shows more detailed voltammograms obtained using a phosphate transfer ion in the aqueous phase (0.1 M) with a 5 mM *n*-BuFc in a 200 µL DCE droplet, both (i) silent and (ii) at a sonication power of 15 Wcm^{-2} with the sonic horn held 15 mm away from the glassy carbon working electrode. **(D)** Cyclic voltammograms recorded at 5 mVs^{-1} showing the effects of intentionally adding 0.1 M Tetrabutylammonium hexafluorophosphate (Bu_4NPF_6) supporting electrolyte to a 200 µL DCE droplet containing 5 mM *n*-BuFc, in the presence of 0.1 M KPF_6 in an adjacent aqueous phase, at a sonication power of 15 Wcm^{-2} with the sonic horn held 15 mm away from the glassy carbon working electrode; (i) With 0.1 M tetrabutylammonium hexafluorophosphate (ii) Without intentionally added electrolyte.

The formation of iron phosphate crystals may have caused the observed decrease in the limiting current, due to the deposit partially blocking the electrode surface. An additional sharp peak feature, *ca.* 0.23 V *vs.* SCE, was seen under silent conditions, as shown in Figure 5.8C. This sharp peak corresponded to the Iron (II/III) phosphate redox couple. This feature was not

seen under ultrasonic conditions since the cavitation effect of the ultrasound effectively removed the deposit.

Throughout this investigation a resistance effect was apparent due to the absence of supporting electrolyte in the organic phase, leading to resistance at the triple phase boundary. This was characterised by the drawn out nature of all limiting currents. Figure 5.8D demonstrates the effect of adding 0.1 M tetrabutylammonium hexafluorophosphate into the organic phase on the triple phase oxidation of *n*-BuFc. The triple phase boundary resistance was reduced as shown by the limiting currents, which became much less drawn out. It was also seen that the limiting current was slightly increased due to a greater reaction zone being formed within the organic droplet. Avoiding the use of electrolyte in the organic phase was however important for ease of separation and cost, and so electrolyte added examples were not further investigated. To combat the effects of resistance in this system without the use of an organic electrolyte a large overpotential was used. Data presented in this work suggested that electrolysis in surface mobilised 1,2-dichloroethane without intentionally added electrolyte was possible.

5.3.4 The Reduction of Benzil as a Synthetic Test Reaction in Triple Phase Boundary System

Benzil was chosen as the initial test reaction for use in the ultrasonically agitated triple phase boundary system, as it exhibits a simple two electron reduction (shown in Scheme 5.3) at relatively low potential (ca. -0.5 V). This value was comparable to the expected reversible reduction seen in a single phase organic system (Figure 5.9C)[50].

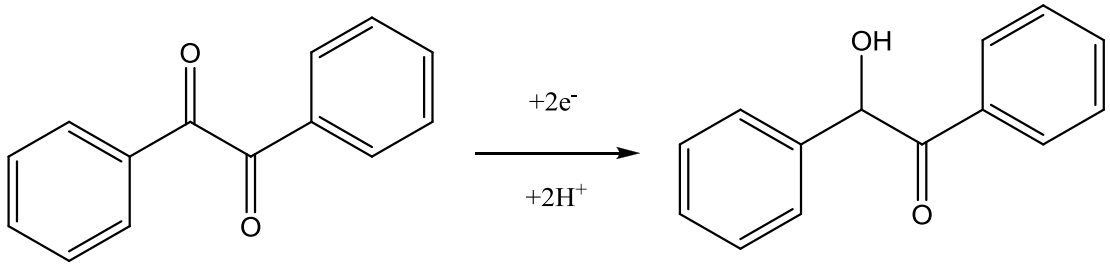

Scheme 5.3 The electrochemical reduction of Benzil.

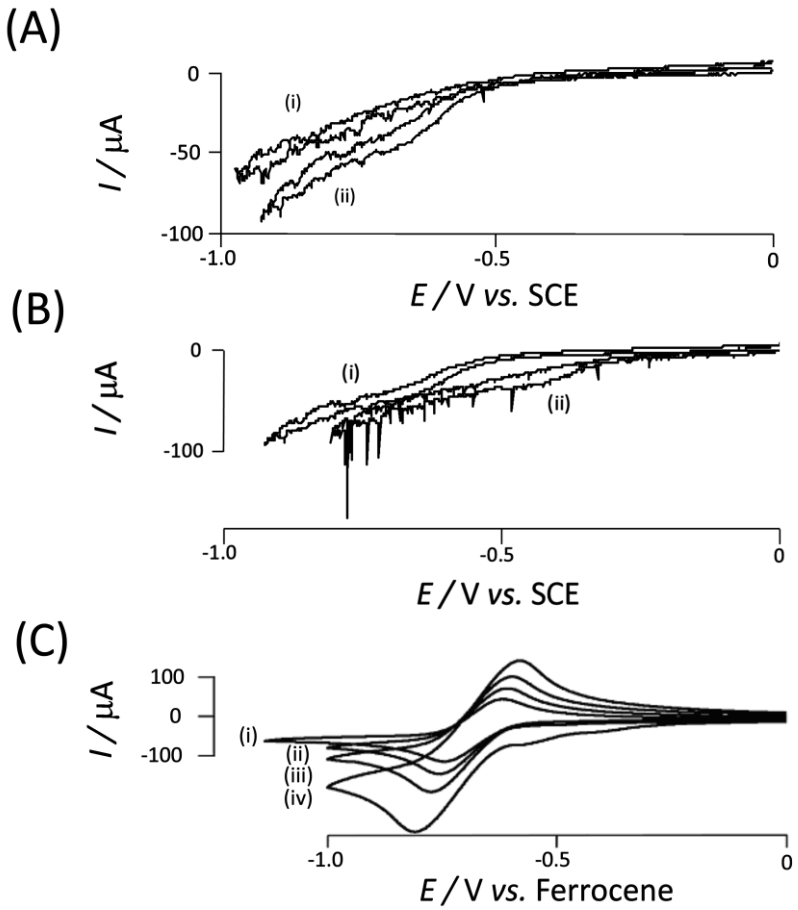

Figure 5.9 (**A)** Voltammograms for Benzil (i) 25mM and (ii) 50mM in a 1ml DCE droplet on a glassy carbon electrode surrounded by an aqueous solution of 0.1M $NaClO_4$ under a sonication power of 15Wcm^{-2} at a distance of 15mm perpendicular to the electrode surface. **(B)** Voltammograms for Benzil under the conditions above with different electrolyte solutions as the aqueous phase (i) 0.1M $NaClO_4$ (ii) 0.1M $HClO_4$. **(C)** Voltammograms for the single phase reversible reduction of 5mM benzil in anhydrous acetonitrile with 0.1M tetrabutylammonium bromide and a 3 mm glassy carbon working electrode (i) 50mVs^{-1} (ii) 100mVs^{-1} (iii) 200mVs^{-1} (iv) 500mVs^{-1}.

Figure 5.9A shows the limiting currents of benzil which appeared highly resistive as would be expected for a triple phase mechanism, but scale with the concentrations measured. Higher concentrations of benzil tended to become immiscible in the emulsified DCE and appeared as floating solid in the aqueous phase. It was thought that protons became the transfer reagent that accompanied the benzil reduction mechanism and were moved from the aqueous phase into the organic phase to balance the generated negative charge in the DCE droplet. This is supported by Figure 5.9B which shows that under acidic aqueous conditions (Figure 5.9Bii) more free protons are

available and the reduction occurred at a lower negative potential, which was expected only if the proton transfer was involved in the reduction mechanism.

Unfortunately, on analysis of the highest achievable limiting currents, it was deemed an unsuitable system for bulk triple phase electrolysis since a low limiting current meant the reaction time would be too long and the limitation of an open system posed problems with oxygen reduction.

5.3.5 The Oxidation of 1,2,3,4-Tetrahydro-1-naphthol as a Synthetic Test Reaction in Triple Phase Boundary System

It was hoped that the use of an oxidative system would eliminate oxygen based side reactions and associated background currents. 1,2,3,4-Tetrahydro-1-naphthol (THN) is the easiest alcohol based oxidation system, since its product α-tetralone is a highly energetically favourable aromatic system which should yield a low proportion of side products (Scheme 5.4).

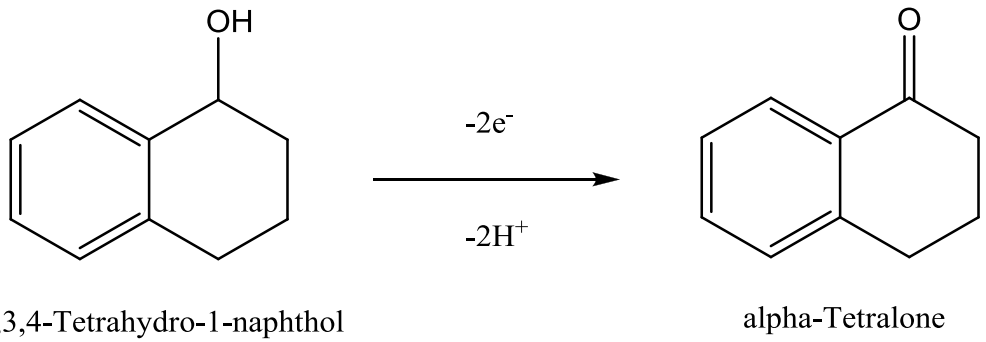

Scheme 5.4 The oxidation of 1,2,3,4-tetrahydro-1-naphthol to α-tetralone.

The proposed mechanism was the reverse of that seen for the benzil reduction. In the case of THN the oxidation caused a positive charge to build up in the DCE droplets which was accompanied by the proton release of generated protons into the aqueous phase to balance this charge. Figure 5.10 shows that although the limiting currents were poorly defined for the THN oxidation system the slopes of the signals did scale with concentration and this suggested that this oxidation may be suitable for electrolysis. It should also be noted that the currents seen were much larger than those achieved for the benzil reduction system, however it is likely that some current may be attributed to background processes.

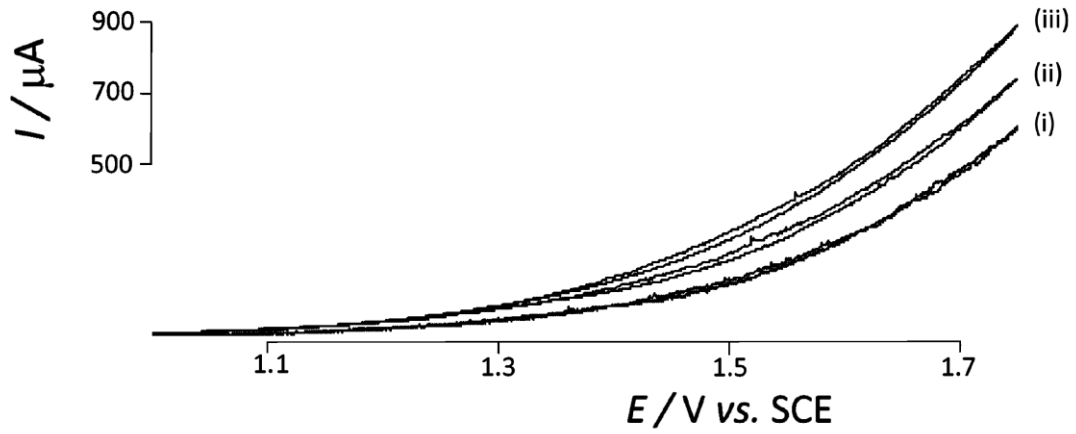

Figure 5.10 Voltammograms for 1,2,3,4-tetrahydro-1-naphthol oxidation with 15 Wcm^{-2} sonication at a distance of 15 mm perpendicular to the glassy carbon working electrode surface using a scan rate of 5 mVs^{-1} in a 200 µL DCE droplet with an aqueous phase of 0.1M KPF_6 and (i) 10 mM (ii) 20 mM (iii) 50 mM of 1,2,3,4-tetrahydro-1-naphthol.

5.3.6 The Oxidation of Benzyl Alcohol as a Synthetic Test Reaction in Triple Phase Boundary System in the absence of solvent

It was thought that using a chlorinated solvent such as DCE might be causing background problems and poor voltammetry, since chlorinated species are liable to dissociate in the presence of radicals to give highly destructive chlorine radicals. The next system aimed to eliminate some of these background problems used a solvent free environment. It was hoped that using a dense, water immiscible alcohol would result in a triple phase boundary system being found where a liquid redox active material could be used free of solvent. Although the oxidation of benzyl alcohol appeared at much higher potential than THN it was found that without DCE present the potential window into the oxidative range was greatly extended. Benzyl alcohol was chosen since it is slightly denser than water and is mostly immiscible with aqueous solutions. The expected oxidation is shown in Scheme 5.5.

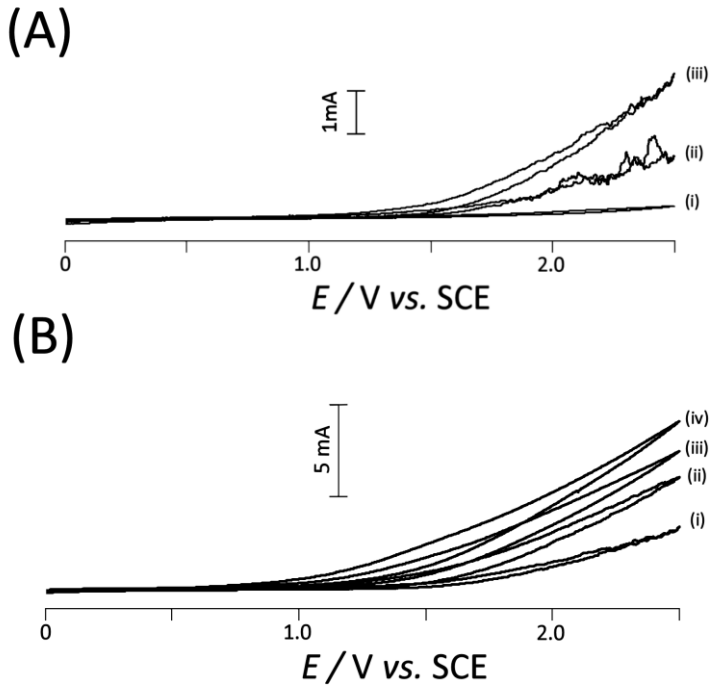

Figure 5.11 Voltammograms for the oxidation of 500 µL benzyl alcohol with no solvent immobilised on a glassy carbon working electrode in an aqueous solution of 0.1 M KPF_6 at a scan rate of 50 mVs^{-1}. **(A)** The effect of sonication power on the limiting currents (i) no sonication (ii) 6Wcm^{-2} (iii) 15 Wcm^{-2}. **(B)** The effect of temperature on the limiting currents with a sonication of 15 Wcm^{-2} 15 mm perpendicular to the GC working electrode (i) room temperature ca. 20 ^{o}C (ii) 40 ^{o}C (iii) 50 ^{o}C (iv) 60 ^{o}C.

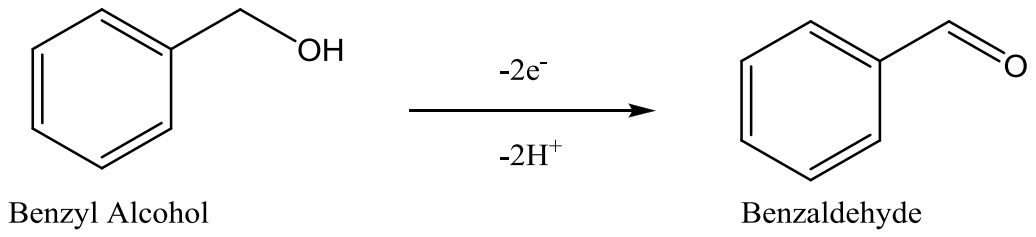

Scheme 5.5 The Oxidation of benzyl alcohol to benzaldehyde

Figure 5.11A revealed the anticipated highly resistive limiting currents but a clear sonication effect was also shown, with currents *ca.* 3 mA observed, using a sonication power of 15 Wcm^{-2}. This current although the highest yet achieved for the synthetic triple phase boundary processes was still insufficient to create a measurable amount of product over a reasonable time period. This increase was hypothesised to be due to the slight miscibility that benzyl alcohol possessed with water. This miscibility allowed a secondary aqueous based mechanism to proceed (Figure 5.12B) in which the benzyl

alcohol first partitioned into the aqueous phase where upon it was oxidised, with the more hydrophobic product likely redissolved in the organic phase.

The aqueous based mechanism and organic based triple phase boundary reaction could both reasonably contribute to the currents achieved. The triple phase boundary mechanism remained essentially unchanged (i) the alcohol in the triple phase boundary layer was oxidised, electrons were transferred to the working electrode (ii) H^+ moved into the pure aqueous phase to balance the positive charge generated (Figure 5.12A). Alternatively it was feasible that instead of a proton expulsion anion incorporation is possible, similar to what was found for the oxidation of *n*-Butylferrocene, especially considering the anion involved is the highly hydrophobic PF_6^-.

To try and boost the limiting current the temperature of the solution was controlled by thermostat and incrementally increased by heating the entire cell from beneath the working electrode. It was hoped that this heating effect would increase the triple phase boundary reaction by increasing diffusion speeds and making the benzyl alcohol more water soluble leading to an even more diffuse triple phase boundary zone. The effects of increasing the temperature are shown in Figure 5.8B and show a clear increase in the achieved currents. Finally, a 1 hour electrolysis was done at a potential of 2.5 V giving a current of *ca.* 10 mA. The resulting solution was separated using three clean aliquots of dichloromethane and washed with water to remove electrolyte. The resulting solution was dried and a ^1H NMR at 250 MHz showed a trace amount of the expected product benzaldehyde but in such a slight conversion that under these conditions either the side reactions dominate the reaction or the triple phase boundary was inefficient for bulk electrolysis under these conditions. This process required further optimisation to be used preparatively.

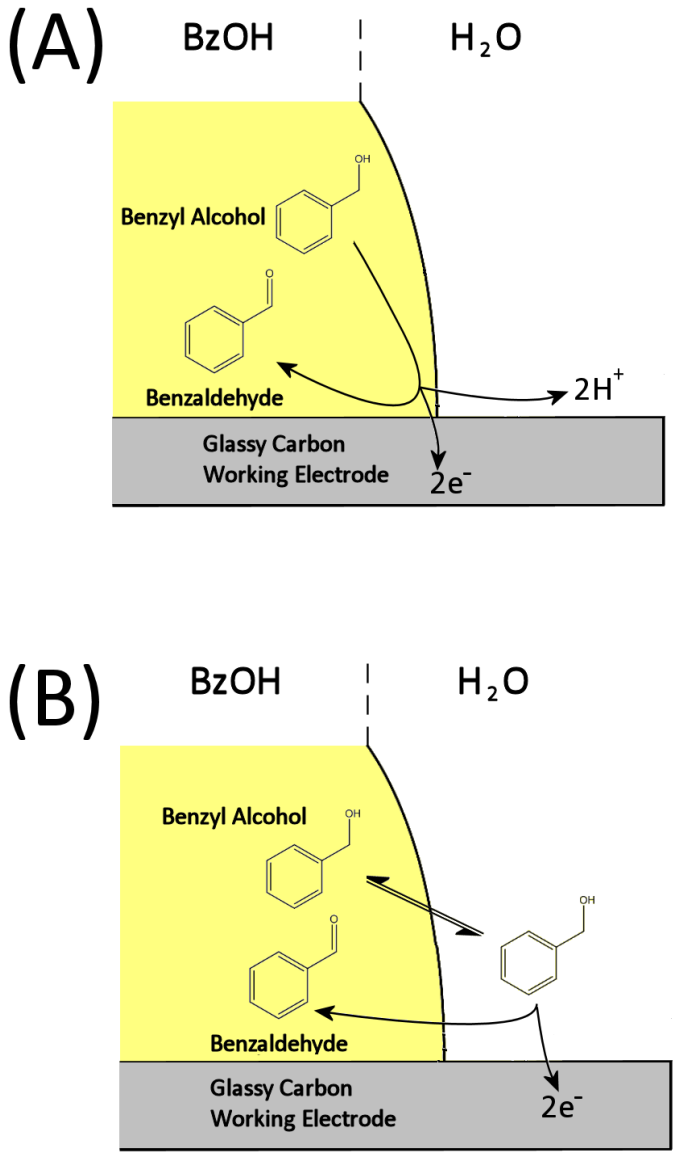

Figure 5.12 A cross-sectional view of a droplet in contact with an electrode surface showing two possible oxidation mechanisms for benzyl alcohol. **(A)** A triple phase boundary reaction where benzyl alcohol is oxidised in a 2 electron process in a concerted proton insertion. **(B)** Benzyl alcohol is suspected to be reasonably soluble in water and will partition significantly thus creating a single phase mechanism where it is likely the benzaldehyde product will be solubilised in the organic phase.

5.4 Conclusions

It has been shown that triple phase boundary processes for droplets of 1,2-dichloroethane on a glassy carbon electrode can be enhanced by low power ultrasound. This meant that larger volume droplets may be studied with all the benefits of micro droplet arrays larger contact area. These larger droplets

were more synthetically viable for bulk electrolysis including ion extraction or possible triple phase organic synthesis. Surface mobilisation of macro-droplets can be achieved without emulsification thus a dynamic triple phase boundary was created with agitation within the organic phase giving rise to increased limiting currents. The advantage of the triple phase system was that the electrolyte and electrode systems were held separate from the organic reaction meaning product extraction and characterisation were greatly improved from single phase systems where excess electrolyte made characterisation complicated.

It has also been shown that both simple oxidative and reductive reactions can be carried out at the triple phase boundary. Although synthetic chemistry at a triple phase boundary was greatly enhanced by using a 'dynamic' system such as ultrasound the results were too limited by the need for a dense solvent such as DCE and further optimisation is required before appreciable conversions of starting materials can be analysed. Reactions at triple phase boundaries were facile and can be achieved cleanly but even after an hour either too little conversion was seen or side reactions destroy potential products. When using pure organic reagents an improvement was seen in current density but even at increased temperature the current was still insufficient for suitable product turnover.

Without further optimisation of processes by the use of effective biphasic mediators or surface modification triple phase chemistry still remains primarily an analytical tool.

5.5 References

(1) Leighton, T. G. *The Acoustic Bubble*; Academic Press, **1997**.

(2) Mason, T. J. *Sonochemistry: The Uses of Ultrasound in Chemistry*; The Royal Society of Chemistry, **1990**.

(3) (a) Gaplovsky, A.; Gaplovsky, M.; Toma, S.; Luche, J. L. *Journal of Organic Chemistry* **2000**, *65*, 8444; (b) Toma, S.; Gaplovsky, A.; Luche, J. L. 7th Meeting of the European-Society-of-Sonochemistry, Biarritz Guethary, France, **2000**; p 201.

(4) Cella, R.; Stefani, H. A. *Tetrahedron* **2009**, *65*, 2619.

(5) Ooi, T.; Tayama, E.; Doda, K.; Takeuchi, M.; Maruoka, K. *Synlett* **2000**, 1500.

(6) Marken, F.; Compton, R. G.; Davies, S. G.; Bull, S. D.; Thiemann, T.; Melo, M.; Neves, A. C.; Castillo, J.; Jung, C. G.; Fontana, A. *Journal of the Chemical Society-Perkin Transactions 2* **1997**, 2055.

(7) (a) Marken, F.; Goldfarb, D. L.; Compton, R. G. *Electroanalysis* **1998**, *10*, 562(b) Akkermans, R. P.; Ball, J. C.; Rebbitt, T. O.; Marken, F.; Compton, R. G. *Electrochimica Acta* **1998**, *43*, 3443; (c) Compton, R. G.; Eklund, J. C.; Marken, F. *Electroanalysis* **1997**, *9*, 509; (d) Compton, R. G.; Foord, J. S.; Marken, F. *Electroanalysis* **2003**, *15*, 1349.

(8) Atobe, M.; Ikari, S.; Nakabayashi, K.; Amemiya, F.; Fuchigami, T. *Langmuir* **2010**, *26*, 9111.

(9) Holt, K. B.; Del Campo, J.; Foord, J. S.; Compton, R. G.; Marken, F. *Journal of Electroanalytical Chemistry* **2001**, *513*, 94.

(10) Mason, T. J. *Chemical Society Reviews* **1997**, *26*, 443.

(11) Banks, C. E.; Compton, R. G. *Analyst* **2004**, *129*, 678.

(12) Marken, F.; Akkermans, R. P.; Compton, R. G. *Journal of Electroanalytical Chemistry* **1996**, *415*, 55.

(13) Eklund, J. C.; Marken, F.; Waller, D. N.; Compton, R. G. *Electrochimica Acta* **1996**, *41*, 1541.

(14) Floate, S.; Hardcastle, J. L.; Cordemans, E.; Compton, R. G. *Analyst* **2002**, *127*, 1094.

(15) Compton, R. G.; Marken, F.; Rebbitt, T. O. *Chemical Communications* **1996**, 1017.

(16) Marken, F.; Eklund, J. C.; Compton, R. G. *Journal of Electroanalytical Chemistry* **1995**, *395*, 335.

(17) Banks, C. E.; Compton, R. G.; Fisher, A. C.; Henley, L. E. *Physical Chemistry Chemical Physics* **2004**, *6*, 3147.

(18) Compton, R. G.; Eklund, J. C.; Page, S. D.; Rebbitt, T. O. *J. Chem. Soc.-Dalton Trans.* **1995**, 389.

(19) Compton, R. G.; Eklund, J. C.; Marken, F.; Rebbitt, T. O.; Akkermans, R. P.; Waller, D. N. Baltic Conference on Interfacial Electrochemistry -

Electrochemical Reactivity of Electrode Surface, Tartu, Estonia, **1996**; p 2919.

(20) Kruusma, J.; Nei, L.; Hardcastle, J. L.; Compton, R. G.; Lust, E.; Keis, H. *Electroanalysis* **2004**, *16*, 399.

(21) (a) Hardcastle, J. L.; Ball, J. C.; Hong, Q.; Marken, F.; Compton, R. G.; Bull, S. D.; Davies, S. G. *Ultrasonics Sonochemistry* **2000**, *7*, 7; (b) Marken, F.; Kumbhat, S.; Sanders, G. H. W.; Compton, R. G. *Journal of Electroanalytical Chemistry* **1996**, *414*, 95.

(22) Low, C. M. R. *Ultrasonics Sonochemistry* **1995**, *2*, S153.

(23) Ando, T.; Bauchat, P.; Foucaud, A.; Fujita, M.; Kimura, T.; Sohmiya, H. *Tetrahedron Letters* **1991**, *32*, 6379.

(24) Cintas, P.; Luche, J. L. *Green Chemistry* **1999**, *1*, 115.

(25) Mason, T. J.; Lorimer, J. P.; Bates, D. M. *Ultrasonics* **1992**, *30*, 40.

(26) (a) Banks, C. E.; Davies, T. J.; Evans, R. G.; Hignett, G.; Wain, A. J.; Lawrence, N. S.; Wadhawan, J. D.; Marken, F.; Compton, R. G. *Physical Chemistry Chemical Physics* **2003**, *5*, 4053; (b) MacDonald, S. M.; Fletcher, P. D. I.; Cui, Z. G.; Opallo, M. C.; Chen, J. Y.; Marken, F. 57th ISE Annual Meeting **2006**, Edinburgh, SCOTLAND, 2006; p 1175.

(27) Marcus, Y. *Ion Properties*; 10 ed.; Marcel Dekker, Inc., **1997**.

(28) McKenzie, K. J.; Marken, F. Workshop on Electchemistry and Interfacial Chemistry in Environmental Clean-Up and Green Chemical Processes, Coimbra, Portugal, **2001**; p 1885.

6. Ultra-turrax Generated Emulsion for Electrosynthetic Reactions at the Triple Phase Boundary

Contents

Chapter 6: Ultra-turrax Generated Emulsion for Electrosynthetic Reactions at the Triple Phase Boundary

Aims

- To use a high shear force ultra-turrax to create bulk emulsions capable of efficient triple phase boundary reactions.
- To analyse redox processes; i) in the aqueous phase with a blank organic phase, ii) in the organic phase at the triple phase boundary.
- To use the mobile organic phase emulsion to solubilise deposits of redox product from electrode surfaces as novel biphasic mediators.

Publication

- Watkins JD, Amemiya F, Atobe M, Bulman-Page PC and Marken F, *Electrochimica Acta,* **2010**, 55, 8808 – 8814.

CHAPTER 6: Ultra-turrax Generated Emulsion for Electrosynthetic Reactions at the Triple Phase Boundary

6.1 Introduction

A particular problem with single phase electrosynthesis is that electrochemical reactions require a 10-20 fold excess of electrolyte to act as charge carriers. Methods which avoid this need for added salt are very important. Biphasic electrochemistry is one such method and will be discussed in this introduction.

It has already been shown that an emulsion can provide a highly suitable environment for effective triple phase boundary electrochemistry, as demonstrated by an ultrasonic system (Chapter 5). In a similar system, an ultra-turrax high shear force generator was used to stabilise a temporary emulsion of oil droplets in water. In this case the action was similar to a blender in which rotating blades cut the oil phase into fine droplets that became dispersed in the aqueous phase.

The potential benefits were two fold for triple phase boundary techniques: i) The small size of droplets created a very large triple phase contact boundary compared to their total volume ensuring effective electrolysis. ii) The rotational motion forced droplets onto an electrode placed below the ultra-turrax allowing the droplets to effectively bombard the electrode, creating a large hydrodynamic effect both in the aqueous phase and within the highly turbulent organic droplet emulsion phase.

When compared to an ultrasonic technique this method avoided the potential cavitational damage to electrode surfaces as well as being suitable for a wider range of solvents, which were less dense than water. However much like the low powered ultrasonic technique discussed previously, the shear force generated emulsion was highly unstable and instantly reformed a bulk phase when the shear force was removed. This instability allowed the facile

extraction of organic products from the oil phase without further separation steps.

The liquid | liquid interface has been used successfully in a wide range of applications, most notably in the formation of polyaniline nanofibres by using the selective reactivity of the liquid interface to better control the polymerisation.[1] In synthetic organic chemistry the liquid | liquid interface can lead to a range of new catalytic chemistries. These involve an aqueous heterogeneous catalyst which is kept separate from a reaction centre in an organic phase.[2] In the emulsion the catalyst is able to operate at the interface, with products being isolated in the organic phase and facile separation and recycling of the catalyst.

The disadvantages of such a system are primarily due to the low reactivity when compared to homogeneous catalysis and often a related loss of selectivity. A notable example is a catalytic oxidation of simple alcohols by a water-soluble palladium (II) bathophenanthroline complex.[3] In this case, water insoluble alcohols formed a phase separation with the aqueous phase containing catalyst. However, these alcohols may partition into the aqueous phase allowing for reaction. The reaction rate was controlled by the solubility of the alcohol in the water, with a post-reaction extraction by ether allowing the aqueous phase to be reused. The conversions were excellent and showed a selective oxidation of unsaturated alcohols as well as the ability to control primary alcohol oxidation to aldehydes or carboxylic acids, by careful adjustment of conditions.

Another major disadvantage of an aqueous | organic biphasic system is the reliance on a partitioning mechanism to aid the reaction rate, so for very hydrophobic organic molecules this process could be very slow. One solution is to use a phase separation based on a fluorous | organic interface. A highly fluorinated hydrocarbon is used as an immiscible phase, and by fluorinating the ligands of standard metal catalysts the catalyst can be immobilised in this phase.[4] This reaction can be run as a direct analogue of the aqueous biphasic reaction, or as a single phase system. Upon heating, the fluorous phase can solubilise in the organic phase giving a single homogeneous mixture allowing a rapid reaction rate. When cooled, the phase separation

reoccurs automatically, separating the reaction mixture and catalytic phases. Perfluorinated solvents can also be used as immiscible partners with aqueous phases as shown by Nishimoto *et al.*[5] in the biphasic diels alder reaction where both fluorous and aqueous conditions are known to enhance this reaction.

Another biphasic system of great interest in synthetic chemistry is the use of ionic liquids. These are a versatile new category of materials which exist as ion pairs but with a sufficiently low melting point as to be easily attainable in liquid form at relatively low temperatures.[8] For a room temperature ionic liquid (RTIL) in general, mismatched ion pairs are used to create a sufficiently weak ionic lattice that at low temperatures the ions form a liquid. Commonly, a bulky asymmetric organic cation is accompanied by almost any anion. Halide based anions generally lead to higher temperature ionic liquids than inorganic ones such as PF_6^-. Some common examples are shown in Figure 6.1.

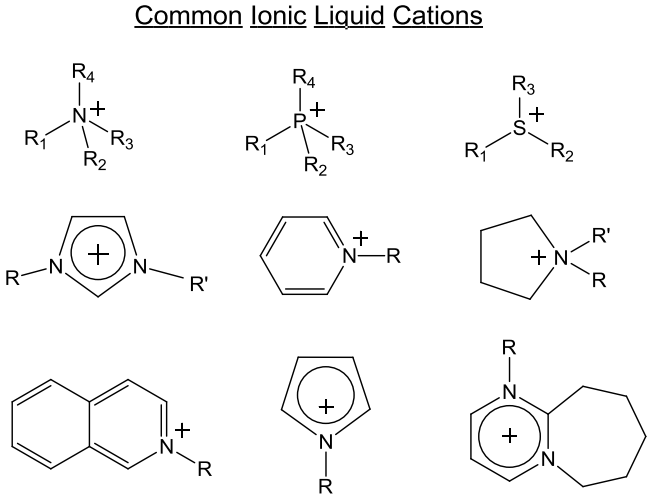

Figure 6.1 Some common cations used to form ionic liquids.

Ionic liquids are useful in catalysis due to their high stability, low reactivity and low vapour pressure as summarised in a review by Sheldon.[6] Furthermore, due to the expansive nature of the combinations of ions possible for ionic liquids, they have very tuneable physical properties such as melting point, boiling point and dipole moment.

In biphasic catalysis it is essential that the catalyst is not degraded during the course of the reaction, it can be easily removed from the reaction mixture and

can be reused multiple times. A biphasic ionic liquid method was used to separate catalysts and reaction materials by using a monophasic mixture of ionic and organic phases. This was followed by the removal of volatile organic products from non-volatile RTIL *in vacuo*[6] or by using a biphasic reaction where catalyst and reactants were kept in separate phases during the reaction and elucidated by decanting.[7] Although, in this final case there must be enough partitioning to ensure good turnover. The use of RTILs in the synthesis and separation of a multitude of organic materials has been reviewed extensively by Tzschucke *et al.*[8]

A further biphasic system can be derived from the use of supercritical fluids. A supercritical fluid is a fluid that is subjected to pressures and/ or temperatures above their 'critical value' which creates a new liquid like state. A commonly used super critical liquid is derived from carbon dioxide ($scCO_2$) and is both environmentally friendly and nonhazardous as well as using only very mild conditions (T_C = 31.1 ^oC , P_C = 73.8 bar)[8] to become supercritical. In the case of supercritical reactions, the separation is simply achieved by depressurisation leaving dry products with no associated solvent. If the $scCO_2$ is combined with ionic liquids in a biphasic system then it is also possible to easily separate catalysts in a reusable ionic liquid phase where trace $scCO_2$ can be completely removed by depressurisation.[9]

An interesting example in the field of electrosynthesis has shown the potentially high yielding oxidation of benzyl alcohol to benzaldehyde in a mixed $scCO_2$ ionic liquid mixed system,[9] The ionic liquid was used as an electrolyte and $scCO_2$ was used at various pressures to control product yields. This overcame the problem of low electrolyte solubility in $scCO_2$ and allowed the same facile product isolation procedure to be used from $scCO_2$ as previously described. Furthermore, the ionic liquid phase was shown to be reused over many reactions and was thus not wasted. A final useful property of supercritical fluids is that they are true designer solvents similar to ionic liquids.[10] The key difference is that instead of a laborious synthetic approach to change chemical compositions, temperature and pressure may be varied to change the solvent properties. The miscibilities of co-solvents such as ionic liquids can be varied such that a reaction may be completed in a

monophasic system and with a change in pressure may be turned into a biphasic system for easy product extraction.[10]

Whatever biphasic mixture is used, the benefits of highly dispersed emulsions are that droplets become pseudo water soluble. This means that the droplet is so small that it can be assumed to be molecular sized within an immiscible phase, thus giving important properties as if it were soluble. Without ultrasound or high shear forces surfactant molecules can be used to stabilise micro-emulsions.[11]

The use of emulsions is especially important in electrosynthesis since the immiscible phase may be an aqueous phase containing electrolyte and the emulsion an organic reagent. In this way electrosynthesis can be achieved in aqueous conditions, ideal for conductivity, even though the substrate is insoluble in water.

This methodology lends itself to a mediation approach, where an insoluble organic reagent is indirectly reduced or oxidised by a mediator. In this case the mediator is in the aqueous phase and once reduced or oxidised can partition into the organic phase in order to pass on this charge to the redox centre in the droplet[12] (Figure 6.2).

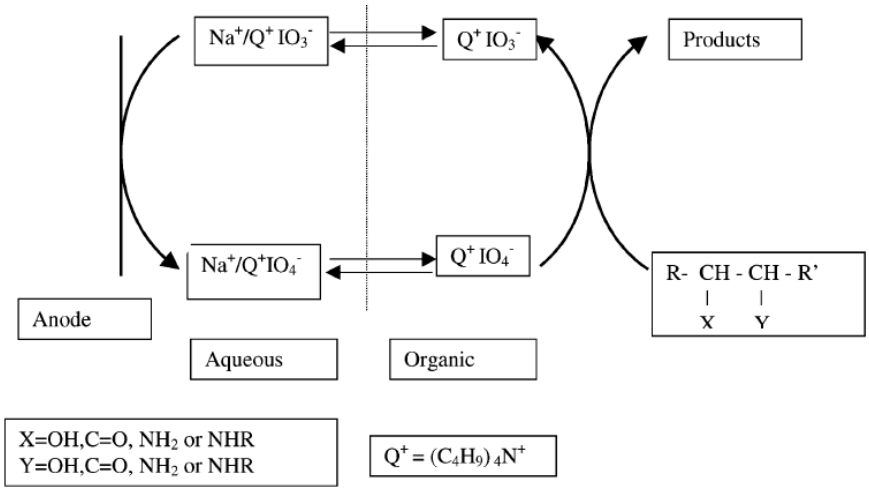

Figure 6.2 A general scheme of a mediated biphasic oxidation reaction.[12b]

Mediation can use any readily oxidised or reduced species and is not strictly a biphasic reaction. Mediated organic systems using a *tris*(4-

bromophenyl)amine$^{+/0}$ couple have been demonstrated in a single phase system by Park *et al.*[13]

A good example of biphasic mediation utilises cobalt based salts and complexes[14] most notably vitamin B_{12}[15] and It has been shown that this can promote asymmetric carbon-carbon bond formation.[12a] Properties of cobalt complexes that make it suitable for mediation are that it has a low reduction potential and is highly reversible. In biphasic applications vitamin B_{12} has an interesting characteristic in that the oxidised form is aqueous soluble, however the reduced form is often aqueous insoluble. This solubility change causes the reduced vitamin B_{12} to form crystals on an electrode surface, which may be characterised by a sharp stripping oxidation peak. This deposit is however highly soluble in organic solution and thus will become dissolved in an organic emulsion, making it an effective mediator to transfer electrons to organic materials in the emulsion. This effect has been investigated by Marken *et al.*[16] under ultrasound conditions to form a stable emulsion using the reduction of cobalticinium hexafluorophosphate. It was found that the stripping oxidation peak disappeared when the ultrasound assisted reduction took place, leaving instead a well defined limiting current. It was even possible to visualise the second reduction of neutral cobaltocene at very negative potentials, as shown in Figure 6.3. Similar results have been found for the oxidation of *leuco*-Methylene Green which forms a water insoluble oxidised product.[17]

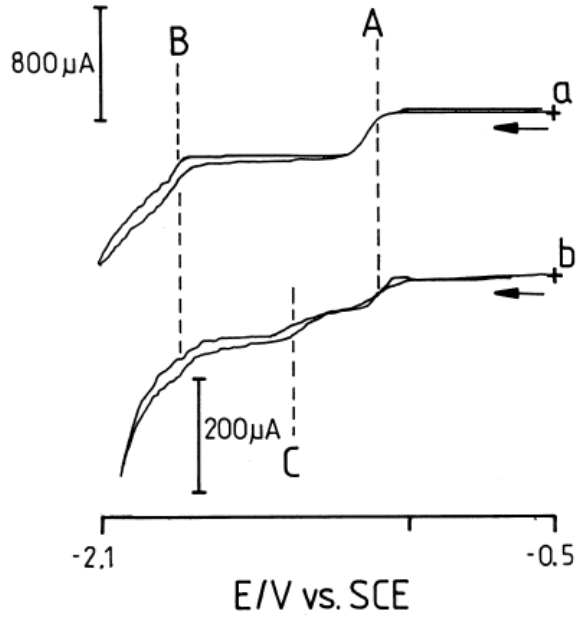

Figure 6.3 Voltammograms showing the ultrasound assisted steady state reduction of cobalticinium hexafluorophosphate at a glassy carbon electrode in the presence of a 1-octanol emulsion as a trapping solvent for the solid neutral cobaltocene product. Process A is the $CoCp_2^{+/0}$ redox couple, process C is the $CoCp_2^{0/-}$ redox couple and process B is yet to be identified.[16]

Biphasic synthetic techniques are already starting to emerge in the field of electrosynthesis. The benefits of biphasic systems are often that side reactions can be suppressed and electrolyte can be excluded as a contaminant from the product mixture. Biphasic alternatives are being developed based on the idea of the 'cation pool' method, as introduced in Section 1.3.6. This system, called the 'cation flow' method,[18] was discovered by Horii *et al.*[19] and used the principle that in one flowing phase stable cations are produced in high concentration. When a second immiscible parallel flow was introduced, containing a nucleophile, the nucleophiles underwent phase transfer by diffusion and reacted with the cations to form products.

The idea of biphasic electrosynthesis is not limited to liquid | liquid systems. Much research has been done into solid | liquid biphasic systems in various circumstances. Tajima *et al.*[20] have used the concept of an electrolyte solution generated *in situ* by solid supported bases. It was found that protic solvents in the presence of a solid supported base dissociated to give protons and these protons acted as charge carriers in electrosynthesis. In

this case, it can now be imagined that the solid supported base may be filtered out of the product mixture, post reaction, leaving just the product containing protic solvent, with no electrolyte contaminant. This also meant that the solid base can be recycled. This idea of an *in situ* generated electrolyte has already been successfully applied to the Kolbe reaction mentioned previously.[21]

Biphasic reactions are useful for isolating very reactive intermediates from a potentially reactive environment, thus allowing less side reactions and giving better control of products. This was found in an example by Chiba *et al.*[22] who used a sodium dodecyl sulphate micellular system with a $Ce^{III/IV}$ mediator to create quinones for a Diels Alder reaction within micelles, which would usually be halted by side reactions with water. This work was followed by a similar example using hydrophobic PTFE fibres on a glassy carbon electrode.[23] In this case the unstable quinones stayed close to the hydrophobic PTFE fibres where the organic based dienes were situated and performed a Diels Alder coupling to capture the unstable intermediates. This same arrangement was then used to make facile euglobal natural products in good yield.[24] Both of these approaches have the benefit of stopping diene oxidation, which would lead to decomposition and a loss of yield, by using modified electrode surfaces.

Another method to avoid the inclusion of excess electrolytes involves micro-gap reactors.[25] This method used paired syntheses with electrodes close enough together in a face to face configuration that the electrochemical conductivity was sufficient using only electro-generated species in the flow cell. This has been applied to synthetic cathodic reactions,[26] sometimes with a porous film between the electrodes,[27] paired synthetic reactions,[28] and with scale up capabilities of such a system being investigated.[29]

In this Chapter an ultra-turrax high shear force generator was used to emulsify an unsupported organic phase in water. Redox processes were conducted either in the aqueous phase, or organic phase as a triple phase boundary system. The unstable nature of the emulsion meant that a separation was easily achieved by removal of the shear force for product extraction. The high shear forces were used to enhance the hydrodynamic

transport at the triple phase boundary, as well as creating large triple phase boundary reaction zones. Finally a blank organic phase was used as a capture phase for insoluble aqueous redox products as a step towards a biphasic mediated process.

6.2 Experimental

6.2.1 Chemical Reagents

Sodium perchlorate (98%, Aldrich), hexaammineruthenium(III)chloride (Aldrich, 98%), *n*-butylferrocene (98%, Alfa Aesar), potassium hexafluorophosphate (Aldrich, 99.9+%), cobaltocenium hexafluorophosphate (Aldrich, 98%), potassium chloride (Sigma, 99.0-100.5%), sodium chloride (Sigma Ultra, 99.5%), sodium tetrafluoroborate (Aldrich, 98%), and sodium nitrate (Aldrich, 98%) were obtained and used without further purification. Filtered and demineralised water was taken from a Millipore water purification system with not less than 18 MOhm cm resistivity.

6.2.2 Instrumentation

Voltammetric measurements were conducted with a μ-Autolab III potentiostat system (Eco Chemie, Netherlands) in staircase voltammetry mode with a 2.3 cm^2 glassy carbon (type 1, Alfa Aesar) working electrode. A platinum counter electrode and a KCl-saturated calomel reference electrode (SCE, REF401, Radiometer) were placed in the side arms of the experimental cell (see Figure 6.4). An IKA ultra-turrax homogenisation system (Fisher Scientific) was employed and a glass cell custom-made to fit the ultra-turrax probe (see Figure 6.4C). The working electrode was placed at the bottom of the cell with a seal ring. All experiments were conducted at 20 +/- 2 ^oC.

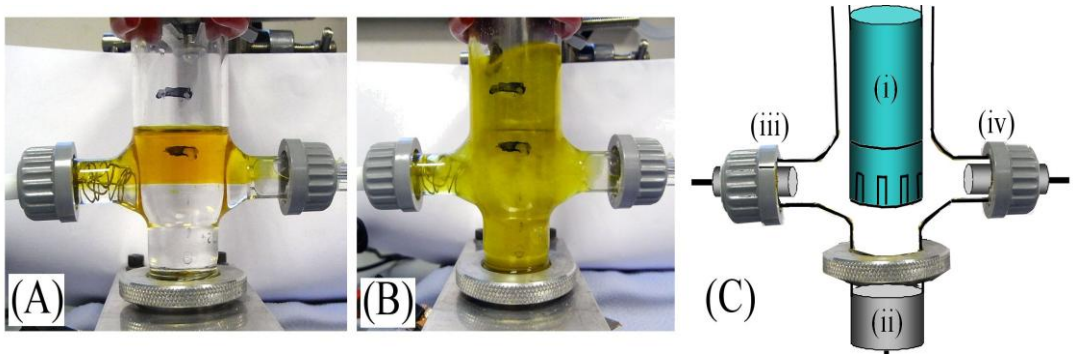

Figure 6.4 (A) Photograph of an acetonitrile | aqueous 2 M NaCl two phase system (14 cm^3 aqueous and 9 cm^3 organic phase, 50 mM n-butylferrocene colours the upper organic phase yellow) in the ultra-turrax electrolysis cell. **(B)** Photograph of the cell during ultra-turrax operation. **(C)** Schematic drawing of the cell with (i) ultra-turrax insert, (ii) working electrode, (iii) counter electrode, and (iv) the reference electrode.

6.3 Results and Discussion

The ultra-turrax high shear force mixer was used to generate an emulsion for multiple electrochemical reactions, as illustrated in Figure 6.5. The first example (A) shows the reaction of a redox probe in a fully electrochemically supported aqueous phase with an emulsified blank organic phase. Alternatively a triple phase reaction (B) was achieved with an emulsified unsupported organic phase containing a suitable redox probe in a bulk aqueous phase containing electrolyte. The triple phase boundary was created at the electrode surface as the microdroplets bombarded it and were rapidly removed. The advantages of the shear force method at the triple phase boundary were two-fold; i) the microdroplets created a large triple phase boundary length compared to droplet area and ii) the stirring forces created a turbulent movement of droplets, with high mass transport conditions in both the emulsified organic and aqueous phases. The final electrochemical reaction that was exploited in the ultra-turrax system was for the case of an aqueous based redox process which formed an insoluble product on the electrode surface (C) which became solubilised in a mobile organic emulsion. This product solubilisation was used to separate products in the organic phase from electrolyte in the aqueous phase by cleaning the electrode surface during an electrochemical reaction to prevent fouling.

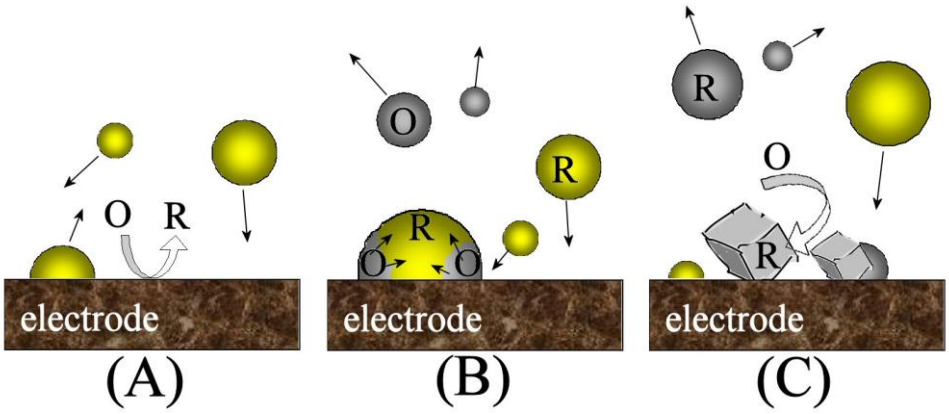

Figure 6.5 This shows a schematic drawing of **(A)** a redox process in the aqueous phase in the presence of inert organic phase, **(B)** a redox process at the triple phase boundary with dynamic removal of product from the electrode surface. and **(C)** a redox process in the aqueous phase producing an organic soluble product which is then removed by dissolution into the organic phase.

6.3.1 Liquid-Liquid Biphasic Electrochemistry I.: Aqueous Phase Reduction of $Ru(NH_3)_6^{3+}$ in Acetonitrile | Aqueous Electrolyte

Initially, a simple aqueous redox probe $[Ru(NH_3)_6]^{3+}$ was analysed with and without an immiscible organic phase being present. This method helped to show the blocking effects of an organic emulsion as well as the effect of mass transport rate on limiting currents. $[Ru(NH_3)_6]^{3+}$ is known to undergo a simple one electron reduction process, *ca.* -0.18 V *vs.* SCE in 0.1 M KCl (Scheme 6.1), and is not known to partition into the organic acetonitrile phase. Acetonitrile is commonly miscible with water so a large amount of sodium chloride was added to ensure a biphasic system.

$$Ru(NH_3)_6^{3+}{}_{(aq)} + e^- \rightleftharpoons Ru(NH_3)_6^{2+}{}_{(aq)}$$

Scheme 6.1 The reversible one electrode redox couple $Ru(NH_3)_6^{3+}$.

The phase separation was clearly shown (Figure 6.4A), where the less dense acetonitrile phase resided on top of the aqueous 1 M NaCl solution and was coloured with a yellow dye. Upon the application of high shear force mixing, provided by an ultra-turrax system, an emulsion was formed. This effect is shown in Figure 6.4B and caused the organic phase microdroplets to rapidly bombard the electrode at the base of the device. Upon removal of the high shear force a biphasic separation reformed spontaneously due to the

instability of the emulsion, allowing for the facile separation of organic molecules and electrolyte.

In Figure 6.6 voltammetric data is presented for the aqueous redox system. In the absence of shear force the expected reversible voltammogram for the single electron reduction of $[Ru(NH_3)_6]^{3+}$ was clearly shown both in the presence (A)(i) and absence (A)(ii) of acetonitrile. On the application of shear force a steady state voltammetric case was seen due to the dominance of a convection based transport process over the diffusional process seen in static solution. The result was a large increase in Faradaic currents, with agitation of 11,000 rpm up to *ca.* -1 mA, as compared to a static solution of *ca.* -0.1 mA. However, it must also be noted that there was not a large increase of limiting currents when the stirring rotation was increased to 33,000 rpm. This suggested that although the mixing had been increased, the mass transport effect towards the electrode was not overly affected by the increased rotation.

By applying Equation 1 the limiting currents were used to estimate a diffusion layer thickness for the reaction under the high shear force conditions. For a rotation speed of 11,000 rpm the diffusion layer thickness appeared to be *ca.* 20 μm which confirmed the presence of a strong agitation but was still only moderate when compared to ultrasound agitation. Considering the very high shear forces used this diffusion layer thickness was much larger than expected. This discrepancy can be attributed to cell geometry where shear forces are dissipated dramatically between the electrode surface and shear force generator over 1cm away. Unlike the ultrasound case, the high shear forces were not directional towards the electrode surface.

(1)
$$\delta = \frac{nFDAc}{I_{\mathrm{lim}}}$$

Here δ is the diffusion layer thickness, n is the number of transferring electrons, F is the Faraday constant, D is the diffusion coefficient of $[Ru(NH_3)_6]^{3+}$, A is the active electrode area, c is the bulk concentration of $[Ru(NH_3)_6]^{3+}$ and I_{lim} is the limiting current measured.

In general, the limiting currents seen in the presence of acetonitrile (40 vol.% solution) appeared diminished by about 20 % due to the partial blocking effect of acetonitrile microdroplets sporadically bombarding the surface.

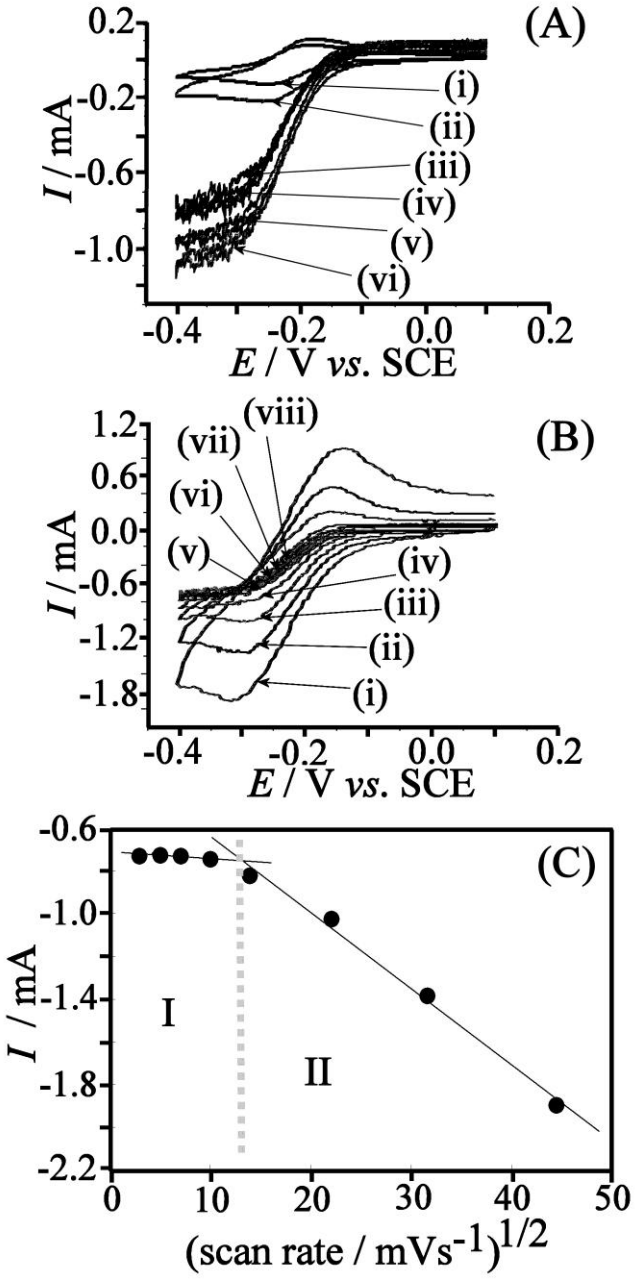

Figure 6.6 (A) Cyclic voltammograms for the reduction of 1 mM $Ru(NH_3)_6^{3+}$ in aqueous 2 M NaCl/0.1 M $NaClO_4$ at a scan rate 10 mVs^{-1}, glassy carbon, area 2.3 cm^2 (i) no agitation with acetonitrile, (ii) no agitation without acetonitrile, (iii) ultra-turrax 22000 rpm with acetonitrile, (iv) ultra-turrax 33000 rpm with acetonitrile, (v) ultra-turrax 11000 rpm without acetonitrile, and (vi) ultra-turrax 33000 rpm without acetonitrile**. (B)** Cyclic voltammograms at scan rate (i) 10 mVs^{-1}, (ii) 20 mVs^{-1}, (iii) 50 mVs^{-1}, (iv) 100 mVs^{-1}, (v) 200 mVs^{-1}, (vi) 500 mVs^{-1}, (vii) 1000 mVs^{-1}, and (viii) 2000 mVs^{-1} for the reduction of 1 mM $Ru(NH_3)_6^{3+}$ in aqueous 2 M NaCl/0.1 M $NaClO_4$ with

ultra-turrax agitation 11000 rpm and with acetonitrile. **(C)** Plot of the peak or limiting current versus the square root of scan rate (lines indicate steady state (I) and transient (II) behaviour.

The last key piece of information that was analysed for the single phase blocking system is shown in Figures 6.6B and 6.6C in which a scan rate dependence on the limiting current was seen. It is well known that the mass transport effect of the agitation only gave rise to steady state behaviour if the scan rate was sufficiently slow compared to the mass transport, such that electroactive material was supplied fast enough to the surface to effectively outrun the timescale of the experiment.

At fast scan rates the experiment time was so short that the mass transport effect was not seen and a transient behaviour was shown, similar to the results seen under static conditions. Graphically the results in Figure 6.6B show a clear transient behaviour for plots (i) – (iii) where plot (iv) shows slight peaks superimposed on a predominantly steady state signal. Plots (v) - (viii) were then of sufficiently low scan rate to show total steady state behaviour, indicative of a mass transport controlled system. When this data was plotted as peak or limiting current against scan rate, the trend became even clearer. Two distinct regions were seen; i) a steady state section of the plot, where the current did not change with scan rate, and ii) a transient controlled region with a direct relationship between peak current and square root scan rate, as predicted by the Randles-Sevcik equation. The scan rate at which this switch between behaviours was observed was important and was used to estimate the diffusion layer thickness (Equation 2). A switchover scan rate of *ca.* 0.22 Vs^{-1} was seen corresponding to a diffusion layer thickness of 22 μm which correlated well with the previously estimated value.

(2)
$$\delta = \frac{1}{0.446}\sqrt{\frac{DRT}{nFv_{trans}}}$$

Here terms are the same as for equation 1 and R is the gas constant 8.314 $Jmol^{-1}K^{-1}$, T is the absolute temperature and v_{trans} is the transition scan rate.

6.3.2 Liquid-Liquid Biphasic Electrochemistry II.: Acetonitrile Phase Oxidation of n-Butylferrocene in Acetonitrile | Aqueous Electrolyte at the Triple Phase Boundary.

A triple phase boundary approach was utilised to analyse the one electron oxidation of *n*-butylferrocene in acetonitrile (Scheme 6.2) at the electrode | aqueous electrolyte | acetonitrile boundary. This approach was explained in Section 1.2 including several examples of previous methods. In this case, the action of the high shear force pushed electroactive acetonitrile droplets to the surface of the electrode. This created a temporary and highly dynamic microdroplet array in which localised mixing within the turbulent droplets was achieved, as well as the continual renewal of the boundary (Figure 6.5).

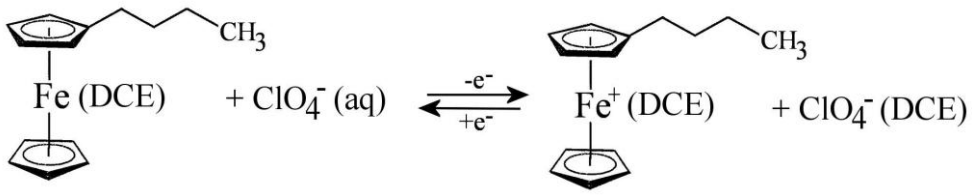

Scheme 6.2 The reversible one electron redox process of *n*-butylferrocene at a triple phase boundary.

The one electron triple phase oxidation of *n*-butylferrocene was highly reversible and the inclusion of 0.1 M $NaClO_4$ as well as 2 M NaCl ensured that a suitable transfer anion (ClO_4^-) was included in the aqueous phase to constrain the ferrocenium to the acetonitrile phase. It has previously been proven that Cl^- ions are too hydrophilic to be useful in this capacity[30] and would instead induce the cationic expulsion mechanism of *n*-$BuFc^+$ into the aqueous phase.

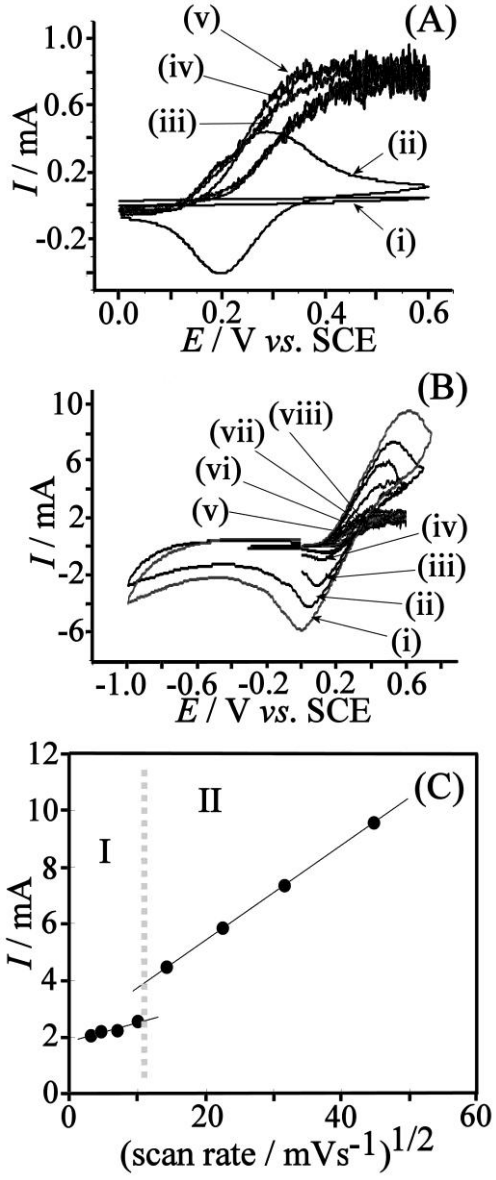

Figure 6.7 (A) Cyclic voltammograms for the oxidation of 50 mM *n*-butylferrocene in acetonitrile/ aqueous 2 M NaCl/ 0.1 M $NaClO_4$ at scan rate 10 mVs^{-1}, area 2.3 cm^2 (i) background without *n*-butylferrocene, (ii) without agitation, (iii) with ultra-turrax agitation 11000 rpm, (iv) with ultra-turrax agitation 22000 rpm, and (v) with ultra-turrax agitation 33000 rpm. **(B)** Cyclic voltammograms for the oxidation of 50 mM *n*-butylferrocene in acetonitrile/ aqueous 2 M NaCl/ 0.1 M $NaClO_4$ with ultra-turrax agitation 11000 rpm and scan rate (i) 10 mVs^{-1}, (ii) 20 mVs^{-1}, (iii) 50 mVs^{-1}, (iv) 100 mVs^{-1}, (v) 200 mVs^{-1}, (vi) 500 mVs^{-1}, (vii) 1000 mVs^{-1}, and (viii) 2000 mVs^{-1}. **(C)** Plot of the peak or limiting current versus the square root of scan rate (lines indicate steady state (I) and transient (II) behaviour.

In Figure 6.7A the single electron oxidation of *n*-BuFc and coupled anion transfer was shown as a chemically reversible signal with a reversible

potential of *ca.* 0.24 V *vs.* SCE under static conditions. Although the acetonitrile phase was separated from the electrode in the static case some acetonitrile containing the redox probe remained immobilised on the electrode surface from previous agitations. This conclusion is supported by the symmetrical wave shapes which suggest a surface immobilised redox process with complete electrolysis over the scan timescale. When compared with the scan in the presence of a blank acetonitrile phase it was shown that the reversible signal was due to the *n*-BuFc in the unsupported organic phase.

With the application of agitation ranging from 11,000 – 33,000 rpm a change in electrochemical signal to a steady state case with higher current appeared. This was due to the mass transport effect of emulsion droplets towards the electrode surface, although it was interesting to note that the limiting current appeared almost independent of rotation speed with a current of *ca.* 0.8 mA.

The effect of scan rate was used again to estimate the mass transport speed of the high shear force stirring and is shown in Figure 6.7B. At high scan rates a transient signal was observed for the reversible anion migration triple phase boundary reaction, however as the scan rate was slowed a steady state signal dominated with a limiting current almost independent of the scan rate, indicative of mass transport control. The switchover scan rate was measured to be 0.22 Vs^{-1} (Figure 6.7C) which corresponded to a diffusion layer thickness of 22 μm assuming an electrode area of 4% of the electrode contact area measured previously. This is a reasonable assumption based on the triple phase boundary contact area being so small for an array of microdroplets compared to a bulk liquid phase process. The diffusion layer thickness measured in this way also corresponded well to the value measured previously for the single phase $[Ru(NH_3)_6]^{3+}$ system (Section 6.3.1). This showed that the agitation conditions were similar for both the aqueous and organic phases in the emulsion. In order to increase the limiting current for this triple phase boundary process either the triple phase boundary length must be increased, by having smaller droplets in the emulsion, or by putting electrolyte into the organic phase.

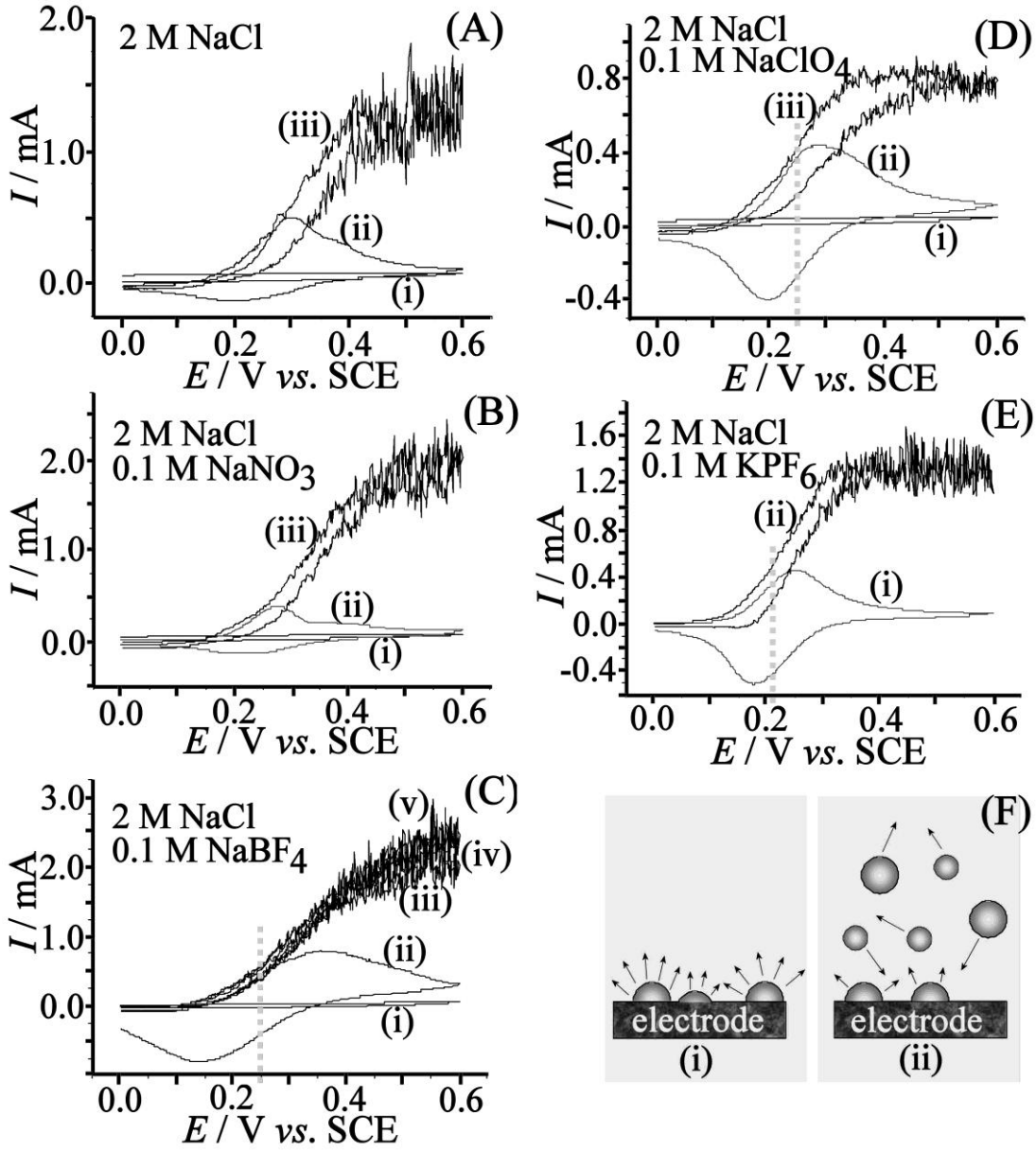

Figure 6.8 **(A)** Cyclic voltammograms for the oxidation of 50 mM n-butylferrocene in acetonitrile/ aqueous 2 M NaCl + 0.1M $NaClO_4$ at a scan rate of 10 mVs^{-1}, and a 2.3 cm^2 glassy carbon electrode (i) background without n-butylferrocene, (ii) without agitation, (iii) with ultra-turrax agitation 11000 rpm. **(B)** As above in acetonitrile/aqueous 2 M NaCl/ 0.1 M $NaNO_3$. **(C)** As above in acetonitrile/ aqueous 2 M NaCl/ 0.1 M $NaBF_4$ including data for ultra-turrax agitation 22000 rpm (iv) and 33000 rpm (v). **(D)** As above in acetonitrile/aqueous 2 M NaCl/ 0.1 M $NaClO_4$. **(E)** As above in acetonitrile/aqueous 2 M NaCl/ 0.1 M KPF_6. **(F)** Schematic drawing of (i) organic phase microdroplets immobilised at the electrode surface and (ii) microdroplets from the solution exchanging with immobilised microdroplets.

It is a well known effect, and has been demonstrated in a multitude of both static and dynamic triple phase boundary processes, that the transfer anion

has a significant effect on the reversible potential (Section 1.2.2) of the redox probe according the relative hydrophobicity. Figure 6.8 shows an example of this effect under both static and dynamic conditions for a range of anions. More hydrophobic anions require less energy to stimulate their insertion into an organic phase and thus oxidation occurs at less positive oxidation potentials. This was shown above by the comparison of the *n*-BuFc oxidation in the presence of ClO_4^- (0.24 V *vs.* SCE) and PF_6^- (0.22 V *vs.* SCE) where PF_6^- was more hydrophobic and thus easier to transfer. Conversely the presence of Cl^-, NO_3^-, BF_4^- appeared to have no effect on the midpoint potential as they all appeared shifted positively of PF_6^-, but all by a roughly equal value. This was due to the change in mechanism described in Section 1.2.2, in which the one electron process now involved the concerted expulsion of *n*-$BuFc^+$ into the aqueous phase to balance the charge, and thus the ion identity had no further effect. The expulsion of the ferrocenium ion lead to a decomposition of the ion to form passivating iron oxide on the electrode surface. This process was especially obvious in the cases with Cl^- and NO_3^-, in which the voltammetry also showed a very weak back peak due to the lack of *n*-$BuFc^+$ for the reverse process to occur.

6.3.3 Liquid-Liquid Biphasic Electrochemistry III.: Aqueous Phase Reduction of Cobaltocene in Acetonitrile | Aqueous Electrolyte

The final system studied using the high shear force generated emulsion was that of an aqueous phase reaction resulting in an aqueous insoluble product. In the absence of the emulsion this product remained as a deposit on the electrode surface and in high enough concentration could block the surface. The resulting voltammetry showed a pronounced stripping peak on the reverse scan. In the presence of a solubilising organic emulsion the product was removed from the surface *in situ* and no stripping peak was seen, since the product was then contained in the organic phase. The chosen reaction used here was the reversible couple of cobaltocene the cobalt analogue of ferrocene.

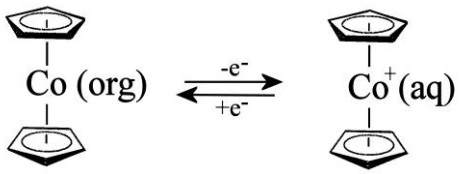

Scheme 6.3 The reversible one electron oxidation of cobaltocene showing a phase transfer process

Scheme 6.3 shows the reversible cobaltocene couple in which the aqueous soluble cobaltocenium solution was, upon reduction, deposited onto the glassy carbon electrode and potentially incorporated into the organic emulsion.

The voltammetry of the cobaltocene couple is shown in Figure 6.9A in the absence of acetonitrile and occurred at *ca.* -1.1V (*vs.* SCE) in an aqueous solution of 2 M NaCl + 0.1 M $NaClO_4$. The reduction wave appeared non ideal due to the onset of a competing hydrogen evolution and electrode fouling by the deposited cobaltocene. Also, the oxidative stripping peak appeared more heavily pronounced at high scan rates with a characteristic shape indicative of an attached redox species.

In the presence of an acetonitrile emulsion the insoluble cobaltocene on the electrode surface became dissolved in the organic emulsion. The rate of this process was linked to the mass transport of organic phase to the surface and the efficiency of the dissolution process. Since the dissolution of the product was in direct competition with oxidative striping the rate constant of the dissolution was probed by changing the scan rate and thus changing the timescale over which the dissolution could act. If the scan rate was too fast then the dissolution would not have time to occur before the stripping process reoxidised the cobaltocene back to cobaltocenium. However, once the scan rate became slow enough that the dissolution could happen before the polarity reversal caused the oxidative stripping, the stripping peak would no longer be visible. The scan rate corresponding to this switch in mechanism corresponded to the dissolution rate.

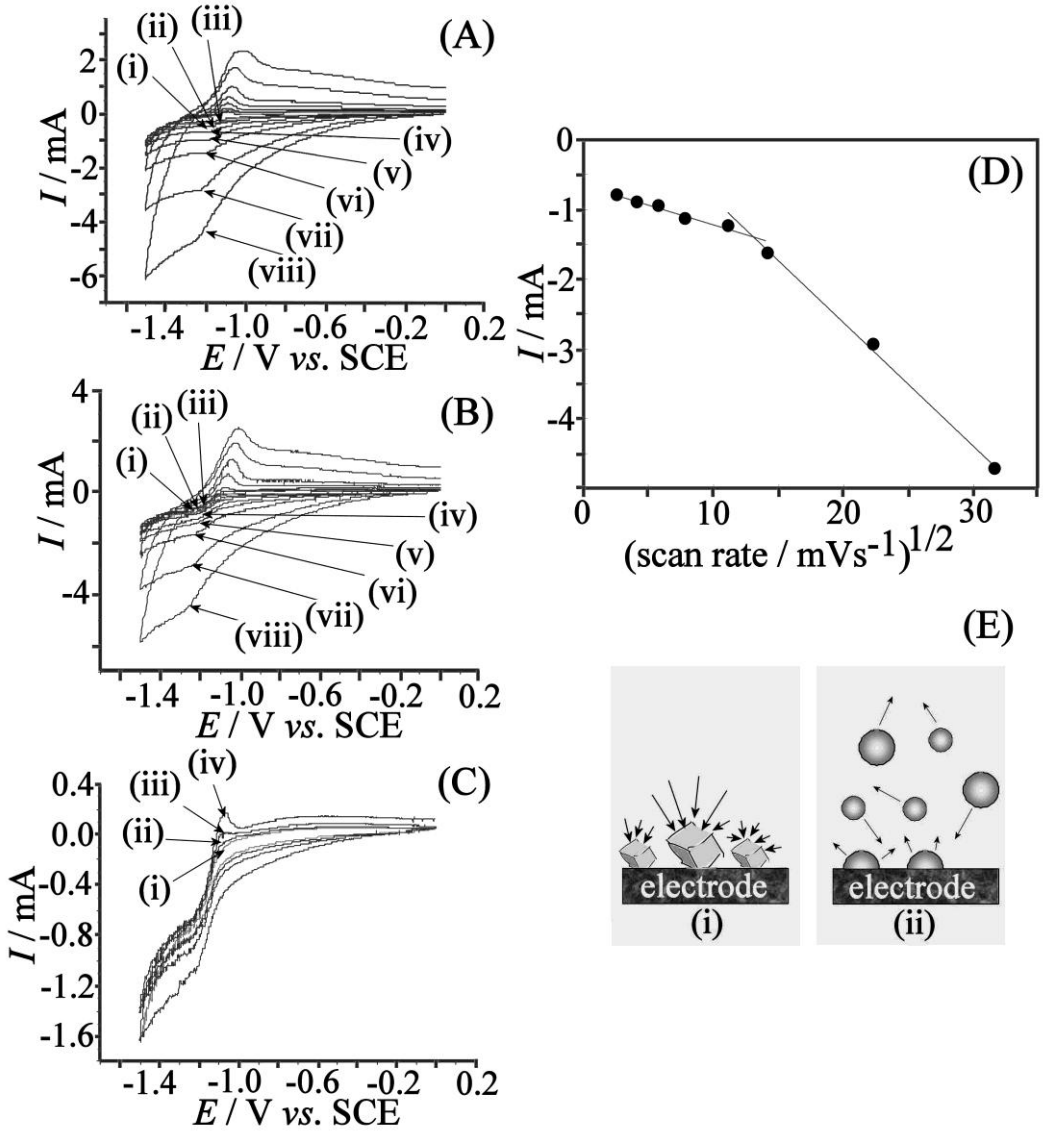

Figure 6.9 **(A)** Cyclic voltammograms for the reduction of 1 mM $Cc^+PF_6^-$ in acetonitrile/ aqueous 2 M NaCl / 0.1 M $NaClO_4$ without agitation at a 2.3 cm^2 glassy carbon electrode with scan rates; (i) 5 mVs^{-1}, (ii) 10 mVs^{-1}, (iii) 20 mVs^{-1}, (iv) 50 mVs^{-1}, (v) 100 mVs^{-1}, (vi) 200 mVs^{-1}, (vii) 500 mVs^{-1}, (viii) 1000 mVs^{-1}. **(B,C)** Cyclic voltammograms obtained with ultra-turrax agitation 11000 rpm. **(D)** Plot of the peak or limiting current versus the square root of the scan rate. **(E)** Schematic drawing of the Co^+ reduction and cobaltocene crystal formation in the absence (i) and in the presence (ii) of ultra-turrax agitation.

In Figure 6.9B voltammograms are shown for a wide range of scan rates during agitation with peak or limiting currents summarised in Figure 6.9D. At fast scan rates the oxidative stripping peak was clearly visible at *ca.* -1.2 V and in order to best compare low scan rates these were plotted separately in Figure 6.9C. At 50 mVs^{-1} a stripping peak was still visible, at 20 mVs^{-1} the

peak was still slightly visible as a hump but at 10 mVs^{-1} the mechanism had clearly changed and now the dissolution of the product was faster than the reversible stripping process. When the peak height was plotted against the scan rate (Figure 6.9D) the crossover scan rate was estimated more accurately and appeared to correspond to about 0.13 Vs^{-1}. This value was very similar to the mass transport limit for the redox process seen in a single phase with Ru^{3+}. This showed that the dissolution was effective and mostly controlled by the mass transport of the droplets to the surface. This result was replicated for concentrations of $CoCp_2^+$ up to 5 mM in which the currents seen for the reduction scale linearly with the concentrations. The removal of $CoCp_2$(s) products remained effective with a roughly constant rate of removal.

Previous experiments have been concerned with the use of a blank acetonitrile phase to trap an electro-generated insoluble product which could be used to depassivate electrodes *in situ*.[31] This example utilised a similar trapping mechanism with an ultrasound agitation and was used to isolate '1 electron' products preferentially. This was achieved by encapsulating the products in an inert organic phase to prevent further reduction.

6.4 Conclusions

In conclusion it has been shown that a non-surfactant stabilised high shear force generated emulsion can act as an effective organic phase for triple phase boundary mechanisms. The currents recorded are nearing levels required for efficient triple phase boundary synthetic processes and the unstable nature of the emulsion meant that separation *via* decantation was possible.

The emulsion has been analysed in blank conditions where the organic phase blocked the electrode surface for aqueous phase redox processes and in a triple phase mode where a redox probe in the organic phase was addressed without the need for supporting electrolyte in that phase.

A third more interesting case showed that the emulsion could be effectively used as a passivating agent to remove electrochemically generated solids at the electrode surface with the rate of dissolution was controlled mainly by the

rate of mass transport of the microdroplets to the surface. This methodology could be used to depassivate surfaces, avoid electrode fouling in metal analysis, or as a phase transfer mediator system where electrons can be shuttled into the organic phase for mediation of novel redox processes.

6.5 References

(1) Huang, J. X.; Kaner, R. B. *Journal of the American Chemical Society* **2004**, *126*, 851.

(2) Sheldon, R. A. *Green Chemistry* **2005**, *7*, 267.

(3) Brink, G. J.; Arends, I.; Sheldon, R. A. *Science* **2000**, *287*, 1636.

(4) Horvath, I. T.; Rabai, J. *Science* **1994**, *266*, 72.

(5) Nishimoto, K.; Kim, S.; Kitano, Y.; Tada, M.; Chiba, K. *Organic Letters* **2006**, *8*, 5545.

(6) Sheldon, R. *Chemical Communications* **2001**, 2399.

(7) Sirieix, J.; Ossberger, M.; Betzemeier, B.; Knochel, P. *Synlett* **2000**, 1613.

(8) Tzschucke, C. C.; Markert, C.; Bannwarth, W.; Roller, S.; Hebel, A.; Haag, R. *Angewandte Chemie-International Edition* **2002**, *41*, 3964.

(9) Zhao, G. Y.; Jiang, T.; Wu, W. Z.; Han, B. X.; Liu, Z. M.; Gao, H. X. *Journal of Physical Chemistry B* **2004**, *108*, 13052.

(10) Kroon, M. C.; Shariati, A.; Costantini, M.; van Spronsen, J.; Witkamp, G. J.; Sheldon, R. A.; Peters, C. J. *Journal of Chemical and Engineering Data* **2005**, *50*, 173.

(11) Danov, K. D.; Kralchevsky, P. A.; Ivanov, I. B. *Chapter 26 in Encyclopedic Handbook of Emulsion Technology "Dynamic Processes In Surfctant Stabilized Emulsions"*; Marcel Dekker: New York, **2001**.

(12) (a) Rusling, J. F.; Zhou, D. L. *Journal of Electroanalytical Chemistry* **1997**, *439*, 89; (b) Khan, F. N.; Jayakumar, R.; Pillai, C. N. *Journal of Molecular Catalysis a-Chemical* **2003**, *195*, 139.

(13) (a) Park, Y. S.; Little, R. D. *Journal of Organic Chemistry* **2008**, *73*, 6807; (b) Park, Y. S.; Wang, S. C.; Tantillo, D. J.; Little, R. D. *Journal of Organic Chemistry* **2007**, *72*, 4351.

(14) Rusling, J. F. Workshop on Electchemistry and Interfacial Chemistry in Environmental Clean-Up and Green Chemical Processes, Coimbra, Portugal, **2001**; p 1895.

(15) Njue, C. K.; Nuthakki, B.; Vaze, A.; Bobbitt, J. M.; Rusling, J. F. *Electrochemistry Communications* **2001**, *3*, 733.

(16) Marken, F.; Compton, R. G. *Electrochimica Acta* **1998**, *43*, 2157.

(17) Akkermans, R. P.; Roberts, S. L.; Compton, R. G. *Chemical Communications* **1999**, 1115.

(18) Suga, S.; Okajima, M.; Fujiwara, K.; Yoshida, J. *Journal of the American Chemical Society* **2001**, *123*, 7941.

(19) (a) Horii, D.; Amemiya, F.; Fuchigami, T.; Atobe, M. *Chemistry-a European Journal* **2008**, *14*, 10382; (b) Horii, D.; Fuchigami, T.; Atobe, M. *Journal of the American Chemical Society* **2007**, *129*, 11692.

(20) (a) Tajima, T.; Fuchigami, T. *Angewandte Chemie-International Edition* **2005**, *44*, 4760; (b) Tajima, T.; Fuchigami, T. *Chemistry-a European Journal* **2005**, *11*, 6192.

(21) Kurihara, H.; Fuchigami, T.; Tajima, T. *Journal of Organic Chemistry* **2008**, *73*, 6888.

(22) Chiba, K.; Jinno, M.; Nozaki, A.; Tada, M. *Chemical Communications* **1997**, 1403.

(23) Chiba, K.; Jinno, M.; Kuramoto, R.; Tada, M. *Tetrahedron Letters* **1998**, *39*, 5527.

(24) Chiba, K.; Arakawa, T.; Tada, M. *Journal of the Chemical Society-Perkin Transactions 1* **1998**, 2939.

(25) Paddon, C. A.; Pritchard, G. J.; Thiemann, T.; Marken, F. *Electrochemistry Communications* **2002**, *4*, 825.

(26) (a) Horii, D.; Atobe, M.; Fuchigami, T.; Marken, F. *Electrochemistry Communications* **2005**, *7*, 35; (b) Horii, D.; Atobe, M.; Fuchigami, T.; Marken, F. *Journal of the Electrochemical Society* **2006**, *153*, D143; (c) He, P.; Watts, P.; Marken, F.; Haswell, S. J. *Green Chemistry* **2007**, *9*, 20; (d) He, P.; Watts, P.; Marken, F.; Haswell, S. J. *Angewandte Chemie-International Edition* **2006**, *45*, 4146; (e) He, P.; Watts, P.; Marken, F.; Haswell, S. J. *Electrochemistry Communications* **2005**, *7*, 918.

(27) Horcajada, R.; Okajima, M.; Suga, S.; Yoshida, J. *Chemical Communications* **2005**, 1303.

(28) Amemiya, F.; Horii, D.; Fuchigami, T.; Atobe, M. *Journal of the Electrochemical Society* **2008**, *155*, E162.

(29) He, P.; Watts, P.; Marken, F.; Haswell, S. J. *Lab on a Chip* **2007**, *7*, 141.

(30) Komorsky-Lovric, S.; Lovric, M.; Scholz, F. *Journal of Electroanalytical Chemistry* **2001**, *508*, 129.

(31) Wadhawan, J. D.; Del Campo, F. J.; Compton, R. G.; Foord, J. S.; Marken, F.; Bull, S. D.; Davies, S. G.; Walton, D. J.; Ryley, S. *Journal of Electroanalytical Chemistry* **2001**, *507*, 135.

7. Liquid–Liquid Electro-synthetic Mechanisms at the Triple Phase Boundary in a Nano-Carbon Membrane Microreactor

Contents

Chapter. 7: Liquid–Liquid Electro-synthetic Mechanisms at the Triple Phase Boundary in a Nano-Carbon Membrane Microreactor.

Aims

- To characterise the novel carbon membrane material with an aqueous single phase redox process with a blank organic phase.
- Use the carbon membrane to stabilise the organic | aqueous boundary and allow triple phase boundary reactions within the membrane.
- To apply the new triple phase boundary procedure to synthetic reductions with accompanying proton transfers.

Publication

- Watkins JD, Ahn SD, Taylor JE, Bulman-Page PC, Bull SD and Marken F, *Electrochimica Acta,* **2011,** 56, 6764 - 6770.

CHAPTER 7: Liquid–Liquid Electro-synthetic Mechanisms at the Triple Phase Boundary in a Nano-Carbon Membrane Microreactor

7.1 Introduction

A new carbon material, 'bucky paper', purchased from Nanolab gave unique properties for use in triple phase boundary reactions. Bucky paper is a carbon nanofibre membrane made from multiwalled carbon nanotubes (MWCNTs) which were first purified with hydrochloric acid then functionalised with carboxylic acid groups by etching with nitric acid. The functionalised nanofibres were then suspended in distilled water as a highly stable suspension and filtered under high pressure to give a compacted porous carbon nanofibre paper.[1] The resulting paper is strong and malleable and highly suited as an electrode membrane. The paper combines porosity and durable mechanical properties with the high electrochemical window and chemical resistance of carbon electrodes.

MWCNTs are best described as several carbon nanotube sleeves inside one another creating a pseudo-graphitic structure. The spacing of these layers tends to be *ca.* 0.3–0.4 nm. And the overall tubes generally have diameters from 2–100 nm.[2] In a review of carbon nanotubes it was suggested by Pumera[3] that oxidisation processes can introduce many more defects into the MWCNT walls thus increasing the heterogeneous electron transfer rate and this is generally achieved by an electrochemical oxidative process. He also suggested that the catalytic activity of carbon nanotubes reported was more likely due to the presence of the metallic impurities used in their initial production, so this possibility in bucky paper electrodes cannot be discounted. The natural catalytic ability of carbon nanotubes is of some debate and Moore *et al.*[4] have suggested a rigorous comparison of any new nanocarbon material be made with graphite powder before conclusions of catalytic nature are assumed. For the purposes of enhancing the triple phase boundary length MWCNTs are highly useful due to their high surface area and porosity.

MWCNTs are primarily synthesised by an arc discharge process[5] and used in a wide range of applications. Most notably MWCNTs are used in electroanalytical applications.[2] First, the carbon nanotubes require immobilisation onto an electrode surface[6] or incorporation into a paste electrode[7] or solid carbon based composite material.[8]

A key example of this type of analytical investigation is in the detection of DNA which has been achieved on MWCNT arrays.[6b,9] Nanotube electrochemistry is ideal for the detection of subtle changes such as DNA binding events due to its sensitive nature and ability to form high surface area arrays for signal amplification.

In this chapter a novel methodology for electroorganic synthesis is presented based on the triple phase boundary mechanism described in previous chapters. The concept was first introduced in Chapter 1 with a subsequent introduction to electroorganic synthetic techniques already in use. In Chapters 5, 6 and 7 triple phase boundary techniques were described towards a bulk synthetic technique using various triple phase boundary methods, namely; solid electrolyte (Chapter 5), ultrasound[10] (Chapter 6) and ultra-turrax[11] (Chapter 7). Another relevant example pertinent to this discussion is of a flowing triple phase boundary,[12] previously investigated although not discussed at length in this thesis.

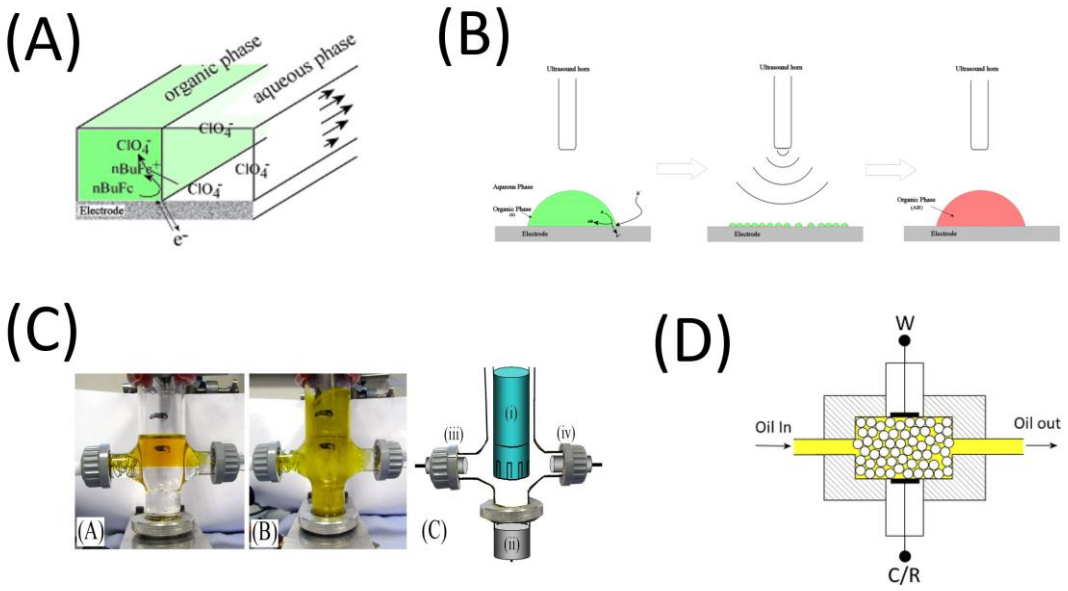

Figure 7.1 Schematic representation of the previously studied synthetic triple phase boundary systems **(A)** Biphasic flow, **(B)** Low power ultrasound, **(C)** High shear force ultra-turrax and **(D)** The salt matrix cell.

Each method is summarised in chronological order with a comparison containing various advantages and disadvantages. The flowing triple phase boundary technique investigated utilised a very short triple phase boundary length but a high mass transport to the triple phase zone where it was shown that slower flow rates lead to a greater efficiency in an acetonitrile | water biphasic flow system. A major advantage in a flowing synthetic system is that a continuous electrolysis process was possible but the current was found to be too small for further investigation for synthetic purposes.

Next, a solid electrolyte salt matrix was described where a dense matrix of highly solvated salt crystals created a pseudo-aqueous phase around which a solvent existed, allowing redox processes to occur. The advantages of this approach were that a solid electrolytic phase allowed even easier electrolyte separation than in aqueous solution, as well as the potential for a flow system giving a continuous process. The triple phase boundary length itself was greatly increased by the highly divided powder in contact with the electrode surface at a multitude of nano-contacts. The key disadvantage was that in a two electrode system with a calomel electrode acting as a counter and reference it was impossible for this approach to be used for the high current conditions necessary for an effective turnover rate in synthetic applications.

Next, a low powered ultrasound system was utilised to break large droplets (*ca* 1 ml) into an unstable localised emulsion of microdroplets at an electrode surface. This method was effective in enhancing triple phase boundary processes both by increasing the triple phase boundary length and by causing turbulent mixing of droplets for enhanced mass transport to the triple phase boundary. However a major disadvantage was that the current found was still too low to make useful synthetic processes in an appropriate timescale and only liquids denser than water could be used as organic carrier solvents. This was a very limiting feature since most solvents with a density greater than water are halogenated and a potential source of side reactions and inefficiency in synthetic processes.

Finally an ultra-turrax driven process was presented in which a high shear force ultra-turrax apparatus was used to generate an unstable micro-emulsion from a biphasic system. This setup appeared very similar to the low power ultrasound approach except that much higher stirring forces were generated and the resulting emulsion was mobile within the entire aqueous phase rather than being localised to the electrode surface. Although this approach generated a much improved current (1 – 10 mA) and allowed for the use of less dense organic phases, the dispersed nature of the emulsion still lead to poor synthetic turnover of products. Separation by removal of the high shear force remained facile.

The new concept utilised a very large triple phase boundary contact zone at an amphiphilic carbon membrane, which readily absorbed both aqueous and organic phases, and in the case of a phase separation preferentially stabilised the organic | aqueous interface. The membrane was used as the working electrode at the liquid | liquid interface when a suitable carbon contact was created. The triple phase boundary process was thought to occur within the carbon membrane at the points where both liquids simultaneously contacted a nanofibre of the carbon (Figure 7.2). The result was a microreactor where the aqueous side of the carbon contained supporting electrolyte and a plentiful supply of transferable ions and the organic side contained redox probes which were suitably hydrophobic so as not to partition or transfer into the aqueous phase.

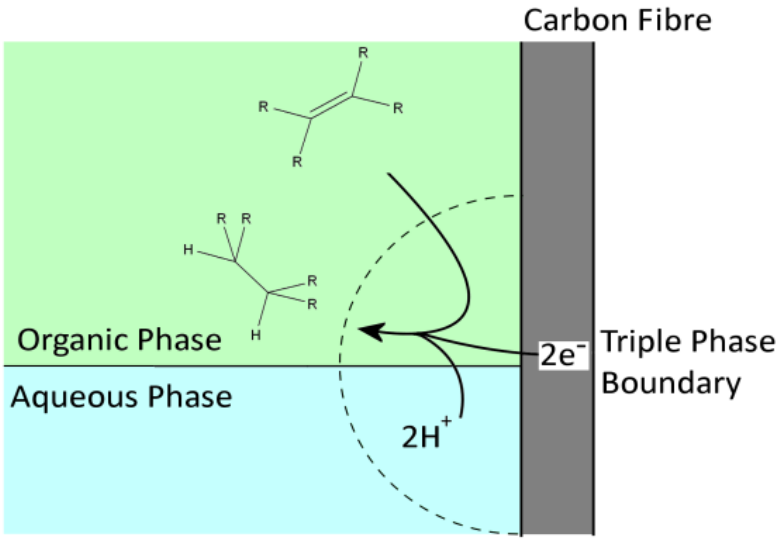

Figure 7.2 The triple phase boundary mechanism for the organic test system tetraethyl ethylenetetracarboxylate where a concerted two electron / two proton process occurs with protons being supplied from the aqueous phase.

The mechanism of the triple phase boundary process has been discussed in Chapter 1 in which an electron transfer must be accompanied by a concerted ionic transfer across the liquid | liquid boundary. For characterisation purposes the studied process has generally been a ferrocene oxidation with an accompanying anion transfer from the aqueous phase, assuming that a suitably hydrophobic anion exists in the aqueous phase.

For the synthetic test system a highly activated alkene was chosen with four ester group attachments. This molecule was chosen as a model process for reduction due to its low reduction potential and symmetry which simplified product identification. This test molecule had previously been used by Paddon *et al.*[13] in a study of electrosynthetic processes in an electrolyte free thin layer flow cell.

In all the cases presented here, reductive reactions were exclusively considered leading to the inclusion of protons from the aqueous phase to balance the charge. An interesting difference that arose as a result of this subtle mechanistic change was that the proton underwent a chemical reaction with the reduced species in the organic phase and formed a bond rather than an ion pair, as shown in Figure 7.2.

7.2 Experimental

7.2.1 Chemical Reagents

Sodium perchlorate monohydrate (98%, Sigma Aldrich), sodium sulphate decahydrate (≥99%, ACS reagent, Sigma Aldrich), *n*-butylferrocene (98%, Alfa Aesar), phosphoric acid (Sigma Aldrich ACS reagent, 85 wt%), sodium chloride (≥95%, SigmaUltra reagent, Sigma Aldrich), sodium hydroxide (≥97%, ACS reagent, Sigma Aldrich), hydroquinone, and tetraethyl-ethylenetetracarboxylate (98+%, Lancaster Synthesis) were used without further purification. Demineralised and filtered water was taken from a Millipore water purification system with not less than 18 MΩcm resistivity

7.2.2 Instrumentation

Voltammetric experiments were performed with a microAutolab III system (Ecochemie, Netherlands) in staircase voltammetry mode. The step potential was maintained at approximately 1 mV. The counter and reference electrodes were platinum gauze and KCl-saturated calomel (SCE, Radiometer), respectively. The working electrode was a 4 mm diameter carbon nanofibre membrane disc ('Bucky paper', Nanolabs US, with low resistivity (~0.1 Ωcm) and relatively low impurity levels (Fe 0.36, Si 0.31, Al 0.23, Na 0.32, S 0.23 at%) mounted with Ambersil silicone (Silicoset 151) on a glass capillary of 3.5 mm inner diameter and 5 mm outer diameter. The electrical contact was made with a 1 mm stripe of pyrolytic graphite film (Goodfellow, UK) inside of the glass capillary. Solutions were deaerated with argon (Pureshield, BOC). The pH was measured with a glass electrode (3505 pH meter, Jenway). All experiments were conducted at a temperature of 22 ±2 °C

7.2.3 Procedure I: Creation of Carbon membrane microreactor

First a glass tube of internal diameter 3.5 mm and external diameter 5 mm was cut to be 50 mm in length. A strip *ca.* 3 mm wide of graphite foil was cut to be 70 mm in length and attached to the inside of the glass tube by a chemically resistant silicon based adhesive and the ends of the foil folded

around the top and bottom of the glass tube. A contact was formed at one end of the tube by the adhesion of a copper wire by silver epoxy. At the other end a carbon membrane disc was cut to 5 mm diameter and placed in contact with the foil. Silicon adhesive was used to seal the carbon to the tube with a circle of carbon *ca.* 3.5 mm exposed on both the inside and outside of the glass tube. Upon curing the silicon adhesive contracted and forced the carbon membrane and foil into a physical electrical contact suitable for electrochemical study.

7.2.4 Procedure II: Synthetic reactions

In order to perform a synthetic reduction in the microreactor the electrode as prepared in 7.2.3 was first placed *ca.* 50mm deep in an aqueous solution containing electrolyte (Figure 7.3). After visual inspection for leaking of aqueous phase into the tube 100 µL of organic phase containing redox probe was added to the inside of the glass tube. The electrode was left to equilibrate for several minutes to confirm no leaking of either phase though the carbon membrane. A cyclic voltammogram was performed to ascertain the suitability of the electrode for synthesis and a suitable potential for potentiostatic reduction was chosen. Resistance variations were seen to change the voltammetric shape slightly between electrodes. The overhead stirrer was inserted into the glass tube to a depth of *ca*. 50 mm from the surface of the electrode and was engaged at a rotation speed of *ca.* 300 Hz while the potential was held at a value corresponding to a suitable reductive current (1–10 mA). After the synthesis was complete the overhead stirrer was removed and the internal organic solution separated by pipette as well as several washings of the inside of the glass tube by fresh acetonitrile. The electrode was then immersed in clean acetonitrile followed by 1 M H_3PO_4 followed by distilled water for about an hour each before reuse. The aqueous phase may be recycled immediately.

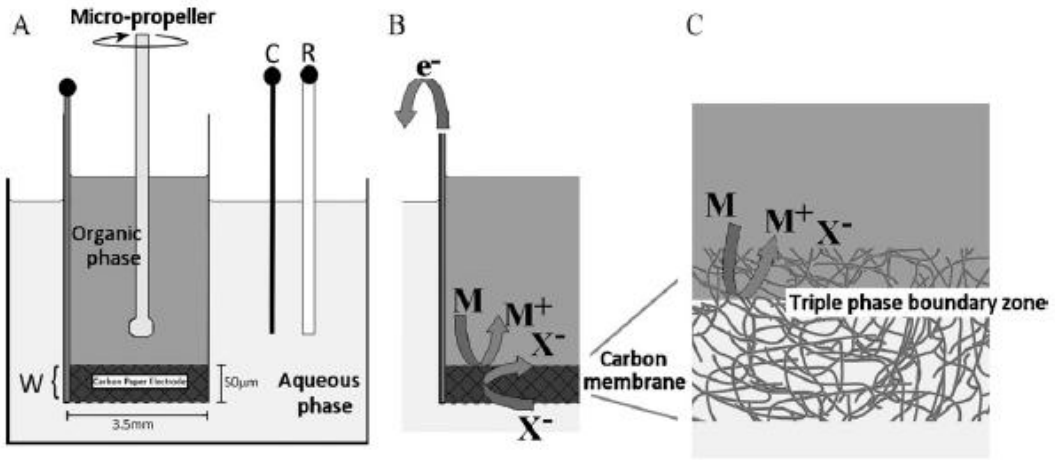

Figure 7.3 (A) A schematic diagram of the carbon paper membrane microreactor, And **(B/C)** the site of triple phase boundary processes.

7.3 Results and Discussion

7.3.1 Non-Electrochemical characterisation of carbon membrane

The carbon membranes were first characterised by microscopy, energy dispersive X-ray spectroscopy (EDS) and qualitative liquid behaviour analysis. Scanning electron microscopy (SEM) images shown in Figure 7.4 gave an idea of the density of the carbon film and an accurate value for the thickness of the film by end on visualisation. The film was clearly composed of randomly orientated carbon fibre of diameter *ca.* 50 nm (Figure 7.4C) as well as having a thickness of between 50 and 100 μm.

The photographs in Figure 7.4D clearly illustrated the amphiphilic nature of the carbon membrane by showing that in both aqueous (1 M $NaSO_4$ + 0.1 M PBS pH 7. aq) and organic (acetonitrile) phases the carbon membrane was able to absorb the solution and sunk to the bottom of the vial. However in a biphasic mixture of both phases (with the aqueous phase suitably salted as to cause immiscibility) the carbon membrane spontaneously equilibrated to the phase boundary of the two liquids even after vigorous shaking, a trait seen previously with carbon nanoparticles.[14] The EDS spectrum confirmed that the film is mostly carbon with *ca.* 7% oxygen and, more significantly, no trace metal contaminants.

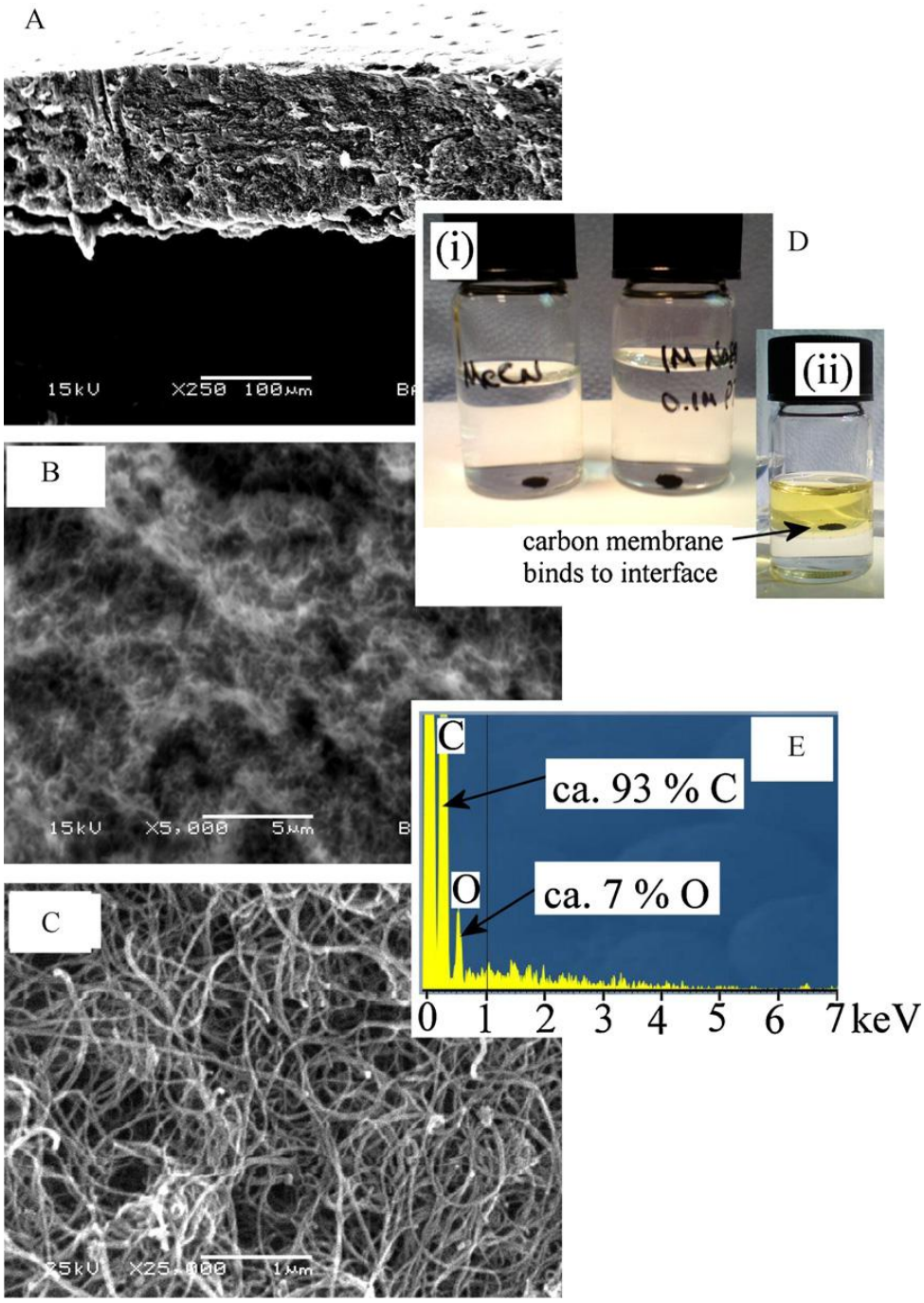

Figure 7.4 (A) – (C) SEM images of the carbon membrane as a cross section (A) and as a face on view (B)/(C). **(D)** Photographs showing the amphiphilic nature of the carbon film with immersions in water and acetonitrile separately (i) and as a biphasic mixture (ii). **(E)** Energy dispersive X-ray spectroscopy (EDX) data of the film.

7.3.2 Electrochemical Oxidation of Hydroquinone in the Aqueous Phase

Electrochemically the new carbon membrane electrodes were first calibrated with the single phase aqueous redox couple of hydroquinone / benzoquinone as shown in Scheme 7.1.

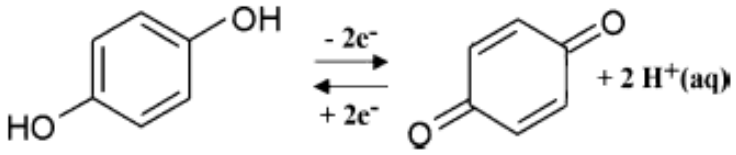

Scheme 7.1. The hydroquinone / benzoquinone redox couple

The voltammetry for the hydroquinone oxidation process is shown in Figure 7.5A for increasing concentrations of hydroquinone. In Figure 7.5B the relationship of charge and concentration of hydroquinone was confirmed to give a linear relationship. The oxidation occurred at a midpoint potential of *ca.* 0.38 V *vs.* SCE and appeared to have a high capacitive component of *ca.* 8 F/g consistent with a highly porous carbon electrode.[15] A significant peak distortion was also seen due to a large resistive component (*ca.* 200 Ω) arising either from the physical contact of the conducting graphite strip and the carbon paper or as a result of ion transport within the membrane. It was for this reason that the charge and not the peak heights were taken as a comparison for the concentrations of hydroquinone.

Interestingly, it was determined that the immersion depth of the carbon electrode into the solution had no effect on the peak heights of the voltammogram (not shown) since the inside of the glass tube was kept reasonably dry. It was therefore assumed that water penetration into the membrane was highly effective and the hydrostatic pressure of the water did not play a role in the contact area. This observation was also confirmed by the constant and high capacitance which suggested that the majority of the internal conductive pathway within the electrode was active.

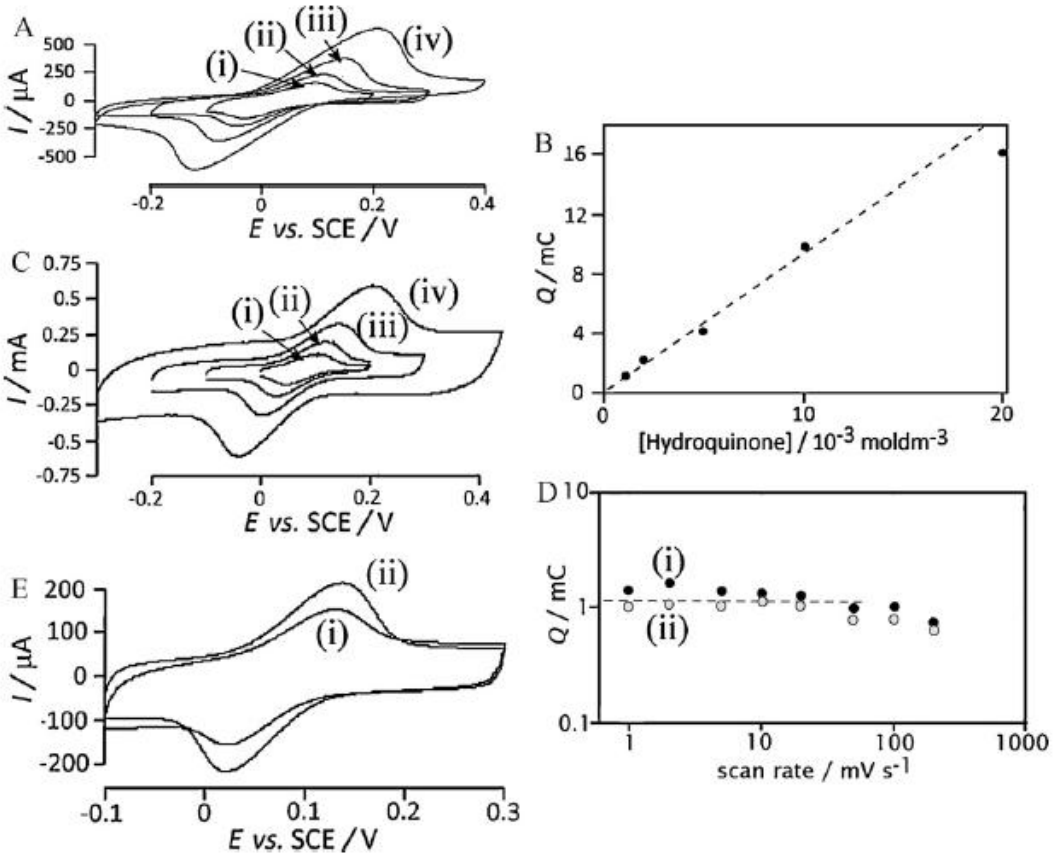

Figure 7.5. (**A)** This figure shows voltammograms for increasing concentrations of hydroquinone (i) 1, (ii) 2, (iii) 5, (iv) 10mM. Which were recorded at a depth of 5 mm into a solution containing hydroquinone and 0.1 M PBS pH 7 with no organic phase present and left to equilibrate for 5minutes between scans. A scan rate of 10 mVs^{-1} was used. **(B)** This shows the variation of the charge with the concentration of hydroquinone used under the same conditions as (A). **(C)** This shows voltammograms for increasing scan rates (i) 5, (ii) 10, (iii) 20, (iv) 50 mVs^{-1}. The scans were measured on a 2 mM solution of hydroquinone in 0.1 M PBS pH 7 and at a depth of 0 mm with no organic phase being present. **(D)** This shows the variation of the oxidative and reductive charge with the scan rate under the same conditions as (C). **(E)** These voltammograms show the effect of adding a blank organic layer of 50 µL acetonitrile into the electrode body. Both are recorded at a scan rate of 10 mVs^{-1} using 2 mM hydroquinone in 0.1 M PBS pH 7 + 1 M Na_2SO_4 and a depth of 0 mm (i) no acetonitrile, (ii) 50 µL acetonitrile.

The dependence on scan rate is analysed in Figure 7.5C and summarised in Figure 7.5D and showed almost no change of the Faradaic charges with scan rate. This suggested a diffusion independent process in which the redox reaction occurred only within the carbon membrane and that hydroquinone which was trapped within the carbon membrane was the only significant

contributor to the charge. External diffusion processes were determined to be insignificant at the scan rates analysed (1 – 200 mVs^{-1}).

Finally, a blank acetonitrile phase was inserted into the glass tube to analyse the rough position of the triple phase boundary within the carbon film. This correlation is shown in Figure 7.5C and showed a reduction in the charge by about a factor of 2. This suggested that the carbon membrane became partially blocked by the acetonitrile phase as the water was no longer able to penetrate as far into the membrane, and thus less hydroquinone was trapped and a lower charge was recorded. This result was also not affected by the fill height of the organic phase or the immersion depth of the electrode probably due to the domination of surface tension and capillary forces within the carbon membrane.

7.3.3 Electrochemical Oxidation of *n*-Butylferrocene at the Triple Phase Boundary

The next redox process for interrogation was that of the *n*-butylferrocene oxidation, the same standard triple phase boundary test system used for the majority of interrogations thus far (Scheme 7.2).

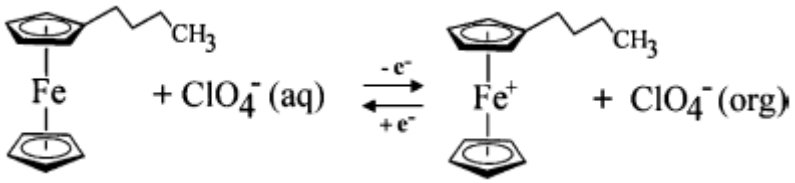

Scheme 7.2 This shows the one electron reversible oxidation of n-butyl ferrocene at the triple phase boundary.

This triple phase test system has been discussed many times throughout this thesis and is the one electron oxidation of *n*-butylferrocene in the organic phase with the concerted transfer of an anion from the aqueous phase to balance the charge. This is however the first time that this reaction has been studied as a potential bulk process.

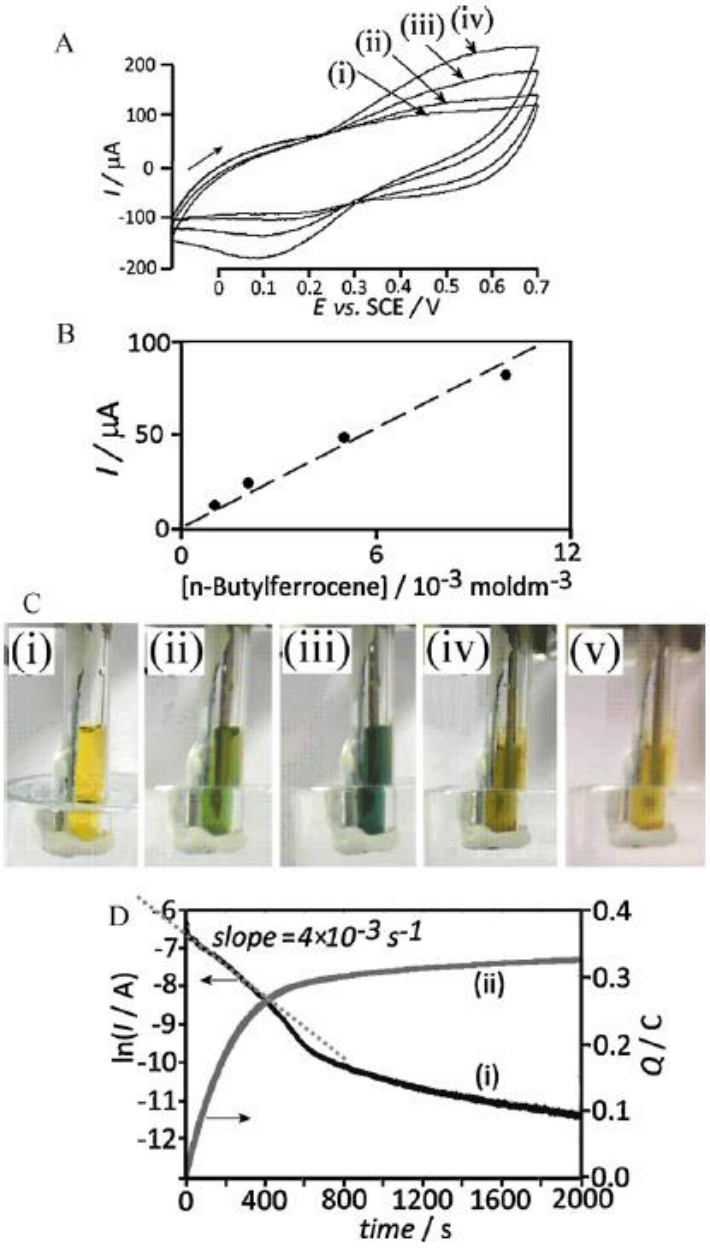

Figure 7.6 (A) This shows voltammograms for increasing concentrations of *n*-butylferrocene (i) 1, (ii) 2, (iii) 5, (iv) 10 mM, all recorded at a scan rate of 10 mVs^{-1} in 0.1 M $NaClO_4$ + 2 M NaCl and 100 µL of acetonitrile **(B)** shows a plot of the peak current for the *n*-BuFc oxidation against the concentration of *n*-BuFc in the organic phase under conditions as in (A). **(C)** Shows a picture of the carbon paper electrode during electrolysis. Here, *n*-BuFc was used as a test reagent in a concentration of 2 mM. The starting state is shown in (i). The electrolysis is maintained at 0.9 V under stirring by and overhead stirrer, and after about 1 minute the solution goes to the state shown in (ii) and finally after 15 minutes (iii), the green colour is characteristic of *n*-butylferrocenium the oxidised form of *n*-butylferrocene. The reaction can then be reversed by electrolysis at -0.1 V for 15 minutes which shows the re-emergence of the yellow n-butyl ferrocene colour. **(D)** Chronoamperometry data for the oxidation

of *n*-BuFc with a plot of (i) log of current *vs.* time and (ii) charge *vs.* time with a dashed line representing the initial first order decay.

Initially, voltammetry was obtained for the *n*-BuFc redox probe in an electrically unsupported organic phase at the triple phase boundary and a chemically reversible voltammogram with midpoint potential *ca.* 0.28 V *vs.* SCE was observed (Figure 7.6A). This voltammogram appeared superimposed on a capacitive background as seen in the case of hydroquinone and suffered a large degree of distortion by resistance. This resistance was to be expected in the case of triple phase voltammetry due to the non-conductive effect of the organic phase without supporting electrolyte. The voltammetry presented in Figure 7.6A was performed under static conditions. It was found perhaps surprisingly that agitation of either the aqueous phase (by magnetic stirrer) or organic phase (by overhead stirrer) showed no effect on the voltammetry (not shown) again leading credence to the membrane effects shown in Section 7.3.1.

Next bulk electrolysis was investigated both visually and by chronoamperometry. In the visual example shown in Figure 7.6C a series of photographs were taken after holding the potential at values suitable for the oxidation and subsequent reduction of *n*-BuFc. In the initial diagram (i) no voltage was applied and the organic phase within the microreactor was clearly visible showing a characteristic yellow colour for *n*-BuFc. When the potential was set to an oxidising level (0.96 V *vs* SCE) for 15 minutes a change in colour to green was seen (Figure 7.6Ciii) characteristic of the oxidised species *n*-BuFc^{+}. This showed that the bulk electrolysis was taking place effectively. The final diagram shows the effect of setting the potential back to a reducing level with the *n*-BuFc colour being regenerated showing that the expected reversible reaction was obtained.

The chronoamperometry data shown in Figure 7.6D for a 20 mM solution of *n*-BuFc in 100 µL of acetonitrile is presented as a log(current) *vs.* time and charge *vs.* time plot. The charge plot suggests a total charge of *ca*. 300 mC is passed overall which was slightly more than the expected 193 mC for complete conversion. This discrepancy was attributed to a decomposition of the product allowing additional electron transfer processes supported by the

emergence of a brown material after polarity reversal (Figure 7.6C, diagram v).

The current plot was initially seen to decrease with time but then began to level off as the current efficiency decreased. By analysing the initial decay of the current it was seen that a first order decay occurred,[16] represented by the dashed line. This decay can be predicted by Equation 1 for a typical bulk electrolysis process.

$$\textbf{(1)} \qquad I(t) = I_0 \times \exp(-m(A/V)t)$$

Here: $I(t)$ is the current at time = t, I_0 is the initial value of electrolysis current, m is the apparent mass transfer coefficient, A is the geometric area (10^{-5} m^2), V is the acetonitrile volume (10^{-7} m^3) and t is the time.

From the decay shown the mass transport coefficient was found to be approximately 4 x 10^{-5} ms^{-1}. This prediction was made based on a constant mass transfer coefficient which was reasonable given the aqueous ion transfer dependence and only small effect of stirring in the organic phase shown. Since a highly buffered and agitated aqueous solution was used this was thought to be supplied at a constant rate. Assuming a diffusion controlled process, this value was used to find a diffusion layer thickness (δ) by using the estimation, $m = D/\delta$, where D is the diffusion coefficient of *n*-BuFc in acetonitrile[17] (1.56 x 10^{-9} m^2s^{-1}). This gave an estimate of the diffusion layer thickness to be 40 µm which, when compared to the carbon membrane thickness was seen to be quite similar. This result suggested that the diffusion into the carbon membrane from solution was slow and thus for faster electrolysis a thinner membrane may be required.

7.3.4 Electrochemical Reduction of Tetraethyl-ethylenetetracarboxylate in the Organic Phase

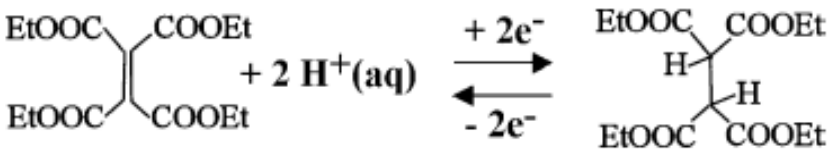

Scheme 7.3 The two electron / two proton reduction of tetraethyl-ethylenetetracarboxylate.

The next redox system that was investigated in the carbon membrane microreactor was an organic test system commonly used in electrochemistry, tetraethyl-ethylenetetracarboxylate[13] (TET). This species is a highly activated alkene and is thus very easy to reduce making a good test system. Another positive property of this redox probe is that the reduction in a single phase reaction is known to be reversible meaning that the radical intermediate is relatively stable which was hoped would limit radical combination forming unwanted dimer products.

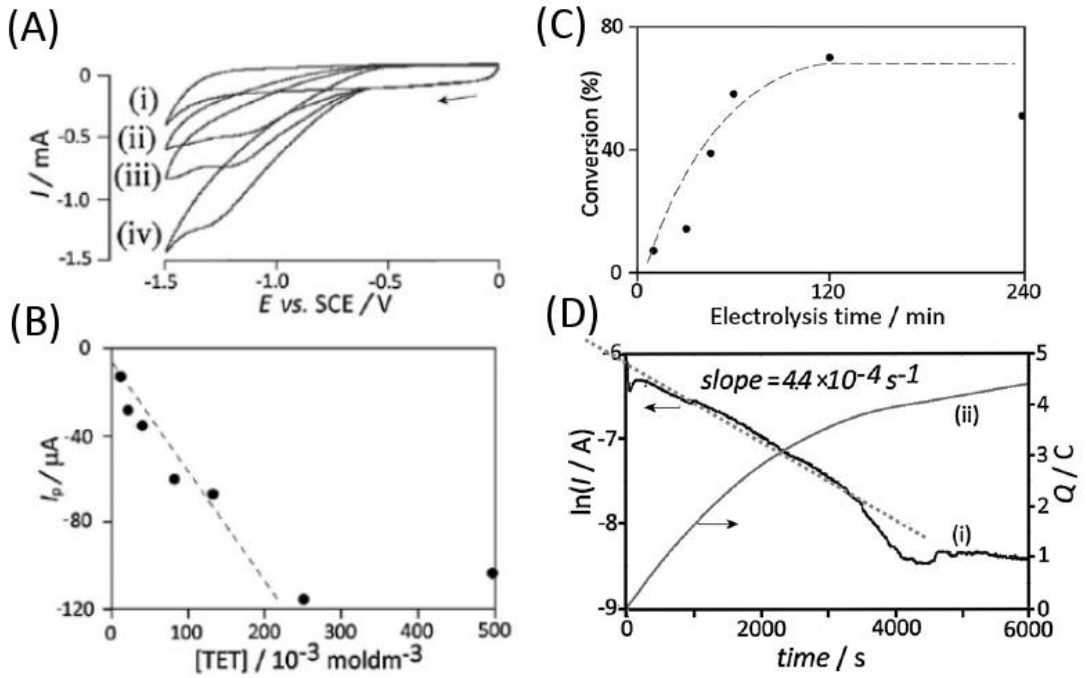

Figure 7.7 **(A)** This shows voltammograms for the triple phase reduction of tetraethyl-ethylenetetracarboxylate (i) 0, (ii) 10, (iii) 20, (iv) 40mM in 100 μL of acetonitrile. Electrodes were held at 5 mm depth for 30 minutes prior to scans to equilibrate. Scans were performed at 10 mVs^{-1} in 0.1 M PBS pH7 + 1 M Na_2SO_4. These scans were performed under static conditions. The data is summarised in **(B)** a plot of peak height against concentration. **(C)** Electrolysis was performed on 80 mM tetraethyl-ethylenetetracarboxylate in 0.1 M PBS pH7 + 1 M Na_2SO_4 and held at a potential of -1.25 V for varying amounts of time while being stirred by a rotating needle at 300 Hz.

From the voltammetry in Figure 7.7A a clear irreversible reductive wave was seen with an onset potential of *ca* -0.6 V *vs*. SCE and peak potential of *ca.* -1.25 V *vs.* SCE for the cathodic process. This represented the concerted addition of two electrons and the insertion of two protons from the aqueous

phase. The concentration dependence shown in Figure 7.7A is summarised in 7.7B and gives a clear linear increase in Faradaic charge with an increasing concentration up to a concentration of *ca* 250 mM. At higher concentrations the charge was instead found to remain roughly constant suggesting that another factor was instead limiting the current. This limitation was possibly due to the resistive nature of the electrochemical reaction.

From the proposed mechanism it was known that a plentiful proton supply was required for the reaction to be viable and from the single phase results in Section 7.3.3 it was thought that diffusion from the bulk aqueous phase into the membrane was relatively slow. As a result it may be inferred that the local proton concentration within the membrane near to the triple phase boundary became diminished during the reaction, especially at very high reagent concentrations, and as a result the reaction would be inhibited by the lack of protons in the locality of the triple phase boundary reaction zone. For further investigations it was determined that a concentration of 160 mM, corresponding to a total mass of 6 mg would be a suitable concentration for electrolysis due to it not being current limited and being of sufficient strength to be detectable by ^{1}H NMR.

Bulk electrolysis experiments were carried out as summarised in Figure 7.7C showing the change in conversion of TET into the product as monitored by ^{1}H NMR and plotted against time. From this plot it was possible to see that the electrolysis up to about one hour appeared to proceed in an almost linear fashion with a current efficiency of 20 – 40 %. It was also possible to determine that in two hours the conversion reached a maximum value of 78% and did not increase further with increased time. At higher time values the conversion was found to decrease possibly due to the effect of side reactions or ester hydrolysis. For each of these reactions an overhead stirrer was used at a stirring frequency of 300 Hz. It was found that the agitation speed does not greatly affect either the limiting current or the conversion time but that in the absence of stirring the conversion was found not to be so efficient. Thus, a high stirring speed was used to ensure rapid mass transport of reagents to the electrode surface.

The use of 1 M Na_2SO_4 and 0.1 M phosphate buffer solution (PBS) pH 7 was determined as the best combination of salts for high conversion of alkene. A high concentration of salt must be used to keep the acetonitrile and water phases immiscible, so 1 M Na_2SO_4 was used initially due to its resistance to electrochemical side reactions but with only very low conversion (*ca.* 22%). It was thought that buffering may be important for the continuation of the reaction due to the availability of protons being crucial and so reactions were undertaken with a 1 M PBS pH 7 aqueous solution but again yielded poor conversions (*ca.* 20%). It was only when a combination of both 1 M Na_2SO_4 and 0.1 M PBS pH 7 was used that a high conversion (*ca.* 78%) was seen. It was reasoned that if a high proton concentration may help the reaction, then 1 M H_3PO_4 could prove beneficial but this effect was not seen. Finally a 1 M Li_2SO_4 solution was used to discount the possibility of a metal cation transfer which would be expected to be easier for Li^+ ions than Na^+ ions due to the higher hydrophobicity of Li^+. The effect of changing the cation showed no effect on the conversion seen after two hours and so it may be assumed that the cation plays no role in the reaction.

For further analysis of the electrolysis a chronoamperometry experiment was performed to analyse the change in current with time, as well as the progression of charge transferred as a measure of the progress of the reaction. From the current profile it was seen that the trend was very similar to that seen in the case of *n*-BuFc with a logarithmic decay however the timescale was now much longer and the gradient was 4.4×10^{-4} s^{-1}. This equated to a value of $m = 4 \times 10^{-6}$ ms^{-1} for the mass transfer coefficient ($m=D/\delta$ with $D = 1.2 \times 10^{-9}$ m^2s^{-1} from the Wilke-Chang estimation[18]), and an estimated diffusion layer thickness of δ= 260 μm. This was an unrealistic value of diffusion layer thickness and may be attributed to a much slower process for the reduction of TET than the oxidation of *n*-BuFc due to a less efficient triple phase boundary process.

This phenomenon may be explained by a result found by Aoki *et al.*[19] in which the efficiency of a triple phase boundary process for *n*-BuFc was seen to increase over time. This was due to the formation of a charge pair in the organic phase, which acted as an electrolyte in the organic phase and

increased the distance into the organic phase over which the triple phase boundary is extended. In the case of TET a charge pair was not formed since the transferring protons became chemically bound to the TET and thus the triple phase boundary was not able to extend which lead to the lower efficiency of the process.

7.4 Conclusions

In conclusion a novel triple phase boundary electrode was presented that overcame the problem of low currents that have existed in previous systems. This problem has been addressed by the use of a very large triple phase boundary zone within a porous carbon fibre membrane. The amphiphilic carbon membrane was shown to stabilise the organic | aqueous interface and allowed a triple phase boundary to exist inside the membrane which was used as the working electrode.

The triple phase boundary was probed by the use of an *n*-BuFc redox probe which allowed anion transfer from the aqueous phase. The electrolysis of this was found to be highly efficient and is analysed both visually and by chronoamperometry to give a mass transfer coefficient $m = 4 \times 10^{-5}$ ms^{-1}.

When compared to the synthetic test system of tetraethyl-ethylenetetracarboxylate the process appeared much less efficient with a mass transfer coefficient $m = 4 \times 10^{-6}$ ms^{-1}. Despite this decrease in efficiency the reduction was still shown to be effective with a conversion to alkane shown to be *ca.* 78% in two hours as analysed by ^{1}H NMR.

7.5 References

(1) Nanolab; http://lib.store.yahoo.net/lib/nanolab2000/preparation-of-buckypaper.pdf, **2006**.

(2) Merkoci, A.; Pumera, M.; Llopis, X.; Perez, B.; del Valle, M.; Alegret, S. *Trac-Trends in Analytical Chemistry* **2005**, *24*, 826.

(3) Pumera, M. *Chemistry-A European Journal* **2009**, *15*, 4970.

(4) Moore, R. R.; Banks, C. E.; Compton, R. G. *Analytical Chemistry* **2004**, *76*, 2677.

(5) Ando, Y.; Iijima, S. *Japanese Journal of Applied Physics Part 2-Letters* **1993**, *32*, L107.

(6) (a) Wang, J.; Musameh, M. *Analyst* **2004**, *129*, 1; (b) Wang, J.; Kawde, A. N.; Musameh, M. *Analyst* **2003**, *128*, 912.

(7) (a) Shul, G.; Murphy, M. A.; Wilcox, G. D.; Marken, F.; Opallo, M. *Journal of Solid State Electrochemistry* **2005**, *9*, 874; (b) Rubianes, M. D.; Rivas, G. A. *Electrochemistry Communications* **2003**, *5*, 689.

(8) Pacios, M.; del Valle, M.; Bartroli, J.; Esplandiu, M. J. *Journal of Electroanalytical Chemistry* **2008**, *619*, 117.

(9) (a) Li, J.; Liu, Q.; Liu, Y. J.; Liu, S. C.; Yao, S. Z. *Analytical Biochemistry* **2005**, *346*, 107; (b) Li, J.; Ng, H. T.; Cassell, A.; Fan, W.; Chen, H.; Ye, Q.; Koehne, J.; Han, J.; Meyyappan, M. *Nano Letters* **2003**, *3*, 597.

(10) Watkins, J. D.; Bull, S. D.; Marken, F. *Journal of Physical Chemistry C* **2009**, *113*, 15629.

(11) Watkins, J. D.; Amemiya, F.; Atobe, M.; Bulman-Page, P. C.; Marken, F. *Electrochimica Acta* **2010**, *55*, 8808.

(12) (a) MacDonald, S. M.; Watkins, J. D.; Bull, S. D.; Davies, I. R.; Gu, Y.; Yunus, K.; Fisher, A. C.; Page, P. C. B.; Chan, Y.; Elliott, C.; Marken, F. *Journal of Physical Organic Chemistry* **2009**, *22*, 52; (b) Watkins, J. D.; MacDonald, S. M.; Fordred, P. S.; Bull, S. D.; Gu, Y. F.; Yunus, K.; Fisher, A. C.; Bulman-Page, P. C.; Marken, F. *Electrochimica Acta* **2009**, *54*, 6908; (c) MacDonald, S. M.; Watkins, J. D.; Gu, Y.; Yunus, K.; Fisher, A. C.; Shul, G.; Opallo, M.; Marken, F. *Electrochemistry Communications* **2007**, *9*, 2105.

(13) Paddon, C. A.; Pritchard, G. J.; Thiemann, T.; Marken, F. *Electrochemistry Communications* **2002**, *4*, 825.

(14) MacDonald, S. M.; Fletcher, P. D. I.; Cui, Z. G.; Opallo, M. C.; Chen, J. Y.; Marken, F. *Electrochimica Acta* **2007**, *53*, 1175.

(15) Marken, F.; Gerrard, M. L.; Mellor, I. M.; Mortimer, R. J.; Madden, C. E.; Fletcher, S.; Holt, K.; Foord, J. S.; Dahm, R. H.; Page, F. *Electrochemistry Communications* **2001**, *3*, 177.

(16) Bard, A. J.; Faulkner, L. R. *Electrochemical Methods, 2nd Ed.*; 2nd ed.; Wiley, **2001**.

(17) Clegg, A. D.; Rees, N. V.; Klymenko, O. V.; Coles, B. A.; Compton, R. G. *Journal of Electroanalytical Chemistry* **2005**, *580*, 78.

(18) Wilke, C. R.; Chang, P. *Aiche Journal* **1955**, *1*, 264.

(19) Tasakorn, P.; Chen, J. Y.; Aoki, K. *Journal of Electroanalytical Chemistry* **2002**, *533*, 119.

8. Liquid–Liquid Electro-reduction Processes in a Triple Phase Boundary Microreactor

Contents

Aims

- To investigate further alkene reduction processes at the triple phase boundary for activated alkenes.
- To investigate the electro-reductions of a range of aldehydes and imines at the triple phase boundary.
- To investigate the mechanism and optimise synthetic reactions by varying pH, concentration and electrolyte composition.

Publication

- Watkins JD, Taylor JE, Bull SD and Marken F, In preparation for submission to Tetrahedron Letters

CHAPTER 8: Liquid–Liquid Electro-reduction Processes in a Triple Phase Boundary Microreactor

8.1 Introduction

The triple phase boundary was introduced in Section 1.2 as a novel electrochemical reaction environment. The mechanism for triple phase boundary processes involves a simultaneous electron and ion transfer between aqueous and organic phases at the point where they simultaneously contact an electrode. The triple phase boundary mechanism allows redox material and electrolyte to be separated during reactions and this avoids issues of separation in electrosynthetic processes post reaction. It is for this reason that the triple phase boundary is an ideal platform for the rapid and clean synthesis of materials.

Electrosynthetic reactions have been introduced in Section 1.3 showing the current syntheses as well as many advantages and disadvantages of the technique over traditional syntheses. Electrochemistry offers a more efficient and clean approach although its disadvantages are rooted in the need to use excess electrolytes and the difficulty in controlling radical reactions. These issues have been addressed in many ways as described but the triple phase boundary approach has been investigated in this thesis.

In summary the problem of triple phase boundary electrosynthesis has been approached *via* a salt matrix cell (Chapter 4), a localised ultrasound enhanced emulsion process (Chapter 5) and a high shear force emulsion process (Chapter 6). Each of these was found to yield too low current densities to be synthetically viable. In Chapter 6 a new method based on an amphiphilic porous carbon membrane microreactor was introduced and characterised with success in the reduction of an organic test system based on a highly ester substituted alkene. In this chapter the microreactor was used for further hydrogenation reactions of several activated organic functional groups.

The hydrogenation reaction is a well established reduction process in synthetic organic chemistry[1] and can be readily achieved for unsaturated carbon-carbon, carbon-oxygen and carbon-nitrogen bonds. The mechanism involves the addition of hydrogen across the bond. In general, the source of hydrogen is high pressure hydrogen gas which can be an explosion hazard. A solid catalyst is usually required onto which hydrogen may dissociate as bound atoms for easy addition to unsaturated bonds bound to the catalyst surface.[1]

A full discussion of catalysts is beyond the scope of this introduction but common examples include precious metals, most commonly palladium. Often the choice of catalyst can determine selectivity, stereochemistry and reaction conditions and many new catalysts are available to suit the reaction. For less hazardous conditions raney nickel allows the reduction of unsaturated bonds by generated hydrogen but requires harsh conditions to achieve this.[2]

Some less common examples of hydrogenation reactions using exotic conditions and environments can often give rise to interesting mechanistic effects. With the popularity of nano-structured materials it is no surprise that hydrogenation reactions are being targeted as model processes with examples involving solid supported palladium nanoparticles,[3] copper nanoparticles,[4] polymer encapsulated platinum nanoparticles[5] and water soluble nanostructured platinum.[6]

There was an example by Chang *et al.*[7] who detailed a solvent free hydrogenation of alkenes by solid supported palladium nanoparticles where reagent melting points were found to be crucial for effective reaction of the exothermic hydrogenation.

As already alluded to, a key problem with the hydrogenation of alkenes was that the use of hydrogen, especially at high pressure, posed a serious safety hazard especially for scale up applications. It is for this reason that much research was directed to the use of hydrogen donors other than hydrogen gas, a so called ‘transfer hydrogenation’. Classically, this methodology involved the simultaneous, thermodynamically driven, oxidation of a donor molecule in order to reduce the target unsaturated bond. Most famously

Noyori *et al.*[8] have used isopropanol and a ruthenium based catalyst for asymmetric transfer hydrogenation. Isopropanol was a popular choice for such reactions as it was easily oxidised to acetone which was easily removed during the reaction to drive the equilibrium and release a H_2 equivalent. Other examples of proton donation from simple molecules include the use of water,[9] methanol[10] and even ammonium hydroxide.[11] Although generally these required metal catalysts, they also avoided the use of hydrogen gas.

Examples of the electro-reduction of unsaturated alkenes to their corresponding alkanes has been demonstrated in a mediated approach by da Silva *et al.*[12] and single phase alkene electrolysis as well as many other electro-reductions have been reviewed by Popp *et al.*[13] The electro-reduction of aldehydes and ketones was also of great interest due to the complexity of the product distribution. The radical mechanism involved in electro-reduction primarily lead to coupled products although competing reaction pathways have lead to alcohol and condensation products. Kise *et al.*[14] have reported a cross coupling procedure of aromatic aldehydes and ketones with aliphatic aldehydes and ketones, by elimination of imidazole. In order to favour this cross coupling it was necessary to use chlorotrimethylsilane, tetrabutylammonium hexafluorophosphate and an excess of the aliphatic reagent. In another publication Kise *et al.*[15] showed that the same procedure can be used for the intramolecular cyclisation of carbonyl compounds.

An alternative electrochemical strategy to the direct reduction of carbonyl compounds, followed by the abstraction of hydrogen, was the electrogeneration of hydrogen at an electrode surface prior to addition to the carbonyl compound. The challenge in this methodology was to find an electrode material suitable for the efficient evolution of hydrogen as well as the catalytic hydrogenation of the carbonyl. Santana *et al.*[16] reported an efficient hydrogenation of a range of substrates both alkene and carbonyl using optimised conditions for hydrogen evolution at a nickel deposit on iron electrodes.

In this study, the triple phase boundary reaction characterised in Chapter 7 was extended to encompass a range of alkenes, aldehydes and imines. The effect of pH variation, substrate concentration, supporting electrolyte identity

and substrate electronic properties was assessed to try and describe a suitable mechanism for the electro-reduction.

8.2 Experimental

8.2.1 Chemical Reagents

Sodium perchlorate monohydrate (98%, Sigma Aldrich), sodium sulphate decahydrate (≥99%, ACS reagent, Sigma Aldrich), *n*-butylferrocene (98%, Alfa Aesar), phosphoric acid (Sigma Aldrich ACS reagent, 85 wt%), sodium chloride (≥95%, SigmaUltra reagent, Sigma Aldrich), sodium hydroxide (≥97%, ACS reagent, Sigma Aldrich), diethyl fumarate (Aldrich, 98%), ethyl cinnamate (Aldrich, 99%), cinnamic acid (Aldrich, 97%), Ethanol (Aldrich, absolute, ≥99.8%), benzaldehyde (Aldrich, redistilled, ≥99.5%), toluene (Sigma-Aldrich, Chromasolv, HPLC grade), 4-(trifluoromethyl)benzaldehyde (Aldrich, 98%), *p*-tolualdehyde (Aldrich, 97%), *m*-tolualdehyde (Aldrich, 97%), *o*-tolualdehyde (Aldrich, 97%), *p*-chlorobenzaldehyde (Aldrich, 97%), *p*-anisaldehyde (Aldrich, 98%), benzylamine (Aldrich, redistilled, ≥99.5%), isopropylamine (Aldrich, ≥99.5%), lithium sulphate (Aldrich, ≥98.0%), lithium hydroxide, monohydrate (Aldrich, 98%), trifluoroacetic acid (Sigma-Aldrich, Reagent Plus, 99%), tetrabutylammonium hexafluorophosphate (Fluka, analytical grade, ≥99.0%) were used without further purification. Demineralised and filtered water was taken from a Millipore water purification system with not less than 18 MΩcm resistivity

8.2.2 Instrumentation

Voltammetric experiments were performed with a microAutolab III system (Ecochemie, Netherlands) in staircase voltammetry mode. The step potential was maintained at approximately 1 mV. The counter and reference electrodes were platinum gauze and KCl-saturated calomel (SCE, Radiometer), respectively. The working electrode was a 4 mm diameter carbon nanofibre membrane disc ('Bucky paper', Nanolabs US, with low resistivity (~0.1 Ωcm) and relatively low impurity levels (Fe 0.36, Si 0.31, Al 0.23, Na 0.32, S 0.23 at%) mounted with Ambersil silicone (Silicoset 151) on a glass capillary of 3.5 mm inner diameter and 5 mm outer diameter. The

electrical contact was made with a 1 mm stripe of pyrolytic graphite film (Goodfellow, UK) inside of the glass capillary. Solutions were deaerated with argon (Pureshield, BOC). The pH was measured with a glass electrode (3505 pH meter, Jenway). All experiments were conducted at a temperature of 22 $\pm$2 oC

8.2.3 Procedure I: Triple Phase Boundary Electro-reductions

The electrolysis was carried out as described in Chapter 7 Section 7.2.4.

8.2.4 Procedure II: Synthesis of ethyl 4-(trifluoromethyl)cinnamate

Since ethyl 4-(trifluoromethyl)cinnamate was not commercially available it must first be synthesised. The procedure was a facile transformation based on a literature method by Rai *et al.*[17] from 4-(trifluoromethyl)cinnamic acid and ethanol. To a solution of 750 mg of 4-(trifluoromethyl)cinnamic acid in absolute ethanol (17 ml) 2 molar equivalents of trimethylsilyl chloride were added at room temperature under air. The mixture was stirred for 12 hours and upon completion the solvent was removed by rotary evaporation and the residue redissolved in ethyl acetate. This solution was washed with saturated $NaHCO_3$ followed by water, and then brine. It was then dried with magnesium sulphate and extracted by rotary evaporation to give the ethyl 4-(trifluoromethyl)cinnamate in an 86 % conversion by ^{1}H NMR comparison of 6.7 ppm (1H, d) and 4.3 ppm (2H, q) and was used without further purification.

8.2.5 Procedure III : Synthesis of Imines

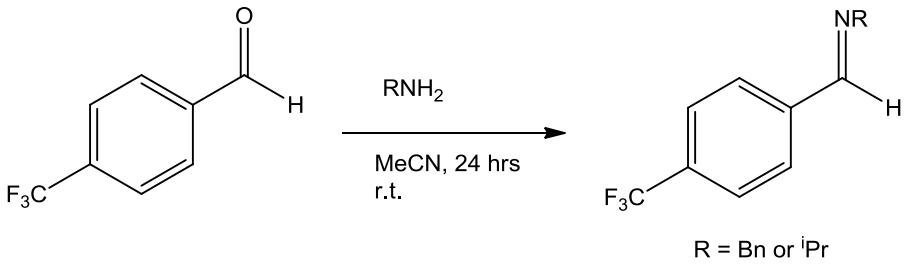

Scheme 8.1 The general preparation of imines used.

Both imines were produced by the same reaction process. To a solution of 4-trifluoromethylbenzaldehyde (3.8 mmol) in anhydrous acetonitrile (20 ml) was

added 3.8 mmol benzylamine under nitrogen and the mixture was stirred at room temperature for 24 hours. In some cases a white precipitate had formed due to the acid base pairing of oxidised aldehyde and amine but was removed by gravity filtration. The acetonitrile was removed by rotary evaporation and the residue analysed by ^{1}H and ^{13}C NMR showing the imine product with no aldehyde being present. The sample was used without further purification.

8.3 Results and Discussion

8.3.1 Electro-reduction of unsaturated alkenes

In Chapter 7 the electro-reduction reaction of a tetra-substituted alkene was investigated and it was found that a reduction wave appeared starting at *ca.* -0.8V *vs.* SCE, with a peak current occurring at *ca.* -1.25V *vs.* SCE. The electrolysis was carried out at the peak potential and resulted in a conversion of 78% to the corresponding alkane (Scheme 2).

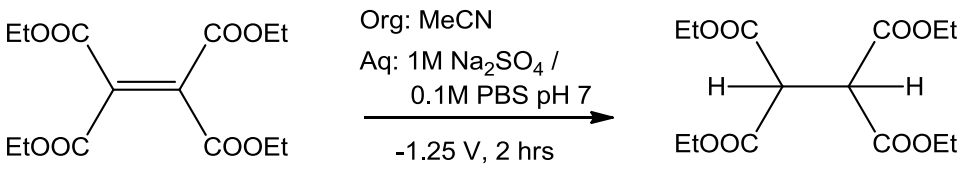

Scheme 8.2 The two electron / two proton reduction of tetraethyl-ethylenetetracarboxylate.

For the carbon nanofibre paper, a scan of a blank acetonitrile phase with the same 1 M Na_2SO_4 + 0.1 M phosphate pH 7 buffer solution revealed a background reduction after -2.0 V *vs.* SCE. This cathodic process was suspected to be related to a surface reduction of the carbon nanofibre paper. Solution based processes of sulphate and phosphate could generally be ignored as these electrolytes were chosen to be electrochemically inert. These background processes not only meant that reductions requiring a greater cathodic driving potential than -2.0 V could not be electrochemically resolved but also that the current efficiency of these reactions would become negligible.

Voltammetric data in Figure 8.1 is shown for both the single phase voltammograms (Figure 8.1A) in a fully supported acetonitrile phase, as well as at a triple phase boundary (Figure 8.1B) within the carbon membrane microreactor. These results showed the shift in reduction potential with electron density of the alkenes. As less esters were incorporated, the alkenes became more electron rich and harder to reduce, shown by a shift to higher reduction potentials.

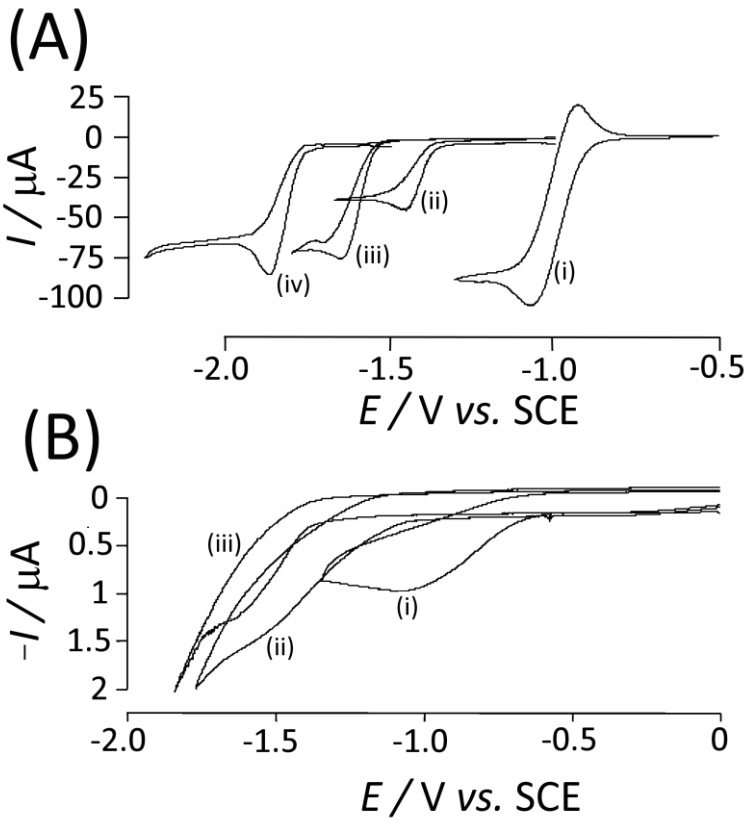

Figure 8.1 (A) Voltammograms summarising the reduction reactions of substituted alkenes on a 3 mm glassy carbon electrode at a scan rate of 10 mVs^{-1} in a single organic phase of 0.1 M Bu_4NPF_6 after saturation by argon gas (i) 8 mM tetraethyl-ethylenetetracarboxylate, (ii) 8 mM diethylfumarate ester and (iii) 8 mM ethyl 4-(trifluoromethyl)cinnamate. (iv) 8 mM ethyl cinnamate **(B)** Voltammograms summarising the triple phase boundary reduction reactions of substituted alkenes at a scan rate of 10 mVs^{-1} in a 100 µL organic phase of MeCN with a 1 M Na_2SO_4 + 0.1 M PBS pH7 aqueous phase. (i) 160 mM tetraethyl-ethylenetetracarboxylate, (ii) 160 mM diethylfumarate ester and (iii) 160 mM ethyl 4-(trifluoromethyl)cinnamate. The reduction of ethyl cinnamate could not be seen before the background reduction wave of the carbon membrane material.

The different alkene reactions are summarised in Table 8.1, and show different reduction potentials for the various alkenes used, as well as the conversion to alkanes for a 2 hour reduction conducted at the peak potential. From Table 8.1 it was clear that a dramatic change in both reduction potential and conversion occurred as the identity of the alkene was changed. The trend showed that for more substituted species, the alkene became electron poor and was easier to reduce. The conversion followed a similar trend with alkene identity, where those easier to reduce gave higher conversions, possibly due to a greater ability to compete with background reactions and lead to a greater current efficiency.

Table 8.1 A table summarising reduction potentials for a single phase experiment in MeCN + 0.1 M Bu_4NPF_6, triple phase reduction potentials under conditions shown in figure 1 and the conversions for a 2 hour synthesis of 160 mM of each alkene.

Entry	Reactant	Single Phase Reduction Potential (in MeCN) *vs.* SCE	Triple Phase Reduction Potential *vs.* SCE	Conversion[1]
1	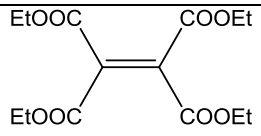	-1.08	-1.25	75 %
2	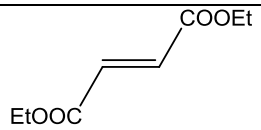	-1.46	-1.80	32 %
3	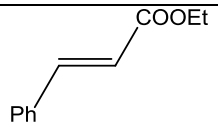	-1.87	-[2]	No Reaction
4	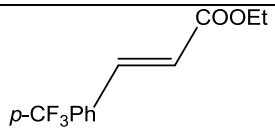	-1.65	-1.80	85 %

[1] Conversion calculated from 1H NMR integration comparison of the overlapping CH2 quartets δ= 4.2 ppm and the new singlet δ= 4.1 ppm.
[2] In the triple phase boundary microreactor the reduction of ethyl cinnamate was hidden in the electrode background and synthesis was not possible.

The exception was for the example of ethyl (trifluoromethyl) cinnamate, which showed a much larger conversion despite having a similar reduction potential to diethyl fumarate. The cause was most likely a stabilising effect of the

benzene ring on the radical anion produced giving an increased time for proton interaction.

Initially an ester di-substituted alkene was used (Scheme 8.3) and was found, as expected, to have a more negative reduction potential compared with the tetra-substituted alkene, due to the di-substituted alkene being less electron poor. The effect of less substitution also had a profound effect on the conversion of the alkene being greatly reduced from 78 % to 32 %, with the bulk of the remainder being unreacted starting material.

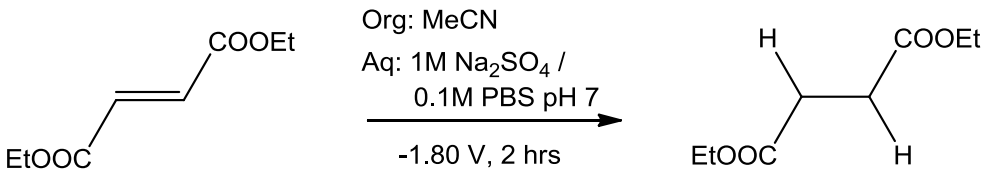

Scheme 8.3 The two electron / two proton reduction of diethylfumarate ester.

For the singly substituted alkene, ethyl cinnamate ester, the reduction potential was now too high to be seen voltammetrically prior to the background reduction, and thus no electrolysis could be attempted. In order to overcome this problem the phenyl ring of the cinnamate ester was substituted by a highly electron withdrawing *para*-trifluoromethyl substituent. This electron withdrawing character had an activating effect on the alkene, similar to substitution by esters. This 4-(trifluoromethyl)cinnamate ester had a lower reduction potential than the unsubstituted cinnamate ester, allowing voltammetry to be visualised and electrolysis to be achieved (Figure 8.1B).

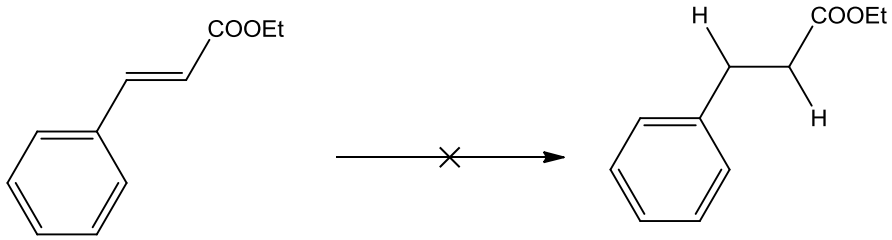

Scheme 8.4 The two electron / two proton reduction of ethyl cinnamate.

With the phenyl group modified by a *para*-trifluoromethyl substituent, the reduction potential was lowered by *ca.* 200 mV, putting it within the -2.0 V limit of the electrode material. Interestingly the *para*- CF_3 group also greatly

increased the conversion to alkane reaching now 85 % in 2 hours (Scheme 8.5).

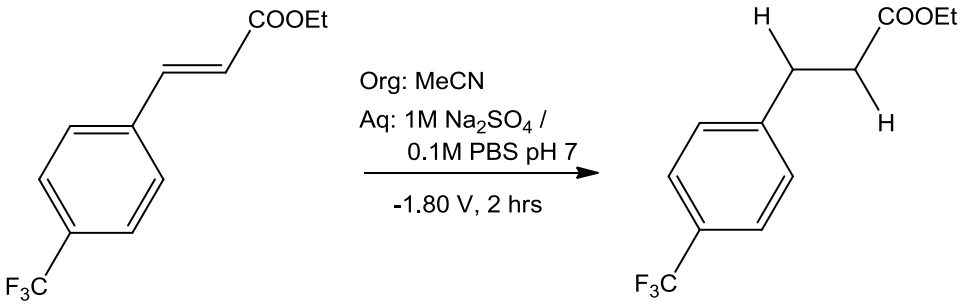

Scheme 8.5 The two electron / two proton reduction of ethyl 4-(trifluoromethyl)cinnamate.

8.3.2 Electro-reduction of benzaldehyde

Aldehydes are of significant interest in electrochemical reductions and were also studied in the triple phase boundary carbon nanofibre microreactor. Benzaldehyde was selected as a test system due to its electron poor nature, which resulted in a facile reduction, as well the inherent ability to easily substitute the benzene ring for further mechanistic analysis. At the triple phase boundary, the reduction wave of benzaldehyde was found to occur at *ca* -1.85 V *vs.* SCE with a well defined but resistive irreversible reduction wave shown in Figure 8.2.

When the products of the benzaldehyde reduction were analysed by ^{1}H NMR (300 MHz), it was found that although the conversion from starting material was 100 %, two distinct products were formed (Scheme 8.6). These were attributed to the expected alcohol as well as a coupled product, seen in previous studies by Bian.[18] The two products were identified by ^{1}H NMR as singlets at *ca.* 4.75 ppm and 4.60 ppm. These peaks were confirmed as the pinacol and alcohol respectively by comparison with pure samples spiked into the reaction mixture, as well as comparison of thin layer chromatography.

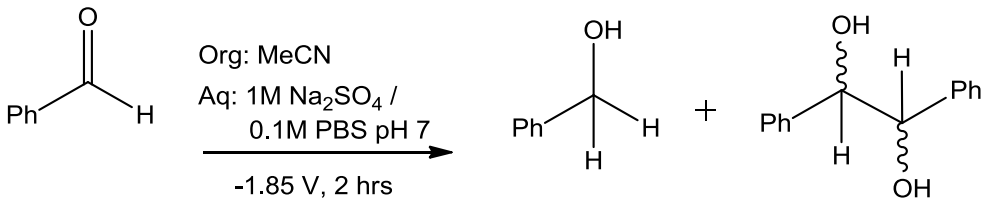

Scheme 8.6 The two electron two proton reduction of benzaldehyde to a mixture of pinacol and alcohol.

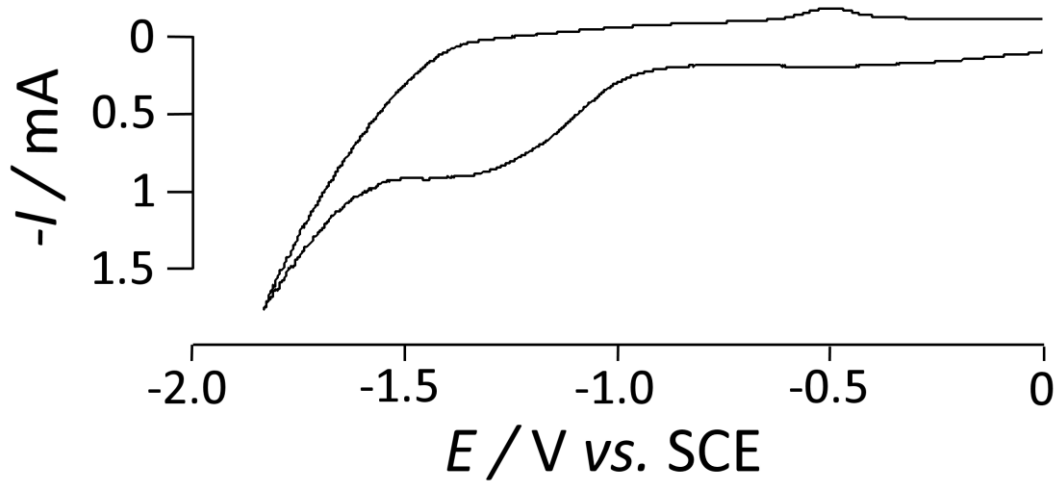

Figure 8.2 A Voltammogram showing the reduction reactions of 160 mM benzaldehyde at the triple phase boundary at a scan rate of 10 mVs^{-1} in a 100 µL organic phase of MeCN with a 1 M Na_2SO_4 + 0.1 M PBS pH7 aqueous phase.

The two products under the conditions in Scheme 5 with a 160 mM benzaldehyde concentration appeared in a 1 : 1.8 ratio in favour of the alcohol. The favouring of an alcohol product from the direct reduction of an aldehyde was in direct contrast with the findings of Bian, who found exclusively the coupled product. This discrepancy was hardly surprising due to the procedural differences used; Bian has used metallic electrodes in a single phase reaction as opposed to the triple phase mechanism in effect here.

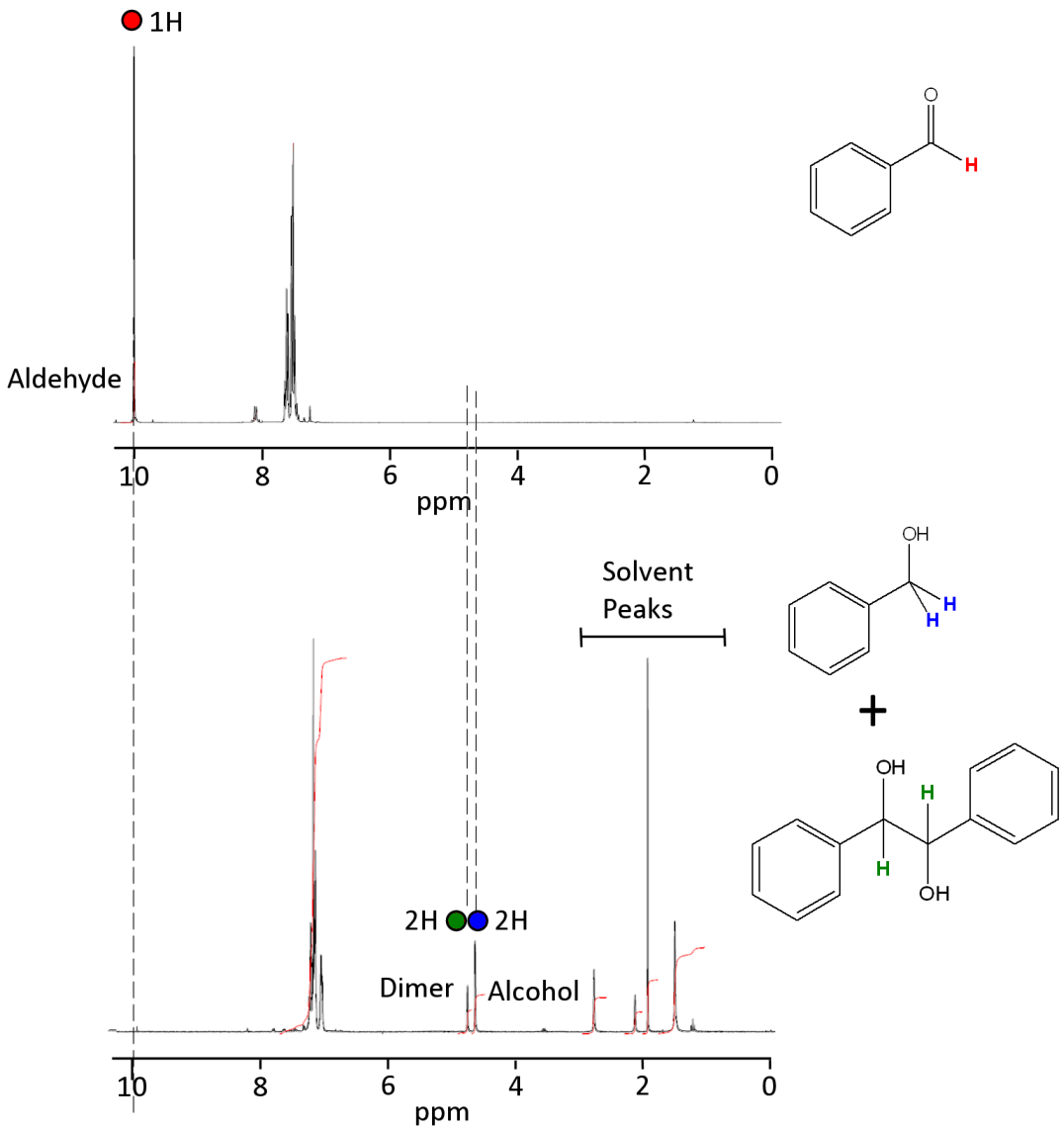

Figure 8.3 This figure shows the ^{1}H NMR (300 MHz) traces of benzaldehyde and a mixture of dimer and alcohol products. The aldehyde peak appears at ca. 10.0 ppm the dimer at ca. 4.75 ppm and the alcohol at ca. 4.6 ppm. The product spectrum corresponds to a reaction of 2 hours for a 320 mM benzaldehyde solution and an aqueous phase of 1M Na_2SO_4 + 0.1 M PBS pH7.

As an example of the methodology for obtaining conversion and product distribution data for the aldehyde reaction, spectra of benzaldehyde and a reaction mixture are compared in Figure 8.3. To determine the conversion and product distribution of each reaction mixture a comparison of ^{1}H NMR (300 MHz) spectra was used (Figure 8.3). The aldehyde peak appeared prominently at *ca.* 10 ppm as well as a phenyl multiplet in the benzaldehyde spectrum, but with no other discernable peaks. The product spectrum was

analysed after a 2 hour reduction of a 320 mM benzaldehyde solution and an aqueous phase of 1M Na2SO4 + 0.1 M PBS pH7. The product spectrum showed solvent peaks for acetonitrile (2.10 ppm) and water (1.6 ppm), since the product sample was far less concentrated than the starting material sample. The product spectrum also gave rise to the appearance of two new singlets between 4.5 ppm and 5 ppm corresponding to the alcohol and dimer protons. The dimer always appeared upfield of the alcohol, but their positions were subject to change depending on the substituents of the phenyl ring. By comparing the integrals of these peaks the product ratio was obtained by. Integration of these signals, which combined with the residual aldehyde peak integral, gave an overall product conversion.

It was hypothesised that the mixture of products was due to the availability of protons compared to radicals for dimerisation, and so lower pH and less benzaldehyde concentration should favour the alcohol product. Upon testing it was found that at a benzaldehyde concentration of 80 mM under the same conditions gave a product ratio of 1 : 1.4 in favour of alcohol. At 40 mM the ratio appeared to change to 1 : 1, but at this low concentrations there was error associated with difficultly in resolving NMR peaks above the background. At the higher concentration of 320 mM the ratio remained at *ca.* 1 : 1.8 but pleasingly the conversion achieved was 98 % in two hours or 100% in four hours. These results appeared to contradict the original hypothesis and so it must be assumed that a more complex mechanism was in effect.

The pH dependence was analysed by changing the aqueous phase buffer pH from pH 7 to pH 2. There was no effect seen on either the conversion or the product distribution. Next, a very large concentration of protons was analysed by using a 1 M H_3PO_4 aqueous phase which gave ratio of 1.4 : 1, now in favour of the dimer. It should be noted also, that the pH change did not appear to cause a Nernstian shift in the voltammetric response as would be expected in a single phase experiment. This result appeared counter intuitive and lends further credence to the conclusion reached in Chapter 7, that the inclusion of Na_2SO_4 in the aqueous phase was highly important.

It is known from Chapter 7 that protons are the transfer ion that completes the triple phase boundary reaction, so it was surprising to see that their concentration in the aqueous phase had no effect on the reaction. Even with a proton source included in the organic phase, in the form of trifluroracetic acid, the conversion became lower. The competition of transferring cations could also be ruled out as a possible mechanism by experiments conducted in a lithiated aqueous phase. It was hoped that Li^+ transfer would effectively compete with proton transfer but instead no changes in conversion or product distribution were detected.

The results so far suggested that external parameters in both the organic and aqueous phases had very little effect on the triple phase boundary mechanism. This oddity may be attributed to the domination of local effects. In this study, the carbon membrane used was 50 – 100 μm thick which was significant compared with the triple phase boundary thickness. This paper was ideal for forming a robust membrane but, given the thickness, it must be assumed that the local proton and aldehyde concentrations were far more important than external factors. This observation also explained why an overhead stirrer in the organic phase had no effect on the reduction currents, since the mass transport effect could not be felt close to the triple phase boundary.

Solvent effects were analysed, and showed that the reaction was feasible in non-polar solvent toluene, with no detriment to either product distribution or conversion. In contrast to Chapter 4, the reaction was not possible in hexane with no triple phase current visible in this solvent.

Further analysis was conducted to determine the functional group compatibility of the reaction, with substituted phenyl rings and other potential reduction centres, a summary of which is found in Table 8.2.

Table 8.2 This shows a table summarising the reduction of substituted benzaldehydes in the carbon membrane microreactor in an organic phase of 100 µL MeCN and an aqueous phase of 1 M Na_2SO_4 + 0.1 M PBS pH7.

Entry	Reactant	Solvent	Triple Phase Reduction Potential *vs.* SCE	Product Ratio[1] Alcohol : Dimer	Conversion[2]
1	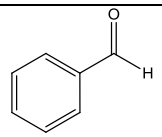	MeCN	-1.90 V	1.8 : 1	100 %
2	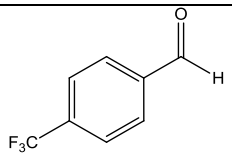	MeCN	-1.80 V	1.65 : 1	100 %
3	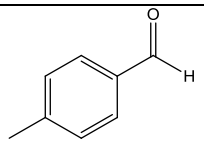	MeCN	-2.1 V	3.1 : 1	66 %
4	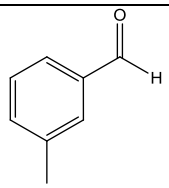	MeCN	-2.1 V	1.82 : 1	94%
4	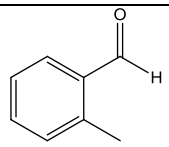	MeCN	-2.1 V	1.65 : 1	70 %
6	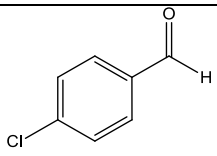	MeCN	-2.1 V	1.8 : 1	99 %
7	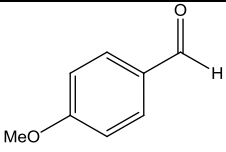	MeCN	-2.1 V	-	Negligible
8	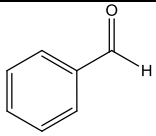	Toluene	-1.85 V	1.6 : 1	100 %

[1.] Product distribution calculated from the integration comparison of dimer (2H) and alcohol (2H) at *ca.* 4.75 and 4.6 ppm

[2.] Conversion calculated from ^{1}H NMR (300 MHz) integration comparison of the aldehyde peak (1H) at *ca.* 10 ppm and the new singlet peaks for dimer (2H) and alcohol (2H) at *ca.* 4.75 and 4.6 ppm.

It was also found that the reduction was not greatly selective and other centres of reduction were liable to reduction as well as the aldehyde. This was to be expected for an electrolysis in which a large driving overpotential was used to complete synthesis in a reasonable time. It may be found by further investigation, that through metal deposition modified electrodes or a lower reduction potential, that greater control of products may be gained. Pleasingly however, the tolerance of a *para*-chloro substitution was found which is unusual in such a reduction, as it would be expected that the C – Cl bond may be cleaved under severe reductive conditions.

A substitution by a *para*-methoxy group completely shut down the reaction with almost no conversion seen, due to a destabilising effect of the radical anion intermediate and the increase in reduction potential required. *Para* nitro and *para*-cyano substituents also appeared incompatible with the reaction, due to their tendency to reduce with the aldehyde resulting in a complex product mixture (results not shown). *Para*-trifluoromethylbenzaldehyde showed very similar results to the unsubstituted reactant but with a lower reduction potential. This meant that a lower driving potential was used and helped in increasing the current efficiency by limiting side reactions.

The *ortho*, *meta* and *para* substitutions of a methyl group were analysed with some interesting results. As expected all three showed a decrease in conversion, probably due to the inclusion of an electron donating functional group to the phenyl ring. This problem could potentially be overcome by using a longer reduction time. The *para* substituted reaction seemed to favour the alcohol product in a 1 : 3.1 ratio, the highest yet recorded, but in an only 66 % overall conversion. This change may be rationalised by the stabilising effect of this electron donating *para* substituent which was not seen in the *meta* case due to relative ring positioning. O*rtho* substitutions did not show a similar selectivity effect due to steric hindrance. The *meta* substituted benzaldehyde however, showed a higher conversion as the electron donating nature of this group was unable to affect a position in a *meta* configuration.

Since the resolution of the triple phase boundary was thought to be important, a series of experiments were conducted with a lower contrast triple

phase boundary. This was easily achieved by changing the overall concentration of electrolyte salts in the aqueous phase. With no salt acetonitrile and water were found to be miscible, but with 1 M salt a well defined phase separation was observed which reformed quickly after vigorous mixing. In all reactions conducted in the carbon membrane microreactor thus far a 1 M concentration of Na_2SO_4 has been used to ensure a well defined phase separation, and so by varying this concentration the resolution of the triple phase boundary may be changed. When a higher concentration (2M Na_2SO_4) was used, almost no change in product distribution was seen, 1 : 1.7 in favour of the alcohol, and still with a 100 % conversion. This was attributed to there being an insignificant increase in boundary resolution over that seen for 1 M salt. If however, a concentration of 0.1 M Na_2SO_4 as well as the same 0.1 M PBS pH 7 was used, then the boundary resolution was seen to decrease significantly by visual inspection. The consequence for the triple phase boundary reaction was that a change in the mechanism was seen, resulting in a switch of product distribution to a ratio of 1 : 1.3 – 1.7 in favour of the dimer.

The mixture of products could be explained by a reaction zone model shown in Figure 8.4. In this case a gradient of proton availability was hypothesised extending into the organic side of the carbon membrane, with reaction zone 1 being more proton rich than reaction zone 2. It was for this reason that zone 1 tended to form alcohol products, whereas the less proton rich zone 2 tended to form dimeric products. The variation in the relative zone volumes determined the distribution of these products but it was still hard to predict how product distributions would change with external effects.

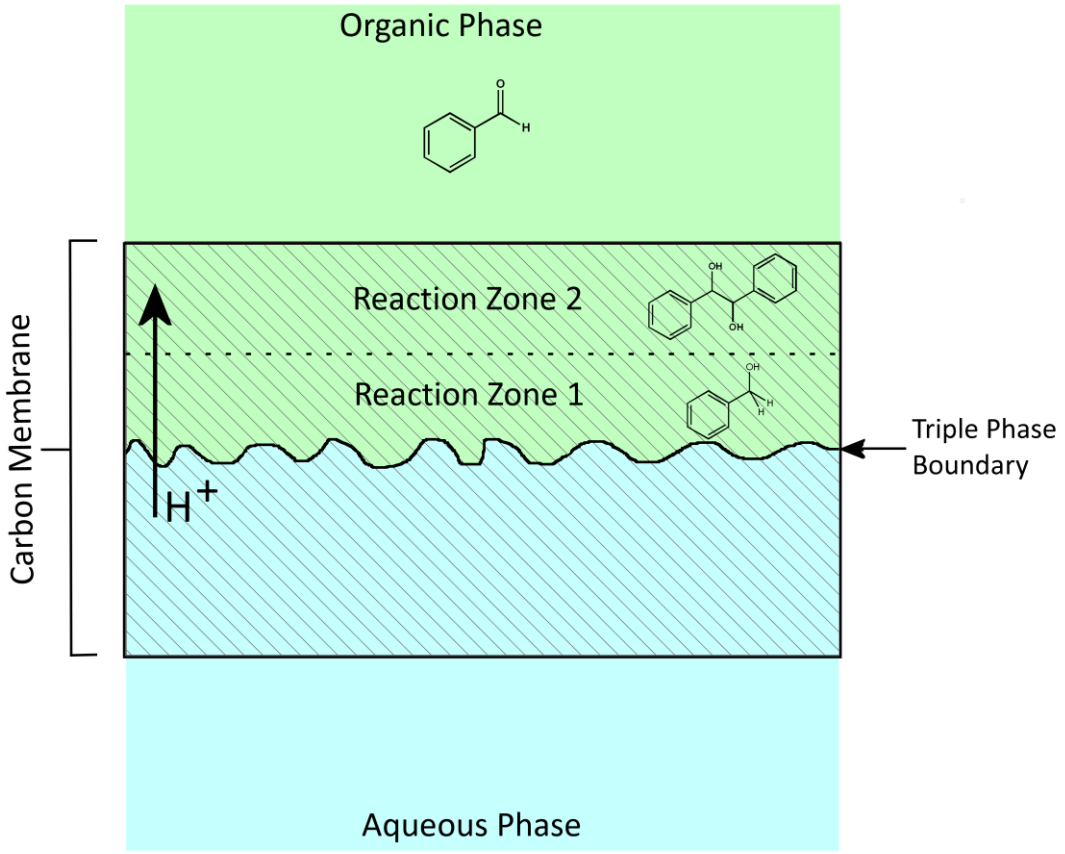

Figure 8.4 This shows a schematic diagram of the carbon membrane during the reduction reaction. The triple phase boundary within the carbon membrane is shown as a non-uniform line with two reaction zones creating products.

8.3.3 Electro-reduction of Imines

Imines are a functional group analogous to carbonyls but with nitrogen in place of oxygen. These compounds are highly reactive, especially in aqueous environments, although Simion *et al.* [19] have shown that an efficient synthesis of them was highly possible in aqueous media. Since they are also readily reduced, they seem to be an ideal compound for study in the carbon membrane microreactor (Scheme 8.7). A benzyl amine was first used to synthesise imines from the *para*-trifluoromethyl substituted benzaldehyde. This aldehyde was chosen to facilitate the characterisation of the imine by ^{1}H NMR.

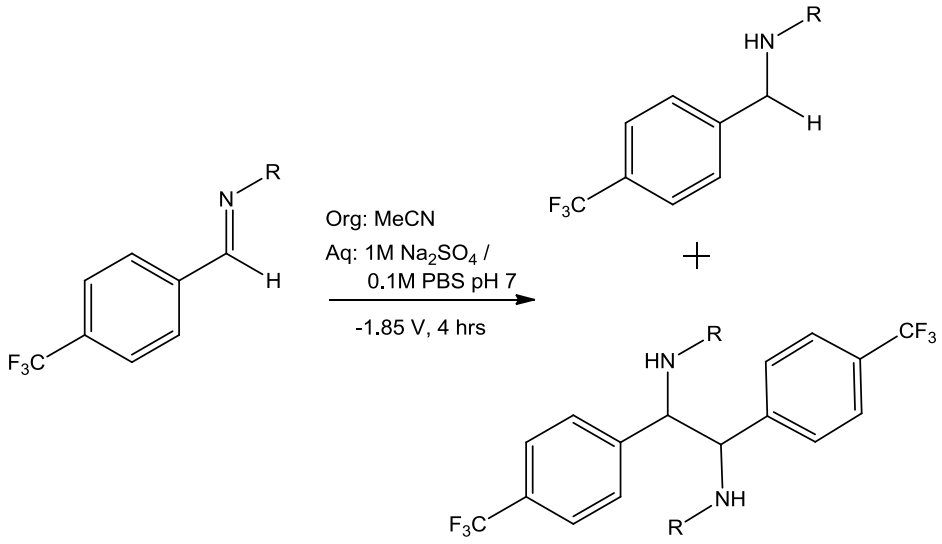

Scheme 8.7 The two electron two proton reduction of imines to a potential mixture of amine and dimeric products.

The first imine synthesised was derived from benzylamine and showed a reduction wave around -1.7 V. This corresponded to a thermodynamically easier reduction than was found for benzaldehyde, although in 2 hours only a very slight conversion was seen (11 %) from a 160 mM sample of imine. After repeating the reaction for 4 hours, the conversion was raised to 50 %, which may suggest a kinetic component of the reduction causing it to be it slower than benzaldehyde. Interestingly however, only a single reduction product was seen for this imine reduction. As analogues of carbonyl groups it was expected that the reduction of imines would lead to a similar mixture of reduction products, of both mono-amine and a coupled diamine products. For the benzyl derivitised imine only the mono-amine product was seen.

A second imine derived from isopropylamine was synthesised from the same aldehyde and showed very different reduction characteristics. In this case, a 100 % conversion was found in a 4 hour synthesis, but with a mixture of products comprising of a 1 : 1 mixture of amine and coupled products, as summarised in Table 8.3.

Table 8.3 This shows a table summarising the reduction of imines in the carbon membrane microreactor in an organic phase of 100 µL MeCN and with an aqueous phase of 1 M Na_2SO_4 + 0.1 M PBS pH7.

Entry	Reactant	Reaction Time	Triple Phase Reduction Potential *vs.* SCE	Product Ratio Amine : Dimer	Conversion
1	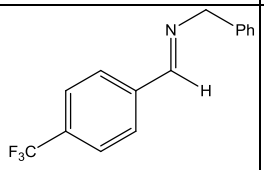	2 hrs	-1.7 V	Amine Only	11 %
2	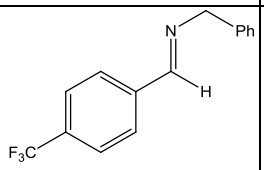	4 hrs	-1.7 V	Amine Only	50 %
3	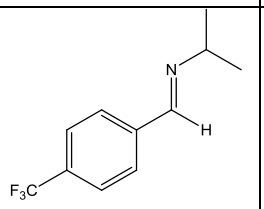	4 hrs	-1.85 V	1 : 1	100 %

[1.] Product distribution calculated from the integration comparison of dimer (2H) and amine (2H) at *ca.* 4.8 and 4.65 ppm
[2.] Conversion calculated from ^{1}H NMR (300 MHz) integration comparison of the imine peak (1H) at *ca.* 8.4 ppm and the new singlet peaks for dimer (2H) and alcohol (2H) at *ca.* 4.8 and 4.65 ppm.

In the case of the isopropyl derived imine a much faster reaction was seen with a conversion of 100 % in 4 hours. This suggested that the steric hindrance of the reductive species was important for the rate of reduction, due to the porous nature of the carbon membrane and the speed of diffusion within the membrane. Furthermore, the steric effect either directly or indirectly had an effect on the product distribution. Although the benzyl substituted imine had a much slower reaction, it only formed a single reduction product. This may be due to the steric effect on the radical coupling not permitting dimer formation. Alternatively, the slow formation of radical anion intermediates may mean that, the local concentration of them was always kept low enough to favour a proton based coupling and resulted in the mono-amine rather than a dimerisation.

8.4 Conclusions

In conclusion, the new triple phase boundary microreactor procedure first introduced in Chapter 7 was extended beyond characterisation, towards bulk reductive syntheses. Initially, the reduction of alkenes was continued for less substituted substrates. As the ester substitution decreased, and the alkenes became more electron rich, the reduction potential increased and the reaction yielded a lower conversion. This effect could however be counteracted by the use of electron withdrawing substituted benzenes instead.

Aldehydes were also the subject of electrolysis in the triple phase boundary microreactor. Benzaldehyde was first analysed and showed excellent conversions but to a pair of products, an alcohol and a dimer. The ratio of these products was altered by changing the triple phase boundary conditions. The reaction was shown to be feasible on a range of substituted benzaldehydes, although was intolerant of other reduction centres under the conditions used.

Finally the reduction of imines was achieved and shown to be much slower than for benzaldehydes. For a more sterically hindered imine a single amine product was seen but for a less sterically hindered imine a product distribution between amine and dimer was found.

8.5 References

(1) Clayden, J.; Greeves, N.; Warren, S.; Wothers, P. *Organic Chemistry*; Oxford University Press, **2001**.

(2) Nishimura, S. *Handbook of Heterogeneous Catalytic Hydrogenation for Organic Synthesis*; Wiley-Interscience, **2001**.

(3) (a) Lim, M.; De Castro, K. A.; Oh, S.; Lee, K.; Chang, Y.-W.; Kim, H.; Rhee, H. *Applied Organometallic Chemistry* **2011**, *25*, 1; (b) Hemantha, H. P.; Sureshbabu, V. V. *Organic & Biomolecular Chemistry* **2011**, *9*, 2597; (c) Kim, S.; Kitano, Y.; Tada, M.; Chiba, K. *Tetrahedron Letters* **2000**, *41*, 7079.

(4) Yoshida, K.; Gonzalez-Arellano, C.; Luque, R.; Gai, P. L. *Applied Catalysis A-General* **2010**, *379*, 38.

(5) Atobe, M.; Okamoto, M.; Fuchigami, T.; Park, J.-E. *Ultrasonics Sonochemistry* **2010**, *17*, 26.

(6) Maity, P.; Basu, S.; Bhaduri, S.; Lahiri, G. K. *Journal of Molecular Catalysis A-Chemical* **2007**, *270*, 117.

(7) Chang, F.; Kim, H.; Lee, B.; Park, S.; Park, J. *Tetrahedron Letters* **2010**, *51*, 4250.

(8) Noyori, R.; Hashiguchi, S. *Accounts of Chemical Research* **1997**, *30*, 97.

(9) Muhammad, O.; Sonavane, S. U.; Sasson, Y.; Chidambaram, M. *Catalysis Letters* **2008**, *125*, 46.

(10) Xiang, Y.; Li, X.; Lu, C.; Ma, L.; Zhang, Q. *Applied Catalysis a-General* **2010**, *375*, 289.

(11) Gaviglio, C.; Doctorovich, F. *Journal of Organic Chemistry* **2008**, *73*, 5379.

(12) da Silva, A. P.; Mota, S. D. C.; Bieber, L. W.; Navarro, M. *Tetrahedron* **2006**, *62*, 5435.

(13) Popp, F. D.; Schultz, H. P. *Chemical Reviews* **1962**, *62*, 19.

(14) Kise, N.; Agui, S.; Morimoto, S.; Ueda, N. *Journal of Organic Chemistry* **2005**, *70*, 9407.

(15) Kise, N.; Shiozawa, Y.; Ueda, N. *Tetrahedron* **2007**, *63*, 5415.

(16) Santana, D. S.; Melo, G. O.; Lima, M. V. F.; Daniel, J. R. R.; Areias, M. C. C.; Navarro, M. *Journal of Electroanalytical Chemistry* **2004**, *569*, 71.

(17) Rai, G.; Thomas, C. J.; Leister, W.; Maloney, D. J. *Tetrahedron Letters* **2009**, *50*, 1710.

(18) Bian, Y. J.; Bai, D. S. *Indian Journal of Chemistry Section B-Organic Chemistry Including Medicinal Chemistry* **2007**, *46*, 1890.

(19) Simion, A.; Simion, C.; Kanda, T.; Nagashima, S.; Mitoma, Y.; Yamada, T.; Mimura, K.; Tashiro, M. *Journal of the Chemical Society-Perkin Transactions 1* **2001**, 2071.

9. Conclusions and Summary

9.1 Conclusions

The primary focus of this thesis has been on the development of new triple phase boundary strategies towards potential use as bulk electrosynthetic systems. A secondary focus has been on the surface modification of carbon nanoparticles as potential platforms for high surface area carbon nanostructured electrodes.

The surface modification of carbon nanoparticles was achieved by the synthetic reaction of commercially available sulphonate functionalised nanoparticle with diamines *via* a sulphonyl chloride intermediate (Chapter 2). In so doing, a cationic carbon nanoparticle was characterised and used in a layer by layer deposition technique with anionic carbon nanoparticles to create highly porous nanostructured carbon thin films. Further modification of the terminal amine has also lead to the attachment of anthraquinone groups for use as highly pH sensitive nanostructured porous carbon films (Chapter 3).

The triple phase boundary is the boundary that exists where three phases are in simultaneous contact at a line boundary. In this thesis the liquid | liquid | solid triple phase boundary has been exclusively investigated, at the boundary between an organic phase, an aqueous phase and a carbon based electrode. The triple phase boundary methodology technique is unique in that redox probe materials and electrolytes may be kept separated, making this technique ideal for use in electrosynthetic processes where product separation from electrolytes can be problematic. In the past, triple phase boundary techniques have been limited to microdroplet arrays but it was the key objective of this work, to scale this technique in such a way that allowed useful synthetic processes to be investigated. The synthetic reduction mechanism involved the transfer of electrons from the electrode surface to the substrate in the organic phase, with the concerted transfer of ions to balance the charge. Generally in organic electrosynthesis, this was a proton transfer from the aqueous phase.

To create a suitable triple phase boundary for electrosynthetic applications a high enough current must be achieved to allow a synthetically viable product turnover. This was achieved in two ways; i) by increasing the triple phase boundary contact zone or ii) by creating mass transport of transfer ions and redox probes to the triple phase boundary.

In previous publications a flow cell was used as a fast mass transport system for flowing triple phase boundary processes.[1] This research showed the first example of a dynamic triple phase boundary, but with currents too low for synthetic applications.

In this thesis four different triple phase boundaries were described. The first example, described in Chapter 4, used a solid salt matrix aqueous phase and a non-polar organic phase. In this example, a series of nano-contact points of salt crystals on a glassy carbon electrode were used as a pseudo-nanoelectrode array, which was best suited as an analytical technique and not a synthetic system.

The next example, described in Chapter 5, used low power acoustic mixing to create a localised surface confined emulsion, in which both the triple phase boundary zone area was increased, and enhanced by increased mass transport. This configuration was tested with synthetic systems and gave good triple phase boundary enhancement, but afforded currents too low for bulk electrosynthesis.

The next example, described in Chapter 6, used a high shear force ultra-turrax system to generate a highly unstable bulk emulsion, in which a large mass transport effect and large triple phase boundary reaction zone lead to very high currents. Unfortunately, despite the large and synthetically viable currents the dispersed nature of the emulsion made synthesis impractical.

The final triple phase boundary described in this thesis (Chapter 7) utilised a commercially available amphiphilic carbon nanofibre paper. This amphiphilic carbon nanofibre paper was able to stabilise the organic | aqueous boundary without the need for further modification. When addressed as the working electrode, the carbon nanofibre paper was able to create a triple phase boundary at the interface of the aqueous and organic phases within the

paper at each point where the two liquid phases simultaneously contacted a nanofibre. In this case, a triple phase boundary microreactor was demonstrated, where an organic phase was contained inside a glass tube and formed a phase separation with an organic phase within the carbon membrane. The use of a high mass transport system was not possible due to the domination of diffusional parameters within the carbon membrane but was necessary for effective bulk electrolysis. Synthetic reactions were demonstrated within this new microreactor (Chapter 8) and showed a high degree of success for the electro-reduction of activated alkenes, aldehydes and imines.

For alkenes, the reactions were found to be most efficient for electron poor alkenes affording the alkane products exclusively. Aldehyde reductions were highly efficient (100% conversion to products in most cases) but generally gave a mixture of products, governed by different reaction zones, to both alcohols and dimers. The external conditions of the aqueous phase were found to have little effect on the mechanism but the incorporation of a combination of Na_2SO_4 (0.1 M – 1 M) as well as a phosphate buffer was found to be critical. Imine reductions, on the other hand, were very slow, and often required a 4 hour reaction time to give an appreciable conversion. In the case of sterically hindered imines a single amine product was isolated whereas less sterically hindered imines gave rise to multiple products. In all of these cases the triple phase boundary reaction was found to be less efficient than ferrocene based anion transfer reactions, but still allowed high conversions in a reasonable timescale.

This thesis represents a significant step towards a bulk triple phase boundary electrosynthetic technique allowing, for the first time, a mechanism suitable for the bulk conversion of *ca.* 10 mg of organic reagents, with analysis by ^1H NMR. This technique requires further optimisation and scale up however to become synthetically viable. To overcome the limitations of diffusion and local reaction conditions within the carbon membrane, it is necessary to reduce the thickness of the carbon membrane to allow external mass transport effects to further enhance the triple phase boundary reaction but care must be taken not to compromise the robustness of the carbon film.

9.2 Publications List

- "Decamethylferrocene Redox Chemistry and Gold Nanowire Electro-Deposition at Salt Crystal | Electrode | Non-Polar Organic Solvent Contacts" Watkins JD, Hotchen CE, Mitchels JM and Marken F, Organometallics, **2011**, Submitted.

- "Liquid–Liquid Electro-Organo-Synthetic Processes in a Carbon Nanofibre Membrane Microreactor: Triple Phase Boundary Effects in the Absence of Intentionally Added Electrolyte" Watkins JD, Ahn SD, Taylor JE, Bulman-Page PC, Bull SD and Marken F, Electrochimica Acta, **2011**, 56(19): 6764-6770.

- "Ion-Transfer- and Photo-Electrochemistry at Liquid | Liquid | Solid Electrode Triple Phase Boundary Junctions: Perspectives" Marken F, Watkins JD, Collins AM, *Physical Chemistry Chemical Physics,* **2011,** 13, 10036-10047.

- "Carbon Nanoparticle Surface Electrochemistry: High Density Covalent Immobilisation and Pore Reactivity of 9,10-Anthraquinone" Watkins JD, Lawrence K, Taylor JE, James TD, Bull SD and Marken F, *Electroanalysis*, **2011**, 23, 1320 – 1324.

- "Liquid | Liquid Biphasic Electrochemistry in Ultra-Turrax Dispersed Acetonitrile | Aqueous Electrolyte Systems" Watkins JD, Amemiya F, Atobe M, Bulman-Page PC and Marken F, *Electrochimica Acta,* **2010**, 55, 8808 – 8814.

- "Three Dimensional Film Electrode Prepared From Oppositely Charged Carbon Nanoparticles as Efficient Enzyme Host" Szot K, Watkins JD, Bull SD, Marken F and Opallo M, **2010**, *Electrochemistry Communications*, 12, 737 – 739.

- "Carbon Nanoparticle Surface Functionalisation: Converting Negatively Charged Sulphonate to Positively Charged Sulphonamide" Watkins JD, Lawrence R, Taylor JE, Bull SD, Nelson GW, Foord JS, Wolverson D, Rassaei L, Evans NDM, Gascon SA and Marken F, *Physical Chemistry Chemical Physics,* **2010**, 12, 737 – 739.

- "High-Yield Acetonitrile | Water Triple Phase Boundary Electrolysis at Platinised Teflon Electrodes" Watkins JD, MacDonald SM, Fordred PS, Bull SD, Gu Y, Yunus K, Fisher AC, Bulman-Page PC and Marken F, *Electrochimica Acta,* **2009,** 54, 6908 – 6912.

- "Ultrasound Mobilisation of Liquid | Liquid | Solid Triple Phase Boundary Redox Systems" Watkins JD, Bull SD and Marken F, *Journal of Physical Chemistry C*, **2009,** 113, 15629 – 15633.

9.3 Presentations List

- Liverpool, Electrochem 2008, poster presentation, "Comparing N-Octyl-2-Pyrrolidone |Aqueous and Acetonitrile | Aqueous Three Phase Boundary Reactions".

- Hull, RHINE 2009, oral presentation "Ultrasound in Triple Phase Reactions – Via Localised Emulsion".

- Weingarten, Germany, ECHEMS 2009, oral presentation "Electrochemical Processes at Flowing Liquid | Liquid | Electrode Interfaces".

- Krakow, Poland SMCBS 2009, oral presentation "Synthesis and Characterisation of Cationic Modified Carbon Nanoparticles".

- Hawaii, Pacifichem 2010, poster presentation "Synthesis, Characterisation and Applications of Cationic Carbon Nanoparticles".

- Hull, RHINE 2011, oral presentation "Electrosynthetic Processes at the Carbon Membrane Stabilised Triple Phase Boundary Interface".

- Warwick, 2011, poster presentation “Liquid – Liquid Electro-Organo-Synthetic Processes at the Triple Phase Boundary Interface”.
- Bath, Electrochem 2011, oral presentation “Electrosynthetic Processes at the Carbon Membrane Stabilised Triple Phase Boundary Interface”.
- Hirschegg, Austria, Bio-Nano summer school, oral presentation “Electron Transfer at the Solid | Liquid Interface: An Introduction to Voltammetry”.

9.4 References

(1) (a) MacDonald, S. M.; Watkins, J. D.; Bull, S. D.; Davies, I. R.; Gu, Y.; Yunus, K.; Fisher, A. C.; Page, P. C. B.; Chan, Y.; Elliott, C.; Marken, F. *Journal of Physical Organic Chemistry* **2009**, *22*, 52; (b) Watkins, J. D. “Clean Electrochemical Processes in Single-Phase and Dual-Phase Microfluidic Devices,” University of Bath, **2008**; (c) MacDonald, S. M.; Watkins, J. D.; Gu, Y.; Yunus, K.; Fisher, A. C.; Shul, G.; Opallo, M.; Marken, F. *Electrochemistry Communications* **2007**, *9*, 2105.